京都大学
KYOTO UNIVERSITY

Title	Study on Porosity of Sediment Mixtures and a Bed-porosity Variation Model(Dissertation_)
Author(s)	Muhammad, Sulaiman
Citation	Kyoto University ( )
Issue Date	2008-03-24
URL	http://dx.doi.org/10.14989/doctor.k13795
Right	
Type	Thesis or Dissertation
Textversion	author

Study on Porosity of Sediment Mixtures and a Bed-porosity Variation Model
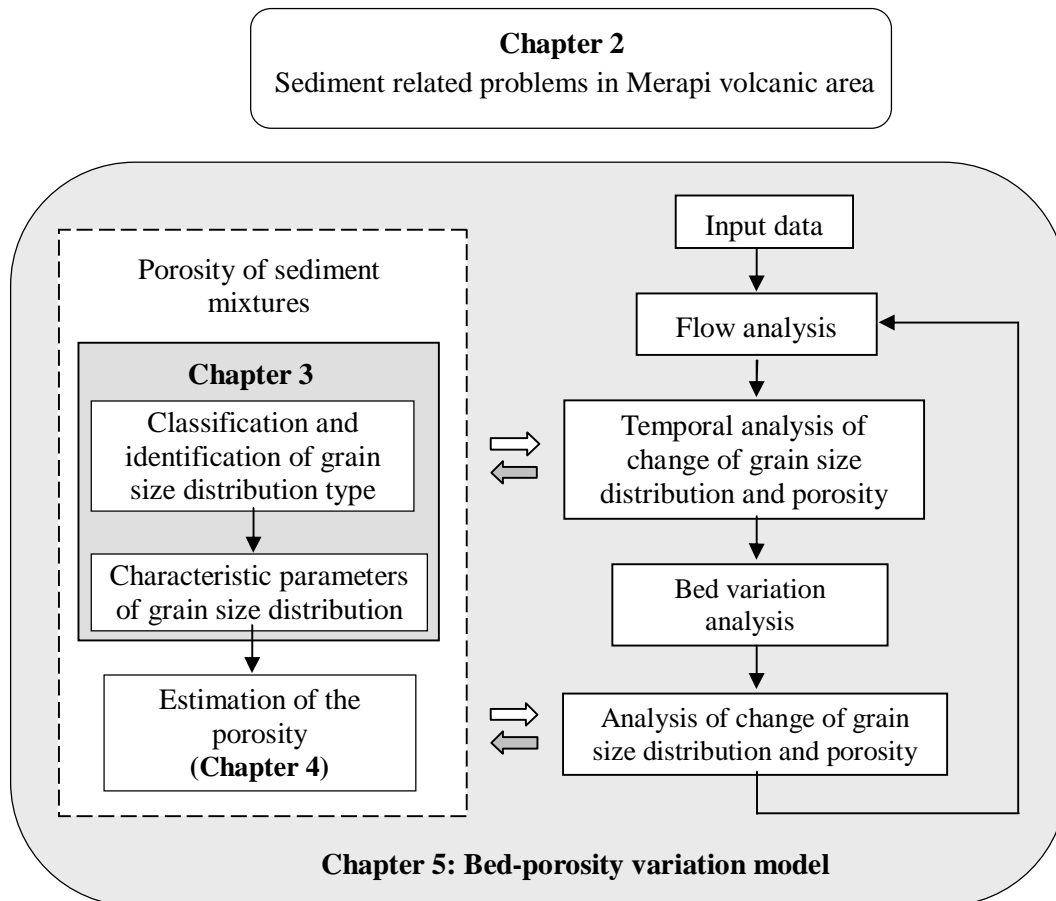
By

Muhammad Sulaiman

2008

Abstract

The sediment movement system in a river basin consists of sediment production process in the mountainous region, sediment supply process to the torrents and sediment deposition process in the lower reach and coastal area. There are human impacts as well as natural impacts in the system. These impacts affect the topographical feature and ecosystem in the basin including the coastal area. Bed variation model is one of the tools for assessing the topographical feature of river. In previous riverbed variation calculations, engineers or researchers conventionally assumed that the porosity in riverbed material is a constant, regardless of whether the grain sizes of the riverbed material was uniform. Since there is no doubt that the porosity depends on the grain sizes distribution, fixing the porosity at a constant value is inadequate for simulating practical sediment movements, such as the removal of fine materials out of the riverbed material or the deposition of fine material into voids between the coarse material. Voids in a riverbed themselves are also important as habitat for aquatic biota. Not only natural sediment transport phenomena, such as floods and debris flows induced by heavy rainstorms, but also artificial impacts, such as the construction of dams or sediment flushing from reservoirs, seriously affect the voids in the riverbed. So far no bed variation model has been available for the analysis of the change in porosity. As the void of bed material plays an important role in fluvial geomorphology, infiltration system in riverbeds and river ecosystem, a structural change of the void with bed variation is one of the concerned issues in river management. Thus, a bed-porosity variation model is strongly required and it is expected that the model contributes the analysis of those problems as a tool for integrated sediment management.

The objectives of this work are: 1) to point out recent problems in a volcanic river basin, as well as the impacts on riverbed variation and ecosystem; the problems in Merapi volcano area and Progo River, Indonesia were chosen as case studies; 2) to develop a method for identifying the type of grain size distribution and two methods for obtaining the porosity for the different type of grain size distribution; 3) to develop a framework and a bed variation model available for the analysis of the change in porosity of bed

material as well as the bed variation. The report consists of four subjects and organized into six chapters as shown in the diagram below (Figure 1). The following diagram shows the framework of proposed bed-porosity variation model and the correspondence of each chapter of this report.

Chapter 2
Sediment related problems in Merapi volcanic area

Porosity of sediment mixtures

Chapter 3

Classification and identification of grain size distribution type

Characteristic parameters of grain size distribution

Estimation of the porosity
(Chapter 4)

Input data

Flow analysis

Temporal analysis of change of grain size distribution and porosity

Bed variation analysis

Analysis of change of grain size distribution and porosity

Chapter 5: Bed-porosity variation model

Figure 1. The framework of proposed bed-porosity variation model and its correspondence of each chapter

In **Chapter 2**, the sediment-related problems in volcanic area, particularly in Mt. Merapi and Progo River, Indonesia and the impacts on bed variation and ecosystem were pointed out. The sediment-related problems persist in the upper reach, middle reach, also in lower reach. Some problems are triggered by natural activities such as volcanic activity of Mt. Merapi and heavy rainfall, and many others are occurred due to the human interfere such as deforestation, construction of sabo dam and sand mining. Uncontrolled sand mining is the serious problem in this area. Those

problems are increasing the susceptibility in the downstream and deteriorating the watershed. A flume experiment was conducted to realize the impact of mining pit on bed variation. Countermeasures of sediment problems, which have been done in Mt. Merapi area and Progo River, were also presented. Finally, the necessity of a tool for integrated sediment management in consideration of the ecosystem in river was indicated.

In **Chapter 3**, the method for classifying and geometrically identifying the type of grain size distribution was presented. First, grain size distribution was classified into some typical types and those characteristic parameters were found out. Then a method for geometrically identifying the type of grain size distribution by using geometric indices β and γ was presented. Based on the geometrical analysis of typical grain size distributions, a diagram on classification of grain size distribution type was indicated. The presented identification method was then applied to the natural grain size distribution data and the validity of the method was verified.

In **Chapter 4**, two methods for estimating the porosity of sediment mixtures were presented. One was based on a particle packing simulation model and the other was based on a measurement method. The porosity of particle mixtures depends on not only the grain size distribution but also the compaction degree. However, the compaction degree could not be intentionally controlled in the model. Both of the methods were applied to estimate the porosity of three typical grain size distributions, namely lognormal distribution, modified-Talbot distribution and bimodal distribution. Particularly in the measurement, it was very difficult to mix the sediment evenly. Consequently, the coarser particle lies at higher position than the finer particle. This grading process made the porosity larger, while in the simulation the particles were mixed evenly. Thus, the particles packing in the simulation might be denser than the packing of particles in the measurement. The results showed that the relationship between grain size distribution and porosity could be determined by using the characteristic parameters of typical grain size distribution. This relation could be introduced into the bed variation model.

In **Chapter 5**, a one dimensional bed-porosity variation model was developed for simulating the changes in porosity of bed material as well as the bed variation. Analytical model for binary mixtures with much different grain sizes and the relationship between the characteristic parameters of grain size distribution and porosity presented in Chapter 4 were introduced into the bed variation model. Two numerical methods were employed to solve the governing equations, i.e., standard successive approximation and MacCormack scheme. A flume experiment was conducted to realize the transformation processes of void structure for two conditions; one was the only fine sediment was removed from a sediment mixture and another was the fine sediment deposited into a coarser bed material. After the validity of the presented model was verified using a data set provided by the experiment, the model was applied to the bed and porosity variation process for bed material with binary mixtures and continuous grain size distribution. Its performance was examined in detail for two conditions; (1) no sediment supply condition and (2) sediment supply condition. The simulation results showed the model could produce a reasonable distribution of porosity of the riverbed material in the longitudinal and vertical directions for both conditions.

A one-dimensional bed-porosity variation model proposed in this study is different from the previous model from a viewpoint of considering the porosity of bed material. Hence, the proposed model is available for the analysis of the change in porosity of bed material as well as the bed variation. The model contributes in two aspects; from the hydraulics point of view, the model provides an improvement of the accuracy in the riverbed variation calculation and from ecological point of view, the model provides the changes in porosity with the bed variation. In the case of binary mixtures, the validity of the model has been verified using a data set provided by the experiment and the simulation result showed that the model produced a reasonable result on the change in porosity as well as the bed variation. In the case of sediment mixtures with continuous grain size distribution, although the validity of the model has not been verified yet, the simulation result showed the model available for analysis of bed and porosity variation.

Key words: *bed variation model, porosity, grain size distribution, sediment mixtures.*

Contents

Chapter 1

Introduction

1.1 Background

A sediment region is defined as the areas extending from the source of sediment to its ultimate destination. A sediment region may extend from the headwaters of a river to the sea, and includes land, riverine, estuarine, littoral, and marine zones. The sediment movement system in a river basin consists of sediment production process in the mountainous region, sediment supply process to the torrents and sediment deposition process in the lower reach and coastal area. Schumm (1977) roughly divided the overall longitudinal profile of most streams into three zones; headwaters (it often has the steepest gradient), transport zone (it is usually characterized by wide floodplains and meandering channel patterns), and depositional zone.

The sediment movement system is influenced by the natural impacts as well as human-induced impacts. Both impacts affect the topographical feature and ecosystem in the basin including the coastal area. In the volcanic basins, particularly in Indonesia, topographical changes of the rivers are mainly dependent upon some factors as follows: (1) the impact of volcanic eruption whose tremendous sediment production causes the severe bed aggradation (DGWR, 1971) and reservoir sedimentation (Sukistijono *et al.*, 2005), (2) the development of the sediment control works for the trapping sediment causes the bed degradation in the downstream (Sumaryono *et al.*, 1996), (3) the construction of dams and weirs for the development of the water resources causes the bed degradation in the

downstream and coastal erosion, (4) uncontrolled sediment mining at a particular site reduces sediment discharge and causes the riverbed degradation in the downstream (DGWR, 2001), (5) deforestation and illegal logging that cause the severe erosion in river basins and sedimentation in reservoirs (Lavigne and Gunnel, 2006).

Due to the volcanic eruption, the supply of sediment from the active volcano in considerable large amount, can impact river channel hydraulics and may cause severe damage on the downstream. At another side, the sediment can be a good material for construction purposes; therefore, many people exploit the sediment for their own additional income. The first condition occurs naturally; whereas the second condition exists under human interfere. If those conditions are unbalance, the unacceptable degree of river morphology change (including the aggradation and degradation of riverbed) may persist. Some features are found in the major rivers in Indonesia, where the riverbed degradation has reached the critical condition (Legono, 2005). The examples of negative impacts due to the riverbed degradation are as follows: 1) the instability of the bridge piers that causes the bridge collapse, 2) the lowering of the water surface profile that makes difficulties of irrigation operation, 3) bank erosion, and 4) undermining of bank protection. It is obvious that the riverbed degradation occurs when there is unbalance situation between the sediment supplied from the upstream part of the river and the sediment extraction from the river reach. In addition, sediment deficit caused by the sand mining leads to selective sorting of finer grains from bed material and the development of the bed armor (Rinaldi *et al.*, 2005). Photo 1.1 shows the sand mining activities at a tributary of volcanic stream in Indonesia, and Photo 1.2 shows the riverbed condition and the bed material after sand mining.

Photo 1.1 Sand mining activities in Senowo River, one of the tributaries of Progo River, Indonesia. The tributary is originated from Merapi Volcano.

Photo 1.2 Riverbed condition and bed material in Senowo River after sand mining.

Installation of dams on a river typically blocks the downstream delivery of sediment and causes the bed degradation and the morphological change. After the construction of dam, the riverbed changes qualitatively and it is covered by an armor coat that composed of coarse sediment. For such reservoir sedimentation issues, some sediment managements have been recently implemented, for example in Japan (Kashiwai, 2004). In order to control reservoir sedimentation, several different approaches such as upstream sediment trapping, dredging, bypassing, sluicing, and flushing have been developed. Among them, the flushing approach was an efficient technique of the hydraulic sediment removal to restore the reservoir storage

3

capacity (Liu *et al.*, 2004a). Flushing removed the accumulated sediments after they have been deposited. The first time a flushing was done, a channel would form in the deposited material, and the next time this channel would be maintained by the flushing flows (Morris and Fan, 1997). During the flushing process, large quantities of suspended matter were carried in suspension down the river over long stretches. Such an artificial sediment supply might influence the downstream reach quantitatively and qualitatively, such as, channel aggradation and flooding, as well as adverse impact on fisheries and the environment (Morris and Fan, 1997). The adverse impacts of flushing were mainly due to the high sediment concentration (Liu *et al.*, 2004b). An example of the impact of sediment flushing on the riverbed material in Japan is shown in Photo 1.3 and the changes of riverbed material before and after sediment flushing are shown in Photo 1.4. The grain size of deposited sediment was found to be finer than the bed material before the flushing.

From an ecological point of view, those human-induced impacts (sand mining and sediment flushing) on habitat for fish and aquatic insects are very important and particularly the importance of assessing the change in void structure of the bed material has been strongly pointed out (Milhous, 1982; ASCE Task Committee, 1992; Owens *et al.*, 2005). As the void of bed material played an important role in fluvial geomorphology (Boulton *et al.*, 1998), exchange processes between river and groundwater (Brunke and Gonser, 1997) and river ecosystem (Gayraud and Philippe, 2003), this study concerns to develop a tool for evaluating the bed variation including the changes of porosity. A structural change of the void with bed variation is one of the concerned issues in river management as well as bed variation. Thus, a bed-porosity variation model is strongly required and it is expected that the model will contribute for analyzing those problem as a tool for integrated management.

Photo 1.3 Upstream views of Kurobe River, Japan before and after sediment flushing from Dashidaira Dam and Unazuki Dam. (Photo courtesy Masaharu Fujita)

Photo 1.4 Changes of riverbed material in Kurobe River, Japan before and after sediment flushing from Dashidaira Dam and Unazuki Dam. (Photo courtesy Masaharu Fujita)

1.2 Problem Definition

The sediment-related problems are conventionally addressed locally for each control area. The local countermeasure for sediment-related problems may give a negative influence on the other reach, and thus the integrated sediment control measure is necessary. Targets of the integrated sediment management are disaster prevention, reduction of negative influence of sediment on rivers, effective utilization of sediment resources and environmental conservation. For sediment management from an

5

ecological point of view, it is essential to evaluate the quantitative and qualitative changes of riverbeds. A numerical simulation method for bed variation is one of the tools of sediment management for assessing the erosion and sedimentation in a river system. Some bed variation models are available to the numerical analysis on topographical and morphological changes of rivers (Lopez and Falcon, 1999; Papanicolau *et al.*, 2004; Meier and Reichert, 2005). However, the models are not useful for assessing the change in porosity at all because they are not equipped with a routine for the porosity change.

So far, engineers and researchers have conventionally assumed that the porosity of bed material is constant in their bed variation models, regardless of whether the particle size of the bed material is uniform (Fujita *et al.*, 2005). However, if only fine sands are removed from a riverbed composed of sediment mixtures or they deposit into the voids of coarser bed material, the porosity of the bed material must change significantly. For these conditions, fixing the porosity at a constant value is inadequate for calculating the riverbed variation. Hirano (1971) has presented a bed variation model for sediment mixtures, and pointed out the necessity of considering the change of porosity in some cases. Therefore, it is essential to develop a framework of bed variation model considering porosity change in riverbed material.

The porosity is generally dependent on the compaction degree. However, if the bed material is assumed to be always mixed at the same compaction degree, the porosity is dependent only on the grain size distribution. A different type of grain size distribution must have a different porosity. The porosity itself must change with the characteristic parameters of each type of the grain size distribution. The porosity can be analytically obtained in the case of binary mixtures. However, in the case of continuous grain size distribution, it is difficult to obtain the relationship between the porosity and the characteristic parameters of grain size distribution. If the

grain size distribution type is identified and the porosity is related to the characteristic parameters of the grain size distribution type, the relationship can be obtained.

Actual sediment mixtures have various types of grain size distribution. It is necessary to obtain the porosity for each grain size distribution one by one in calculation of bed variation. However, it is not practical. Therefore, it is better to install some relationships between the porosity and typical grain size distribution in the bed variation model in advance. For that modeling, it is essential for classifying and identifying the grain size distribution.

1.3 Objectives of the Research

This research study focuses on the developing a framework of bed variation model considering the porosity change in riverbed material. The objectives of this study can be described as follows;

(1) as a background, this study will figure out the recent sediment-related problems in a volcanic river basin as well as the impacts on riverbed variation and ecosystem. The sediment problems in Merapi volcanic area and Progo River basin Indonesia are chosen as case studies,

(2) developing a method for classifying and identifying the type of grain size distribution,

(3) developing two methods for estimating the porosity of different type of grain size distribution,

(4) developing a fundamental framework of quantitative and qualitative bed variation model providing the changes in porosity and grain size distribution type of bed material and a bed porosity variation model.

1.4 Thesis Outline

The thesis is composed of six chapters. The synopsis of each chapter is described as follows:

In **Chapter 2**, the sediment-related problems in volcanic area (particularly in Merapi volcanic area and Progo River, Indonesia) and the impacts on bed variation and ecosystem are figured out and discussed. Countermeasures of sediment problems that have been done in Merapi volcanic area are also presented. To get a better understanding of the impacts of the sand mining on the bed variation, a flume experiment on transformation process of mining pit in a channel is conducted. The environmental and management issues of sand mining are discussed, including the influence of sabo facilities and sand mining in Progo River on ecosystem. The necessity of a tool for integrated sediment management in consideration of the ecosystem in river is then described.

In **Chapter 3**, a method for classifying and geometrically identifying the type of grain size distribution is presented. Based on the geometrical analysis of typical grain size distribution, a diagram on classification of grain size distribution type is proposed. The presented identification method is applied to the natural grain size distribution data and the validity of the method is verified.

In **Chapter 4**, two methods for estimating the porosity of sediment mixtures are presented. One is based on a particle packing simulation model and the other is based on a measurement method. The porosity of binary mixtures is analyzed and a simulation method for estimating the porosity for different types of grain size distribution is described. A measurement method for obtaining the porosity of actual sediment mixtures is then introduced. Finally, a relation between the porosity and the characteristic parameter of grain size distribution obtained in Chapter 3, is indicated. This relation can be introduced into the bed variation model.

In **Chapter 5**, a one-dimensional bed-porosity variation model is developed for the purpose of simulating the changes in porosity of bed material as well as the bed variation. Analytical model on porosity of binary sediment mixtures and the relationship between the characteristic parameters of the grain size distribution and the porosity presented in Chapter 4 are introduced into the bed variation model. A flume experiment is conducted to realize the transformation processes of void structure for two conditions; one is the only fine sediment is removed from a sediment mixture (no sediment supply) and another is the fine sediment deposits into a coarser bed material (sediment supply). Two numerical methods are employed to solve the governing equations, i.e. standard successive approximation and MacCormack scheme. The bed-porosity variation model with standard successive approximation is applied to simulate the bed and the porosity variation process observed in the flume experiment. The bed-porosity variation model by means of MacCormack scheme is applied to simulation of the bed variation processes in some cases under two conditions of no sediment supply and sediment supply.

In **Chapter 6,** the results obtained in the present study are summarized and the future perspectives of researches are pointed out.

References

ASCE Task Committee on Sediment Transport and Aquatic Habitats. (1992). "Sediment and aquatic habitat in rivers systems." *J. Hydraul. Eng.,* Vol.118, No.5, pp.669-687.

Boulton, A. J., Findlay, S., Marmonier, P., Stanley, E. H., and Valett, H. M. (1998). "The functional significance of the hyporheic zone in streams and rivers." *Annu. Rev. Ecol. Syst.*, Vol.29, pp.59-81.

Brunke, M. and Gonser, T. (1997). "The ecological significance of exchange processes between rivers and groundwater."*Freshwater Biology*, Vol.37. pp.1-33.

DGWR (Directorate General of Water Resources), Ministry of Public Works and Power, Government of Indonesia. (1971). "Progo Basin Study", Main Report.

DGWR (Directorate General of Water Resources), Ministry of Settlement and Regional Infrastructure, Republic of Indonesia. (2001). "Review Master Plan Study on Mt. Merapi", Main Report.

Fujita, M., Tsutsumi, D., and Sulaiman, M. (2005). "A simulation method for quantitative and qualitative changes of riverbed." *Proc. Int. Symp. on Fluvial and Coastal Disaster* (CD-ROM), Kyoto, Japan.

Gayraud, S., Philippe, M. (2003). "Influence of bed-sediment features on the interstitial habitat available for macroinvertebrates in 15 French streams." *Internat. Rev. Hydrobiol.*, Vol. 88, pp.77-93.

Hirano, M. (1971). "River-bed degradation with armoring." *J. Japan Soc. Civil Eng.*, Vol.195, pp.55-65. (in Japanese with English summary)

Kashiwai, J. (2004). "Reservoir Sedimentation and Sediment Management in Japan." Public Work Research Institute, Japan.
http://www.pwri.go.jp/eng/kokusai/reportlist.htm

Lavigne, F. and Gunnel. Y. (2006). "Land cover change and abrupt environmental impacts on Javan volcanoes, Indonesia: a long-term perspective on recent events." *Reg. Env. Change.,* Vol. 6, pp.86-100.

Legono, D. (2005). "Important issues on sediment-related disaster management in Indonesia." *Proc. Int. Symp. on Fluvial and Coastal Disaster* (CD-ROM), Kyoto, Japan.

Liu, J., Minami, S., Otsuki, H., Liu, B-Y., and Ashida, K. (2004a). "Prediction of Concerted Sediment Flushing." *J. Hydraul. Eng.*, Vol.130, No.11, pp.1089-1096.

Liu, J., Minami, S., Otsuki, H., Liu, B-Y., and Ashida, K. (2004b). "Environmental impacts of coordinated sediment flushing." *J. Hydraul. Res.*, Vol.42, No.5, pp.461-472.

Lopez, J.L. Falcon, M.A. (1999). "Calculation of bed changes in mountain streams." *J. Hydraul. Eng.*, Vol.125, No.3, pp.263-270.

Meier, W.K. and Reicchert, P. (2005). "Mountain streams-modeling hydraulics and substance transport." *J. Env. Eng.*, Vol.131, pp.252-261.

Milhous, R.T. (1982). "Effect of sediment transport and flow regulation on the ecology of gravel-bed rivers." *Gravel-bed Rivers.* Edited by Hey, R.D., Bathurst, J.C. and Thorne, C.R, John Wiley & Sons, pp.819-842

Morris, G.L. and Fan, J. (1997). "Reservoir Sedimentation Handbook: Design and Management of Dams, Reservoirs, and Watersheds for Sustainable Use." McGraw-Hill, New York, 848 pages.

Owens, P. N., Batalla, R. J., Collins, A. J., Gomez, B., Hicks, D. M., Horowitz, A. J., Kondolf, G. M., Marden, M., Page, M. J., Peacock, D. H., Petticrew, E. L., Salomons, W., and Trsutrum, N. A. (2005). "Fine-grained sediment in river systems: environmental significance and management issues." *River Res. Applic.*, Vol. 21, pp.693-717.

Papanicolau, A.N., Bdour, A., and Wicklein, E. (2004). One-dimensional hydrodynamic/sediment transport model applicable to steep mountain streams. *J. Hydraul. Res.*, Vol.42, No.4, pp.357-375.

Rinaldi, M., Wyzga, B. and Surian, N. (2005). "Sediment Mining in alluvial Channels: Physical effects and management perspectives." *River Res. Applic.*, Vol.21, pp.805-828

Schumm, S.A., (1977). "The fluvial system." John Wiley & Sons, New York, 338 pages.

Sukistijono, Harnanto, A. and Hidayat, F. (2005) "Effect of Volcanic Eruption on Sedimentation: Case Study of Mt. Kelud in Brantas River Basin, East Java-Indonesia." *Proc. Int. Conf. on Monitoring, Prediction and Mitigation of Water-related Disaster*. Kyoto. Japan.pp.551-556.

Sumaryono, A., Churiyah, and Artha, IGM. (1996). "Geomorphological Changes at Progo River Caused by Lahar." *Proc. Workshop on Disasters Caused by Floods and Geomorphological Changes and Their Mitigations*. Yogyakarta, Indonesia.pp.198-209.

Chapter 2

Sediment-related Problems in Merapi Volcanic Area

2.1 Introduction

Merapi volcano is one of the most active and feared volcanoes in the world (Voight, *et al.*, 2000). The word "*Merapi*" is a compound word derived from Sanskrit "meru" that means "high mountain", and from an old Javanese word "api" that means "fire". The volcano is located approximately 30 km north-northeast from Yogyakarta Indonesia, as shown in Figure 2.1. Frequent eruptions have induced pyroclastic flows due to collapse of lava dome or lava tip, resulting in disasters in the downstream area and a tremendous amount of volcanic loose deposit on the slope of Mt. Merapi. Once there is an intensive rainfall, the loose deposit flows downstream as the debris flows endangering the downstream resident lives, assets and social infrastructures. River facilities in the foothills of Mt. Merapi, particularly irrigation weirs, have been damaged by debris flows, causing the negative impact on agriculture.

Progo River is located in the southern part of Central Java, Indonesia. The river flows through the Province of Central Java and Yogyakarta Special Region. Progo River originates in Mt. Sindoro (3,136 m), which is naturally bounded by Mt. Sumbing (3,240 m) at the west side and Mt. Merbabu (3,142 m) as well as Mt. Merapi (2,986 m) at the east side, as shown in Figure 2.1. Those four volcanoes dominate general topography of the Progo River basin. The basin covers an area of 2,380 km² and the slope of Mt. Merapi has an area of 620 km², corresponding to 26% of the total
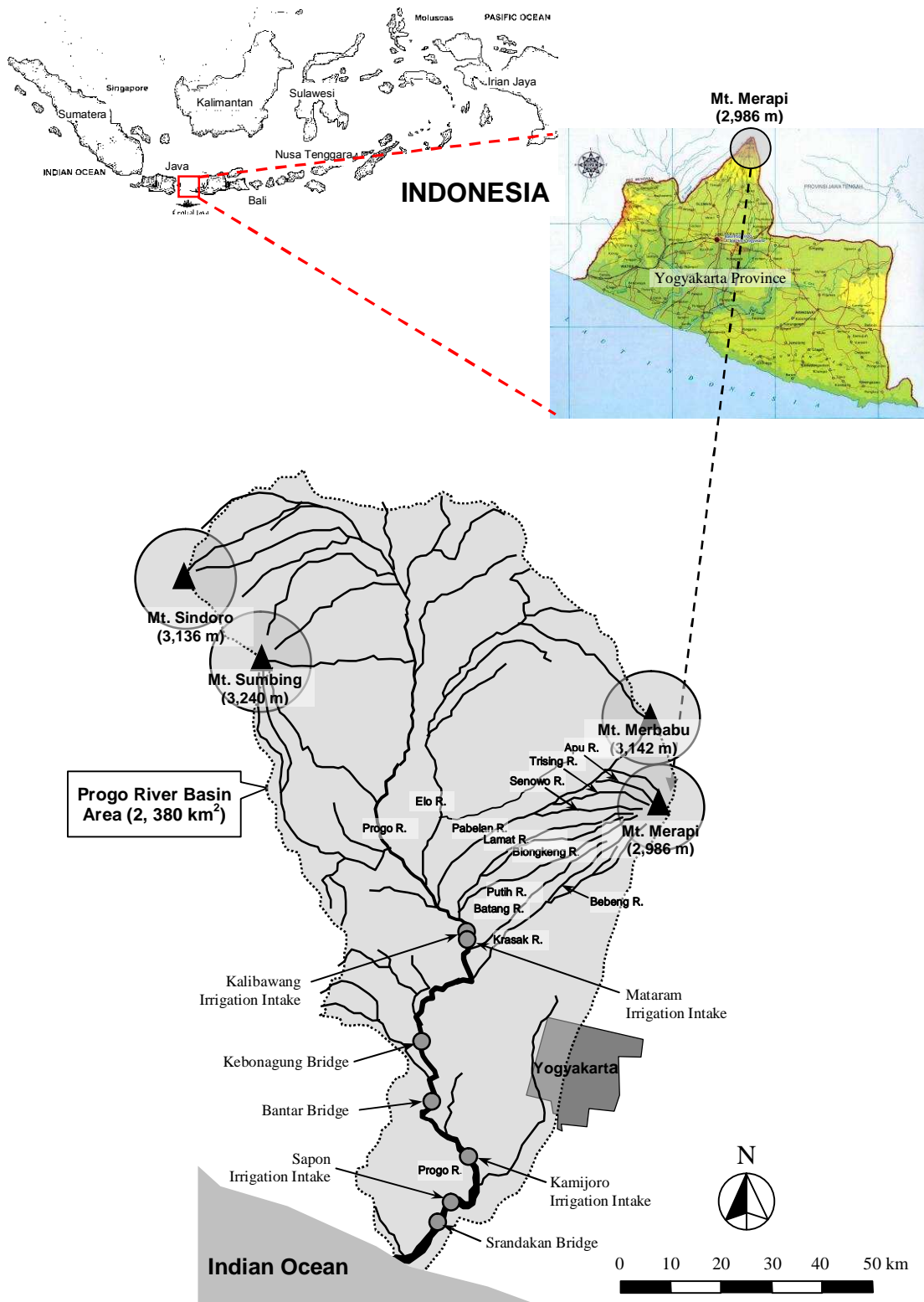
Fig.2.1 Location map of Mt. Merapi and Progo River Basin area.

basin of Progo River. The main river channel is 140 km in total length flowing from the North to the South and drains into the Indian Ocean. The water in Progo River has been contributed to the people daily lives along the river, mainly for irrigation and domestic water. The Progo River basin can be divide into two groups, namely the rivers unaffected by the eruptions of Mt. Merapi (Upper Progo) and the rivers affected by the eruptions of Mt. Merapi (Middle and Lower Progo). The Upper Progo area consists of the catchments of Progo River and Elo River up to their confluence. The rivers affected by the eruptions of Mt. Merapi carry a heavy load following eruption, and are characterized by considerable variation with time depending on eruptions of Mt. Merapi. The tributaries of Progo River on the slope of Mt. Merapi consist of Pabelan, Apu, Trising, Senowo, Lamat, Blongkeng, Putih, Batang, Krasak, and Bebeng Rivers (Figure 2.1). Almost all rivers have parallel flow patterns. Bellow its confluence with Elo River, Progo River starts to receive the recent volcanic material of Mt. Merapi. This material enters Progo River as both of the normal and the flood sediment load, and sometimes forms the deposit in the main stream. The river mouth of Progo River is shallow and has small tidal basin. In front of the river mouth, the accumulation of sediment forms a relatively large submerged delta and blocks up the river mouth.

Sediment deposit in Mt. Merapi area has threatened people and asset in the downstream. On the other side, the sediment has a good quality for construction material and attracts the sand miners. Recently, the sand mining in the Mt. Merapi area has expanded rapidly and becomes the dominant income source of the rural people. However, uncontrolled sand mining has caused serious problems in the watershed, such as bank erosion, riverbed degradation, unstableness of river structures and environmental effects (Lagasse *et al.*, 1980; Kondolf, 1997 and Rinaldi *et al.*, 2005). These physical impacts cause the erosion of riparian and the destruction of aquatic

habitat. Bed coarsening and removal of gravel suitably sized for spawning are of particular concern on river supporting salmonids (Kondolf, 1994).

Riverbed degradation is one of the critical issues of uncontrolled sand mining in Merapi volcanic area.   For example, in the lower reaches of Progo River, two irrigation intakes had a difficulty in conducting water to irrigate 4,500 ha area and three bridges were in danger of collapse, due to riverbed degradation. The locations of those river structures are shown in Figure 2.1.

This chapter presents the recent sediment-related problems in Merapi volcanic area and discusses the impacts on bed variation and ecosystem, as well as the management issues of sustainable sand mining. Firstly, the sediment-related problems from the mountain area to the coastal area and its countermeasures are figured out. It consists of the volcanic activities of Mt. Merapi, the sediment disasters and its countermeasures, the sand mining activities, the riverbed variation and river mouth closure. The sediment disasters that caused by pyroclastic flows and debris flows are presented, including its countermeasures. The present sand mining activities in the foothills of Mt. Merapi and the lower reach of Progo River (hereinafter referred as Lower Progo River) are described. To get a better understanding of the effects of the sand mining on the riverbed variation, a flume experiment on transformation process of mining pit in a channel is conducted. The recent riverbed degradation in the Lower Progo River and its effects on the river structures are also discussed, including the problem of river mouth closure. Secondly, the environmental and management issues of sand mining are discussed. The impacts on ecosystem of sabo facilities and sand mining in Progo River are presented. The necessity of sand mining is then analyzed qualitatively as a method for controlling the excess of sediment.

2.2 Sediment-related Problems

2.2.1 Volcanic activities of Mt. Merapi

Mt. Merapi has been giving various volcanic activities such as eruptions, lava flows, pyroclastic flows, glowing clouds, volcanic ash falls and volcanic debris flows. Of those activities, the pyroclastic flows and debris flows have been causing serious damages around Mt. Merapi. In the historical age, the oldest record of the eruption in 1006 A.D. was engraved in the stone monument with Sanskrit inscription of old Javanese stories (Newhall *et al.*, 2000). This inscription described heavy casualties and the lost of the old kingdom by huge eruption and consequent debris flows. The next record was the eruption in 1672 which caused three thousands deaths by pyroclastic flows, glowing clouds and volcanic debris flows (DGWR, 2001b).

The volcanic activities were continuously recorded after 1800s (Voight *et al.*, 2000). Mt. Merapi has frequently erupted, counting more 40 times include 14 times of major eruptions in the last 200 years as follows (bold denote the major eruption): 1821, **1822,** 1832, 1837, 1846, 1848, **1849,** 1862, 1865, 1869, **1872,** 1883, **1888,** 1891, **1902,** 1909, 1915, **1920, 1930,** 1933, 1939, **1942,** 1948, **1953,** 1956, 1957, **1961**, 1967, **1969,** 1972, 1975, 1976, 1979, **1984,** 1986, 1992, **1994,** 1997, **1998,** 2001 (DGWR, 2001b), and recently in 2006. Thus, Mt. Merapi has erupted once every 5 years, or once 14 every years for major eruptions during the 200 years, while in the last 50 years, Mt. Merapi erupted once every 3 years, and major eruption occurred at intervals of 9 years. The lava production data since 1890 have been compiled by Siswowidjoyo *et al.*, (1995), and the result is shown in Figure 2.2. The production rates of individual eruptive events are varied widely, but the cumulative volume is increased nearly linear (Fig.2.3). This

data showed that the lava production rate was approximately constant for a century, at around $1.2 \times 10^6 m^3$ per year.

Voight *et al.*, (2000), have compiled a comprehensive descriptive history of recent eruptive growth and destructive activities at Merapi Volcano during 1768-1998. Volcanic activities during 1830-1870 occurred on the western slope and on the northwestern slope at the end of 1800s. The volcanic activities moved to the eastern slope during 1903-1904, to the southeastern slope during 1905-1906 and to the northwestern slope during 1909-1913. From 1940 up to 1994 the activities remained mainly on the southwestern slope, except on the northern slope during 1954-1956. From 1998 up to 2001 the activities slightly changed to the western slope from the southwestern slope (DGWR, 2001b). On June 2006, volcanic activities changed to the eastern slope. The activities of Merapi Volcano have caused severe sediment-related disasters, including pyroclastic flows and debris flows.
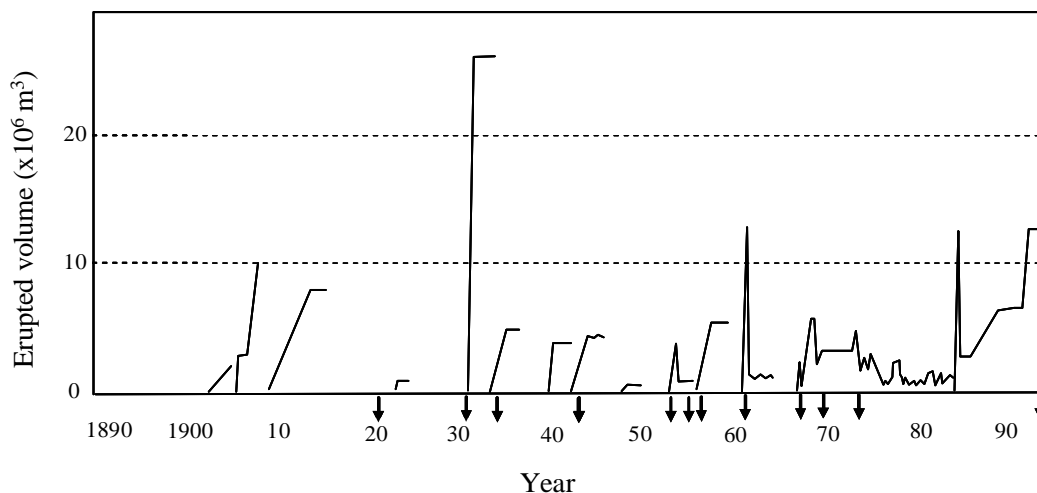
Fig. 2.2 Volume of lava production at Mt. Merapi and its major eruption between 1890 and 1992 (Siswowidjoyo *et al.*, 1995).
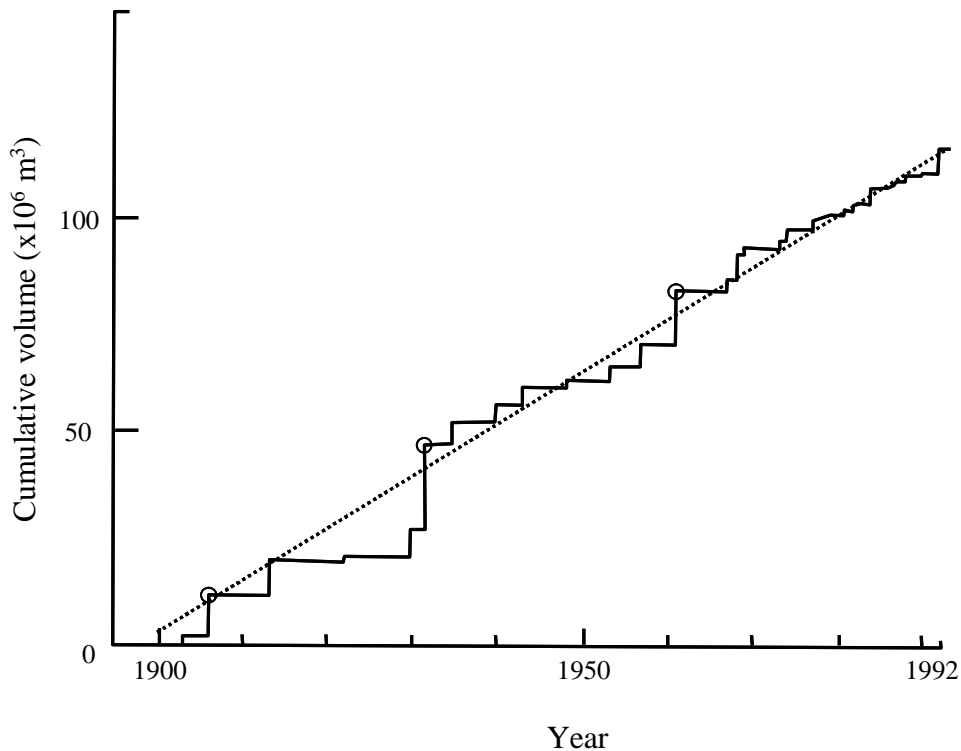
Fig. 2.3 Cumulative volume of lavas from Merapi volcano since 1890 (Siswowidjoyo *et al.*, 1995); circles denote accumulation of lava volumes exceeding 10^7 m^3 in a single eruption episode.

2.2.2 Sediment disasters and its countermeasures

(1)   Pyroclastic flows

Pyroclastic flows are fluidized masses of rock fragments and gases that move rapidly in response to gravity. Pyroclastic flows have occurred during last 100 years toward every direction of the tributaries on the slope of Mt. Merapi (Thouret, *et al.*, 2000; Voight, *et al.*, 2000 and DGWR, 2001b). The direction of pyroclastic flows stayed almost on southwest slope during 37 years from 1961 to 1997. The former direction of pyroclastic flows in 1998 and 2001 was limited just on the western slope. However, in the eruption on June 2006, the pyroclastic flows flowed to Gendol River and Woro River

19

(Mananoma, et al., 2006) and the direction changed towards southeast, as shown in Figure 2.4.
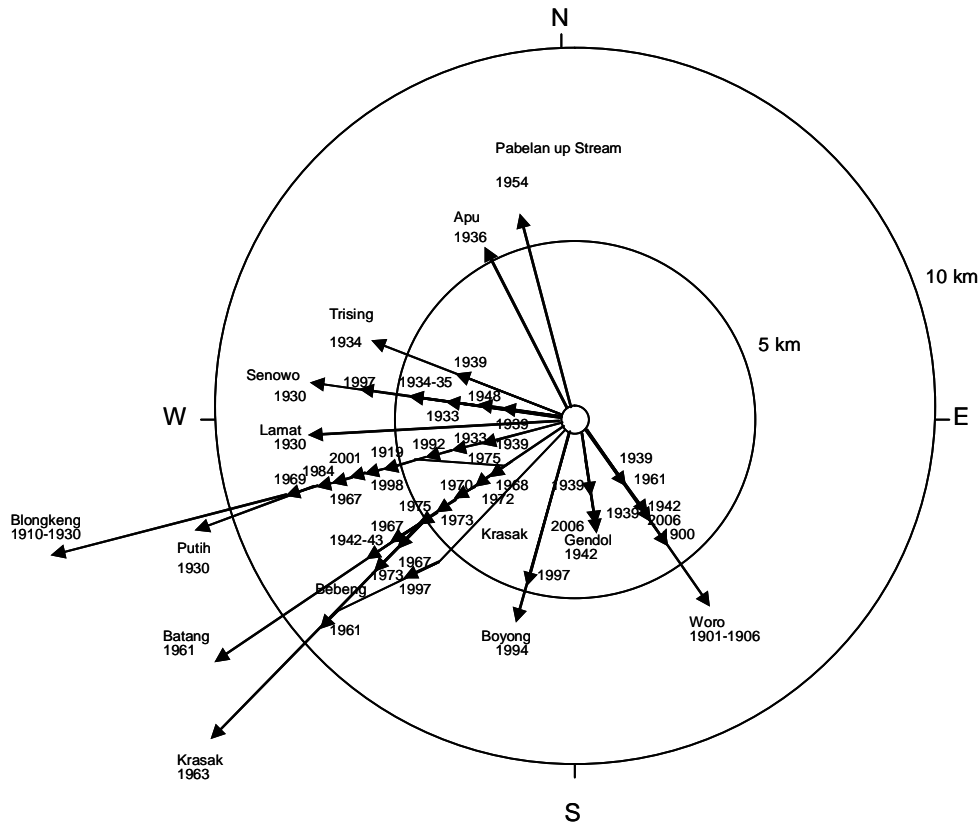
Fig. 2.4 Diagram of dominant directions of pyroclastic flows. (modified from DGWR, 2001b)

Pyroclastic flows have caused tremendous damages by the main body and glowing cloud around Mt. Merapi. The destructive disasters with casualties caused by pyroclastic flows from 1006 to 1996 are listed up in Table 2.1. The situations of upstream Gendol River before and after the eruption on June 2006 are shown in Photo 2.1. The pyroclastic flows damaged the vegetation and filled the valley of upstream Gendol River with a large quantity of gravelly sand.

Table 2.1 Destructive disasters with casualties caused by pyroclastic flows. (source: Lavigne *et al.*, 2000 and DGWR, 2001b)

Year	Duration of activity (year)	Total sediment volume (million m^3)	Remarks (casualties and damages of property)
1006	-	-	Heavy casualties and the old kingdom were lost.
1672	-	-	3,000 casualties
1832-35	3	-	32 casualties
1930-31	0.7	43	Area of 20 km^2 was burned, 13 villages were completely swept away along Blongkeng River, 369 persons were killed and 2000 animals were died. Glowing cloud reached 12.5 km in Blongkeng River, 10.5 km in Putih River, 7.75 km in Lamat River and 8 km in Senowo River.
1969	0.4	10.8	3 casualties
1976	-	-	29 casualties, damages of properties: 3 villages, 349.3 ha tiled land, 4 bridges, and 323 houses
1994	0.9	Over 5.2	Whole lava dome was collapsed, the pyroclastic flows and glowing cloud reached 7.5 km, burning Turgo village and 66 people were killed.
1995	-	-	Damages properties: 1 bridge, 11 trucks
1996	-	-	Damages properties: 14 trucks

Photo 2.1 Situations of upstream Gendol River, (a) before eruption and (b) after eruption on June 2006. (Photo courtesy Tini Mananoma)

(2) Debris flows

A debris flow is water-saturated debris flowing downstream slope under the gravity force. Debris flows consists of material varying in size from clay to rock with a size of several meters. Debris flows have frequently occurred just after eruptions because pyroclastic flows pile up a huge quantity of loose sediments and ashes in the river basins of the volcano. Debris flows start on the upper slope of Mt. Merapi between the elevation of 1,000 and 2,000 m (DGWR, 2001b). Many debris flows have occurred for long years. At least 23 of the 61 reported eruptions since the mid-1500s have produced source deposits for lahars, including debris flows (Lavigne *et al.*, 2000). Damages by debris flows have occurred all the way from the upper slopes to the hamlet and agricultural area on the middle slopes of Mt. Merapi. Debris flows tend to occur when the volcano becomes active. The total number of debris flows recorded from 1931 to 1996 was more than 500 times in almost all the rivers on the slope of Mt. Merapi (DGWR, 2001b). The number of debris flows were: 1) 212 times in almost all the rivers during 17 months from December 1930 to April 1932 after the eruption on November 1930, 2) 247 times in many rivers during 10 years from 1969 to 1978 after the eruption in 1969, and 3) 103 times mainly in Putih, Bebeng and Boyong Rivers during 12 years from 1985 to 1996 after the eruption in 1984. Locations of debris flows disasters are shown in Figure 2.5.

The historical lahar events and related damages at Mt. Merapi have been reported in the previous papers (e.g. Lavigne *et al.*, 2000 and DGWR, 2001b). In January 1969, the large-scale pyroclastic flows occurred and filled the upper reaches of Batang River, Blongkeng River and Putih River (Fig.2.5). As a result, a large-scale debris flows occurred in several rivers. A large amount of sediment flowed down to all the downstream area of the rivers, and a lot of unstable sediment was deposited. Debris flows by heavy rainfalls in the upstream of Putih, Bebeng and Krasak Rivers (Fig.2.5), have

destroyed 291 houses, 10 bridges, and 320 ha of agriculture fields. In November 1976, a large-scale debris flows also occurred and caused large damages in the villages along Putih, Bebeng and Krasak Rivers. Examples of damages by debris flows are shown in Photo 2.2.

(3) Countermeasures

To prevent or mitigate the volcanic sediment disasters, sediment control plans are formulated in combination of structural measures and non-structural measures. Structural measures are the measures to prevent volcanic sediment disasters, which are controlling sediment discharge by layout of sediment control facilities. Sediment control facilities are planned for efficiently controlling the excess of sediment, integrating the available sediment control methods and considering the characteristics of the rivers and basins in Mt. Merapi area. Structural measures programs, which have been implemented, based on the previous master plan and the review master plan (DGWR, 2001a). The previous master plan was established in 1980. The objectives of this plan were to prevent sediment flooding and sediment problems such as difficulty of irrigation water intake caused by sedimentation in river course. Following this master plan, sediment control facilities have been constructed on the slope of Mt. Merapi. By 2001, 192 facilities including 50 check dams, 101 consolidation dams and 12 km dykes were built. Sediment control facilities have been constructed for stabilizing the riverbed and keeping the security of residents by controlling the sediment discharge, as well as generating the economic development by the preparation of a stable social structure.

The relationship between debris flows disasters and the sediment control facilities in Mt. Merapi, which constructed following the master plan 1980 is shown in Figure 2.6. It showed that the debris flows tend to occur when the volcano became active. Although no disasters occurred since 1987, the debris flows have occurred more frequently in the recent years. The

debris flows were recorded 64 times since 1981 (DGWR, 2001b), but the disasters were only counted 2 times in the river courses. It indicated that the sabo facilities were effective to prevent the debris flows disasters.
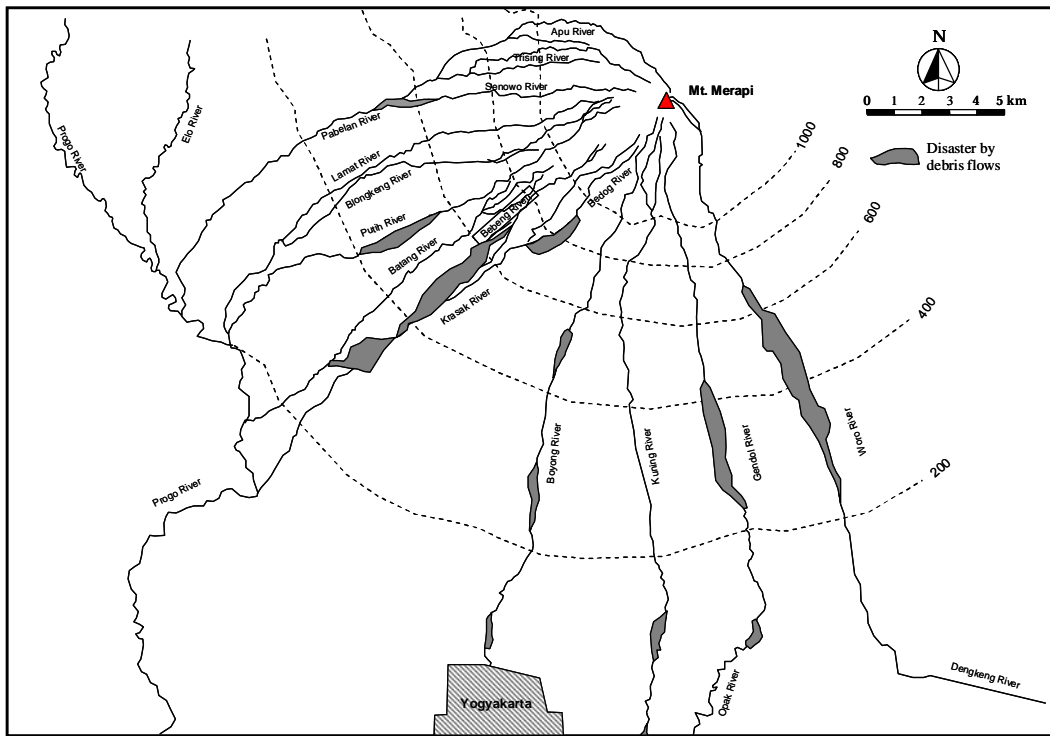
Fig. 2.5 Locations of debris flows disasters. (source:DGWR, 2001b)

(a)   (b)
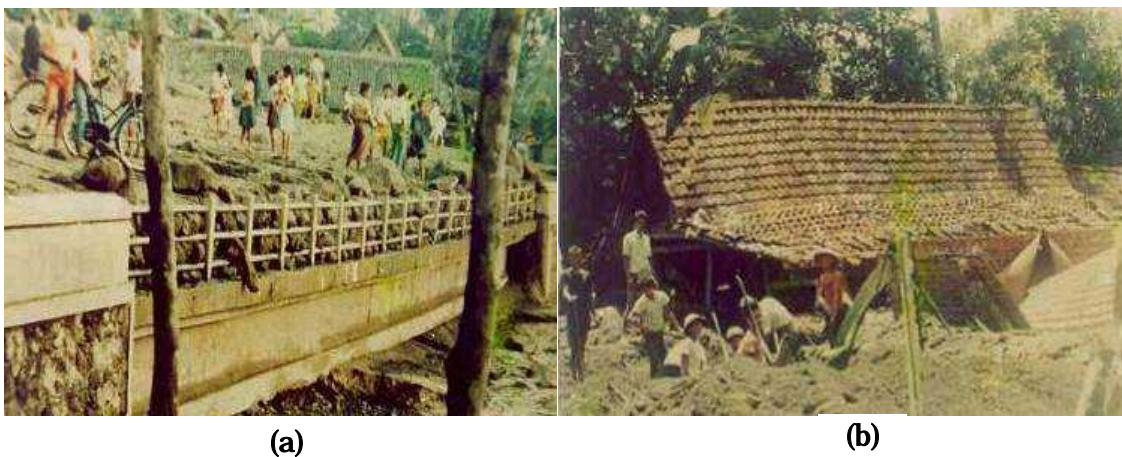
Photo 2.2 Debris flows buried a bridge (a) and houses (b).
(Photo courtesy Fatchan Nurrochmad)
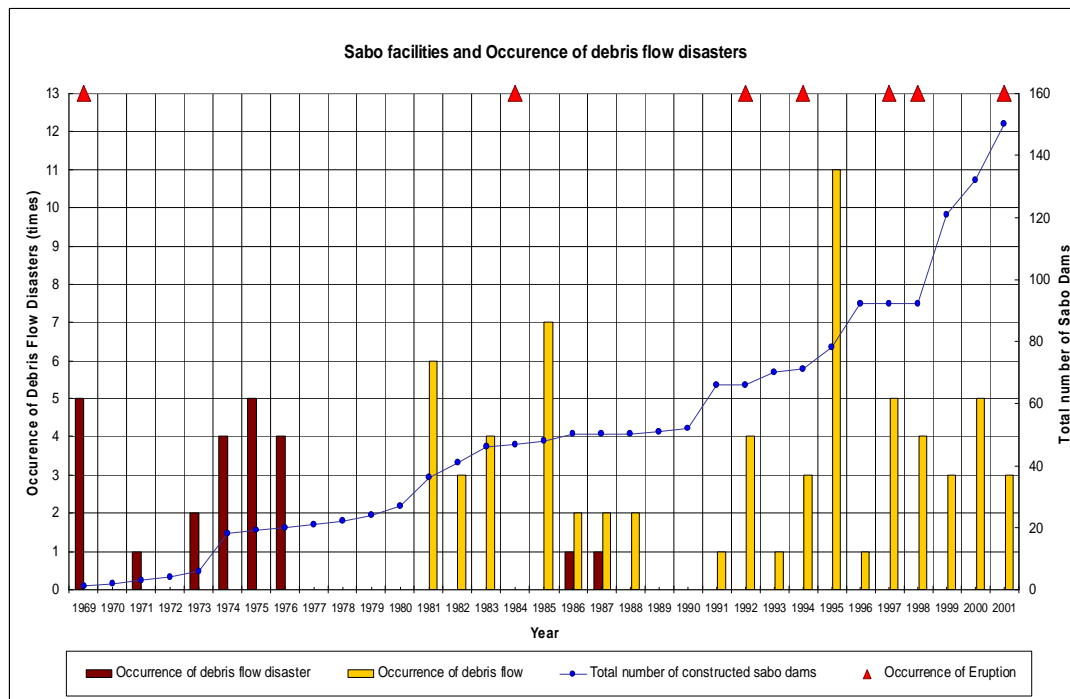
Fig. 2.6 Debris flows disasters and sediment control facilities in Mt. Merapi which constructed following the master plan 1980. (source: DGWR, 2001b).

However, other unexpected sediment problems have arisen. Discharged sediment from Merapi volcano caused the damages of irrigation facilities. The uncontrolled sand mining induced the collapse of sabo facilities as well as the riverbed degradation in Lower Progo River. To cope those unexpected sediment problems, the previous master plan was reviewed and the review master plan on Mt. Merapi was formulated in 2001 (DGWR, 2001a). The objective of the review master plan was a regional development through the disaster mitigation that consists of; 1) countermeasures of volcanic disaster mitigation, 2) riverbed stabilization, 3) sustainable sand mining management and 4) regional development through sediment disaster control.

Non-structural measures are defined as the measures for saving human lives and disaster mitigation by; 1) monitoring/forecasting of pyroclastic flows and debris flows, 2) warning to inhabitants about disasters,

3) adequate evacuation, 4) land use regulation including resettlement, and 5) information of disaster prevention. Non-structural measures programs against sediment disasters in Mt. Merapi area proposed by review master plan study on Mt. Merapi (DGWR, 2001a) are summarized in Table 2.2.

Table 2.2 Non-structural measures programs. (source: DGWR, 2001a)

| Program	Sub-program
1. Monitoring, Forecasting and Warning System for Debris Flows	1) Enhancement of Telemetering System for Observation of Rainfall and Debris Flows
	2) Renewal of Radar Rain Gauge System
	3) Establishment of Forecasting Method
	4) Capacity Building and Institutional Strengthening
2. Warning Communication System	1) Siren and Speaker Warning System
	2) Radio Communication System
	3) Capacity Building and Public Consultation
3. Evacuation System	1) Education to residents on Disaster Prevention and Evacuation
	2) Preparation of Evacuation Facilities
	3) Capacity Building, Public Consultation and Institutional Strengthening
4. Promotion of Resettlement of Residents in Disaster Prone Area	

2.2.3 Sand mining

(1) Present condition

Sand in Mt. Merapi originated from andesit lava rocklike type has a good quality and is popular as construction material. Due to the increasing of economy growth, the regional development stimulated the consumption of sand that caused the sand mining has extended rapidly. Another side, agriculture as a chief industry in the foothills of Mt. Merapi is presently generating low income due to the unfavorable conditions of agricultural economy. This condition also stimulated the sand mining to become an important income source of the rural. The sand mining persists not only in the foothills of Mt. Merapi but also in Progo River channel, especially in the lower reach.

The sand mining volume in the foothills of Mt. Merapi in 2000 was estimated about 6 million m³/year (DGWR, 2001a). The volume was increasing tremendously compared to annual volume of 3.2 million m³/year in 1997 and 5.2 million m³/year in 1998. The locations of sand mining quarry in the foothills of Mt. Merapi are shown in Figure 2.7. The distribution of sand mining volume by the rivers on the slopes of Mt. Merapi is shown in Figure 2.8. Quarry sites extending on Mt. Merapi slope were not only riverbed, but also private lands and riverbanks. Photo 2.3. shows the example of sand mining activity in the foothill of Mt. Merapi.
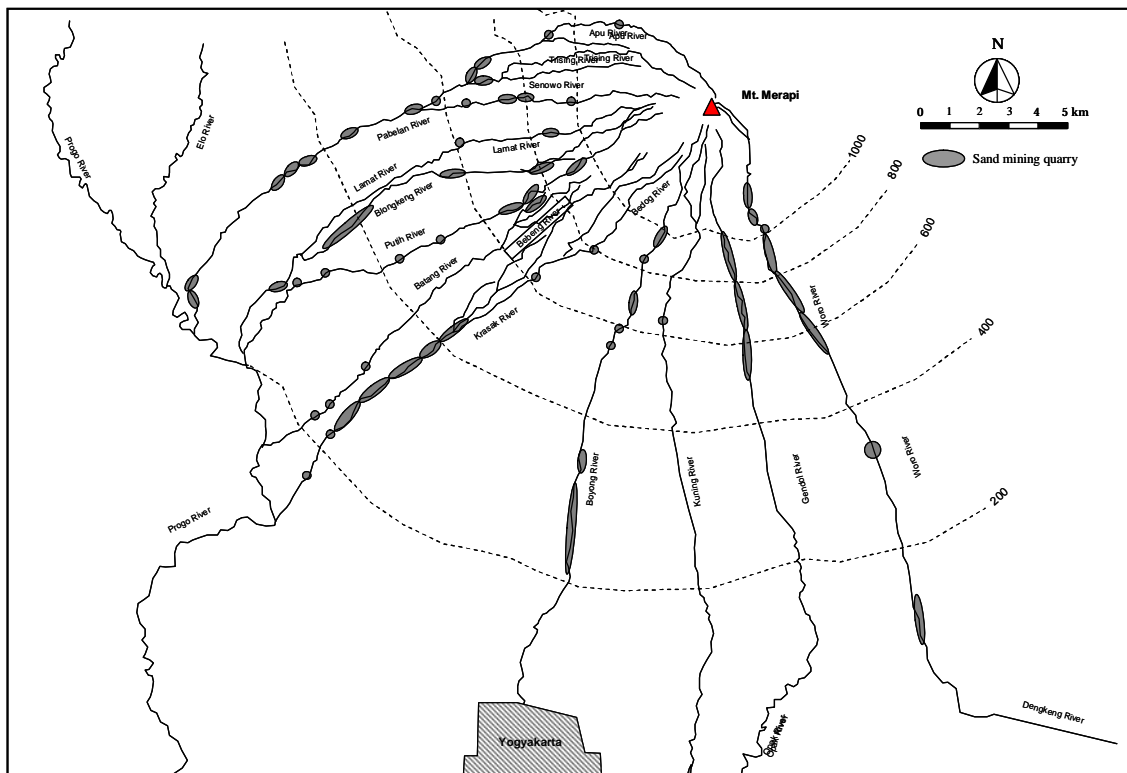
Fig. 2.7 Locations of sand mining quarry in the slopes of Mt. Merapi. (source:DGWR, 2001a)
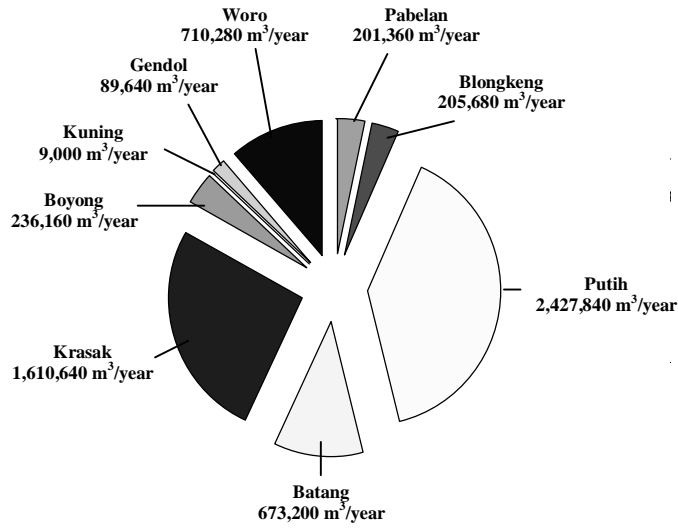
Fig.2.8 Distribution of sand mining volume by river on the slopes of Mt. Merapi. (source: DGWR, 2001a)

Photo 2.3 Sand mining activity in the foothill of Mt. Merapi.

In Progo River, the sand mining activities concentrated in the lower reach area. Figure 2.9 shows the locations of sand mining activity in the Lower Progo River. The annual sand mining volume in the Lower Progo River was estimated at about 2,933 m³/day or 1.07 million m³/year (Indra Karya, 1999). Photo 2.4 shows the example of sand mining activity in the Lower Progo River.
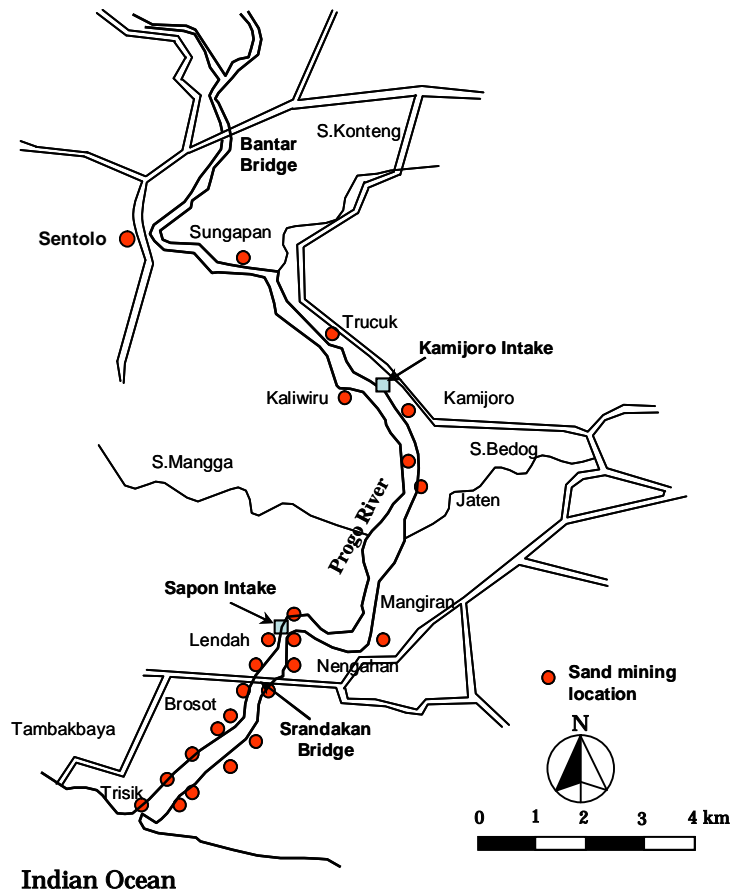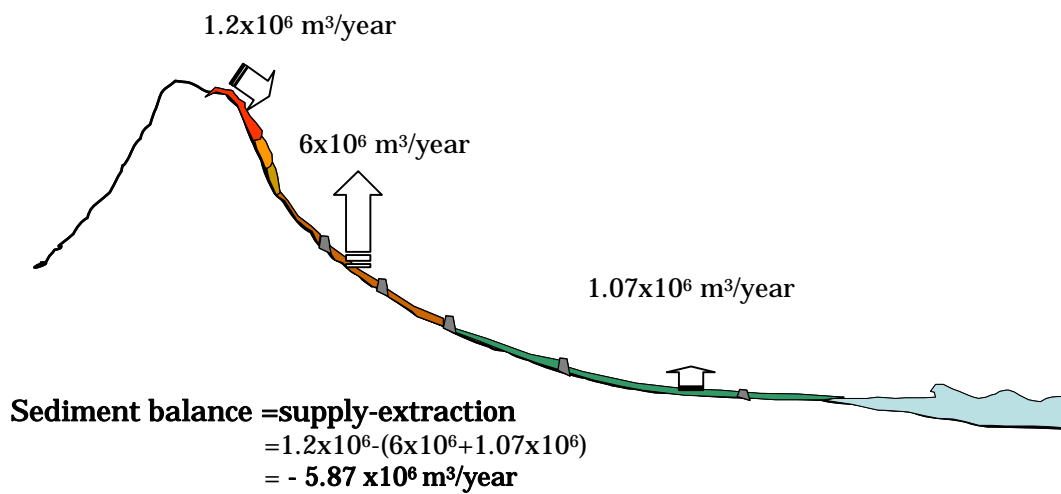

Fig.2.9 Locations of sand mining in Lower Progo River.

Photo 2.4 Sand mining activity in Lower Progo River

The sediment balance in present condition can be roughly estimated based on the lava production rate and the volume of sand mining in the Mt. Merapi area (in the foothill and in the Lower Progo River), as schematized in Figure 2.10. The lava production rate was estimated constant at 1.2 million m³/year (Siswowidjoyo *et al.*, 1995). The sand mining rate in the foothill of Mt. Merapi is assumed equal to the annual sand mining volume in 2000 (DGWR, 2001a), that is about 6 million m³/year. The mining rate in Lower Progo River is assumed equal to the annual sand mining volume in 1999 (Indra Karya,1999), that is about 1.07 million m³/year. Even though the volume of sediment transported to the sea is assumed equal to zero; the sediment balance shows a negative value (Fig.2.10). It means that the severe degradation exists in the Progo River channel due to the sand mining activities.

1.2x10^6 m^3/year

6x10^6 m^3/year

1.07x10^6 m^3/year

Sediment balance =supply-extraction
=1.2x10^6-(6x10^6+1.07x10^6)
= - 5.87 x10^6 m^3/year

Fig. 2.10 Sediment balance in the present condition.

The uncontrolled sand mining has caused the following serious problems;

– unstableness of existing river structures, such as sediment control facility, bridge and irrigation intake by digging nearby,

– increase in channel and riverbank instability,

– riverbed degradation in the downstream,

– artificial armoring due to selective mining,

– destruction of aquatic and riparian habitat,

– environmental issues, such as noise and dust by day and night mining, and damage to the rural roads by overload of trucks

Those problems have been increasing the susceptibility in the downstream and deteriorating the watershed. One of the critical issues of uncontrolled sand mining is the riverbed degradation, which will be more described in sub-section 2.2.4.

(2) Experiment on sediment mining

To get a better understanding of the influence of sand mining on the riverbed variation, an experiment on transformation process of mining pit in a channel is conducted. The complex phenomena in the river are simplified in a laboratory by simplifying the involved parameters such as the utilization of constant or adjustable discharge and uniform channel cross section. To investigate the influence of the sand mining on the riverbed variation, the initial channel bed elevation is flat and six sand mining pits with the simple geometry are created in the middle of the mobile bed.

The flume is filled with the sediment with a thickness of 11.5 cm and it is leveled to keep all the sediment in the same level. Grain size distribution of the sediment mixtures is shown in Figure 2.11. To simplify the form of sand mining pit in the middle of the flume, the simple geometry with a height of H and a length of L is adopted (Fig.2.12). Six different pit geometries are chosen in the experiment. The water discharge is increased gradually to the predefined discharge, Q, and the discharge is maintained. The hydraulic parameters used in this study are summarized in Table 2.3. A thin metal protective sheet is placed on the sediment bed in the upstream and downstream of the mining pit to maintain the initial condition. By paying attention not to disturb the mobile bed, the flume is slowly filled with water until the water level touched the crest of the weir.

The experiment start at t = 0, when the protection sheet is rapidly pulled out of the flume. The formation of the channel is recorded from the beginning to the end of the experiment. After a certain time interval, the flow is stopped to measure the bed elevation, following by reproducing the same discharge. Further bed level measurements are carried out after a certain time interval. The results of the experiment are shown in Figure 2.13.
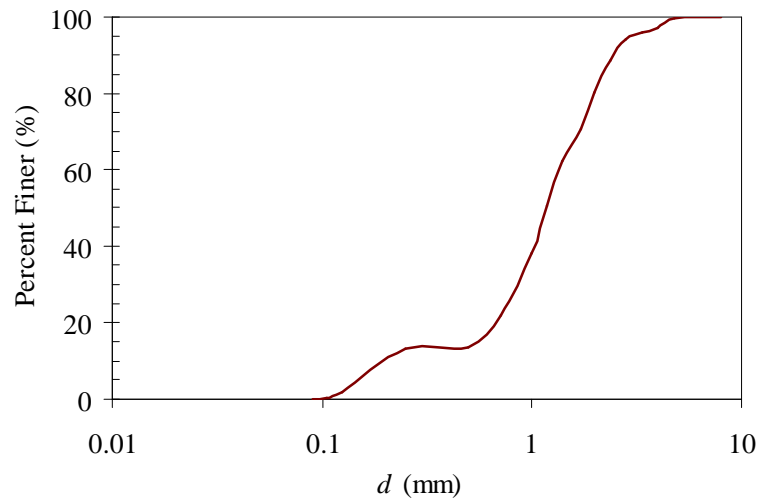
Fig.2.11 Grain size distribution used in the present experiment
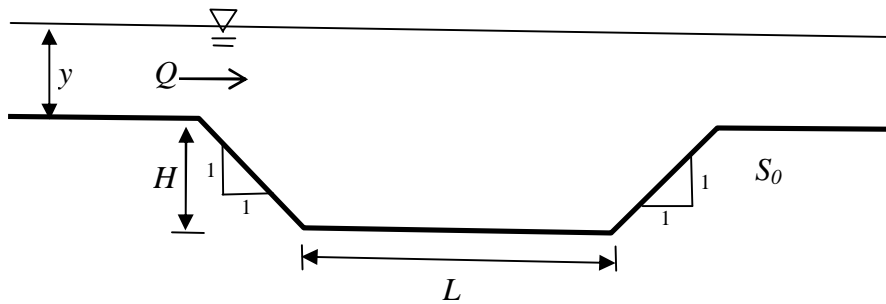
Fig.2.12 Sketch of the mining pit.

Table 2.3 Hydraulic parameters used in the present experiment

Run	Q (m³/s)	Slope, S_o (-)	H (m)	L (m)	H/L
Run SM01	0.0136	0.005	0.05	0.5	0.1
Run SM02	0.0136	0.005	0.05	1.0	0.05
Run SM03	0.0136	0.005	0.05	1.5	0.033
Run SM04	0.0136	0.005	0.025	0.5	0.05
Run SM05	0.0136	0.005	0.025	1.0	0.025
Run SM06	0.0136	0.005	0.025	1.5	0.07

The results show that the sediments are transported into the mining pit and the degradation occurs in the downstream of the mining pit. A mining pit locally increases flow depth. When water flows over the mining pit, the separation occurs and eddy rollers are developed, causing local erosion. The sediment arrived from upstream pit is trapped in the pit that causes the upstream end of the pit migrates to downstream. At the downstream end of the pit, stream flow moves beyond the pit and another separation zone is formed. The flow energies increase and the sediment carrying capacity of the flow is more than the amount of transported sediment. This flow erodes the bed downstream, causing bed degradation. The instream sediment mining causes the degradation upstream and downstream of mining pit. The bed degradation process produced by instream sediment mining is schematized in Figure 2.14.

2.2.4 Riverbed variation

In the Lower Progo River, the riverbed is very unstable depending on the supply of sediment from Mt. Merapi. It is difficult to predict the future natural river behaviour because it depends on the frequency and severity of the eruptions of Mt. Merapi. The other factor that gave influence on the riverbed fluctuation in the Lower Progo River was the construction of sabo facilities in the upper reach during last two decades (Sumaryono *et al.*, 1996). Before the completion of the sabo facilities, the riverbed elevation had increased rapidly and it caused some irrigation intake structures function ineffectively. After the sediment control facilities had been constructed, the sediment discharge from the tributaries to Progo River was decreased and caused the riverbed degradation in the Lower Progo River. Beside, the active instream sand mining that has been practiced nowadays also stimulated the bed degradation as mention in sub-section 2.2.3.
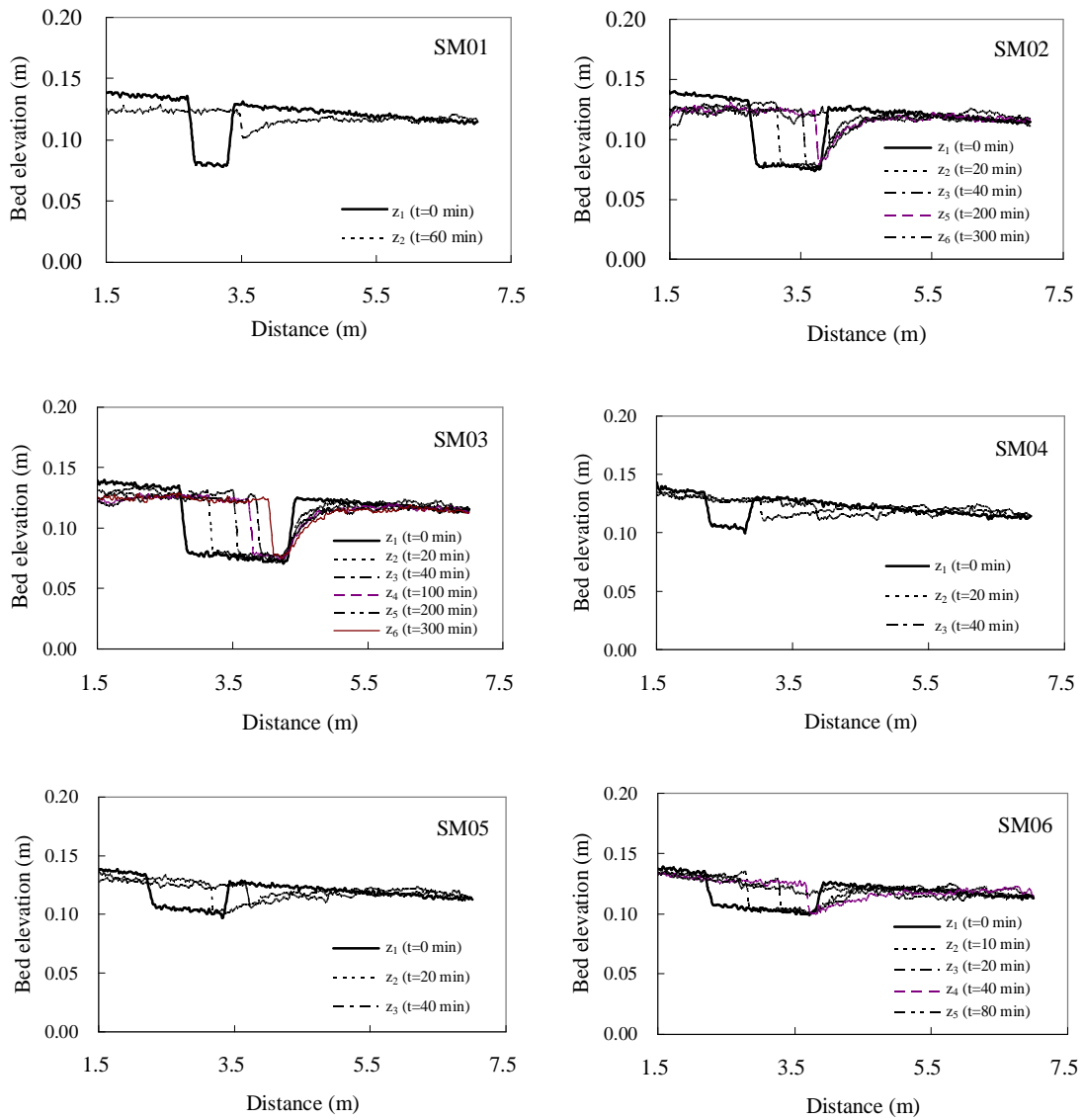
Fig.2.13 Experiment results on the mining pit migration
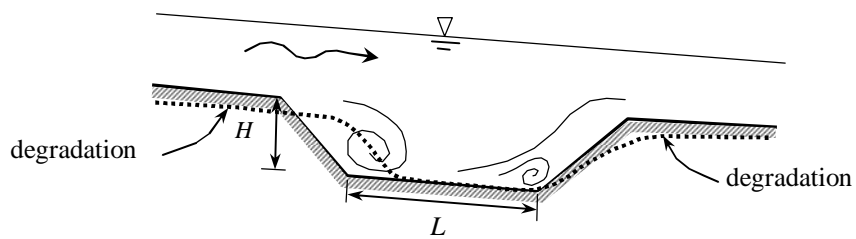
Fig.2.14 Bed degradation produced by instream sediment mining

The sediment balance studies in the Lower Progo River have been recently reported. Study of Progo River Basin in 1971 (DGWR, 1971) reported the riverbed fluctuation surveys for the section of the river close to Kamijoro irrigation intake, Srandakan and Sentolo (shown in Figure 2.9). The survey result showed that the average riverbed level at the Kamijoro irrigation intake has risen by 1.25 m during the period 1961-1970. The survey result at Srandakan and Sentolo indicated the riverbed aggradation by about 0.30 m at Srandakan and 0.45 m at Sentolo during twelve months from March 1970 to March 1971. Study of review master plan on Mt. Merapi (DGWR, 2001a) reported the roughly estimation of the riverbed degradation until 2000 at the major structures in the Lower Progo River. The riverbed levels at the existing structures between in 2000 and in the construction year are compared as shown in Table 2.4. The estimation results showed the characteristics of the riverbed fluctuation. The long-term fluctuation from 1920s to 2000 showed the riverbed aggradation and degradation in Srandakan Bridge and Kamijoro Intake. Since 1970, the riverbed degradation was obviously estimated at 10-30 cm/year. The riverbed in 1970 was one of the highest elevations.

Suwartha (2002) analyzed the bed load sediment transport under two flow conditions; the peak flow (Q_5, 5 years return period) and the low flow (daily discharge) at several control points, namely Pabelan confluence, Kalibawang, Bantar, Sapon, Srandakan Bridge and Progo river mouth (see Fig.2.1). Analysis has been done by using MPM (Meyer-Peter and Muller), Frijlink and Einstein formula. Based on the analysis result of the peak flow, the maximum erosion per day occurred between Sapon and Srandakan, meanwhile the maximum sedimentation occurred between Srandakan and Progo river mouth. From the low flow analysis result, the maximum erosion per day occurred at Bantar-Sapon reach and the maximum sedimentation occurred at Kalibawang-Bantar reach. Based on the shape of average cross

section river, Suwartha (2002) found that the river degradation depth in Bantar-Sapon reach was about 0.48 m/year.

Maulani (2003) analyzed the sediment balance of Progo River reach from Kebonagung Bridge up to the river mouth by using an empirical equation of sediment transport. The cross section data measured in 1996 and 2000 were used for calculation. The analysis result showed that all of the existing structures have been degradated. The degradation of Kebonagung Bridge was 101 cm/year, Bantar Bridge was 20 cm/year, Kamijoro free intake was 0.91 cm/year, Sapon free intake was 57 cm/year, and Srandakan Bridge was 33 cm/year.

Table 2.4 Riverbed fluctuation at the existing structure (source: DGWR, 2001a)

Existing Structure	Riverbed level in 2000		Previous Riverbed Level		Difference		Annual Mean Fluctuation (cm/year)
	Lowest (EL.m)	Average (EL.m)	Observation Year	Average (EL.m)	Period (years)	Average (cm)	
Srandakan Bridge	-0.295	6.00	1929	11.25	71	-525	-7.39 (1929-2000)
Kamijoro Intake	20.570	23.20	1924	22.18	76	+102	+1.34 (1924-2000)
			1930	21.68	70	+152	+2.17 (1930-2000)
					6	-50	-8.33 (1924-1930)
			1970	26.13	30	-293	-9.77 (1970-2000)
					40	+445	+11.1 (1930-1970)
Bantar Road Bridge	34.650	36.30	1984	40.93	16	-463	-28.9 (1984-2000)
Kebonagung Bridge and groundsill	51.880	52.00	1982	57.60	18	-560	-31.1 (1982-2000)

Those studies on sediment balance in Progo River clearly indicated that the riverbed degradation occurred significantly in the Lower Progo River. In recent years, the riverbed degradation caused the unstableness of three bridges located along the main river course and the difficulties of irrigation operation on two intake structures. The locations of those river structures are shown in Figure 2.1 and the conditions of each structures are described as follows:

1) Kebonagung Bridge

It was constructed in 1986 with groundsill. The bridge span is 153.60 m and the width is 7 m. A gabion groundsill has been previously constructed to protect the pier structures failure caused by riverbed degradation. However, the most parts of the groundsill have been destroyed by the tractional load during floods. In 1996 a new groundsill was constructed with stone masonry, but the flood occurred in 1999 have destroyed some parts of the structures. Photo 2.5(a) shows the damages of the groundsill downstream of the Kebonagung Bridge (Photo taken in November 2006).

2) Bantar Bridge

Bantar bridges consist of a road, a railway and an oil pipeline. The old road bridge was constructed in 1926-1930, and the new bridge was constructed in the downstream of the old bridge in 1987-1988. Both the bridges have 210 m in length span and 7.0 m in width. Against serious riverbed degradation, a foundation protection by steel sheet pile was installed in 1988 for the abutments and the piers. At present, the riverbed degradation in Bantar bridges was observed more than 2.0 m (DGWR, 2001a) (Photo 2.5(b) taken in November 2006).

3) Srandakan Bridge

Srandakan Bridge was constructed in 1878-1880 as a railway bridge to serve a sugarcane factory, and in 1975-1985, it was modified to a road bridge with 7.0 m in width to accommodate the increase of traffic numbers. The bridge span is 531 m with 33 bridge piers. In 1997 to 1999 a gabion mattress was placed to protect the piers. In April 2000, the piers No.25 and No. 26 were settled down and it caused the bridge floor collapse (Photo.2.5(c)). The bridge collapsed due to heavy local scouring around the foot of the bridge piers. The scouring occurred because of the lack of the sediment supply from upstream and the intensive sand mining near the

bridge piers by local peoples. In 2003-2004, a groundsill was constructed in the downstream of the bridge to stabilize the riverbed and the new bridge was constructed in the downstream of the old bridge in 2005-2006.

4) Kamijoro Irrigation Intake

It was constructed in 1924 to irrigate the area of about 2,074 ha. The sedimentation problem in irrigation tunnel has always occurred. During dry seasons, the intake has no function due to the insufficient water level that caused by riverbed degradation.

5) Sapon Irrigation Intake

The first intake was constructed in 1914 to irrigate the area of about 1,917 ha of paddy field. Because of the riverbed aggradations since 1967, temporary training works have been renewed annually to maintain adequate water supply. In 1979 to 1984, the new intake (the second intake) was constructed for the irrigation area of 2,279 ha. This second intake has no function at present because of the serious riverbed degradation in the river course. In 1997, some free intake channel facilities were constructed about 500 m upstream from the second intake as temporary countermeasures to assure the irrigation water supply. Photo.2.5(d) shows the lowering water table at the Sapon irrigation intake (the second intake).

Without countermeasures, the riverbed degradation in the Lower Progo River will continuously increase and threatening the existing social infrastructures. The instability of bridges and the ineffective function of intakes due to the riverbed degradation induced serious negative impacts on the regional development. To overcome the issues associated with the riverbed degradation, the riverbed stabilization countermeasures are required including structural and non-structural countermeasures. The structural countermeasure is the construction of groundsills at 5 locations:

Kebonagung Bridge, Bantar Bridge, Srandakan Bridge, Kamijoro Intake and Sapon Intake, where there are important public infra-structures for the regional society and economy (DGWR, 2001a). The non-structural countermeasure is sediment mining management in the upstream area and along the Progo River. That measure will contribute for controlling the sediment discharge.


(a)

(b)

(c)

(d)

Photo 2.5 Damages of river structures in Progo River caused by bed degradation; (a) unstableness of Kebonagung bridge piers and damages of the groundsill downstream of the bridge, (b) unstableness of Bantar bridge, (c) collapse of the Srandakan bridge floor, and (d) lowering water table causes difficulties of irrigation operation at Sapon intake. (Photo (a), (b) and (d) courtesy Masaharu Fujita, 2006)

2.2.5 River mouth closure

Progo River is one of the big four rivers that drain to Indian Ocean at the South coast of Yogyakarta. Location of Progo river mouth is shown in Figure 2.15. The south coast of Java is dominated by wave action from the Indian Ocean, and receives a relatively gentle south-westerly swell of distant origin and stronger locally generated south-easterly waves that move shore sediments and deflect river outlets westwards, especially in the dry season (Bird & Ongkosongo, 1980). These processes are responsible for the opening and closing of the river mouths. In front of the river mouths, the accumulation of sediment has formed sand-bar that closes the river mouth (Photo 2.6). The closure mechanisms of the river mouth are described as follows.
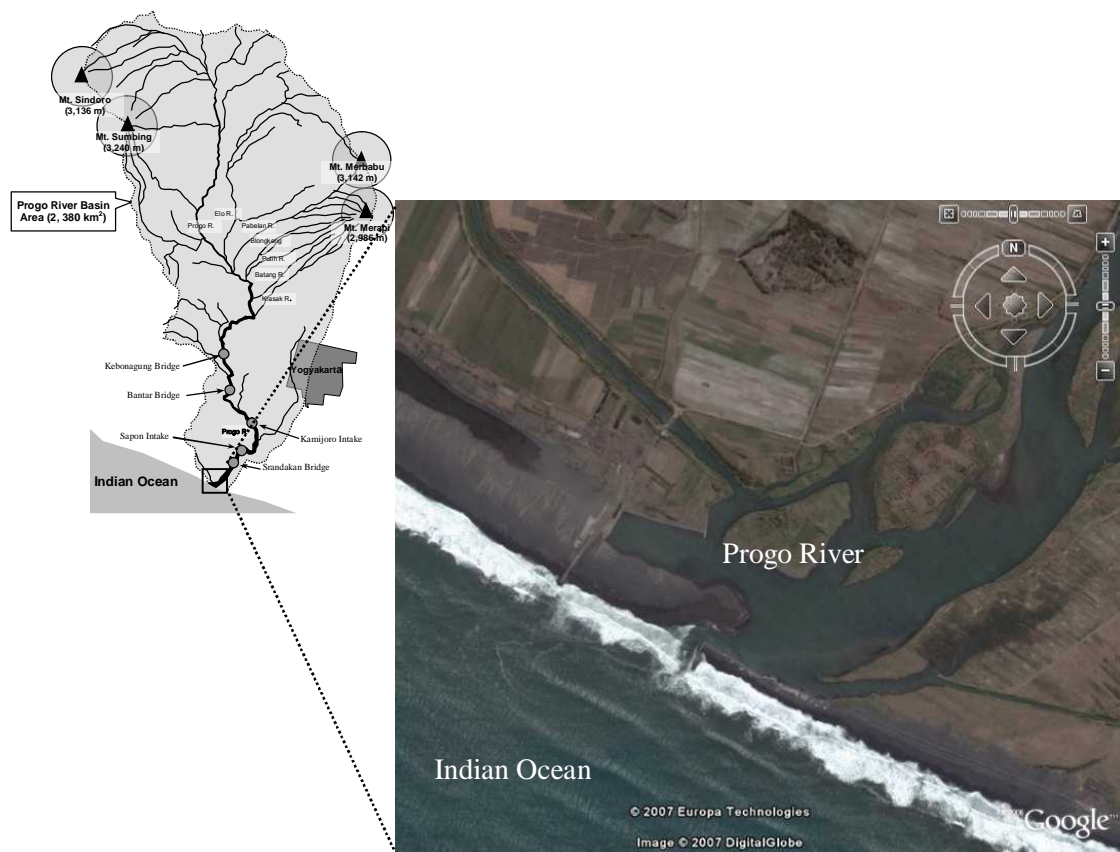
Fig.2.15 Location map of Progo river mouth (from Google Earth)

41
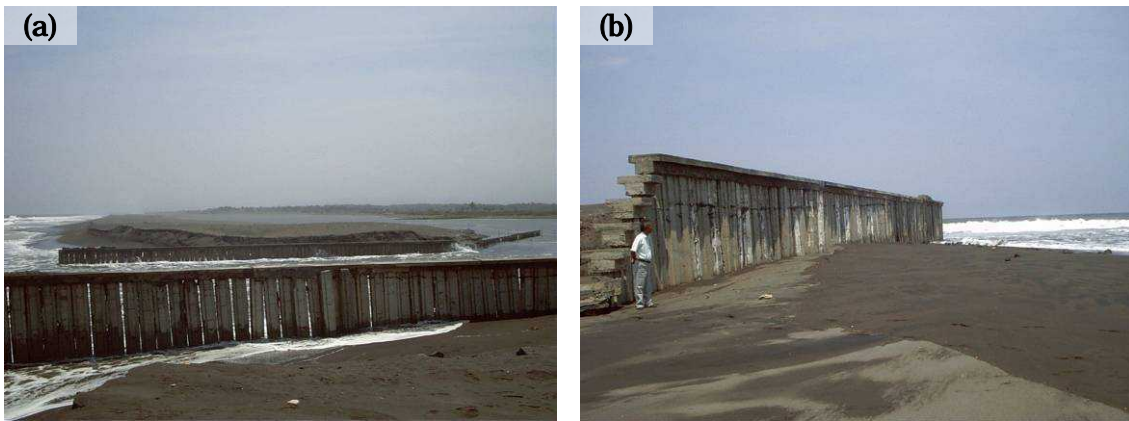
Photo 2.6 (a) Short jetty installed in the sand-bar, (b) Sedimentation at the river mouth due to littoral drift blocking up the river mouth.

During the wet season, the river mouth is opened and the river discharges a large volume of sediment into the sea, which deposits near the river mouth and forms sandbanks. These bank acts as submerged natural groins which interrupt the littoral drift. During this season, wave is predominantly from west to east, associated with a long period swell from the south-west quadrant. Waves converge towards the bank assisting its growth. However, not all of the littoral drift is trapped on the sandbanks and the sediment transport takes place in an easterly direction during the wet season. The intensity of the river flow during this season is far superior to the intensity of the littoral drift. As a result, the position of the river mouth remains fixed, controlled by the river flow.

Towards the end of the wet season, the intensity of the river discharge is reduced and it can no longer control the sediment processes taking place at the river mouth. The sandbank reduces in size and height due to wave action, and tends to shift slightly east relative to the centreline of the mouth. When the sandbank is in this position, swell waves refract around the eastern side of the bank and associated with local sea waves. During this season, the local sea waves changed to the south-east quadrant. The

combination of both waves erodes a wedge at the east bank of the river mouth initiating the process of mouth closure.

During the dry season, the local south-east wind waves take the major role as the driving force behind sediment transport at the South Java Coast, which shifted towards a more easterly direction. In spite of lower magnitude than the south-west swell waves, they reach the shoreline at a much sharper angle and cause the littoral drift to change the direction towards the west. The river mouth proceeds to shift towards the west, unimpeded by the presence of the sandbank and strong river flows. Ultimately, the river mouth may completely close.

In existing circumstances, in the beginning of rainy season, the river flow will be blocking up at the river mouth and it causes overflowing and inundation at the surrounding area (Isnugroho, 2003). The flood in Progo River on November 2000 caused inundation of paddy field covering 13 villages at Kulon Progo District with total area of 1,041 ha including residential areas of 700 ha (DGWR, 2001a).

The river mouth improvement is designed to prevent the rise of water in the river mouth by maintaining all year round communication with the sea. The existing improvement was based on the recommendation of project report of South Java Flood Control Sector Project (DGRD, 2000). The improvement works were constructed to fix the position of the river mouth and prevent it from migrating to the west, where it was more vulnerable to closure. In the dry season the river entrance was fixed further east in the deeper part of the channel, and a short jetty system was provided to converge the dry season flow towards the new mouth, thus increasing the flow velocity through it.

The non-structural countermeasure of river mouth closure that has to be done is a long term monitoring of the coastal zone. The main purpose of this monitoring is to identify any problems that may occur at the earliest possible stage. The monitoring activities consist of: 1) planning activity with

consideration of the long-term beach evolution processes, 2) monitoring the performance of the coastal and river mouth structures, as well as their impacts on the adjacent coastline.

2.3 Environmental and Management Issues

2.3.1 Impacts on ecosystem

(1) Influence of sabo facilities

Sediment control (Sabo) technology has been developed in Indonesia since 1970's. It was obviously developed since technical cooperation on Sabo technology between Indonesian Government and Japanese Government was established. For preventing sediment disasters, sabo technology was introduced in this volcanic area, which has a great deal of discharged sediment and it has given advantages to the people who live in disaster prone area. However, a careful consideration should be paid for attention when the close type of sabo dam is used. Most of sediment will be trapped by sabo dams and the discharged sediment cannot reach the downstream or the main rivers, where the riverbed degradation is observed because of present prosperous sand mining activities.

Thus, to mitigate the present riverbed degradation in the Lower Progo River, the sediment should be positively flowed down, and harmless sediment discharge should be promoted. A large amount of sediment discharge by debris flows has to be captured in the upstream and should be gradually flowed down by consequent middle and small floods. In those rivers, it is necessary to select the dam type such that harmless sediment can flow down in a small or middle flood, and large sediment discharges in debris flows can be captured in the dams. Therefore, permeable check dams such as open type check dams should be installed on those rivers.

44

Sediment control structure for stabilizing the riverbed such as groundsill may have an impact on ecosystem; fish migrations can be stopped or delayed. Fish in the downstream has difficulty to rise up to the upstream because the channel was blocked by the groundsill. Photo 2.7(a) shows the groundsills that have been installed in the Progo River are not equipped with a fish way. It is shown that some fishes have difficulty to migrate to the upstream and caught in the net installed at the groundsill (Photo 2.7(b)).
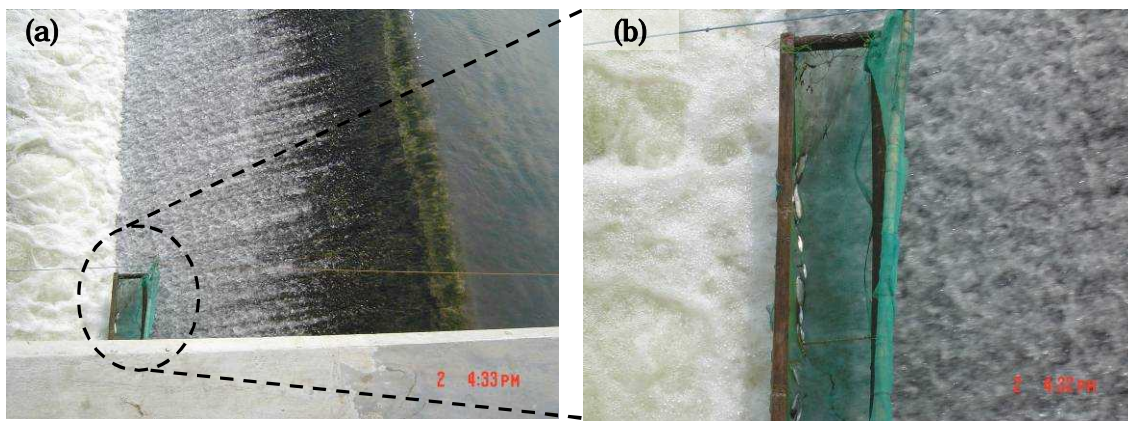
Photo 2.7 Effect of groundsill on fish migration in the downstream of Progo River below the Srandakan bridge. (Photo courtesy Masaharu Fujita)

(2) Influence of sand mining

Uncontrolled sand mining in Mt. Merapi area and Progo River that lead to the removal of channel substrate, resuspension of streambed sediment, clearance of vegetation, and stockpiling on the streambed, will have ecological impacts. These impacts may have an effect on the direct loss of stream reserve habitat, disturbances of species attached to streambed deposits, reduced light penetration, reduced primary production, and reduced feeding opportunities.

In the downstream of sand mining sites, the dynamic system has less fine-grained load and the stream compensates by armoring and riverbed degradation. Photo 2.8 shows the armoring of bed material at the midstream of Progo River due to the sand mining in the foothill of

Mt. Merapi. This situation can adversely affect the aquatic habitats used by various species and their respective life stages. The impacts of sand mining not only dictate the scale and severity of adverse effects on the channel geometry and habitat, but also control the time-scale of recovery following or between disturbances. Streams that are repeatedly harvested at rates in excess of sediment influx undergo channel degradation, possibly causing incision of an entire stream system including its tributaries.

Photo 2.8 Armoring at the midstream of Progo River due to sand mining in the foothill of Mt. Merapi: (a) upstream of Mataram Irrigation Intake, (b) downstream of Mataram Irrigation Intake. (Photo courtesy Masaharu Fujita)

2.3.2 Sustainable sand mining management

Merapi volcano is very active and has been producing much sediments to the downstream. As shown in Figure 2.3, average annual sediment discharge estimated from the cumulative volume of lavas from Merapi volcano was 1.2 million m³/year (Siswowidjoyo *et al.*, 1995). In Merapi volcanic area, other sediment source comes from the non-active basin. The ratio of the sediment discharge from non-active basin was estimated at 20% in the report on the sediment discharge of volcanic active basin (DGWR, 2001b), therefore, the sediment discharge is equal to 0.24 million m³/year. Thus, the average annual total sediment production rate from Merapi Volcano (volcanic active basin) and non-active basin is 1.44 million m³/year.

The cumulative sediment volume from Merapi Volcano from 1900 to 1992 is shown again in Figure 2.16 and the cumulative sediment volume from non-active basin is also plotted in this figure. Using the data on these two kinds of sediment production, the cumulative sediment volume from Merapi Volcano and non-active basin is plotted as shown in Figure 2.16.

In order to reduce the impact of excess sediment discharge in the river system, the excess sediment is necessary to be controlled by sediment control facilities and/or sand mining. To study the necessity of sand mining to control the excess sediment, three cases of sand mining option will be discussed as follows.

1) Case 1: the sand mining rate is assumed equal to the sediment production rate from Merapi Volcano and non-active basin.
2) Case 2: the sand mining rate is assumed equal to the annual sand mining rate in foothill of Mt. Merapi in 1998 at about 5 million m^3/year (DGWR, 2001a).
3) Case 3: no sand mining.

In the Case 1, three condition exist in the river system, i.e. equilibrium condition (E), aggradation condition (A), and degradation condition (D) as shown in Figure 2.17. Circles denote the equilibrium condition. When the cumulative volume of sand mining is equal to the cumulative volume of produced sediments, the equilibrium condition is reached. Aggradation occurs when the cumulative volume of sediments is larger than the cumulative of average sediment volume. In contrary, degradation occurs when the cumulative volume of sediments is smaller than the cumulative of average sediment volume. Fig. 2.17 shows that the aggradation alternates with the degradation in the river system. The degradation occurred during period of 1900 to 1933, 1947 to 1961, 1965 to 1968 and 1977 to 1992. Meanwhile, the aggradation occurred during period of 1933 to 1947, 1961 to 1965, and 1968 to 1977.
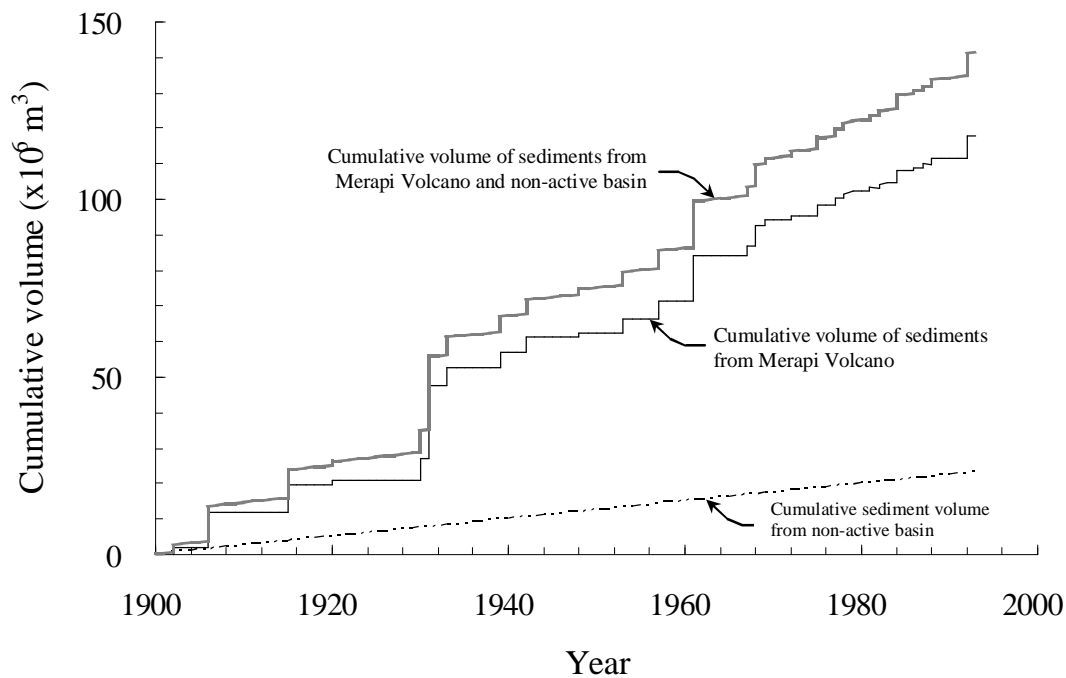
Fig. 2.16 Cumulative volume of sediments from Merapi Volcano from 1900 to 1992, cumulative sediment volume from non-active basin, and cumulative volume of sediments from Merapi Volcano and non-active basin.

The riverbed variation, in the case of sand mining rate equal to the sediment production rate, is shown in Figure 2.18. The riverbed variation depends on occurrence and severity of the eruption of Mt. Merapi. A large eruption can change the riverbed suddenly. However, no sufficient sediment production from the eruption causes the riverbed degradation. Sediment production from the eruption of Mt. Merapi can recover the riverbed from the degradation condition to the equilibrium condition. In order to keep the riverbed in an appropriate level for water utilization and river ecosystem, the allowable deposition depth and allowable erosion depth are necessary to be determined. If the erosion depth in river system is less or equal to the allowable erosion depth, the riverbed elevation is acceptable. However, if the erosion depth is larger than allowable erosion depth, the sand mining rate is necessary to be reduced or sediment control work such as groundsill is

48

necessary to be installed in the downstream of the erosion part. Otherwise, in the case of aggradation, if the deposition depth is larger than allowable deposition depth, the sand mining rate is necessary to be increased or the sediment control work such as a sand pocket is necessary to be installed in the upstream part.

In the Case 2, which the sand mining rate is assumed equal to the annual sand mining rate in the foothill of Mt. Merapi in 1998 (5 millions m³/year), which almost 4 times of sediment production rate, only the degradation condition exists in the river system as shown in Figure 2.19. Severe bed degradation occurred in the riverbed due to the excessive sand mining (Fig. 2.20). Such kind of condition is not appropriate for the water utilization and river conservation. Therefore, sand mining should be regulated strictly.

In the Case 3, which no sand mining, only the aggradation condition exists in the river system as shown in Figure 2.21. Deposition of sediment causes the severe aggradation in the riverbed (Fig. 2.22). It shows that the sand mining can be an effective method to control the excess sediment if the sand mining activities are properly managed.

Both of aggradation and degradation give impacts to the riverbed condition quantitatively and qualitatively, including bed level change and grain size distribution change as well as porosity change. Those effects can be evaluated by using a bed variation model, which considers the change of grain size distribution as well as porosity. This evaluation will be more discussed in Chapter 3, 4 and 5.
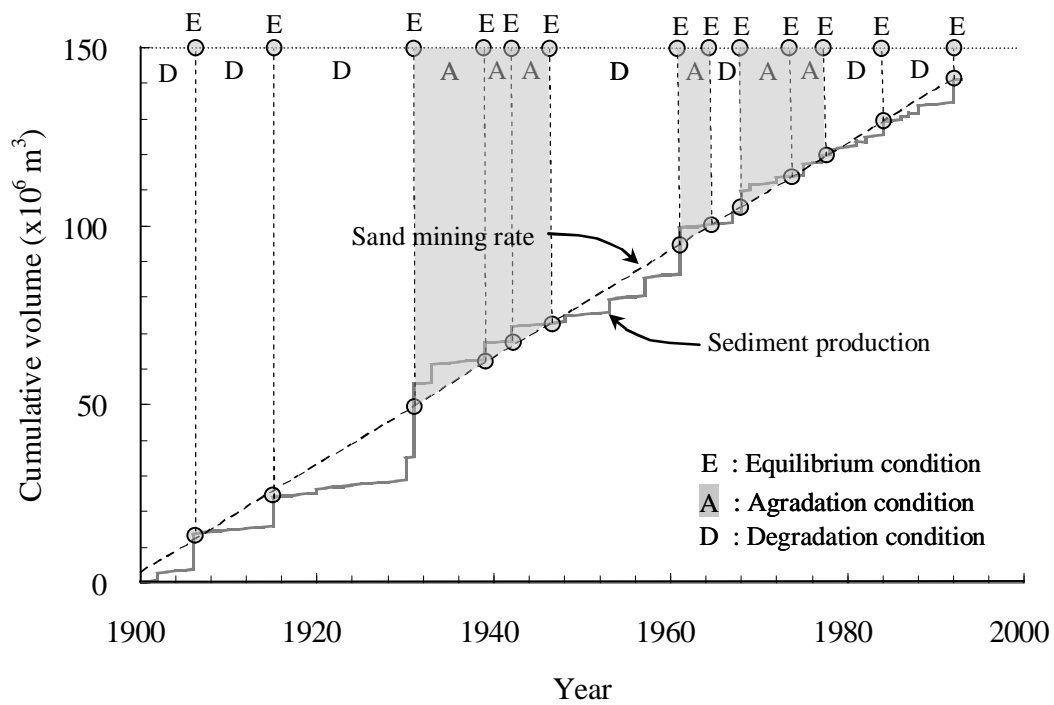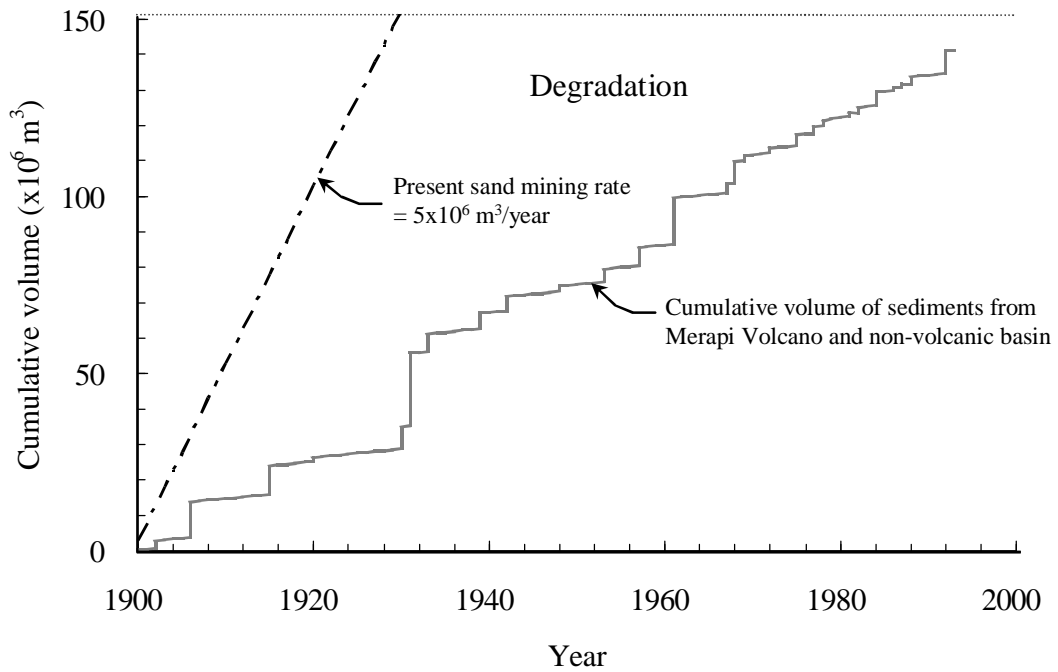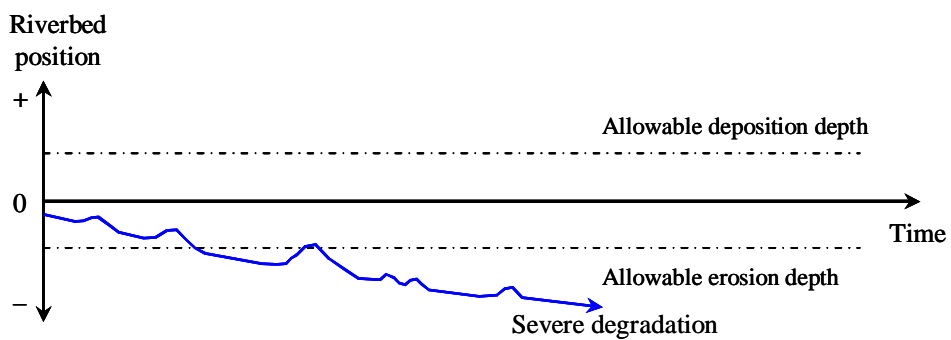
Fig.2.17 Degradation and aggradation condition of the streams in the downstream of Merapi Volcano, in case of sand mining rate equal to sediment production rate from Merapi Volcano and non-volcanic basin (**Case 1**).
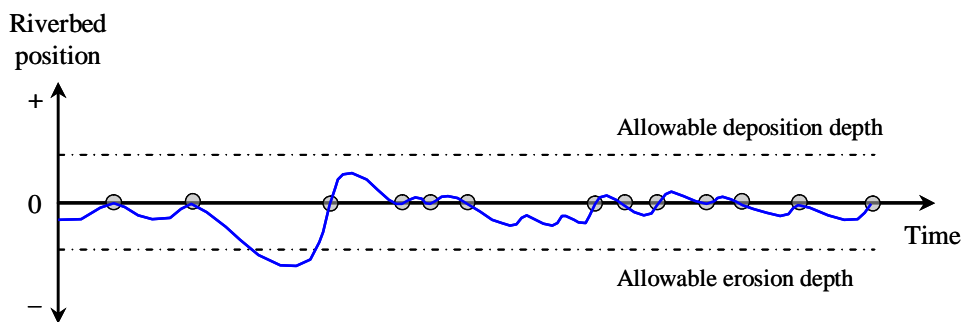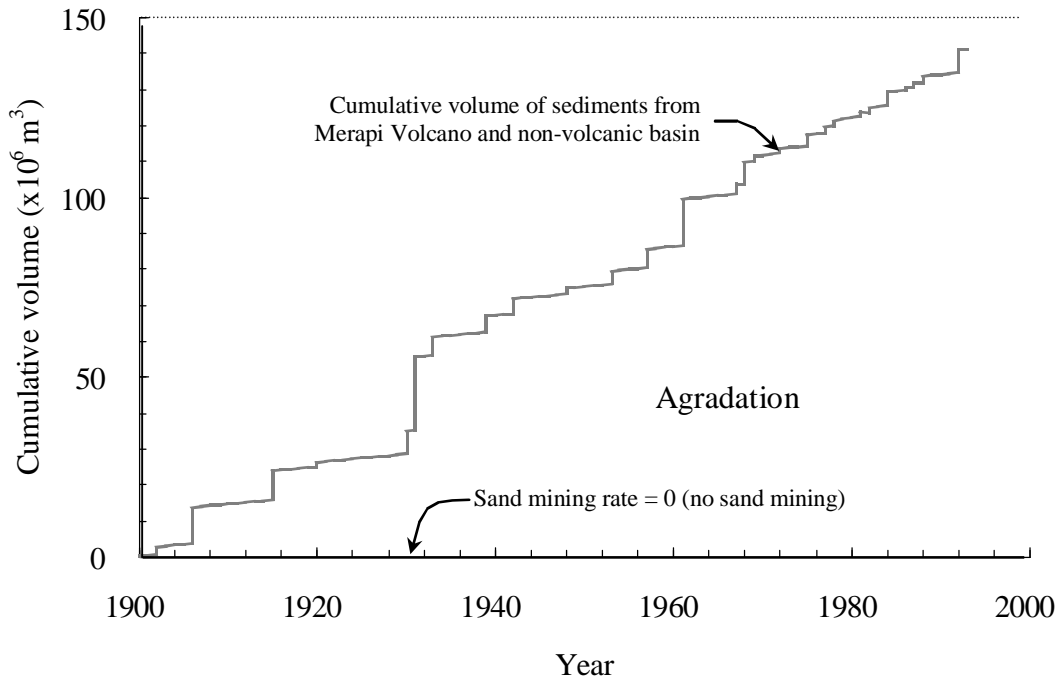

Fig.2.18 Schematic diagram of riverbed variation, in case of sand mining rate equal to the sediment production rate from Merapi Volcano and non-volcanic basin (**Case 1**).

Fig.2.19 Degradation condition of the streams in the downstream of Merapi Volcano, in case of sand mining rate equal to the present sand mining rate = 5×10^6 m³/year (**Case 2**).

Fig.2.20 Schematic diagram of riverbed variation, in case of sand mining rate equal to the present sand mining rate = 5×10^6 m³/year (**Case 2**).

Fig.2.21 Aggradation condition of the streams in the downstream of Merapi Volcano, in case of sand mining rate equal to zero (no sand mining) (**Case 3**).
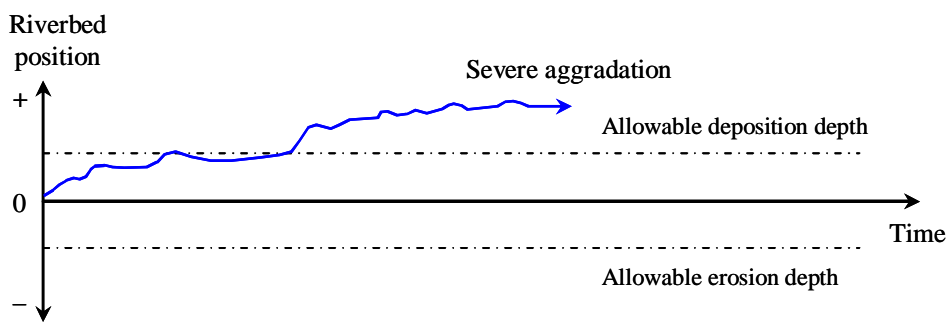
Fig.2.22 Schematic diagram of riverbed variation, in case of sand mining rate equal to zero (no sand mining) (**Case 3**).

As mentioned in sub-section 2.2.3, uncontrolled sand mining caused serious problems in the watershed. The problems related to the sand mining are also stimulated by the expansion of non-registered sand miners and improper method of excavation as well as quarry sites. Actually, there are any laws and regulations to control the sand mining activities. However, it seems that the sand mining is not controlled well by legal reinforcement due to the lack of integrated management system. As long as the sand mining is controlled, it can be one of measures for sediment control plan to give an extra empty capacity in the sediment reservoirs and contribute to the rural economy.

The sand mining management is a part of sediment control plan and the regional development to control the sand mining by providing an alternative income source. In the case of sand mining in Mt. Merapi volcanic area, a sustainable sand mining management has been proposed (DGWR, 2001a) that aimed for public welfare and regional development. The goals of those objectives were as follows.

– Sediment disaster mitigation by increasing empty capacity of sediment reservoir and generating operation and maintenance cost for sediment control facilities.

– Riverbed stabilization to sustain the social infrastructure.

– Protection of river structures and land use.

– Mitigation of environmental issues.

– Sustainable regional income through the sand mining.

The following activities are recommended to achieve the objectives of sustainable sand mining.

- Development of the regulations and guidelines that minimize the environmental impacts from sand mining and have flexibility to fit local needs and conditions.

- Establishment of the sand mining management institution by stakeholders and community with bottom up approach, to facilitate the

sediment control, sustain sands as natural resources, and contribute to the regional economy.

- Dissemination of the knowledge of the proper sand mining technique as well as the effects of excessive sand mining to all of the stakeholders and community.

- Establishment of a long-term monitoring program to assess the effectiveness of sand mining and its effects on the river environment. The monitoring should include volume of aggregate removal, extraction rates, channel change, bank erosion, and ecological conditions of the river.

2.4 Summary

The sediment-related problems in Merapi volcanic area and Progo River are pointed out and summarized in Figure 2.23 and Table 2.5. The problems persist in the upper, middle and lower reach of Merapi volcano area. Some of the problems are triggered by natural activities such as volcanic activity of Mt. Merapi and heavy rainfall, and many others occurred relating to the human interfere such as deforestation, construction of dam and sand mining. The activities of Merapi Volcano have caused severe sediment-related disasters, including pyroclastic flows and debris flows. Frequent eruptions produced a tremendous amount of volcanic loose deposit on the slope of Mt. Merapi and disasters in the downstream area. Sediment supply from the active volcano can affect river channel morphology and the environment. The sediments fill river channels with a large quantity of gravelly sand, which can modify the channel size, shape, and structure, and affect sediment transport and deposition. Sediment transport delivers fine sediment downstream, which aggrades and paves the channel beds.

One of the critical issues of uncontrolled sand mining in Merapi volcanic area is the riverbed degradation in the Lower Progo River. The riverbed degradation has threatened the existing social infrastructures, including three bridges and two irrigation intakes. The instability of the bridges and the ineffective function of the intakes due to the riverbed degradation induced serious negative impacts on the regional development. Removal of finer material through sand mining also causes bed coarsening due to changes in grain size distribution. Otherwise, the qualitative analysis shows that the sand mining can be an effective method to control the excess sediment if the sand mining activities are properly managed. Therefore, the sustainable sand mining management is an important point as a part of the sediment control plan and the regional development to reduce and mitigate the disasters.

Assessing the bed variation is one of the methods to evaluate the riverbed change that is caused not only by the natural sediment transport but also by artificial movement including the removal of sand from the rivers. For that purpose, a bed variation model can be used as a tool for the comprehensive sediment management. As the void of bed materials plays important role in fluvial geomorphology and river ecosystem, this study is concern at developing a tool to evaluate the bed variation quantitatively and qualitatively including the changes of grain size distribution and porosity. To achieve the purposes, a classification of grain size distribution and a method for identifying the type of grain size distribution will be presented and analyzed in Chapter 3. Some methods for estimating the porosity of sediment mixtures for different types of grain size distribution to get a relationship between the porosity and grain size distribution are analyzed and discussed in Chapter 4. This relationship is then to be installed into a bed variation model, which is developed and simulated in Chapter 5. This tool is expected to be available to identify the problems concerning sediment transportation with consider the quantity and quality.
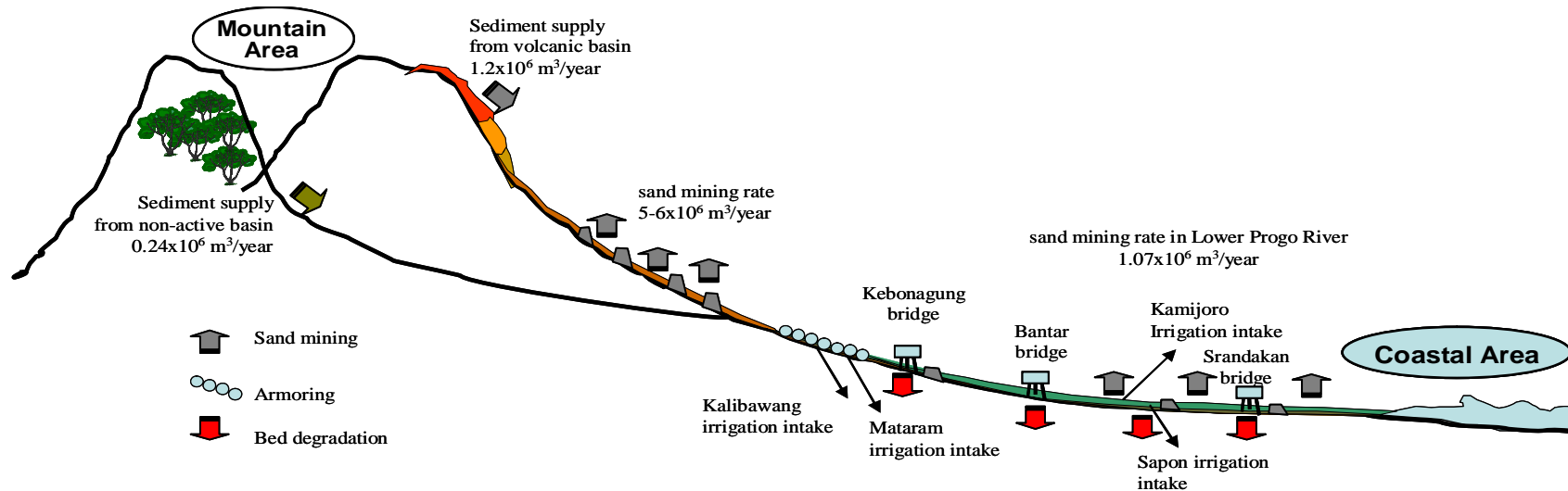
Fig.2.23 Schematic diagram explaining the sediment-related problems in Merapi Volcanic area and Progo River

Table 2.5 Summary of sediment-related problems in Merapi Volcanic area

Stream section	Up reach		Middle reach	Lower reach	Coastal
	Non-active basin	Volcanic basin			
Disturbances	Deforestation	1. Construction of sabo dams since 1970's 2. Sand mining	Construction of groundsill at Kebonagung in 1986	1. Construction of groundsill at Srandakan in 2003 2. Construction of weir at the downstream of Sapon Irrigation Intake in 2006 3. Sand mining	Construction of jetty
Sediment related problems	Surface erosion	1. Pyroclastic flows 2. Debris flows 3. Aggradation	1. Bed degradation 2. Surface bed coarsening	1. Bed degradation	River mouth closure due to longshore sed. transport
Sediment production	0.24 x 10^6 m^3/year (20% of sediment production from volcanic basin)	1.2x10^{6}m^3/year			
Sediment extraction	-	5~6x10^6 m^3/year		1.07 x10^6 m^3/year	
Effects on structures and environment			Unstableness of bridges	Unstableness of bridges Effect on irrigation intake	

References

Bird, E.C.F & Ongkosongo, O.S.R. (1980). "Environmental Changes on the Coast of Indonesia" The United Nations University.

DGRD (Directorate General of Rural Development), Ministry of Settlement and Regional Infrastructure, Republic of Indonesia. (2000). "South Java Flood Control Sector Project. " Volume B.

DGWR (Directorate General of Water Resources), Ministry of Public Works and Power, Republic of Indonesia. (1971). "Kali Progo Basin Study. Main Report. "

DGWR (Directorate General of Water Resources), Ministry of Settlement and Regional Infrastructure, Republic of Indonesia. (2001a). "Review Master Plan Study on Mt Merapi. Main Report. "

DGWR (Directorate General of Water Resources), Ministry of Settlement and Regional Infrastructure, Republic of Indonesia. (2001b). "Review Master Plan Study on Mt Merapi. Supporting Report [B] Volcanic Disaster Mitigation Plan. "

Indra Karya. (1999). "Survey of Sediment Balance and Management in Progo River: Final Report (in Indonesian)."

Isnugroho, (2003). "Flooding and River Channel Deformation due to River Mouth Blocking in Progo Lower Reach, Indonesia." *Proc. 1st. International Conference on Hydrology and Water Resources in Asia Pacific Region*, Kyoto, Japan.

Kondolf, G. M. (1994). "Geomorphic and environmental effects of instream gravel mining. " *Landscape and Urban Planning*, Vol. 28, pp.225-243.

Kondolf, G. M. (1997). "Hungry water: Effects of dams and gravel mining on river channels. " *Environ. Management*, Vol. 21, No.4, pp. 533-551.

Lagasse, P.F., Winkley, B.R. and Simons, D. B. (1980). "Impact of Gravel Mining on River System stability." *J. Waterway, Port, Coastal and Ocean Div.*, Vol.106, pp.389-404

Lavigne, F., Thouret, J.C., Voight, B., Suwa, H., and Sumaryono, A. (2000). "Lahars at merapi volcano, Central Java: an overview." *J. Volcanol. Geotherm. Res.*, Vol.100, pp.423-456.

Mananoma, T., Rahmat, A., and Legono, D. (2006). "Prediction of sediment storage capacity of Gendol River after eruption of Mt. Merapi in 2006." *Proc. Annual Meeting of Indonesia Association of Hydraulic Engineers XXIII*, Manado, Indonesia.

Maulani, A. (2003). "Sediment Migration in Progo River Middle Reach." *Thesis presented to Gadjah Mada University*, at Yogyakarta, Indonesia, in partial fulfillment of requirement for the degree of Master of Engineering. (in Indonesian)

Newhall, C.G., Bronto, S., Alloway, B., Banks, N.G., Bahar, I., del Marmol, M.A, Hadisantono, R.D., Holcomb, R.T., McGeehin, J., Miksic, J.N., Rubin, M, Sayudi, S.D., Sukhyar, R., Andreastuti, S., Tilling, R.I., Torley,

R., Trimble, D., and Wirakusumah, A.D. (2000). "10,000 Years of explosive eruptions of Merapi Volcano, Central Java: archeological and modern implications." *J. Volcanol. Geotherm. Res.*, pp.100:9-50.

Rinaldi, M., Wyzga, B. and Surian, N. (2005). "Sediment Mining in alluvial Channels: Physical effects and management perspectives." *River Research and Applications*. Vol.21, pp.805-828.

Siswowidjoyo, S., Suryo, I., Yokoyama, I., (1995). "Magma eruption rates of Merapi volcano, central Java, Indonesia, during one century (1890-1992)." *Bull. Volcanol.*, Vol.57, pp.111-116.

Sumaryono, A., Churiyah, and Artha, IGM. (1996). "Geomorphological Changes at Progo River Caused by Lahar. In *Proceeding of Workshop on Disasters Caused by Floods and Geomorphological Changes and Their Mitigations.*" Yogyakarta, Indonesia.

Suwartha, N. (2002). "Hydraulics Study of Sediment Transport in Lower Progo River." *Thesis presented to Gadjah Mada University*, at Yogyakarta, Indonesia, in partial fulfillment of requirement for the degree of Master of Engineering. (in Indonesian)

Thouret, J.C, Lavigne, F., Kelfoun, K., and Bronto, S. (2000). "Toward a revised hazard assessment at Merapi volcano, Central Java. " *J. Volcanol. Geotherm. Res.*, Vol.100, pp.479-502.

Voight, B., Constantine, E.K., Siswowidjoyo, S., and Torley, R. (2000). "Historical eruptions of Merapi Volcano, Central Java, Indonesia, 1768-1998." *J. Volcanol. Geotherm. Res.*, Vol.100, pp.69-138.

Chapter 3

Classification and Identification of Grain Size Distribution

3.1   Introduction

The grain size distribution of bed material is of particular interest in the field of soil science (Fredlund *et al*., 2000), sediment transport (Dade and Friend 1998) and aquatic habitat (Gayraud and Philippe, 2003; ASCE, 1992). As for estimating the sediment transport, bed variation and porosity changes in riverbed material, identification of grain size distribution was necessary (Fujita *et al*., 2005). Interpretation of grain size distribution has been widely investigated (e.g. Spencer, 1963; Fredlund *et al*., 2000; Rice and Haschenburger, 2004 and Swamee and Swamee, 2005). Spencer (1963) presented the technique of the graphical dissection of heterogonous distribution through statistical procedure. Fredlund *et al.* (2000) proposed two mathematical forms to represent grain size distribution curves, namely, a unimodal form and a bimodal form using five-parameters of unimodal equation. Rice and Haschenburger (2004) proposed a method for size characterization of coarse subsurface fluvial sediment. The method was developed from an empirical demonstration of the approximate similarity of surface and subsurface grain size distributions when compared over a common range of sizes. Swamee and Swamee (2005) presented the equations for unimodal and multimodal grain size distribution curves by using graphical method. The equation proposed for unimodal distribution involved three parameters and for multi modal distribution, the numbers of

parameters were $4N$-1, where N was the number of sediment fractions. These methods could be used to represent the grain size distribution; however, the procedure to determine the parameter was not simple.

In this chapter, a classification of grain size distribution and a method for identifying the type of grain size distribution will be presented. Firstly, the unimodal grain size distributions of sediment mixtures are classified into three typical types, namely lognormal distribution, Talbot distribution and anti-Talbot distribution; and the characteristic parameters of those typical distributions are found out. Secondly, a method for identifying the type of grain size distribution by means of numerical indices γ and β are presented. Thirdly, based on the geometrical analysis, a diagram on classification of grain size distribution type is indicated. Finally, the diagram is used to identify and classify natural grain size distributions.

3.2 Typical Grain Size Distribution

Riverbed always consists of grains with different sizes. Grain size distribution is an important bulk property that influences the sediment transport phenomena, the infiltration system, and the habitat condition. The distribution curve represents the occurrence of cumulative frequency, f (weight/weight bass), of the grain size, d. The curve begins at the origin and monotonically increases to unity. When the probability density of the cumulative frequency $p = \mathrm{d}f/\mathrm{d}(\log d)$ is plotted, it may exhibit one, two or three modes. These grain size distributions are called unimodal, bimodal or multimodal distributions, respectively. The grain size distribution and its probability density distribution associated with unimodal and bimodal distributions are illustrated in Figure 3.1.

In this chapter, the classification of the unimodal distribution and the identification of distribution types are newly discussed. The unimodal distribution can be classified into three typical distributions, namely, Talbot

distribution, lognormal distribution and anti-Talbot distribution. These typical grain size distributions and probability density distributions are shown in Figure 3.2.

3.2.1 Talbot distribution

It is well known that the surface bed material of mountainous rivers and armor layer of gravel bed rivers have Talbot type of grain size distribution as shown in Figure 3.2(a). The shape of grain size distribution curve is concave and the probability density distribution is positively skewed towards a high-end tail of distribution. The original size distribution function of Talbot distribution is as follows:

$$f(d) = \left(\frac{d}{d_{max}} \right)^n \qquad (n>1) \qquad (3.1)$$

where d_{max} = the maximum grain size and n = a coefficient.

Figure 3.3 shows fitting the natural grain size distributions by Eq.(3.1). A-1 and F-1 are the grain size distribution data taken from Ai River (Osaka Prefercture, Japan) and Fukadani bare slope (Gifu Prefercture, Japan), respectively. Distribution of A-1 data is narrower than F-1. A-1 is best fitted by using coefficient n=0.9 and F-1 is best fitted by using coefficient n=0.3. Fitting by Eq.(3.1) gives the good agreement for narrow distribution, but the difference is much larger for the finer size of the wide distribution. This result indicates that the minimum grain size as well as the maximum size should be introduced into the function as a parameter. Thus, the original Talbot distribution function, Eq.(3.1), is modified with considering the minimum diameter of the grain size as shown in Eq.(3.2) and it is called as Modified-Talbot distribution or M-Talbot distribution (hereinafter referred as M-Talbot distribution).
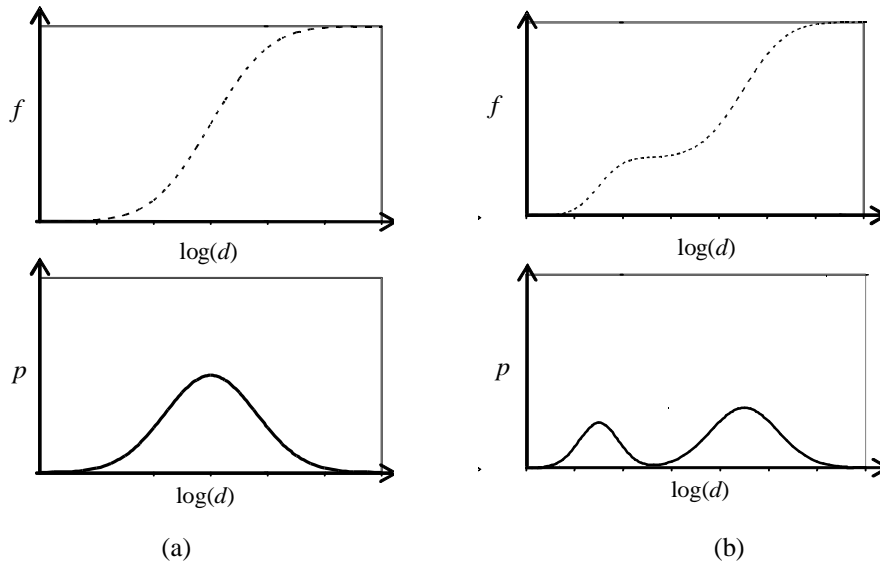
Fig.3.1 (a) Diagram illustrating the grain size distribution and probability density distribution function of unimodal distribution.   (b) Diagram illustrating the grain size distribution and probability density distribution function of bimodal distribution.

(a) Talbot type   (b) Lognormal type   c) Anti-Talbot type
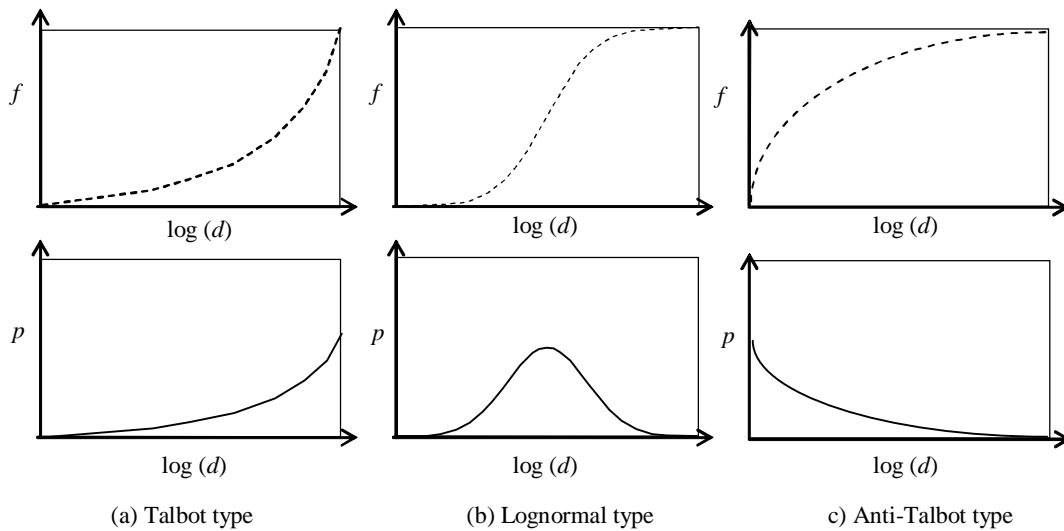
Fig.3.2 Typical types of unimodal grain size distribution and its probability density distribution curves
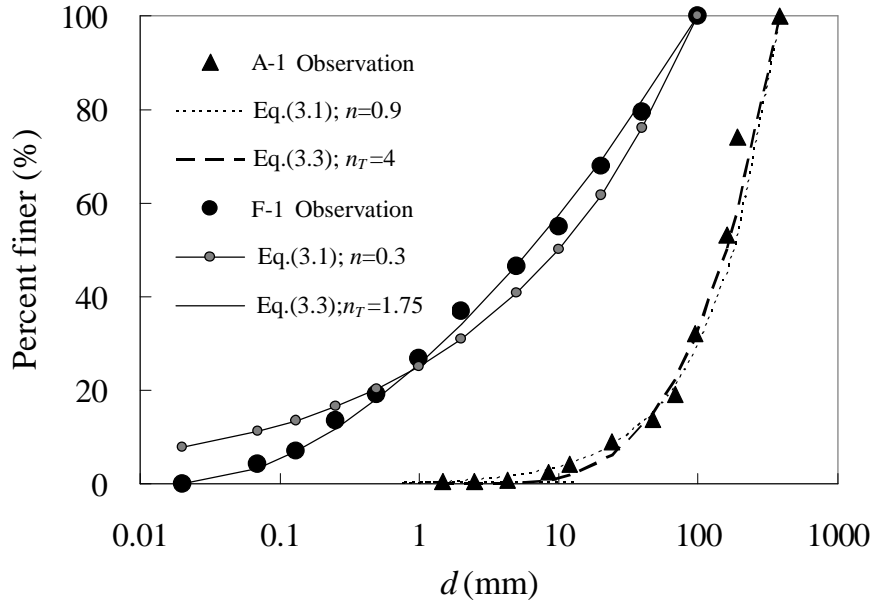
Fig.3.3 Fitting curve for Talbot distribution

$$g(\chi) = \left(\frac{\chi - \chi_{\min}}{\chi_{\max} - \chi_{\min}} \right)^{n_T} \tag{3.2}$$

where $\chi = \log_{10} d$, $\chi_{\min} = \log_{10} d_{\min}$, $\chi_{\max} = \log_{10} d_{\max}$, and n_T = a coefficient more than 1 called Talbot number.

Therefore,

$$p(d) = \frac{1}{\log_e 10} \frac{1}{d} \left(\frac{\log \dfrac{d}{d_{\mathbf{min}}}}{\log \dfrac{d_{\mathbf{max}}}{d_{\mathbf{min}}}} \right)^{n_T} \tag{3.3}$$

Normalizing the diameter d with $d_{\min}$, Eq.(3.3) is written as:

$$p\left(\frac{d}{d_{\min}}\right) = \frac{1}{\log_e 10} \frac{d_{\min}}{d} \left(\frac{\log \dfrac{d}{d_{\min}}}{\log \dfrac{d_{\max}}{d_{\min}}}\right)^{n_T}$$

(3.4)

Probability density distribution of $d/d_{\min}$ is a function of $d_{\max}/d_{\min}$ and n_T. Therefore, the characteristic parameters of M-Talbot distribution are Talbot number, n_T, and ratio of maximum and minimum diameters of particle, $d_{\max}/d_{\min}$. Fitting the natural grain size distribution data A-1 and F-1 by using Eq.(3.3) gives the better results than Eq.(3.1) as shown in Figure 3.3.

3.2.2 Lognormal distribution

Lognormal grain size distribution is one of the most common grain size distributions appearing under natural conditions. Its grain size distribution and the probability density distribution are shown in Figure 3.2(b). The probability density distribution has a single peak and symmetric around the mean of the distribution. The probability density function of lognormal distribution is as follows:

$$g(\chi) = \frac{1}{\sqrt{2\pi}\sigma_L} \exp\left[-\frac{(\chi - \chi_{mg})^2}{2(\sigma_L)^2}\right]$$

(3.5)

where $\chi = \ln d$, $\chi_{mg} = \ln d_{mg}$, d_{mg} = the geometric average of grain size and σ_L = the standard deviation of $\ln d$.

Therefore,

$$p(d) = \frac{1}{\sqrt{2\pi}\sigma_L d} \exp\left[-\frac{(\ln d - \ln d_{mg})^2}{2(\sigma_L)^2}\right]$$

(3.6)

Normalizing d with d_{mg},

$$p\left(\frac{d}{d_{mg}}\right) = \frac{1}{\sqrt{2\pi}\sigma_L}\frac{d_{mg}}{d}\exp\left[-\frac{\left(\ln\frac{d}{d_{mg}}\right)^2}{2(\sigma_L)^2}\right] \qquad (3.7)$$

Probability density distribution of d/d_{mg} is a function of σ_L. The characteristic parameter of the lognormal distribution is, therefore, only σ_L.

3.2.3 Modified anti-Talbot distribution

Typical anti-Talbot distribution and its probability density distribution are shown in Figure 3.2(c). The shape of grain size distribution curve is convex and the probability density distribution is skewed towards the low-end tail of distribution (hereinafter referred as M-anti-Talbot distribution). The size distribution function is same as M-Talbot distribution shown in Eq.(3.3), but the value of Talbot number n_T is less than 1. Therefore, the characteristic parameters of the mixtures are Talbot number, n_T, and ratio of maximum and minimum diameters of particle, d_{max}/d_{min}.

3.3 Identification of Grain Size Distribution

3.3.1   Geometric indices of grain size distribution

Based on the visual discrimination of the shapes of grain size distribution and the probability density distribution, the grain size distribution of natural sediment mixtures can be identified and classified into three typical types. The grain size distribution is classified into the lognormal distribution if the trend of the size distribution curve is similar to the lognormal curve and the density distribution has a single peak. If the
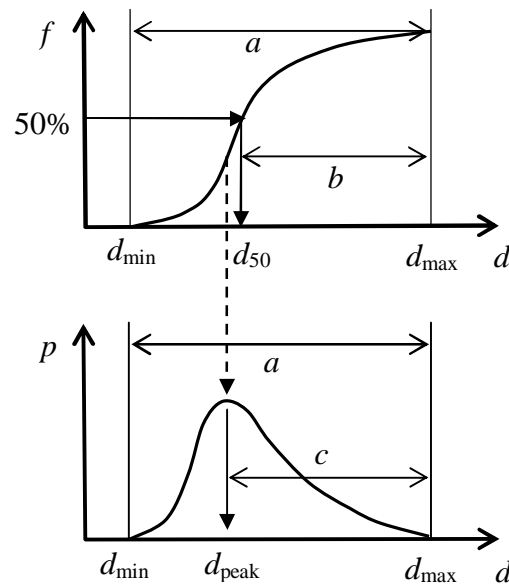
density distribution is skewed towards a high-end tail of distribution, the grain size distribution is classified into M-Talbot distribution. If the probability density distribution has two peaks, the grain size distribution is classified into bimodal distribution.

However, such visual identification is not available to install its result into the riverbed variation model. Thus, the geometric indices γ and β are introduced to identify the distribution type. The indices γ and β are defined as Eq.(3.8) and Eq.(3.9), respectively. Index γ designates the relative location of the median grain size, d_{50}, between the minimum size, d_{min}, and the maximum size, d_{max}. Index β expresses the relative location of the grain size, d_{peak}, for the peak probability density distribution between the minimum size, d_{min}, and the maximum size, d_{max}. Schematic graphs of geometric indices γ and β are shown in Figure 3.4

$$\gamma = \frac{\log d_{max} - \log d_{50}}{\log d_{max} - \log d_{min}} \Rightarrow \frac{b}{a} \quad (3.8)$$

$$\beta = \frac{\log d_{max} - \log d_{peak}}{\log d_{max} - \log d_{min}} \Rightarrow \frac{c}{a} \quad (3.9)$$

Fig.3.4 Schematic graphs of geometric indices γ and β

3.3.2　Indices of typical grain size distributions

The index β of M-Talbot distribution is 0.0. The index γ changes from 0.0 to 0.5 depending on Talbot number, n_T, and the value of γ decreases with increase in Talbot number. If Talbot number, n_T, is 1.0, the distribution is linear and γ is 0.5. M-Talbot distribution curves with the same d_{max}/d_{min} and different Talbot numbers are shown in Figure 3.5(a). The geometric indices for each distribution shown in Figure 3.5(a) are illustrated in Figure 3.6. The indices β and γ of M-Talbot distribution are plotted on the line expressed by $\beta = 0$ and $0 < \gamma < 0.5$.

The lognormal distribution curves with the same mean value and different standard deviation are shown in Figure 3.5(b). Both of indices β and γ of lognormal distributions are always 0.5 as shown in Figure 3.6. The indices β and γ of lognormal distribution are plotted just on the center point (0.5, 0.5).

The index β of M-anti-Talbot distribution is 1.0. The value of γ varies from 0.5 to 1.0 depending on the value of Talbot number, n_T, and the value of γ increases with decrease in Talbot number. If Talbot number, $n_T = 1.0$, the distribution is linier and γ is 0.5. The M-anti-Talbot distribution curves with the same d_{max}/d_{min} and different Talbot numbers are shown in Figure 3.5(c). The indices β and γ of those distributions are illustrated in Figure 3.6. The indices β and γ of M-anti-Talbot distribution are plotted on the line expressed by $\beta = 1.0$ and $0.5 < \gamma < 1.0$.

### 3.3.3　Indices of other grain size distributions

Natural grain size distributions usually have the transition shapes between the typical grain size distributions. The grain size distributions between M-Talbot distribution and lognormal distribution are shown in Figure 3.7(a). M_1 looks like M-Talbot distribution and M_3 is visually close to

lognormal distribution. When the distribution changes from M_1 to M_3, the plot of β and γ approaches the center point (0.5, 0.5) from the origin (0,0) along the line expressed by $\beta = \gamma$ (Fig.3.8(a)). The transition shapes from lognormal distribution to M-anti-Talbot distribution are shown in Figure 3.7(b). N_1, N_2 and N_3 gradually changes from lognormal type to M-anti-Talbot type. N_1 looks like lognormal distribution and N_3 is visually close to M-anti-Talbot distribution. The plot of β and γ shown in Fig.3.8(a) approaches the point (1, 1) from the center point along the line expressed by $\beta = \gamma$.

The distributions that have the transition shapes between linear distribution and lognormal distribution are shown in Figures 3.7(c) and 3.7(d). All of those distributions have same median size. The indices β and γ of those distributions are shown in Figure 3.8(b). If β is close to 0.5, the distribution becomes lognormal type. On the contrary, if β is close to 0.0 or 1.0, the distribution becomes linear.

Five distributions shown in Figure 3.7(e) have the same peak grain sizes, d_{peak}, that is middle of the minimum and maximum sizes, but different mean sizes. P_1 and Q_1 are unimodal distributions, but P_2 and Q_2 are bimodal distributions. The geometric indices of those distributions are shown in Figure 3.8(b). When γ decreases to be less than 0.25 or increases to be more than 0.75 for $\beta = 0.5$, it is impossible to draw the unimodal distribution and the grain size distribution must be bimodal distribution.
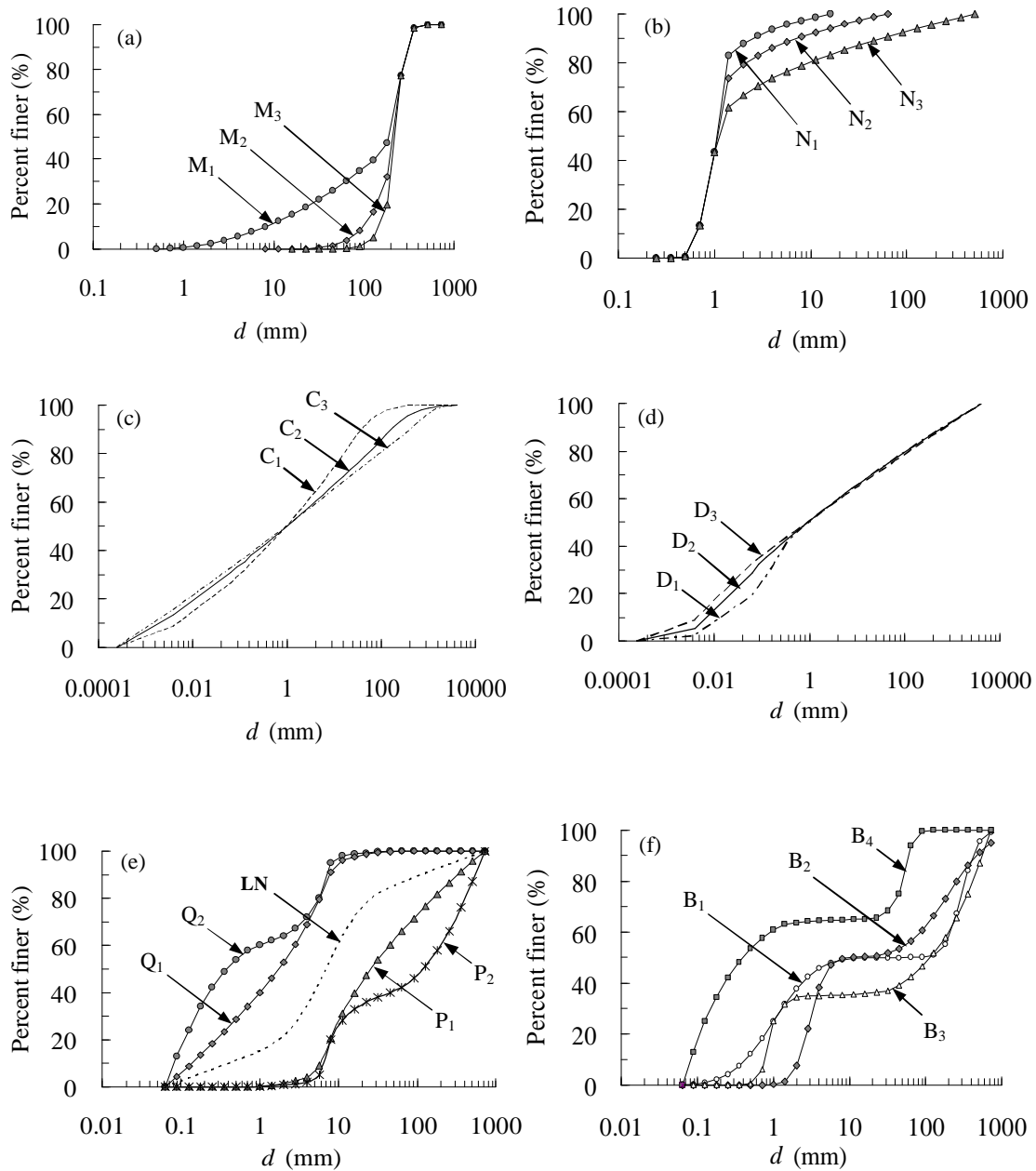
Four bimodal grain size distributions are shown in Figure 3.7(f). The geometric indices β and γ are obtained by the same way and shown in Figure 3.8(a). The indices β and γ of bimodal distribution can be plotted scattered in all region ($0<\beta<1$ and $0<\gamma<1$).
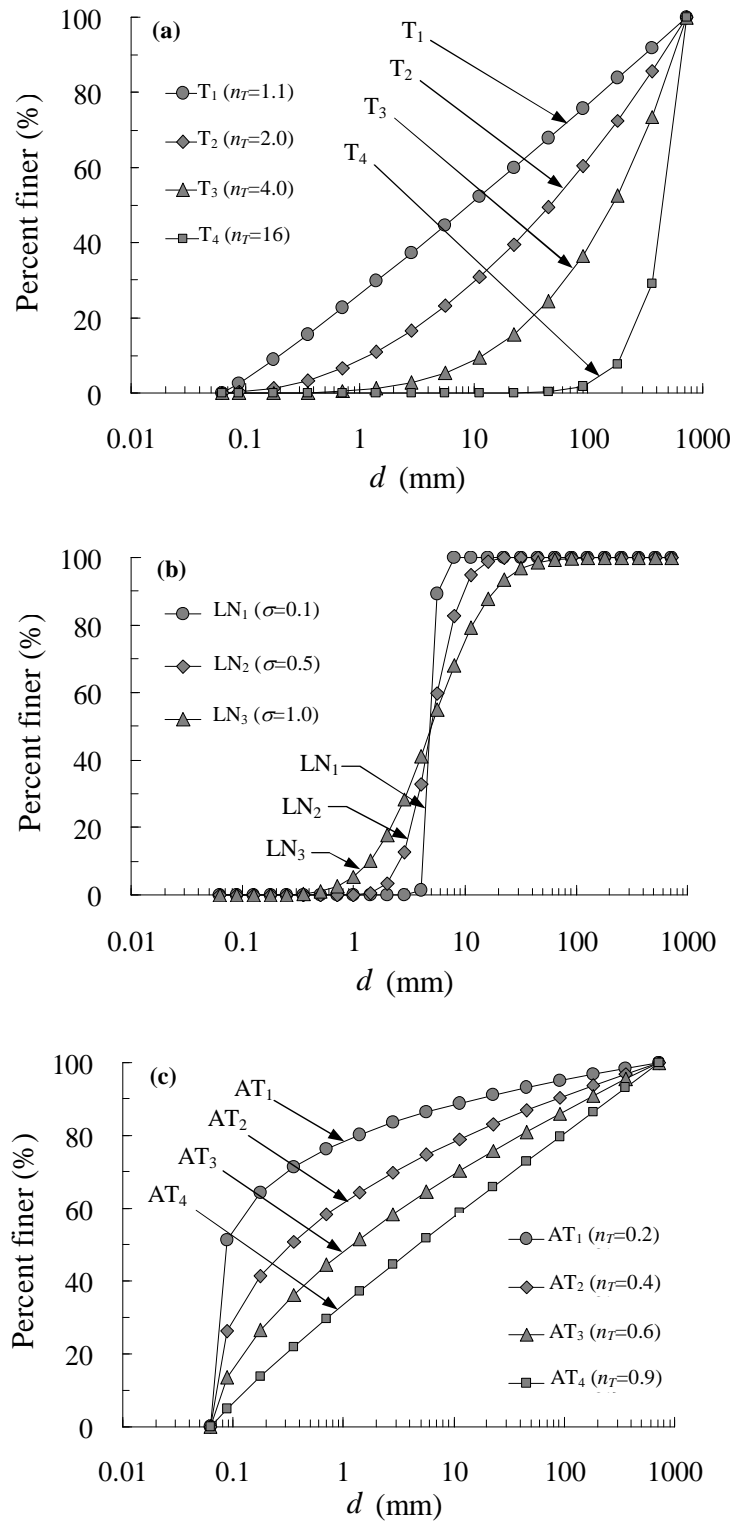
Fig.3.5 (a) M-Talbot distribution with different Talbot numbers, (b) lognormal distribution with different standard deviation, and (c) M-anti-Talbot distribution with different Talbot numbers.
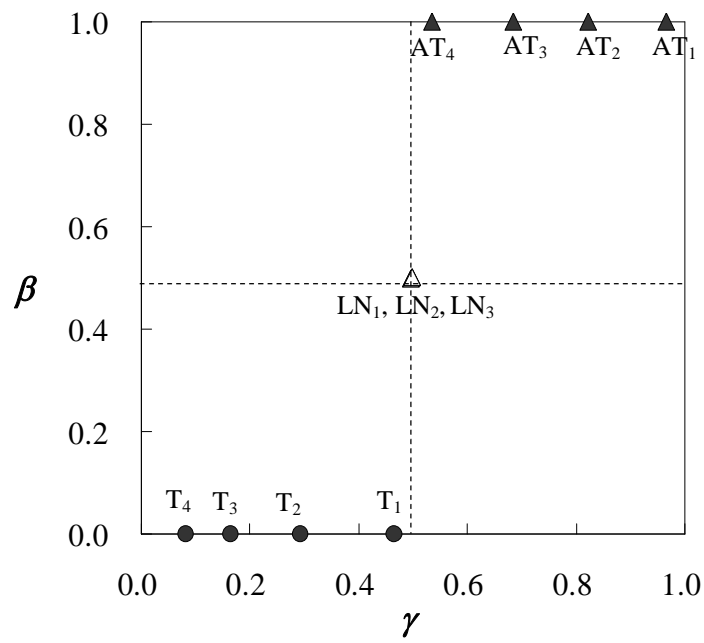
Fig.3.6 The relation between β and γ of M-Talbot, lognormal and M-anti-Talbot distribution shown in **Fig.3.5.**

Fig.3.7 Transition types of grain size distributions: (a) M-Talbot to lognormal, (b) lognormal to M-anti-Talbot, (c) lognormal to linear (Talbot), (d) lognormal to linear (M-anti-Talbot), (e) other distributions with $\beta = 0.5$, and (f) bimodal distributions.
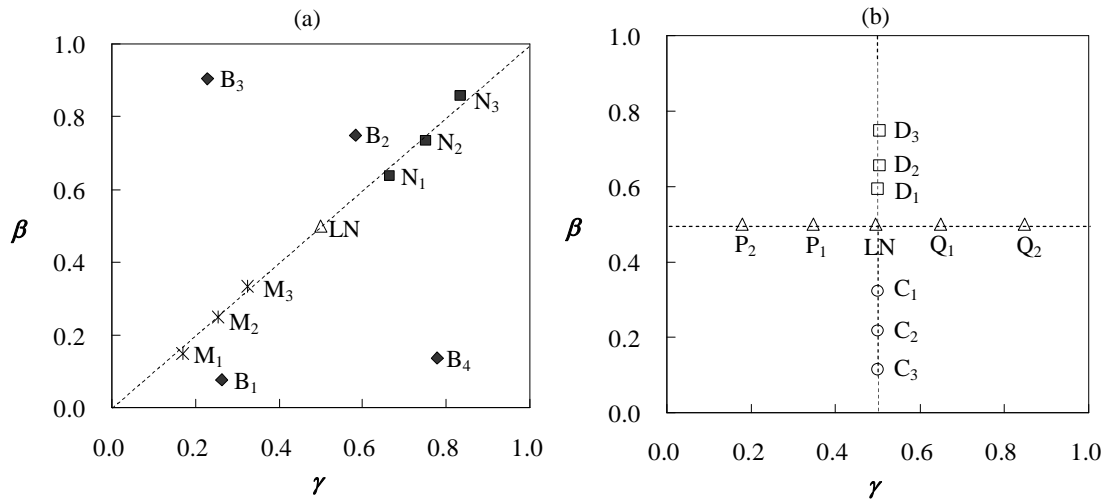
Fig.3.8 The relation between β and γ of the grain size distributions shown in **Fig. 3.7.**

## 3.3.4   Border lines of typical unimodal distributions

Based on the geometric investigation of grain size distribution, as explained before, the region of indices β and γ for each unimodal distribution type can be determined. The region is bordered by four lines, consisting of Line-1, Line-2, Border-1, and Border-2 as shown in Figure 3.9(c).   The indices of M-Talbot and M-anti-Talbot distributions are on Line-1 ($\beta = 0$ and $0 < \gamma < 0.5$) and Line-2 ($\beta = 1.0$ and $0.5 < \gamma < 1.0$), respectively. The indices of lognormal distribution are plotted just on the center point (0.5, 0.5). The indices of the other distribution are plotted on the area of $0<\beta<1$ and $0<\gamma<1$, apart from Line-1, Line-2 and the center point. However, as mentioned before, there is an area where no unimodal distribution exists. From a geometric analysis, an area where unimodal distribution exists is surrounded by Border-1, Border-2, $\beta = 0$ and $\beta = 1.0$ as shown in Figure 3.9(b). For example, distribution P_2 and Q_2, their geometric indices are located in the outside of unimodal area. When $\beta = 0.5$, $\gamma = 0.2$ or

$\beta = 0.5$, $\gamma = 0.85$, it is not possible to draw any unimodal distribution curves. For bimodal distribution, the regions of indices β and γ cover all of the area, as illustrated in Figure 3.9(a).
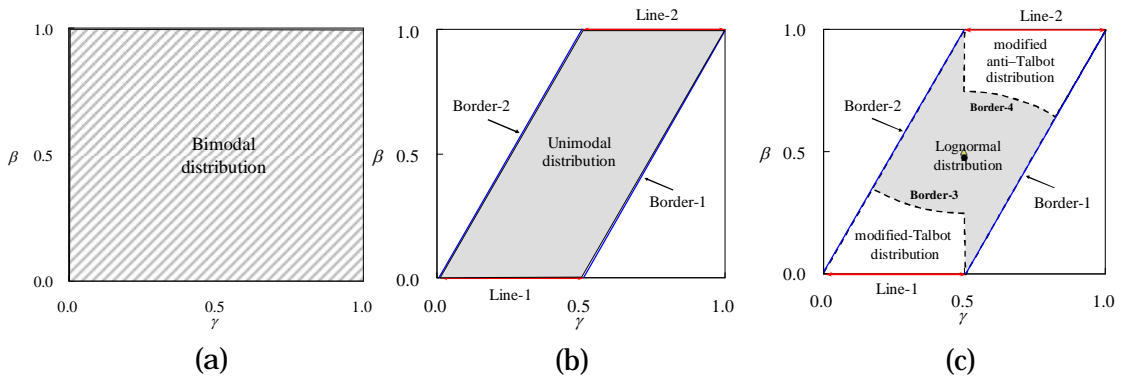
Fig.3.9 Domain of each distribution type; (a) bimodal distribution, (b) unimodal distribution, (c) M-Talbot, lognormal and M-anti-Talbot distribution.
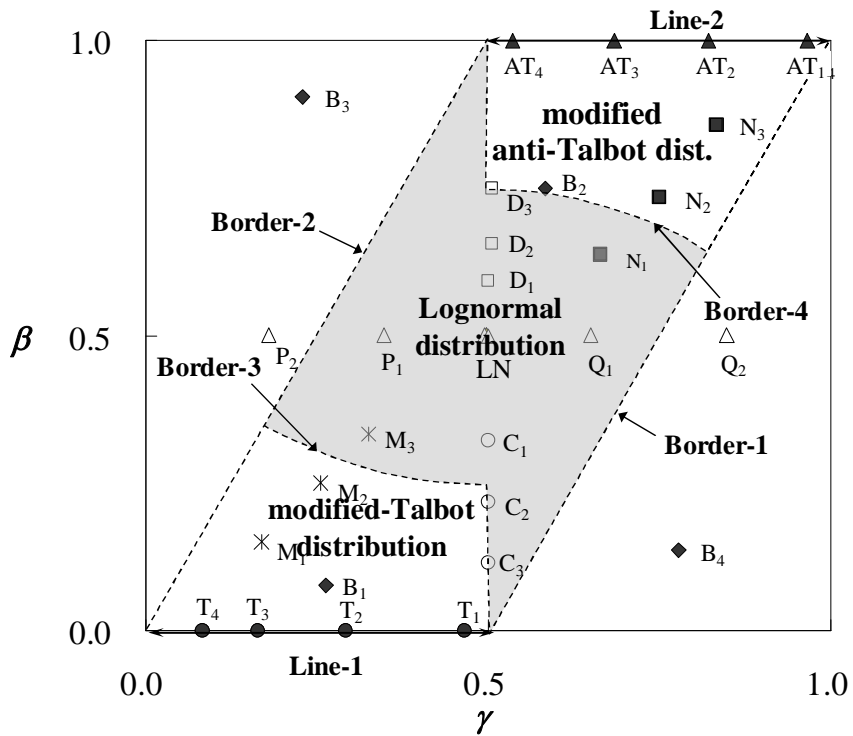
Fig.3.10 Diagram of relation between β and γ that indicating M-Talbot, lognormal, and M-anti-Talbot regions.

It seems reasonable that the grain size distribution type is identified with the distance to the point (γ, β) from Line-1 (corresponding to M-Talbot distribution), Line-2 (corresponding to M-anti-Talbot distribution), or the center point (corresponding to lognormal distribution). According to this criterion, the border line between M-Talbot distribution and lognormal distribution (Border-3) is written as Eq.(3.10) and the border line between M-anti-Talbot and lognormal distribution (Border-4) is expressed as Eq.(3.11).

$$\text{Border-3:} \quad \beta = (0.5 - \gamma)^2 + 0.25 \tag{3.10}$$

$$\text{Border-4:} \quad \beta = -(0.5 - \gamma)^2 + 0.75 \tag{3.11}$$

Since the M-Talbot distribution is available when $\gamma < 0.5$ and the M-anti-Talbot distribution is available when $\gamma > 0.5$, the vertical line $\gamma = 0.5$ is used as the border between M-Talbot and lognormal distribution and between lognormal and M-anti-Talbot distribution. The region of M-Talbot distribution, lognormal distribution, and M-anti-Talbot distribution are indicated in Figure 3.9(c).

The indices of the grain size distribution shown in Figures 3.5 and 3.7 are plotted on the diagram on classification of grain size distribution type (Fig.3.10). According to this criterion, M_1 and M_2 are identified as M-Talbot distribution. N_2 and N_3 are classified into M-anti-Talbot. M_3, N_1, P_1, Q_1, C_1, D_1 and D_2 are identified as lognormal distribution. These results seem to be appropriate visually. P_2 and Q_2 are bimodal distribution and those are out of the unimodal area.

3.4 Application to natural bed material

The presented identification method is applied to the following data and the validity of the method is verified. The grain size distributions of

natural riverbed material and produced sediment are collected for analysis of identification and classification of grain size distribution. The samples are taken from several rivers and a bare slope in Japan i.e. Ai River in Osaka Prefecture (Fujita, 2004), Hino River in Tottori Prefecture (MLIT, 2004), Ohtaki River in Nagano Prefecture (Ashida and Fujita, 1987) and a Fukadani bare slope in Gifu Prefecture. The grain size distributions and those probability density distributions are shown in Figures 3.11 and Figures 3.12, respectively. Capital letter A, H, O and F denote the samples from Ai River, Hino River, Ohtaki River and a Fukadani bare slope, respectively. The sampling points are summarized in Table 3.1. The samples are classified by the characteristics of sampling points as follows:

   a) Surface bed material (A-1, 5, H-1, 2, 3)
   b) Sub-surface bed material (A-2, 6, H-4, 5, 6)
   c) Sand bar (A-3)
   d) Sediment deposition in a sabo dam (A-4)
   e) Sediment deposition in a valley immediately after Ontake Lanslide 1984 (O-1)
   f) Sediment deposition in a reservoir (O-2, 3)
   g) Sediment produced at a bare slope (F-1, 2, 3)

   The indices β and γ and the distribution type of those distributions are also listed in Table 3.1. The relation between indices β and γ of those distributions are plotted on the diagram on classification of grain size distribution type as shown in Figure.3.13. A-1, A-3, A-5, A-6, H-3, O-1, F-1, F-2, and F-3 are identified as M-Talbot distribution and the plots are located in the M-Talbot area. H-1, H-2, O-2, and O-3 are identified as lognormal distribution and the plots are located in the lognormal area.

   The validity of the identification method is verified by using the visual identification based on the shape of grain size distribution curves (Fig. 3.11) and probability density distribution curves (Fig.3.12). The grain size

distributions are categorized into 5 types by the visual identification; namely M-Talbot, lognormal, M-Talbot-lognormal transition, lognormal-M-anti-Talbot transition and bimodal distribution. A-1, A-5, A-6, H-3, F-1, F-2, and F-3 plotted with filled circles are visually identified as M-Talbot distribution. A-3 and O-1 plotted with triangles are visually identified as the distribution between M-Talbot and lognormal, therefore, the plots of indices β and γ are located near the Border-3. H-1, O-2, and O-3 plotted with filled diamonds are visually identified as lognormal distribution. H-2 plotted with cross is visually identified as the distribution between lognormal and M-anti-Talbot and the plot of indices β and γ are located near the Border-4. A-2, A-4, H-4, H-5 and H-6 plotted with rectangular are visually identified as bimodal distribution and the plots are located in M-Talbot and lognormal area. These verification results indicate that the classification and identification method is available for the identification of the grain size distribution.

Types of natural grain size distribution shown in Table 3.1 can be classified by the vertical and longitudinal sampling position as shown in Table 3.2. From this classification, it can be seen that the grain size distributions of surface bed material in the midstream tend to be M-Talbot distribution, while the grain size distributions in the downstream tend to be lognormal distribution. Nakamura and Tockner (2004) pointed out that most Japanese rivers exhibit reduced flow and sediment dynamics. The surface bed materials of midstream have M-Talbot distribution because of the developing of armoring due to the truncation of the sediment transport by sediment control dams, hydropower dams, weirs, and by the afforestation of mountain slopes. However, downstream riverbeds consisted of mostly of fine-grained substrates such as silt and sand (Yoshimura *et al.*, 2005), and the grain size distribution is usually lognormal distribution.
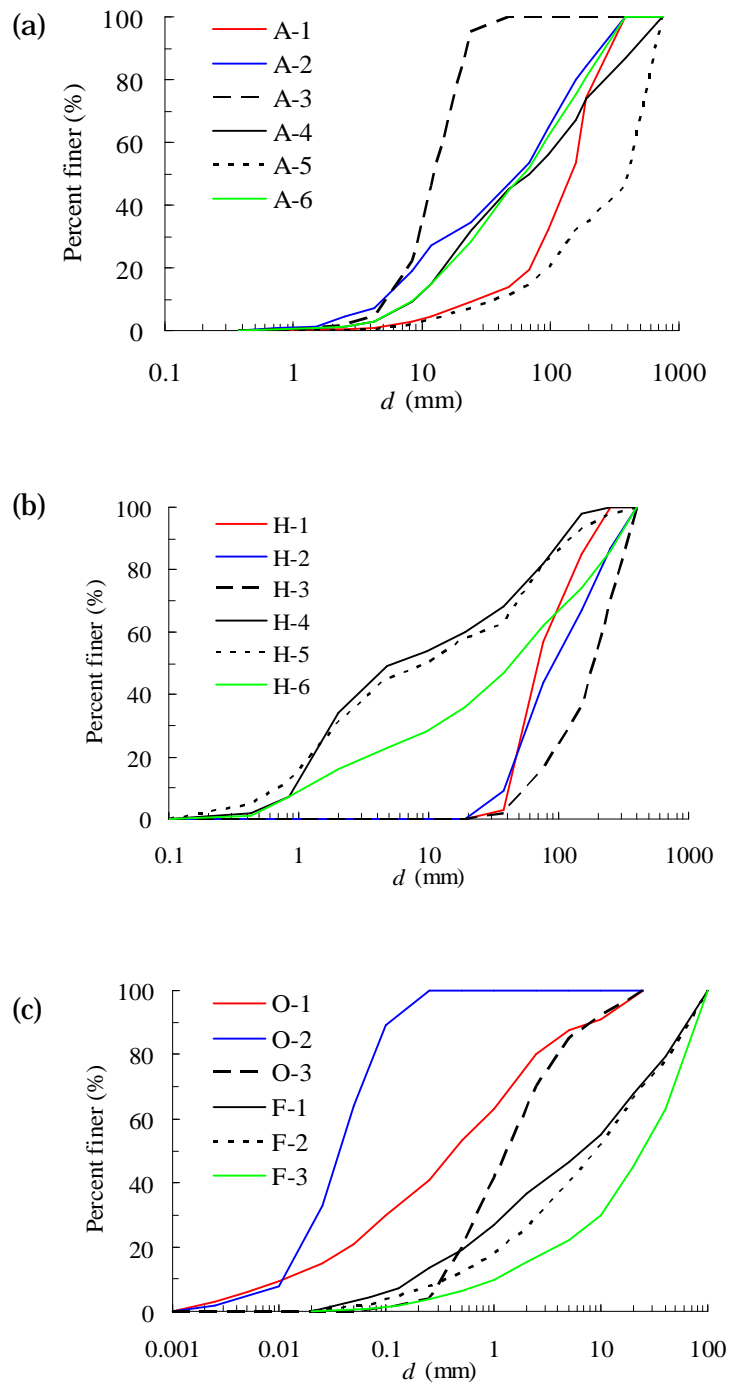
Fig.3.11 Grain size distributions of natural sediment mixtures sampled in (a) Ai River, (b) Hino River and (c) Ohtaki River and a Fukadani bare slope.
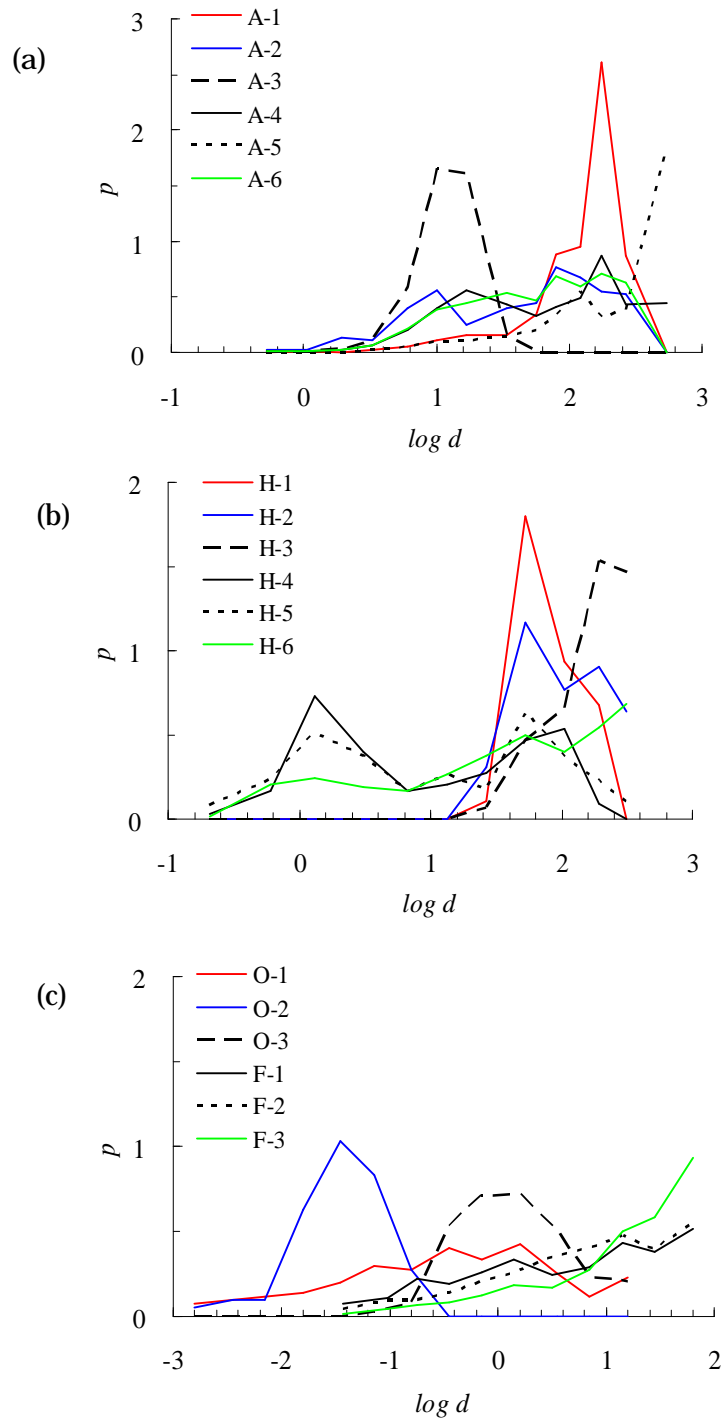
Fig.3.12 Probability density distributions of natural sediment mixtures sampled in (a) Ai River, (b) Hino River and (c) Ohtaki River and a Fukadani bare slope.

Table 3.1 Parameters of actual grain size distribution.

No.	Sample sites	d_{min} (mm)	d_{50} (mm)	d_{peak} (mm)	d_{max} (mm)	β	γ	Type
A-1	Surface bed in upstream of Gokuraku Bridge in Ai River	0.740	149.23	159.00	381.00	0.08	0.11	**T**
A-2	Sub-surface bed in upstream of Gokuraku Bridge in Ai River	0.370	57.70	67.80	381.00	0.19	0.25	**B**
A-3	Sand bar in downsream of Gokuraku Bridge in Ai River	0.370	12.77	8.50	47.60	0.29	0.23	**T**
A-4	Deposit in Ai gawa sabo dam in Ai River	0.370	67.80	159.00	750.00	0.16	0.30	**B**
A-5	Surface bed near Kurumatukuri Bridge in Ai river	2.500	409.49	381.00	750.00	0.00	0.05	**T**
A-6	Sub-surface bed in Kurumatukuri Bridge in Ai river	0.370	62.75	159.00	381.00	0.07	0.23	**T**
H-1	Surface bed in the upstream of river mouth of Hino River	19.000	70.14	37.50	250.00	0.65	0.51	**L**
H-2	Surface bed in Lower Hino River	19.000	94.57	37.50	400.00	0.72	0.49	**L**
H-3	Surface bed in Middle Hino River	19.000	191.18	150.00	400.00	0.20	0.20	**T**
H-4	Sub-surface bed in the upstream of river mouth of Hino River	0.100	5.70	0.85	250.00	0.73	0.52	**B**
H-5	Sub-surface bed in Lower Hino River	0.100	9.50	37.50	400.00	0.24	0.48	**B**
H-6	Sub-surface bed in Middle Hino River	0.100	45.00	250.00	400.00	0.00	0.27	**B**
O-1	Deposit in Ohtaki River immediately after Ontake Landslide, 1984	0.001	0.44	1.00	25.00	0.25	0.39	**T**
O-2	Deposit of wash load in Makio Reservoir	0.001	0.03	0.03	0.25	0.33	0.35	**L**
O-3	Deposit of bed material load in Makio Reservoir	0.050	1.45	1.00	25.00	0.43	0.44	**L**
F-1	Sediment produced at Fukadani bare slope on May 28,2002	0.020	7.08	40.00	100.00	0.00	0.29	**T**
F-2	Sediment produced at Fukadani bare slope on July 1,2002	0.020	9.29	40.00	100.00	0.00	0.26	**T**
F-3	Sediment produced at Fukadani bare slope on November 12,2002	0.020	25.49	40.00	100.00	0.00	0.12	**T**

L: Lognormal distribution ; T: M-Talbot distribution; B: Bimodal distribution
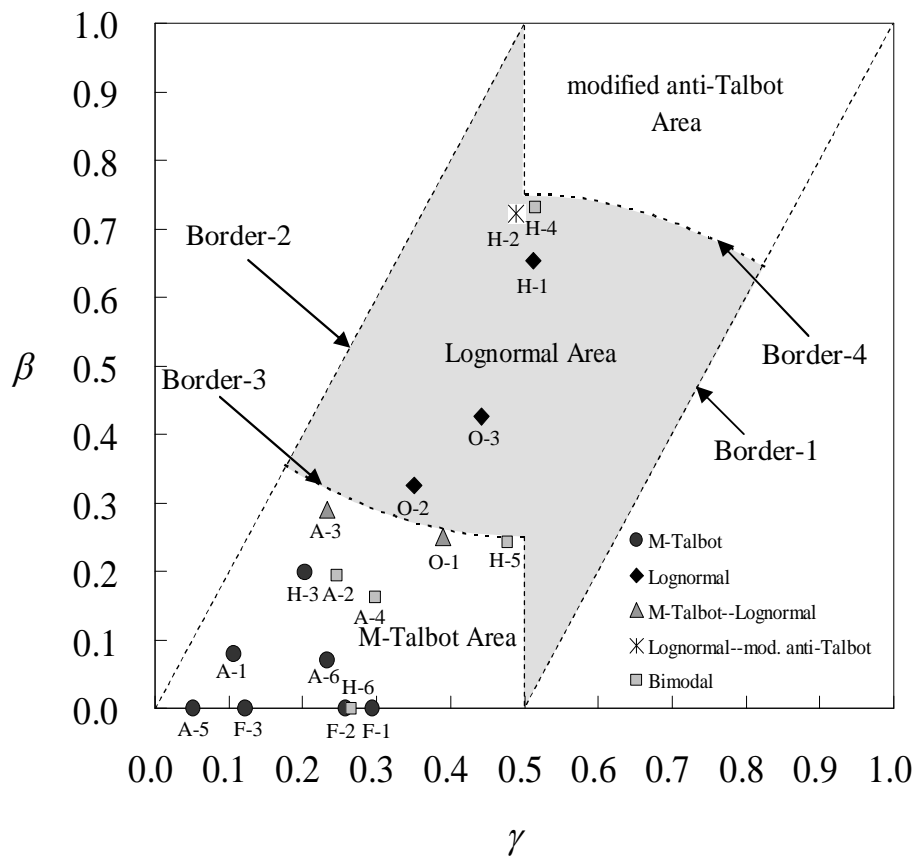
Fig. 3.13 The relation between β and γ of natural grain size distribution shown in Figure 3.11.

Table 3.2 Classification of natural grain size distribution types by the vertical and longitudinal sampling position in the stream.

No.	Sample sites	Vertical position	Type	Longitudinal position
A-1	Surface bed in upstream of Gokuraku Bridge in Ai River	surface	**T**	Midstream
A-3	Sand bar in downsream of Gokuraku Bridge in Ai River	surface	**T**	Midstream
A-5	Surface bed near Kurumatukuri Bridge in Ai river	surface	**T**	Midstream
H-3	Surface bed in Middle Hino River	surface	**T**	Midstream
H-1	Surface bed in the upstream of river mouth of Hino River	surface	**L**	Downstream
H-2	Surface bed in Lower Hino River	surface	**L**	Downstream
A-2	Sub-surface bed in upstream of Gokuraku Bridge in Ai River	sub-surface	**B**	Midstream
A-6	Sub-surface bed in Kurumatukuri Bridge in Ai river	sub-surface	**T**	Midstream
H-6	Sub-surface bed in Middle Hino River	sub-surface	**B**	Midstream
H-4	Sub-surface bed in the upstream of river mouth of Hino River	sub-surface	**B**	Downstream
H-5	Sub-surface bed in Lower Hino River	sub-surface	**B**	Downstream
F-1	Sediment produced at Fukadani bare slope on May 28,2002	source	**T**	Upstream
F-2	Sediment produced at Fukadani bare slope on July 1,2002	source	**T**	Upstream
F-3	Sediment produced at Fukadani bare slope on November 12,2002	source	**T**	Upstream
A-4	Deposit in Ai gawa sabo dam in Ai River	deposit	**B**	Upstream
O-1	Deposit in Ohtaki River immediately after Ontake Landslide, 1984	deposit	**T**	Upstream
O-2	Deposit of wash load in Makio Reservoir	deposit	**L**	Upstream
O-3	Deposit of bed material load in Makio Reservoir	deposit	**L**	Upstream

Almost of the sub-surface materials in the middle reach are identified as bimodal type. Bimodal sediments were common in gravel bed rivers (Smith, 1997). A characteristic feature of Japanese rivers was high sediment transport, particularly during flood events (Yoshimura *et al.*, 2005). The transported sediments usually contain both of coarse and fine sediments and have a lognormal distribution. However, due to the human-induced impact, such as the reduced transportation of the sediments following development of dams, causes the armoring of surface bed material. During flood, only fine sediment such as suspended load and wash load is supplied to the downstream of dams and they will deposit in the bed material after the flood. This means that the sediment much finer than the material of armor coat deposits on the bed. Therefore, the bimodal sediment is developed. After flood, fine sediment in the surface bed material is then transported to the downstream causes the bed coarsening. The grain size

distribution of surface material becomes Talbot distribution, while sub-surface material has bimodal distribution.

Sediments produced from the bare slope are identified as Talbot distribution. Deposited materials have variety typical grain size distribution that depends on the deposit location and the source of material. The deposited materials in the sabo dam have bimodal distribution. The deposited materials in Ohtaki River come from the source; therefore, the typical grain size distribution is similar with the sediment produced from the source, i.e. Talbot distribution.

3.5 Summary

A method for identifying the type of grain size distribution is developed. The results are as follows:

1)   Unimodal distribution can be classified into three typical types of distribution namely, modified-Talbot distribution, lognormal distribution and modified-anti-Talbot distribution and the characteristic parameters of each type are found out.

2)   It is well known that the bed material in mountain streams has Talbot distribution. The characteristic parameters of this distribution are the maximum grain size, $d_{\max}$, and a coefficient, n. However, fitting the Talbot-like wide grain size distribution of bed material by using this function gives the much larger difference in the range of finer sizes. Therefore, the original Talbot distribution function is modified with considering the minimum grain size distribution, and in this study, it is called as modified-Talbot distribution or M-Talbot distribution. The characteristic parameters of M-Talbot distribution are the Talbot number, n_T, and the ratio of the maximum and minimum diameters of particle, $d_{\max}/d_{\min}$.

3) The geometric indices γ and β, that designate the relative locations of the grain size for percent finer of 50%, d_{50}, and the grain size for the peak probability density, d_{peak}, between the minimum size and the maximum size are found out for classification of the distribution type, namely M-Talbot type, lognormal type and M-anti-Talbot type.

4) A diagram on classification of grain size distribution is presented. The diagram presents the relation between geometric indices γ and β and the domain of each typical unimodal distribution, i.e. M-Talbot, lognormal and M-anti-Talbot distribution. The validity of the diagram is verified by comparison with the result by means of visual identification.

5) The diagram on classification of grain size distribution can be applied to classify the natural grain size distributions into three types. The grain size distributions of surface bed material in the midstream of Japanese Rivers tend to be M-Talbot distribution, while the grain size distributions in the downstream tend to be lognormal distribution. The grain size distribution of sub-surface bed material has bimodal distribution. Sediments produced on the bare slope are identified as Talbot distribution. Deposited materials have variety of typical grain size distribution depending on the deposit location and the source of material.

By using the identification method that presented in this chapter, the variation of the grain size distribution type can be identified adequately. The characteristic parameters of grain size distribution type obtained in this chapter are then related to the porosity. The relationship among them will be analyzed and discussed in Chapter 4.

References

Ashida, K. and Fujita, M. (1987). "Simulation of reservoir sedimentation." *Annuals, Disas. Prev. Res. Inst., Kyoto Univ.*, Vol.30 (B-2). (in Japanese).

Dade, W., B. and Friend, P., F. (1998). "Grain-Size, Sediment-Transport Regime, and Channel Slope in Alluvial Rivers." *The Journal of Geology*, Vol. 106, pp.661-675.

Fredlund, M. D., Fredlund, D. G., and Wilson, G. W.(2000). "An equation to represent grain size-distribution." *Can. Geotech. Journal.*, Vol.37, pp. 817-827.

Fujita, M. (2004). "Study on riverbed morphology as habitat for aquatic living things." Report, Foundation of River Watershed Environment Management. (in Japanese).

Fujita, M., Tsutsumi, D., and Sulaiman, M. (2005). "A simulation method for quantitative and qualitative changes of riverbed. " *Proc. International Conference on Fluvial and Coastal Disasters*, CD-ROM, Kyoto, Japan.

Gayraud, S., Philippe, M. (2003). "Influence of bed-sediment features on the interstitial habitat available for macroinvertebrates in 15 French streams." *Internat. Rev. Hydrobiol.*, Vol. 88, pp. 77-93.

MLIT Hinogawa River Office (2004). "Technical Report on Integrated Sediment Management of Hino River Basin 2003." (in Japanese).

Nakamura, K., and Tockner, K. (2004). "River and Wetland Restoration in Japan. " *Proc. 3rd. European Conference on River Restoration*, Zagreb, Croatia.

Rice, S. P. and Haschenburger, K. (2004). "A hybrid method for size characterization of coarse subsurface fluvial sediments." *Earth Surf. Process. Landorms*, Vol.29, pp.373-389.

Smith, G. H. S. (1997). "Measuring and defining bimodal sediment: Problems and implications." *Water Resources Research*, Vol.33, No.5, pp.1179-1185.

Spencer, D. W.(1963). "The interpretation of grain size distribution curves of clastic sediments." *Journal of Sedimentary Petrology*, Vol. 33, No.1, pp.180-190.

Swamee, P. K. and Swamee, N.(2004). "Equation for grain size distribution." *International Journal of Sediment Research*, Vol. 19, No.1, pp.66-74.

Yoshimura, C., Omura, T, Furumai, H., and Tockner, K. (2005). "Present State of Rivers and Streams in Japan." *River Res. Applic.*, Vol.21, pp.93-112.

Chapter 4

The Porosity of Sediment Mixtures

4.1   Introduction

The porosity of mixed grain size populations has been studied by those interested in the packing of particles in artificially created mixture as well as by earth scientists interested in natural geologic materials. Much of the research on particle packing and porosity came from diverse non-earth science disciplines (Cumberland and Crawford, 1987). More recently, particle packing has been examined by earth scientist interested in understanding of voids ratio of non cohesive soils (Aberg, 1992a), void sizes in granular soils (Aberg, 1996), relations between porosity and hydraulics conductivity   (Aberg, 1992b; Kolterman and Gorelick, 1995), and geologists interested in oil reservoir properties (Albert, 2005).

Some lessons have been learned from laboratory and theoretical studies (Han *et al.*, 1986; Marion *et al.*, 1992; Aberg, 1996a).

(i)   The porosity of two component mixtures (binary mixtures) depends on the fractional concentrations of each particle size population and the ratio of the particle diameters.

(ii) The porosity of a mixture of large and small particles is less than the linear combination of the porosities of the pure components.

(iii) The mean grain diameter of a mixture does not predict its porosity.

(iv) A porosity minimum is always observed for some combination of two components in the mixtures. The minimum theoretically occurs when small particles completely fill the voids of the load bearing larger particles.

Riverbed materials typically consist of grain of different sizes. The difference in grain size influences the packing behavior and consequently affects the porosity of riverbed materials. It has been established that the porosity decreased when the sorting became poorer (Kolterman and Gorelick, 1995) and varied with the skewness (Alberts, 2005). Many real particle systems are of continuously distributed sizes. Such systems have often the distributions that resemble either Gaussian or lognormal distributions by weight. Sohn & Moreland (1968) conducted several experiments on such continuous size distributions and reported that an increase in the range of grain size, equivalent to poorer sorting, caused the porosity to be lower. They found that binary mixtures of continuous distributions showed the porosity trend similar to binary mixtures of uniform sizes, although the porosities were somewhat higher for larger ratios. Alberts (2005) evaluated the effects of sorting and skewness of the weight distribution on the porosity of sediment mixtures and indicated a slight trend of decreasing porosity with poorer sorting, while the result showed the lowest porosities for a slight positive skewness.

In previous riverbed deformation calculations, engineers or researchers conventionally assumed that the porosity of riverbed material was a constant (0.3-05), regardless of whether the grain sizes of the riverbed material were uniform. Since there was no doubt that the porosity depended on the particle size distribution, fixing the porosity at a constant value was inadequate for simulating practical sediment movements, such as the removal of fine material out of the riverbed material or the deposition of fine material into voids between the coarse material (Hirano, 1971). Voids in a riverbed material themselves are also important as habitat for aquatic biota, such as fishes and insects, and the effects of void changes due to sedimentation on the riverbed environment have been widely investigated (e.g., Erman & Ligon, 1988, Wood & Armitage, 1997, Yamada & Nakamura, 2002). Not only natural sediment transport phenomena, such as floods and
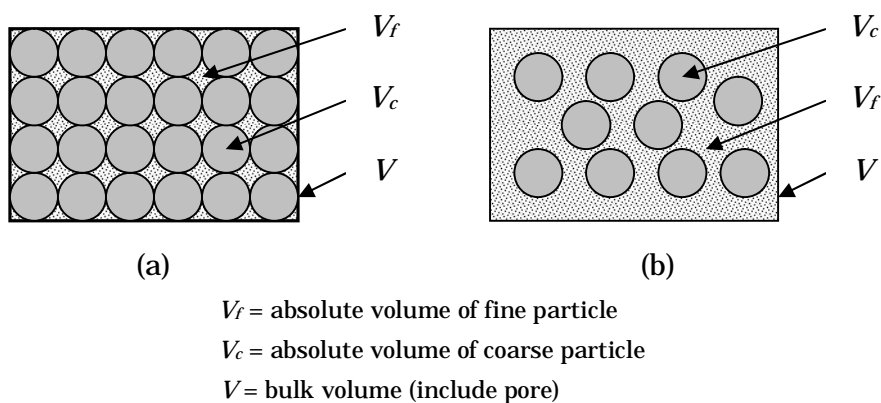
debris flows induced by heavy rainstorms, but also artificial impacts, such as the construction of dams or sediment flushing from reservoirs, seriously affect the voids in the riverbed. To manage both of sediment controls and ecological conservation in an integrated manner throughout an entire river system, it is essential to consider the changes in the voids of the riverbed material. The relationship between porosity and particle size distribution has been studied in the research field on powder technology (Standish and Borger, 1979, Yu and Standish, 1993). A simulation method for the random packing of spherical particles has been developed to calculate the void ratio and the co-ordination number of fine powders (Suzuki & Oshima, 1983). In this model, the coordination number, which was the number of contact points on a particle, was estimated from uniform size particle data, the fractional number of fine particles and the particle diameter ratio. However, in these packing simulation methods, the particle sizes were limited to several discrete components, and the procedure to determine where a particular particle was to be placed was complicated. Many granular materials had a spread of particle sizes that was well described by a lognormal distribution function (Cumberland and Crawford, 1987). A computer simulation of random packing of spheres with lognormal distribution has been developed by Nolan and Kavanagh (1993). The model could produce randomly pack lattices consisting of spheres, which obey the lognormal distribution with absolute standard deviations of 0 to 0.84. However, in this simulation, the standard deviations were limited to less than 1.0. Sediment mixtures of riverbed materials usually had different types of grain size distribution as described in Chapter 3. Thus, the methods to estimate the porosity of sediment mixtures for different types of grain size distribution are necessary.

In this chapter, some methods for estimating the porosity of sediment mixtures for different types of grain size distribution are presented. Firstly, the porosity of binary mixtures is analyzed. Secondly a simulation method

for estimating the porosity for different types of grain size distribution is described. Thirdly, a measurement method for obtaining the porosity of actual sediment mixtures is introduced. Finally, a relation between the porosity and the characteristic parameters of grain size distribution obtained in Chapter 3 is indicated.

4.2 Porosity of Binary Mixtures

There are two types of particle packing in binary mixtures, namely "coarse packing", in which the smaller particles are contained in the pore space created by larger particles (Fig.4.1(a)) and "fine packing", in which the larger particles are dispersed in a fine-grained matrix (Fig.4.1(b)). The porosity of binary mixtures is obtained on the assumption of "ideal packing". The ideal packing model is based on the concept of filling the pores between the large spheres with small spheres, that is, only one type of particle packing (coarse or fine) occurs at a time and each particle type does not disturb the packing of the other particle type. The condition and quantitative porosity of each packing is described below.

V_f = absolute volume of fine particle
V_c = absolute volume of coarse particle
V = bulk volume (include pore)

Fig.4.1 Mixing of two particles groups: (a) coarse packing and (b) fine packing

4.2.1 Coarse packing

In coarse packing, the finer particle group occupies uniformly the pores of the coarser particle group beforehand laid with a normal porosity λ_{sc} (0.35 to 0.4). It is assumed that the difference between two sizes is so large that the filling never disturbs the structure of coarser particle composition. The porosity of coarser particle group, therefore, does not change. Also, the porosity of finer particle group is λ_{sf}. To satisfy the above condition, the grain size of finer group must be thoroughly smaller than the void scale of coarser group. The condition and porosity of coarse packing can be expressed by Eq. (4.1) and Eq.(4.2) as follows;

$$V\lambda_{sc} \geq \frac{V_f}{1 - \lambda_{sf}} \tag{4.1}$$

$$\lambda = \frac{V - \left(V_c + V_f\right)}{V} \tag{4.2}$$

where V = total bulk volume, V_f = absolute volume of fine particle, V_c = absolute volume of coarse particle, λ = total porosity of mixtures, λ_{sf} = normal porosity of uniform fine particle, λ_{sc} = normal porosity of uniform coarse particle.

The mixing ratio of finer particle group, p, is

$$p = \frac{V_f}{V_c + V_f} \tag{4.3}$$

Absolute volume of coarse particle is as follows:

$$V_c = V\left(1 - \lambda_{sc}\right) \tag{4.4}$$

From Eq. (4.3) and (4.4), absolute volume of fine particle is written as:

$$V_f = \frac{pV_c}{1 - p} = \frac{p}{1 - p}V\left(1 - \lambda_{sc}\right) \tag{4.5}$$

Substituting Eq.(4.5) into Eq.(4.1), the condition of coarse packing become as follows:

$$p \leq \frac{\lambda_{sc}\left(1 - \lambda_{sf}\right)}{\left(1 - \lambda_{sc}\lambda_{sf}\right)} \qquad (4.6)$$

Substituting Eq.(4.4) and Eq.(4.5) into Eq.(4.2), total porosity of the mixture is expressed as:

$$\lambda = \lambda_{sc} - \frac{p}{1 - p}\left(1 - \lambda_{sc}\right) \qquad (4.7)$$

If $\lambda_{sc} = \lambda_{sf} = \lambda_s$, from Eq.(4.6), the condition of the coarse packing is written as:

$$p \leq \frac{\lambda_s}{\left(1 + \lambda_s\right)} \qquad (4.8)$$

The porosity of mixture for coarse packing is as follows:

$$\lambda = \lambda_s - \frac{p}{1 - p}\left(1 - \lambda_s\right) \quad \text{for} \quad p \leq \frac{\lambda_s}{\left(1 + \lambda_s\right)} \qquad (4.9)$$

4.2.2 Fine packing

In case of fine packing, the coarser particles scatter in the finer particle layer beforehand laid with a normal porosity λ_{sf} (0.35 to 0.4). The volume outside of the volume of coarse particle is absolute volume of finer particle. Thus the porosity of the mixtures is same as to the porosity of finer fraction.

From Eq.(4.6), the conditions of fine packing can be expressed by using following relation:

$$p \geq \frac{\lambda_{sc}\left(1 - \lambda_{sf}\right)}{\left(1 - \lambda_{sc}\lambda_{sf}\right)} \qquad (4.10)$$

If $\lambda_{sc} = \lambda_{sf} = \lambda_{s}$,

$$p \geq \frac{\lambda_{s}}{(1 + \lambda_{s})} \qquad (4.11)$$

The total bulk volume is expressed as:

$$V = V_{c} + \frac{V_{f}}{1 - \lambda_{sf}} \qquad (4.12)$$

As the void volume contained in the bulk volume is equal to the void volume of fine particles, the following equation is obtained.

$$\lambda V = \frac{V_{f}}{1 - \lambda_{sf}} \lambda_{sf} \qquad (4.13)$$

$$\lambda = \frac{V_{f}}{V} \frac{\lambda_{sf}}{1 - \lambda_{sf}} \qquad (4.14)$$

The total bulk volume of the mixture can be expressed as follows:

$$V = \frac{1 - p}{p} V_{f} + \frac{V_{f}}{1 - \lambda_{sf}} \qquad (4.15)$$

Substituting Eq.(4.15) into Eq.(4.14), the porosity of fine packing is obtained as follows:

$$\lambda = \frac{p\lambda_{sf}}{1 - \lambda_{sf}(1 - p)} \qquad (4.16)$$

4.2.3 Application

The porosity of binary mixtures is calculated in the case of $\lambda_{sc} = \lambda_{sf} = 0.4$. The result is shown in Figure 4.2. The porosity of binary mixtures depends on the fractional concentrations of each particle size population and the minimum porosity exists. For binary mixtures in this case, the minimum porosity is 0.16 and occurs when the proportion of fine particle is 0.286. This minimum value appears when fine particle completely fill the voids of coarse particles.
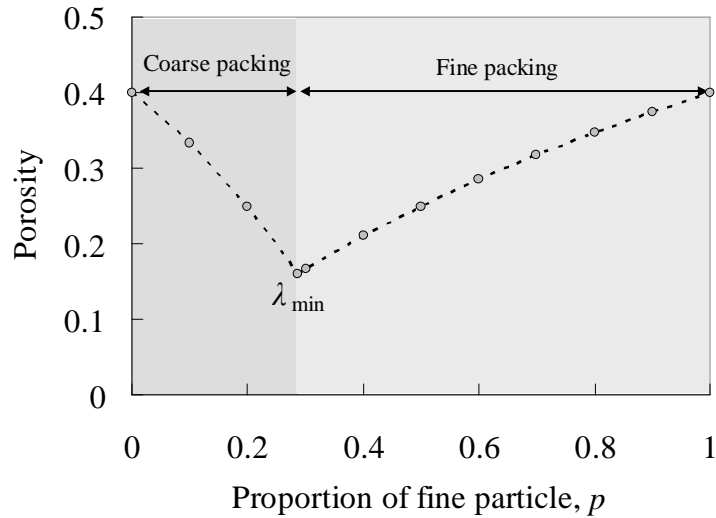
Fig.4.2 Porosity of binary mixtures in the case of $\lambda_{sc}=\lambda_{sf}=0.4$.

4.3 A Simulation Method for Estimating the Porosity of Sediment Mixtures

Tsutsumi, Fujita and Sulaiman (2006) have developed a numerical method for packing spheres in a vessel to obtain the porosity of mixtures of spherical particles. The sizes of packed particles and the packing order were determined from the grain size distribution using random numbers. The particles were placed in the lowest position available in the vessel. The porosity of the particle mixtures depended on not only the grain size distribution but also the compaction degree. However, the compaction degree could not be intentionally controlled in the model. As a result, in the simulation, the compaction degree was given. The defect of this method was that it takes too much time to fill the particles with a wide grain size distribution in a vessel. For such wide distribution, it is practical to use a measurement method for actual sediment mixtures. The simulation procedure, the results, and the evaluation of the model are described in this section.

4.3.1   Simulation method

The simulation model involves four stages: a) preparing a set of random numbers, b) calculating the particle diameter according to the specified particle size distribution for each random number, c) packing the particle into a hypothetical vessel, and d) calculating the volume of voids. The following sections describe each stage in detail.

(1)   A set of random numbers

In the first stage of the simulation model, a set of random numbers between 0.0 and 1.0 is prepared to determine the diameters of particles that will be packed into a hypothetical vessel. The "*RAND*" function in MS Excel software will produce a set of random numbers. A sample set of random numbers is shown in Table 4.1. The random numbers used to determine the diameter have fourth decimal place to give the wider variation of random number and reduce the probability of duplication number. If the decimal place is smaller, the range of random number becomes narrower and the duplication number will easily occur.

(2)   Calculating particle diameters

The grain size distribution of actual riverbed material can be generally approximated by a statistical function (e.g., normal distribution, lognormal distribution, etc). In this simulation model, a dataset of particle diameters that corresponds to any grain size distribution function can be calculated using the set of random numbers shown in the previous section. An example using a lognormal distribution function (Eq.4.17) and the procedure for obtaining the particle diameter d_n corresponding to the given value p_n for $\sigma_L = 0.5$ and $d_{mg} = 0.002$ m is shown in Figure 4.3. For given random number

p_n = 0.4439, the corresponding diameter d_n = 1.972 is obtained by using bisection method.

$$f(d) = \frac{1}{\sqrt{2\pi}\,\sigma_L d}\exp\left[-\frac{\left(\ln d - \ln d_{mg}\right)^2}{2\left(\sigma_L\right)^2}\right]$$ (4.17)

Table 4.1 An example of a set of random values used to determine the diameters of particles before packing into a hypothetical vessel (k is the particle number, p_k is the generated random value).

Particle No. k	Random number p_k [-]	Particle No. k	Random number p_k [-]
1	0.9010	7	0.4033
2	0.2916	8	0.3922
3	0.5387	9	0.6068
4	0.0399	…	…
5	0.3808	n	0.4439
6	0.3068	…	…
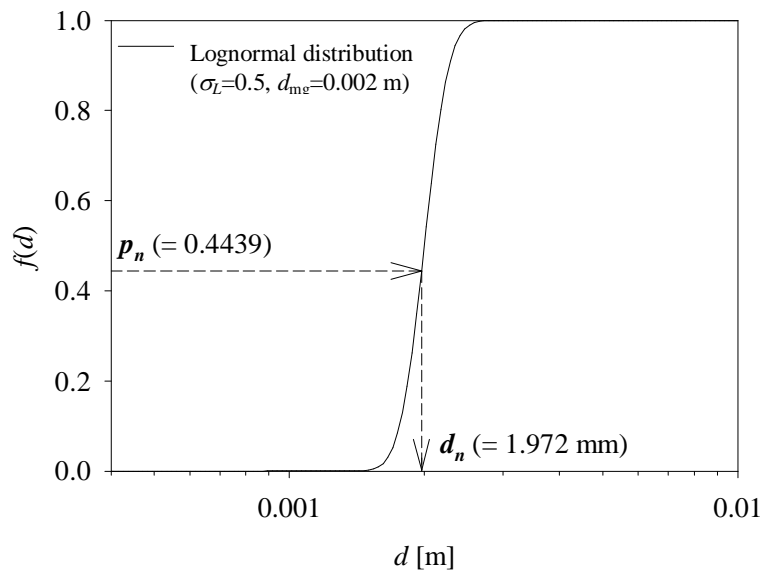
Fig.4.3 An example of the particle size distribution represented by the lognormal distribution function and the procedure for obtaining the particle diameter corresponding to a given value p_n.

(3) Particle packing

A hypothetical cubic vessel, described by dashed-lines in x, y and z coordinates, as shown in Figure 4.4, is prepared for particle packing. The length of the cube, L_v, is given as:

$$L_v = r_d d_{max}$$

(4.18)

where, d_{max} = the maximum diameter of the prepared particles, and r_d = a multiple number.

The particles prepared for packing, as described in the previous section (shown in Figure 4.4(a)), are placed into the hypothetical vessel one by one according to the following packing rules:

(i)   The center of the 1st particle is placed on the origin of the coordinate axes (Fig. 4.4(b)).

(ii)   The center of the 2nd particle is placed on the x-axis so that the particle contacts the 1st particle (Fig. 4.4(c)).

(iii) The center of the 3rd particle is placed on the x-y plane so that the particle contacts the 1st and 2nd particles (Fig. 4.4(d)).

(iv)   The center of nth particle is placed in the lowest position available where it contacts three other fixed particles, or at any available position on the x-y plane where it contacts two other fixed particles (Fig. 4.4(e)).

(i)   If the nth particle overlaps a previously positioned particle, that point is excluded.

(vi)   If the nth particle is placed $d_{max}/2$ away from the sidewalls or bottom plane of the vessel ($x < -d_{max}/2$, $x > L_v + d_{max}/2$, $y < -d_{max}/2$, $y > L_v + d_{max}/2$, $z < 0$), that point is excluded, where d_{max} is the diameter of the largest particle among all those prepared.

(vii) If the nth particle is placed $d_{max}/2$ away from top of the vessel ($z >$ $L_v+d_{max}/2$), the packing simulation terminates.

(4) Calculating the volume of voids

The volume of voids is obtained by subtracting the volume of particles from the volume of the vessel, V_t, given by

$$V_t = L_v^{3}$$
(4.19)

The volume of particles included within the vessel is calculated as follows:

(i)   If the entire particle k is included within the vessel (Fig. 4.5(a)), the volume of particle V_k is,

$$V_k = \frac{\pi}{6} d_k^{3}$$
(4.20)

(ii)   If only a portion of the particle k is included within the vessel (Fig. 4.5 b ,(c),(d)), the volume of the portion that is cut by the vessel walls is calculated analytically, considering the x, y, and z coordinates of the center and the diameter d_k of the particle.

The total volume of the particles that are included within the vessel, V_p, is obtained as,

$$V_p = \sum_k V_k$$
(4.21)

Then, the porosity λ is calculated as,

$$\lambda = \frac{V_t - V_p}{V_t}$$
(4.22)
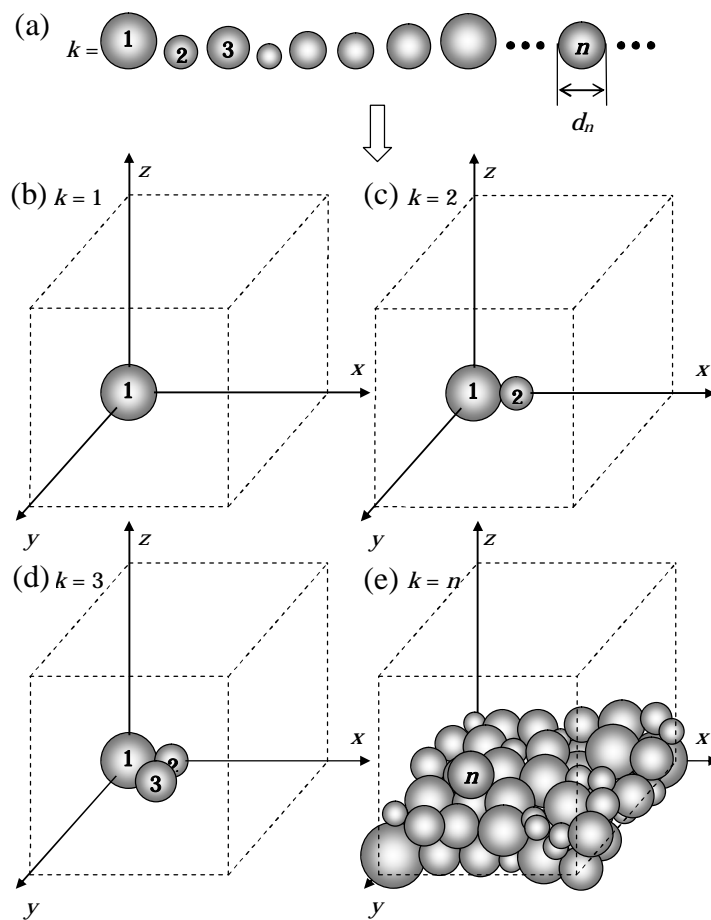
Fig.4.4 Particles whose diameters are previously determined are placed into a hypothetical vessel one by one, until no space remained in the vessel (Tsutsumi, Fujita and Sulaiman, 2006).
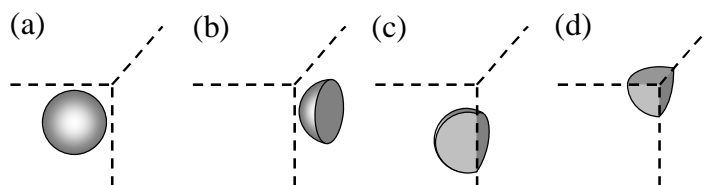
Fig.4.5 Classification of particle position for calculating the particle volume included within the hypothetical vessel (Tsutsumi, Fujita and Sulaiman, 2006).

4.3.2 Model assessment

To assess the validity of the simulation model, a laboratory experiment was conducted. A schematic diagram explaining the experiment is shown in Figure 4.6 and the procedure of experiment is described below:

(i) Spherical glass beads with six different diameters (i.e., 0.2, 0.4, 0.6, 0.8, 1.0, and 2.0 mm) are prepared and mixed well to form six different kind of particle size distributions. The mixing ratios of the different-sized particles to form the six particle size distributions are shown in Table 4.2 and the grain size distribution of these particle mixtures are shown in Figure 4.7.

(ii) The 100 ml glass cylinder with 28 mm of diameter and 233 mm height is prepared and the initial weight (W_1) is measured.

(iii) Then, the mixing particles are filled into the cylinder 3 times and the material was compacted by repeatedly dropping the cylinder from around 20 mm high.

(iv) The total bulk volume (V_t) of particle mixtures is recorded.

(v) Total weight of cylinder including particle mixtures (W_2) is recorded to calculate the total volume of particle mixture.

(vi) The total volume of the particle mixtures in the cylinder, V_p, is obtained as,

$$V_p = (W_2 - W_1)/\rho_p \qquad (4.23)$$

where ρ_p= density of the glass bead = 2.5×10^3 kg/m³

(vii) Then, the porosity is calculated as,

$$\lambda = \frac{V_t - V_p}{V_t} \qquad (4.24)$$
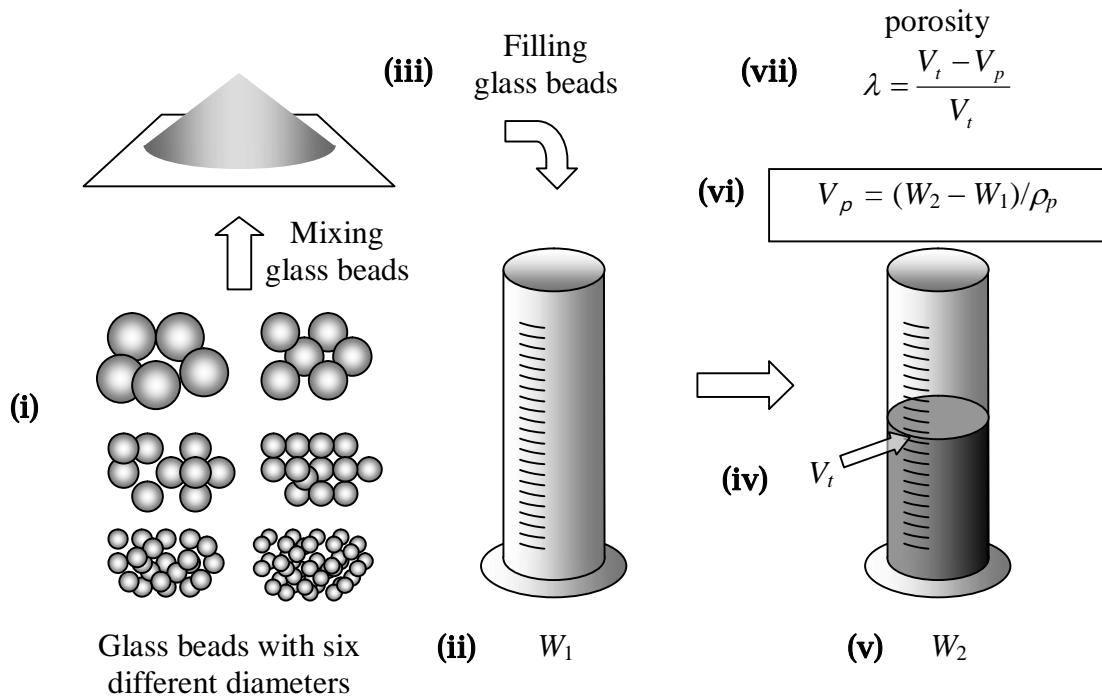
Fig.4.6   A method used in the particle packing experiments conducted to assess the validity of the simulation model (Tsutsumi, Fujita and Sulaiman, 2006).

The porosities obtained in the particle-packing experiment for the six different particle size distributions listed in Table 4.2 are shown in Table 4.3 and the mean porosities of five repetitions are shown in Figure 4.8 (filled circles ●). The error bars indicate the ranges between maximum and minimum values of five repetitions. The porosity varies with the particle size distribution. The porosity decreases as the particle size distribution changes from No. 1 to 6, that is, from a uniform distribution to a wide distribution. The lowest value of the porosity is 0.278 for sample No. 6. It can be shown analytically that the porosity of densely packed spherical particles with a uniform diameter is 0.28. However, the experimental result using glass beads with a uniform diameter is 0.35 (sample No. 1). This discrepancy likely arises from the minor difference in the size of the glass beads, although they are meant to be of uniform particle size.

Table 4.2 Mixing ratio of the six different sized-particles (vol%).

d [mm]	Number of particle size distribution					
	1	2	3	4	5	6
0.2	---	---	---	---	---	16.6
0.4	---	---	---	---	20.0	16.6
0.6	---	---	---	25.0	20.0	16.7
0.8	---	---	33.3	25.0	20.0	16.7
1.0	---	50.0	33.3	25.0	20.0	16.7
2.0	100.0	50.0	33.4	25.0	20.0	16.7
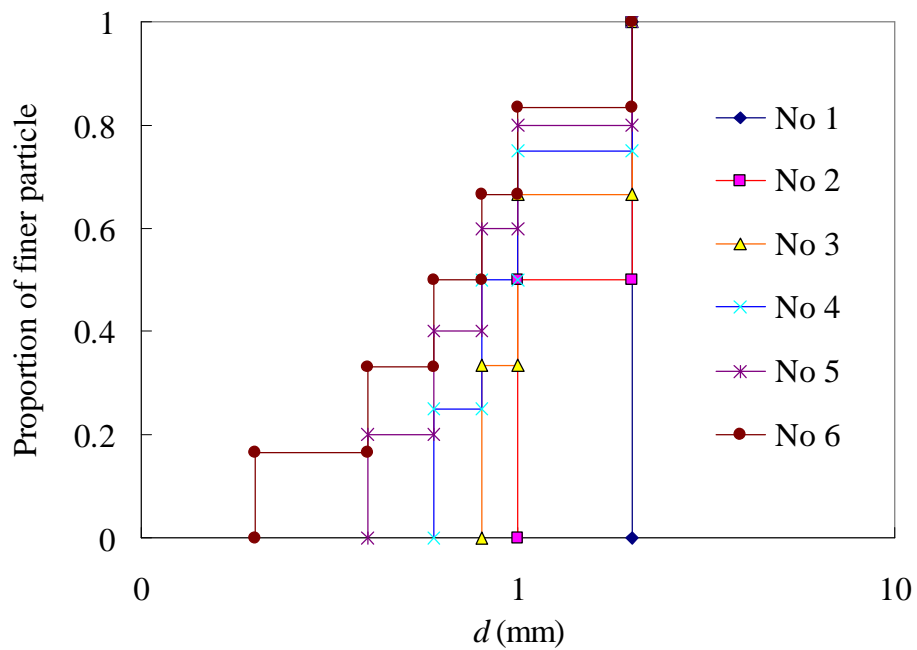
Fig.4.7 Grain size distributions of the six different particle mixtures used in the experiment.

Table 4.3 The porosities of the particle-packing experiment for the six different particle size distributions listed in Table 4.2.

Sample	No.1	No.2	No.3	No.4	No.5	No.6
λ	0.3521	0.3358	0.3375	0.3302	0.3150	0.2795
λ	0.3515	0.3396	0.3438	0.3250	0.3123	0.2740
λ	0.3498	0.3408	0.3421	0.3255	0.3101	0.2760
λ	0.3489	0.3388	0.3360	0.3248	0.3098	0.2798
λ	0.3514	0.3353	0.3396	0.3268	0.3187	0.2792
$\lambda_{average}$	0.3507	0.3381	0.3398	0.3265	0.3132	0.2777
λ_{max}-λ_{min}	0.0032	0.0055	0.0078	0.0054	0.0089	0.0058

The simulated porosities for the six different particle size distributions listed in Table 4.2 are shown in Table 4.4. The vessel size in each simulation is in proportion to the maximum diameter and the ratio, r_d, varies from 5.2 for sample No.1 to 1.7 for sample No.6. If the simulation for sample No.6 employs the same vessel that used for sample No. 1, much more particles must be packed in the vessel because No. 6 contains finer particles. The simulation under this condition needs much executing time. To save the executing time, for the wider distribution, the ratio of vessel size to maximum particle size must be set at a smaller value.

The mean porosities of five repetitions are also shown in Figure 4.8 (open circles ○) together with the experimental results. The simulated porosity of sample No. 1 ranges widely from 0.280 to 0.351, and the mean value differs from the experimental result. The widely variation of simulated porosity for sample No. 1 arises from the packing simulation procedure, as explained in Figure 4.9. An example is shown, where 10 particles are placed in the 1st layer and 2 particles in the 2nd layer. If the next particle is placed at position (a), it is still possible to form the densest packing. However, if the next particle is placed at (b), it will no longer be densest packing. In the former case, the porosity is close to 0.28 and in the later case, it must be larger than 0.28 up to 0.35.

The deviation of simulated porosity increases from sample No.2 to No.6. The variation may be due to the effect of vessel size. Using the smaller vessel, the simulation provides the wider variation in the packing particles formation, and consequently, the variation of calculated porosity becomes much larger.

Table 4.4 The porosities of the particle-packing simulation for the six different particle size distributions listed in Table 4.2.

Sample	No.1	No.2	No.3	No.4	No.5	No.6
r_d	5.2	3.2	3.2	2.7	2.2	1.7
λ	0.2803	0.3325	0.3354	0.3354	0.3266	0.2852
λ	0.3020	0.3387	0.3495	0.3419	0.3279	0.2949
λ	0.3507	0.3508	0.3428	0.3232	0.3206	0.2356
λ	0.3461	0.3477	0.3469	0.3306	0.2915	0.2422
λ	0.3445	0.3429	0.3498	0.3496	0.3280	0.2864
$\lambda_{average}$	0.3247	0.3425	0.3449	0.3362	0.3189	0.2688
$\lambda_{max}-\lambda_{min}$	0.0704	0.0183	0.0144	0.0264	0.0365	0.0593
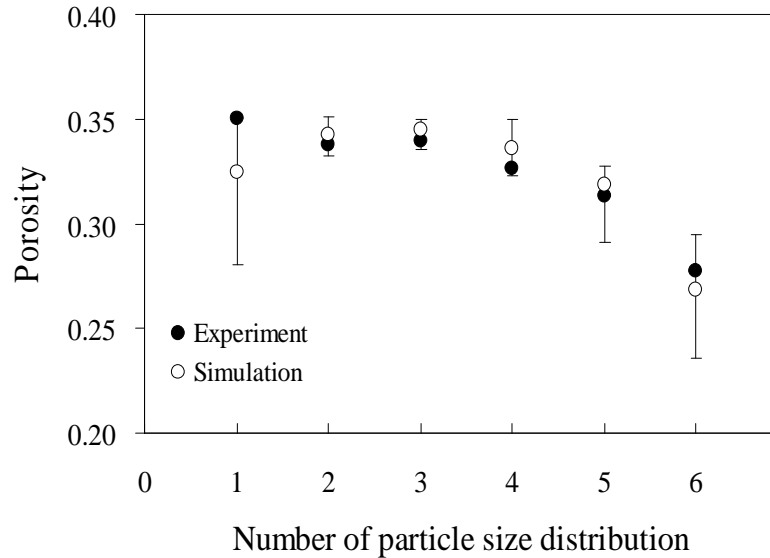
Fig.4.8 Comparison between the experimental and simulated results on the porosity for six different particle size distributions. Error bars indicate maximum and minimum of five repetitions of the experiments or simulations. (Tsutsumi, Fujita and Sulaiman, 2006)

Although there is a discrepancy between the experimental and simulated porosities for sample No. 1, there is a good agreement for samples No. 2 to No. 6. The discrepancy between the experimental and simulated porosities for sample No. 1 may be also due to the minor size differences mentioned above. The average error between the experimental and simulated mean porosities for sample No. 2 to No. 6 is 0.00672. These comparisons between the experimental and simulated porosities show the validity of the particle packing simulation model for obtaining the relationship between the particle size distribution and the porosity for spherical particles, except in the case of uniformly sized particles.
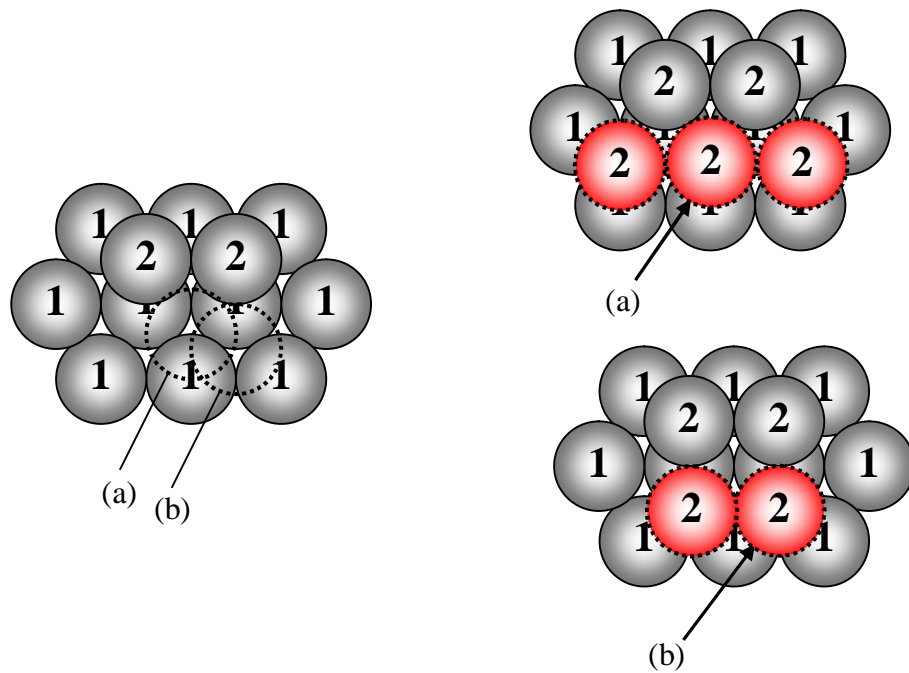
Fig.4.9 Difference in the particle arrangement for uniformly sized spherical particles. An example is shown (10 particles in the 1st layer and 2 particles in the 2nd layer). If next particle is placed at position (a), it is still possible to form the densest packing. However, if it is placed at (b), it will no longer be densest packing.

4.3.3 Simulation results

Actual sediment mixtures have various types of grain size distribution. This section presents the simulation results of particle packing model for lognormal, M-Talbot and bimodal distribution.

(1) Lognormal distribution

Granular materials with a spread of particle sizes are well described by a lognormal distribution function. In other words the weights of the particles are distributed normally with respect to the logarithms of the respective particle diameters. Some riverbed materials obey this distribution.

Porosity of particle mixtures with lognormal distribution was calculated using the particle packing simulation model for 11 different standard deviations of 0.01 to 1.5. The grain size distributions are shown in Figure 4.10. The simulated porosities are shown in Table 4.5. As the particle mixtures with a wider distribution contain the finer particles, the executing time for simulation becomes much larger. The vessel sizes for the wide distributions must be set at a smaller value to reduce the executing time. Therefore, $r_d(=L/d_{max})$ decreases with σ_L. For example, when $\sigma_L = 0.01$, $r_d = 4.9$, but when $\sigma_L = 1.5$, $r_d = 2.1$.

The relationship between the standard deviation, σ_L, and the simulated porosity, λ, is shown in Figure 4.11. If the standard deviation σ_L ranges between 0.01 and 0.1, the calculated porosity is about 0.38, which is close to 0.4 that is the porosity generally assumed in conventional riverbed deformation calculations. The mean value of the simulated porosity decreases from 0.374 to 0.156 as the standard deviation, σ_L, increases from 0.01 to 1.50. When the particle size is distributed over a wider range,

especially with standard deviation, σ_L, larger than 0.5, the simulated porosities are much smaller than 0.4. Takemon *et al.* (2003) reported that the porosity actually measured in a sandbar was to be 0.16 for a standard deviation of 0.054, supporting the small porosity obtained from the simulation. Those small values mean that the assumption of a constant porosity in riverbed material is inadequate for riverbed deformation calculations, if the particle size is distributed over a wide range.
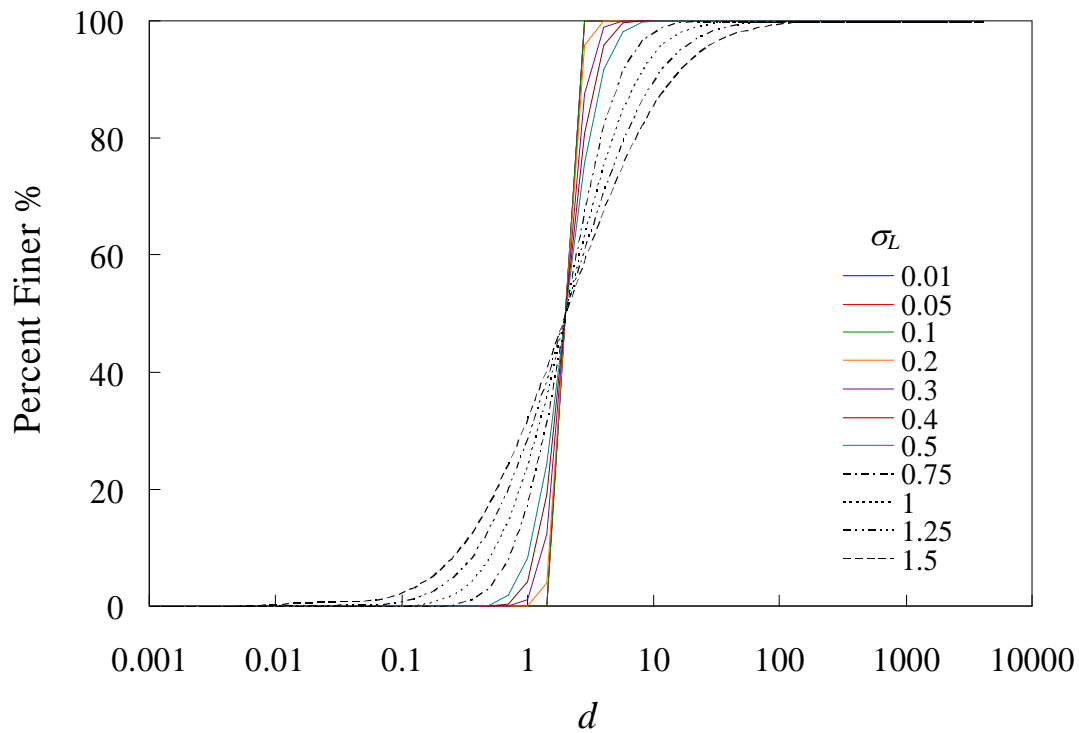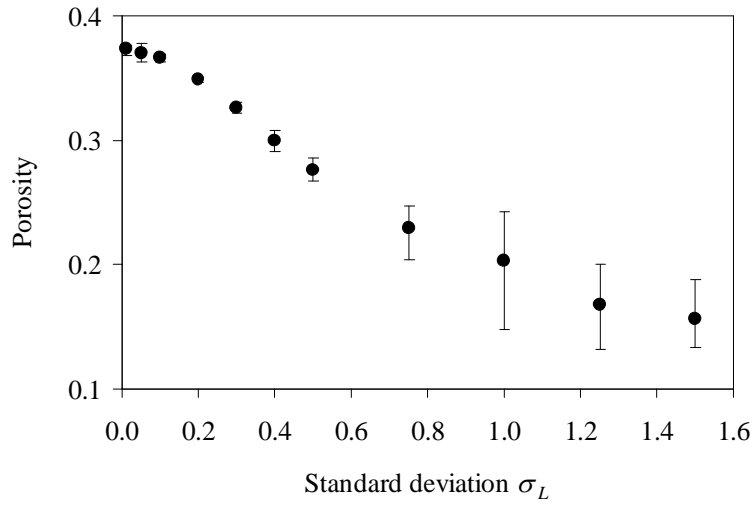

Fig.4.10 Grain size distribution of the lognormal distribution used in the simulation of particle packing.

Table 4.5   The porosities of the particle-packing simulation for the lognormal distributions shown in Figure 4.10.

η_L	0.01	0.05	0.1	0.2	0.3	0.4	0.5	0.75	1	1.25	1.5
d_{mg}	2	2	2	2	2	2	2	2	2	2	2
r_d	4.9	4.4	4.6	5.2	3.9	3.0	2.5	1.8	1.5	2.1	2.1
λ_1	0.376	0.368	0.363	0.351	0.326	0.303	0.275	0.240	0.228	0.192	0.188
λ_2	0.375	0.375	0.368	0.349	0.325	0.308	0.283	0.234	0.243	0.201	0.159
λ_3	0.368	0.366	0.363	0.347	0.322	0.291	0.268	0.222	0.176	0.170	0.166
λ_4	0.373	0.363	0.369	0.348	0.330	0.293	0.270	0.204	0.147	0.131	0.133
λ_5	0.375	0.378	0.369	0.349	0.327	0.304	0.286	0.247	0.221	0.145	0.134
λ_{avr}	0.374	0.370	0.366	0.349	0.326	0.300	0.276	0.229	0.203	0.168	0.156
λ_{max} -λ_{min}	0.008	0.015	0.006	0.004	0.008	0.017	0.018	0.043	0.095	0.069	0.055

Fig.4.11 Relationship between the standard deviation of the lognormal distribution, σ_L, and the porosity. Error bars indicate maximum and minimum of five repetitions of the simulations.

The deviation of simulated porosity increases when the standard deviations increase from 0.75 to 1.5. This deviation arises from the effect of vessel size as shown in Figure 4.12. Figure 4.12(a) shows the packing of particles with a small standard deviation in the vessel, whose size is much larger than the maximum diameter of particles. Figure 4.12(b) shows the packing of particles with a large standard deviation in the vessel, whose size is comparable to the maximum diameter of particles. If the standard deviation is small, the particle size ranges narrowly, while if the standard deviation is large, the particle size ranges widely. In the former case (Fig.4.12(a)), the possible variation of packing arrangement is small or the particles arrangement is relatively homogeneous and consequently the deviation of porosity is also small. In the latter case, the possible variation of packing arrangement is large and consequently the deviation of porosity is large.
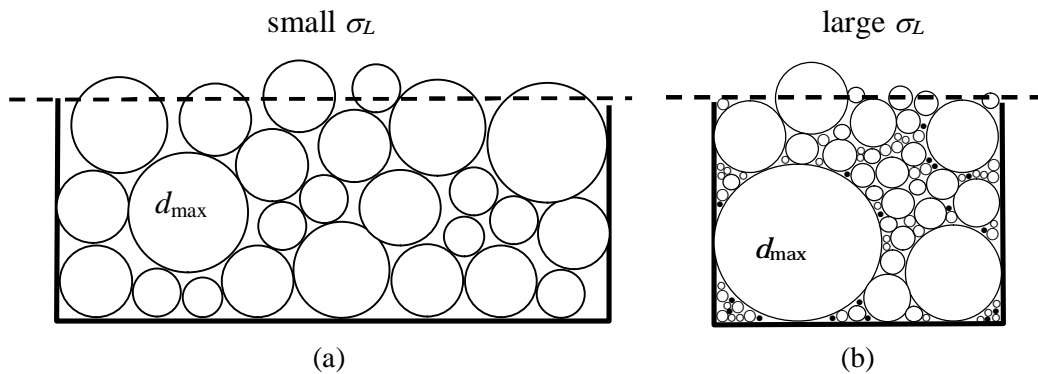
Fig.4.12 Effect of vessel size in the deviation of porosity; (a) particles with small standard deviation packed in the relatively large vessel, (b) particles with large standard deviation packed in the relatively small vessel.

(2) M-Talbot distribution

Porosity of the material whose grain size distribution is M-Talbot distributions with the parameters of Talbot number, n_T, and ratio of maximum and minimum sizes, d_{max}/d_{min}, is calculated by means of the packing model. A relationship between the value of Talbot number, n_T, and the calculated porosity is shown for d_{max}/d_{min} of 10 and 100   in Figure 4.13. The porosity increases from 0.241 to 0.314 for d_{max}/d_{min}=10 when the Talbot number, n_T, increases from 2 to 8. The porosity increases from 0.173 to 0.273 for d_{max}/d_{min}=100 when the Talbot number, n_T, increases from 4 to 12. The simulation for smaller ratio of d_{max}/d_{min} provides the higher value of porosity.
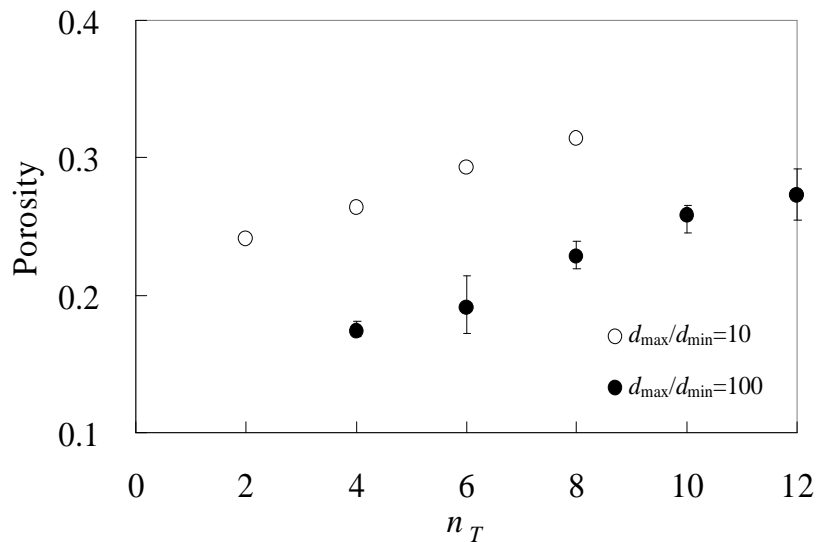
Fig.4.13   Relationship between the Talbot number of the   modified-Talbot distribution, n_T, and the porosity.

The important thing that can be seen in Fig.4.13 is that relationship has the same inclination for different ratio of maximum and minimum diameters. The reason is not clear, but the result is very useful to introduce into the bed variation models.

(3)　Bimodal distribution

A calculation of porosity by means of the packing simulation model needs much time　for a wide bimodal distribution. Considering the executing time, in this study, the simulation is conducted for rather narrow bimodal distribution. The characteristics of two materials A and B are shown in Table 4.6.　Porosities for seven different mixtures of A and B are estimated. The proportion of material A, p_A, is 0.0, 0.2, 0.25, 0.3, 0.5, 0.75 and 1. The relationship between the proportion, p_A, and the porosity for two materials mixtures is shown in Figure 4.14. The porosity of two materials mixtures depends on the fractional concentrations of each material. The result is compared with the porosity of binary particle mixtures (Eq.(4.9) and Eq.(4.16)). Interestingly, the changes of porosity with p_A for binary particle mixtures and binary mixtures are similar and a minimum porosity exists near a p_A of 0.2.

Table 4.6 Characteristic of two materials for bimodal distribution

Material	σ	d_{min} (mm)	d_{50} (mm)	d_{max} (mm)
A	0.2	0.5	1.0	2.0
B	0.2	2.0	4.0	8.0
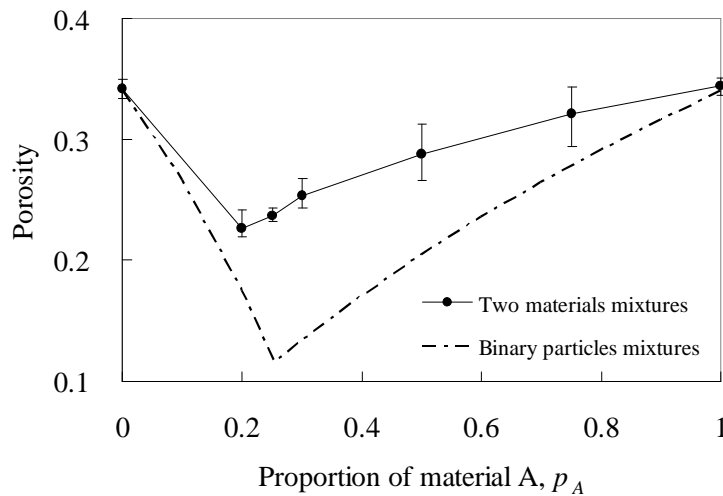
Fig.4.14　Relationship between the proportion of material A, p_A, and the porosity of the mixtures.

4.3.4 Voids within particles assembly

To visualize the void within the packed particles, the hypothetical vessel is cut by three horizontal cross-sections (Figure 4.15). Since it is difficult to visualize the 3-dimensional shapes of the voids within packed particles, the voids are drawn in 2-dimensions on this cross section. The open areas between the circles then substitute for the 3-dimensional shapes of the voids within the packed particles. The lognormal distribution is used and three standard deviations (σ_L = 0.01, 0.1, and 1.5) are used to simulate the particle packing; the results for each case are shown in Figure 4.16.
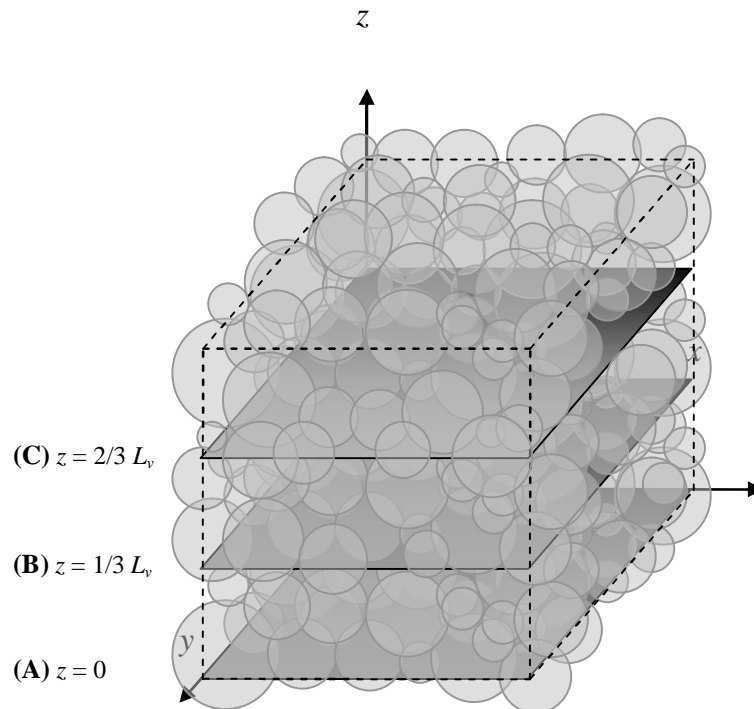
Fig.4.15 Schematic showing three horizontal cross-sections (A, B, and C) cutting the assembly of packed particles within the hypothetical vessel. (Tsutsumi, Fujita and Sulaiman, 2006)

In the case of σ_L = 0.01 (left column in Figure 4.16), the particle size is almost uniform and the particles are arranged systematically on the bottom

(cross-sections (A)). However, the small gaps between the circles cause the systematic arrangement on the cross-sections to be incomplete. Although the systematic arrangements of several particles still remain near the origin of the coordinate axes on the middle cross-section (B), other particles show random arrangements. The arrangement is no longer systematic on the upper cross-section (C), and a larger area is open between the circles.

In the case $\sigma_L = 0.1$ (middle column in Figure 4.16), the particle size shows a moderate distribution on the cross-section (A), and the arrangement of the particles is not systematic. The open areas between circles on the cross-section (A) are slightly larger than those in the case $\sigma = 0.01$, but on the upper cross-sections (B) and (C) they appear similar to those in the case of $\sigma_L = 0.01$.

In the case $\sigma_L = 1.5$ (right column in Figure 4.15), the particle size is distributed over a wide range on the cross-section (A), and the particle arrangement is completely random on every cross-section. The size of the open area seems to be similar to those in the two previous cases. However, the area occupied by the large particles reduces the open area on every cross-section. This reduction of the open area by large particles may contribute to the smaller porosity.

Although the open areas are only 2-dimensional, the tendencies mentioned above agree with the relationship between the particle size distribution and the porosity shown in Figure 4.11. Therefore, it confirms that the decrease in the porosity with increasing standard deviation, shown in Figure 4.11, is due to the reduction of the volume of voids by the large particles. It is also confirmed that if the mean diameter is identical, the size of voids seems similar, although the void ratio changes depending on the particle size distribution.
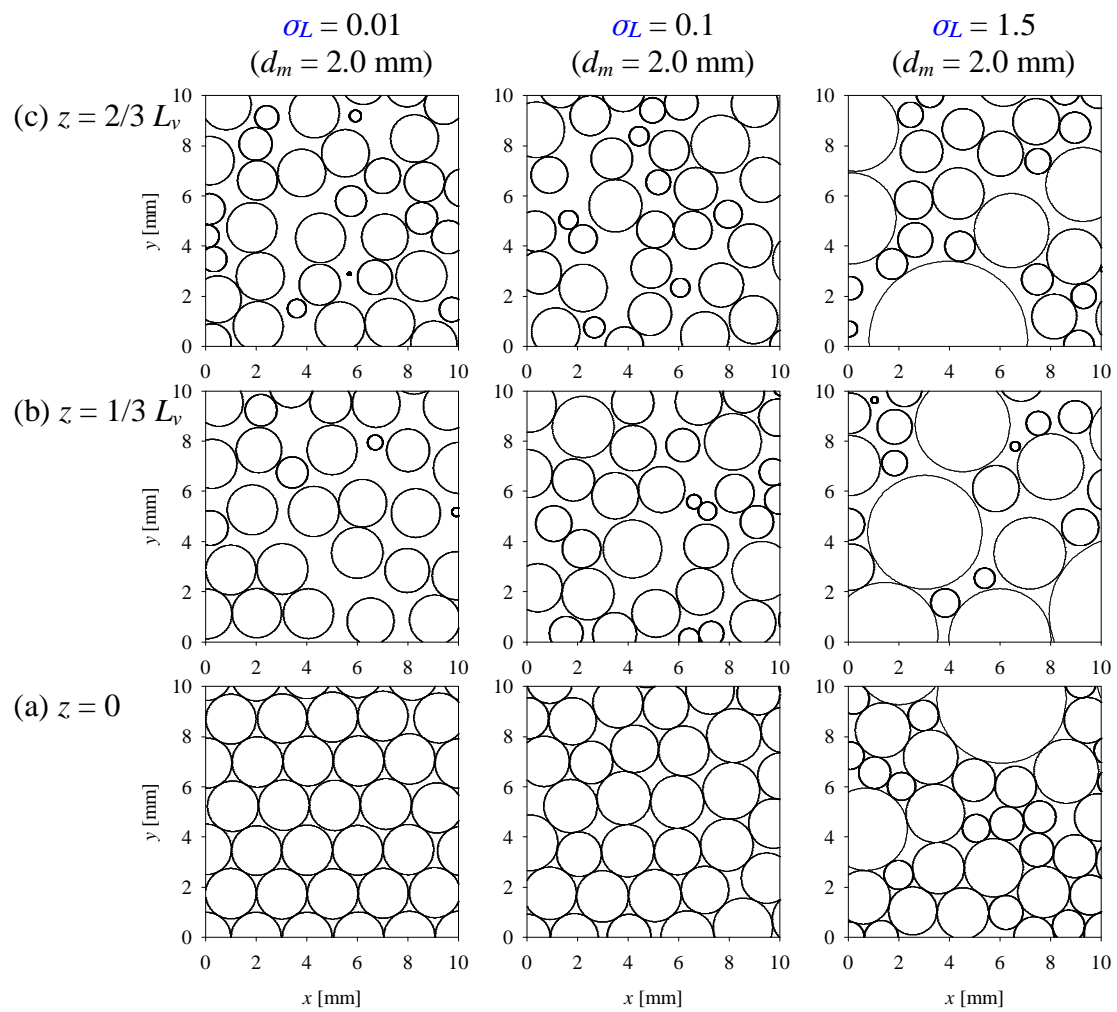
Fig.4.16 Cross sections of the packed particles simulated by the packing model. (Tsutsumi, Fujita and Sulaiman, 2006)

## 4.4 A Measurement Method for Estimating the Porosity of Sediment Mixtures

4.4.1 Previous studies

Methods for the measurement of gravel bed porosity were described by Carling and Reader (1982), Milhous (2002) and Gayraud and Philippe (2003). Carling and Reader (1982) explained the frozen sediment core sampling method. Milhous (2002) developed a simple method for measuring porosity below armor coats using a wooden frame and a plastic sheet. Gayraud and Philippe (2003) analyzed 99 frozen cores collected from 15 French streams to investigate the influence of grain size distribution and vertical bed packing on the interstitial habitat. However, the relation between the parameter of typical grain size distribution and the porosity was not described clearly.

4.4.2 A measurement method

Porosity is the most widely used parameter for assessing the interstitial space both in sediments and in soils. The porosity is normally defined as the ratio of the pore volume to the total volume of a given sample. The porosity can be calculated from the measured sediment volume based on a water displacement process. A schematic diagram explaining the measurement method of the porosity is shown in Figure 4.17. This is a simple method to determine the porosity. The technique is to measure the volume surrounding by a ring-frame and a sediment bed, before and after removal of the sediment sample from the bed below the ring-frame. The difference in the volumes is calculated as the total volume of the sample.
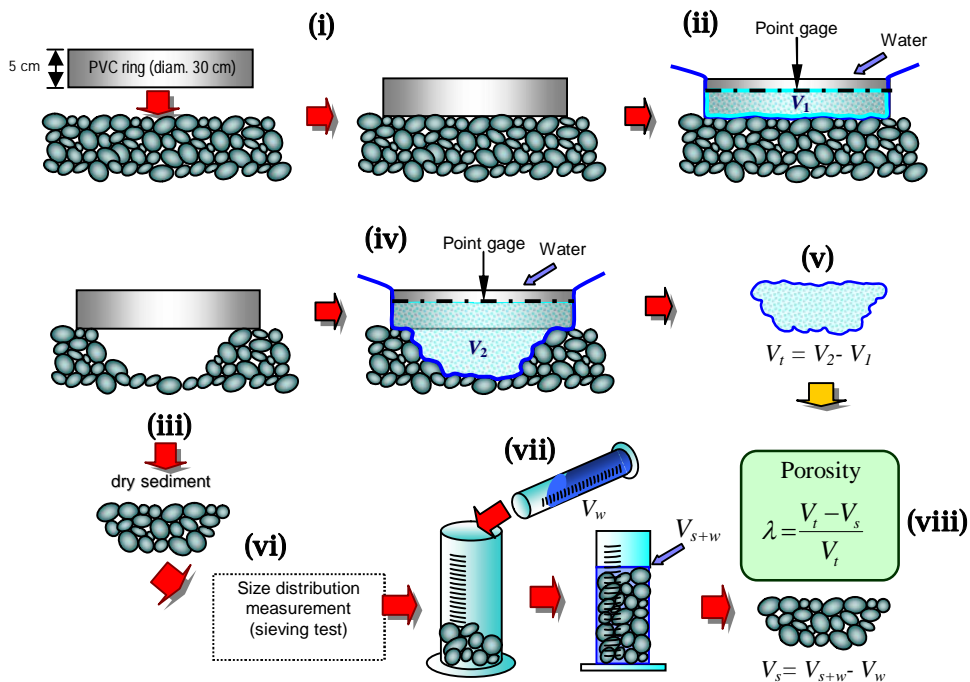
Fig.4.17   Schematic diagram explaining the measurement method
of the porosity.

A PVC (Polyvinyl Chloride) ring-frame with 30 cm of diameter and 5 cm of height is used. The equipments needed to measure the porosity are: a level, a point gauge, a vinyl sheet, 2000 cc cylinder, and vinyl bag. All the equipments can be carried in fields as well as laboratories (Photo 4.1).

(a) Laboratory experiment   (b) Field experiment

Photo 4.1   Equipments used for measurement of porosity.

The procedure for determining the porosity of a sediment sample in a laboratory or bed material in a field is as follows:

(i)   Set a PVC ring-frame horizontally in a stable position by using a level, on the sediment sample or riverbed material whose porosity is to be measured.

(ii) Determine the volume surrounding by the ring-frame and the bed below a datum (V_1); place adjustable point gauge (for laboratory experiment) or the tripod with adjustable point gauge (for field measurement) above the ring-frame to measure the water level. Place a plastic sheet inside of the ring-frame and fill the water up to the datum. Make a careful note of the volume of the water placed into the ring-frame (V_1). Remove the water from the ring-frame carefully without moving the ring-frame.

(iii) Remove the surface sediment of the sample or the surface bed material and carefully keep the ring-frame position. The hole should be as smooth sided as possible. The required sample size is not well known, but in this study, a reasonable result has been obtained when the sample size is between 3 and 5 kg. Retain the removed material for sieve analysis and measurement of the sediment volume.

(iv) Determine the volume of the hole dug after removal of the sediment or bed-material sample; place the plastic sheet inside of the ring-frame and fill the water into the hole and the ring-frame to the same datum as the first volume measurement (controlled by using the point gauge). The volume of the water must be determined during the process of filling (V_2).

(v)   Calculate the volume of the hole (V_t) by subtracting the initial ring-frame volume (V_1) from the hole plus ring-frame volume (V_2).

(vi) Dry the sample and measure its weight. The specific weight is calculated from the weight and the volume. Sieve the sample and determine the grain size distribution.

(vii) Measure the absolute volume of the sediment (V_s); the sediment sample is put into a cylindrical vessel and water is filled into the cylindrical vessel carefully up to a place marked on the inside of cylindrical vessel. Remove the air content in the sediment as much as possible during filling the water by shaking the cylindrical vessel. Note the total volume of sediment and water (V_{s+w}). Record the volume of water that filled into the cylinder (V_w). The volume of sediment (V_s) is calculated by subtracting the water volume (V_w) from the total volume of sediment and water (V_{s+w})

(viii) Calculate the porosity: $\lambda = \dfrac{V_t - V_s}{V_t}$

4.4.3 Laboratory experiment

A laboratory experiment is conducted to measure the porosity of sediment mixtures with different types of grain size distribution. Twenty one different kinds of grain size distributions are prepared; consisting of six lognormal distributions with different standard deviation (i.e., 0.02, 0.253, 0.29, 0.303, 1.23 and 1.6), five bimodal distributions and ten M-Talbot distributions. The characteristic parameters of two materials for bimodal distribution are shown in Table 4.7. A set of the proportions of material A, p_A, is 0.1, 0.2, 0.3, 0.4, and 0.5. The ratio of maximum and minimum diameters (d_{max}/d_{min}) and Talbot number, n_T, of the samples with M-Talbot distribution are shown in Table 4.8. The sediment mixtures with lognormal distribution and bimodal distribution are made of color sands and gravels. As for M-Talbot distribution sample, the materials are taken from the point bar of Uji River.

Table 4.7 Characteristic parameters of sediment mixtures for bimodal distribution.

Fraction	σ	d_{min} (mm)	d_{50} (mm)	d_{max} (mm)
A	0.2	0.5	1.0	2.0
B	0.2	2.0	4.0	8.0

Table 4.8 Talbot distribution parameters.

d_{max}/d_{min}	53	201	1129
n_T	1.2, 2.6, 6.0	2.5, 5.0, 8.0	2.5, 4.3, 4.9, 6.8

The procedure of the experiment in the laboratory is described below.

(i)   Each sediment sample is prepared and mixed well in a plastic box with 60 cm in length, 40 cm in width and 17 cm in height.

(ii)   Then, the mixed sediment is filled into the other plastic box. After each filling, the sediment mixture is scraped flat and compacted evenly by repeatedly dropping the wood cylinder from around 5 cm high. A wood cylinder with a diameter of 15 cm and a height of 10 cm and with a steel handle (total weight = 2.38 kg) is used to compact the material.

(iii) The porosity of material mixture is measured as described in the sub section 4.4.2.

(iv)   The grain size distribution and the porosity are measured five times for each sample.

The grain size distributions of the samples for lognormal, bimodal and M-Talbot distributions are shown in Figure 4.18, Figure 4.19 and Figure 4.20, respectively. Figure 4.18 shows the average observed distribution of six samples and those fitting curve by using lognormal distribution function with different standard deviation (i.e., 0.02, 0.253, 0.29, 0.303, 1.23 and 1.6). Figure 4.19 shows the average observed distribution of five bimodal distributions with different proportion of material A, p_A (i.e. 0.1, 0.2, 0.3, 0.4, and 0.5). Figure 4.20 shows the average observed distribution of ten samples and those fitting curves by using M-Talbot distribution function (Eq.(3.2)) with three different ratios of maximum and minimum diameters, d_{max}/d_{min}, (i.e. d_{max}/d_{min}=53 (Fig.4.20(a), d_{max}/d_{min}=201 (Fig.4.20(b)), and d_{max}/d_{min}=1129 (Fig.4.20(c)).
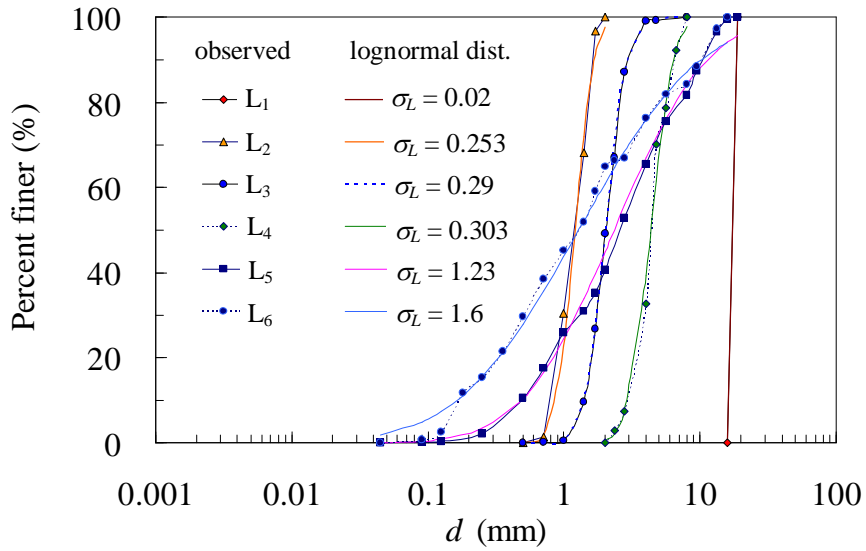
Fig.4.18 Average observed distribution of six lognormal distributions with different standard deviation and its fitting curve of each distribution by using lognormal distribution function.
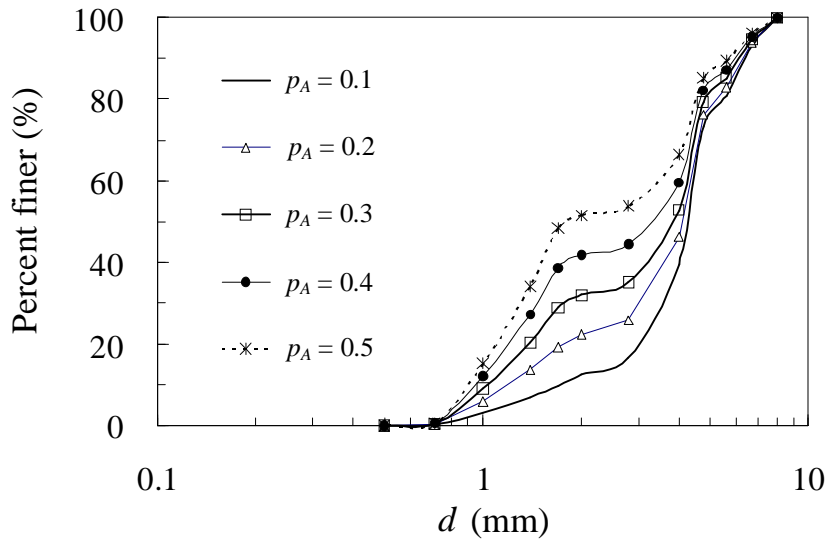
Fig.4.19 Average observed distribution of five bimodal distributions with different proportion of material A, p_A.
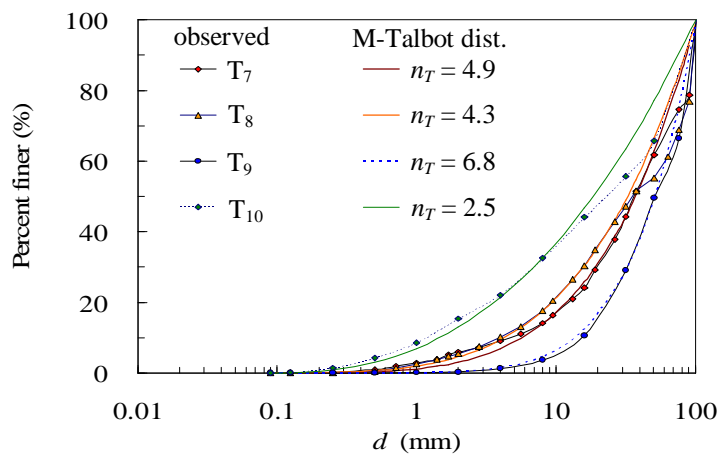
(a) $d_{max}/d_{min} = 53$

(b) $d_{max}/d_{min} = 201$
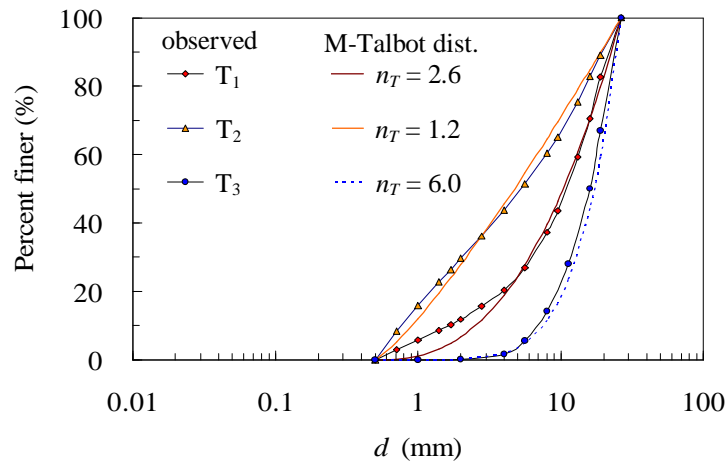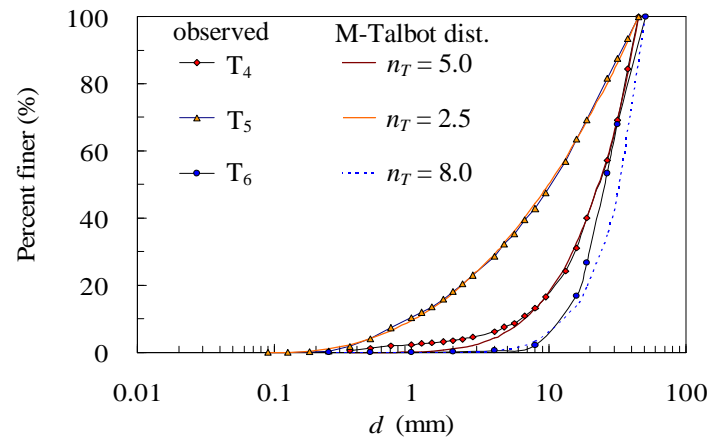
(c) $d_{max}/d_{min} = 1129$

Fig.4.20 Grain size distribution of the sample with M- Talbot distribution.

4.4.4 Relationship between grain size distribution and porosity

(1) Lognormal grain size distribution

The mean values of the measured porosity over five repetitions for six different lognormal grain size distributions (Fig.4.18) are shown in Figure 4.21. The simulation result on the relationship between the standard deviation of lognormal distribution and the porosity described in Section 4.3 is also shown in this figure. The error bars indicate the ranges between maximum and minimum values of five repetitions. The trend of porosity change with the standard deviation between the measurement and the simulation is almost similar. However, the measurement result is somewhat larger than the simulated one. The discrepancy may be due to the difference in the shape of particles, the compaction degree, and the inverse grading of the particles. Particularly in the measurement, it is very difficult to mix the sediment evenly. Consequently, the coarser particle lies at higher position than the finer particle. This inverse grading process makes the porosity larger, while in the simulation, the particles are mixed evenly. Thus, the particle packing in the simulation may be denser than the particle packing in the measurement. However, the diagram shown in Figure 4.21 is available for estimating the porosity of lognormal grain size distribution.

(2) Bimodal grain size distribution

Bimodal grain size distribution generally ranges widely. In this study, the artificial bimodal distributions with narrow distribution are used. The characteristic parameters of materials used in this experiment are shown in Table 4.7. These parameters are similar with the paremeters that used for particle packing simulation in Section 4.3.3. Porosities for seven different samples with proportions of material A, p_A, of 0.0, 0.1, 0.2, 0.3, 0.4, 0.5 and 1.0 are measured (sample with $p_A = 0.0$ and $p_A = 1.0$ are same with

lognormal distribution samples L_4 and L_3, respectively). Relationship between proportion p_A (by volume) of mixtures and the mean value of the five-measured porosity for binary mixtures are shown in Figure 4.22. The porosity of bimodal distribution depends on the percentage of each material in the mixture and a porosity minimum is observed.
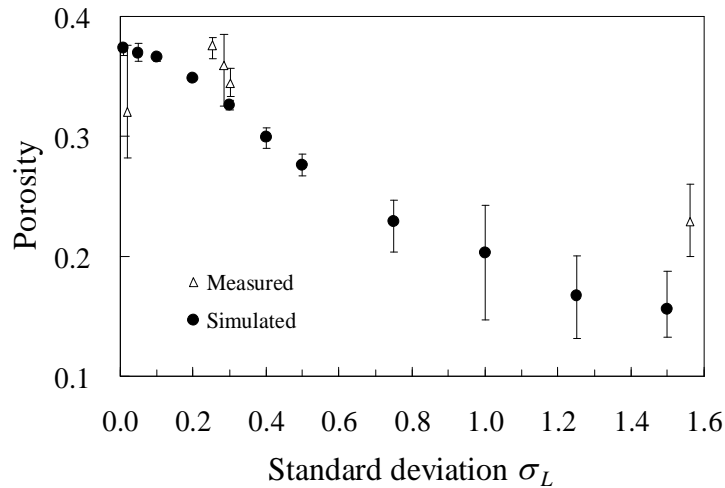

Fig.4.21   Comparison between the measured porosity and simulated porosity for lognormal distribution with different standard deviation.
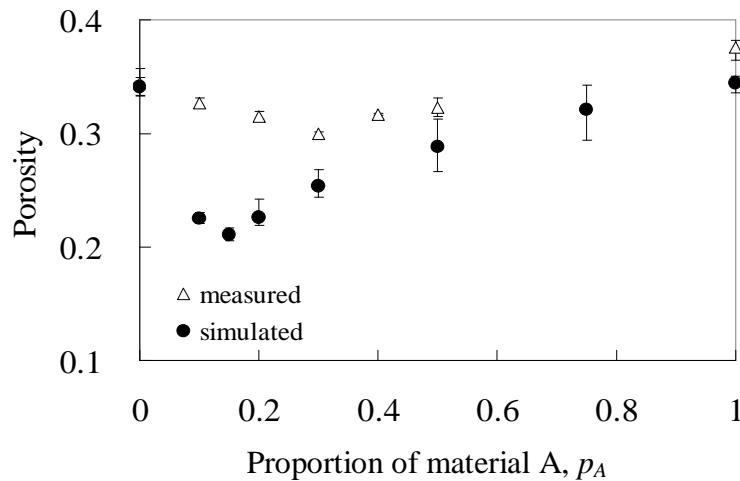
Fig.4.22   Comparison between the measured porosity and simulated porosity for bimodal distribution with different proportion of material A, p_A.

122

The results are compared with the mean value of the five repetitions of the simulated porosity for bimodal distribution by using particle-packing model. It is interesting that the minimum porosity appears for a percentage of finer material as in a binary mixture. The discrepancy between the measured and simulated porosity may be due to the differences in the uniformity of the mixtures of sediment sample and the packing of particle as illustrated in   Figure 4.23. In the simulation (Fig.4.23(a)), the particles are packed evenly in the vessel with dense packing. Consequently, the sediments are mixed uniformly in the vessel and the porosity becomes rather small. However, in the experiment (Fig.4.23(b)), due to the compaction, the coarse fraction lies at higher position and the finer fraction goes down to lower position. As each fraction has almost uniform distribution, the measured porosity is larger than the simulated one and close to the porosity for uniform sediment.
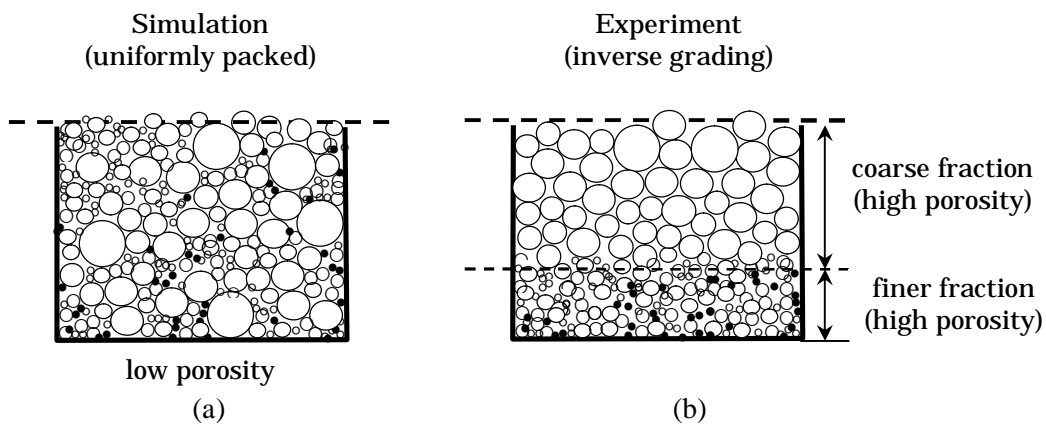
Fig.4.23   Differences in the uniformity of particles mixtures of bimodal distribution in simulation model (a), and experiment (b)

(3) M-Talbot grain size distribution

The mean values of measured porosities over five repetitions for ten different Talbot distributions (Fig.4.20) are shown in Figure 4.24. The relationship between the Talbot number, n_T, and the simulated porosity is also shown in Figure 4.24. Both of the simulation result and the measurement result show that the porosity increases with Talbot number and the ratio of maximum and the minimum grain sizes. However, the porosities in the simulation and the measurement are rather different for the same Talbot number and the same ratio of maximum grain size and minimum grain size. The reason of this discrepancy is also due to the differences in the shape of particles, the compaction degree, and grading of the particle as explained before. The porosity of Talbot distribution can be roughly estimated by means of Figure 4.24, but the more analysis by measurement and simulation is necessary to determine the relation more accurately.
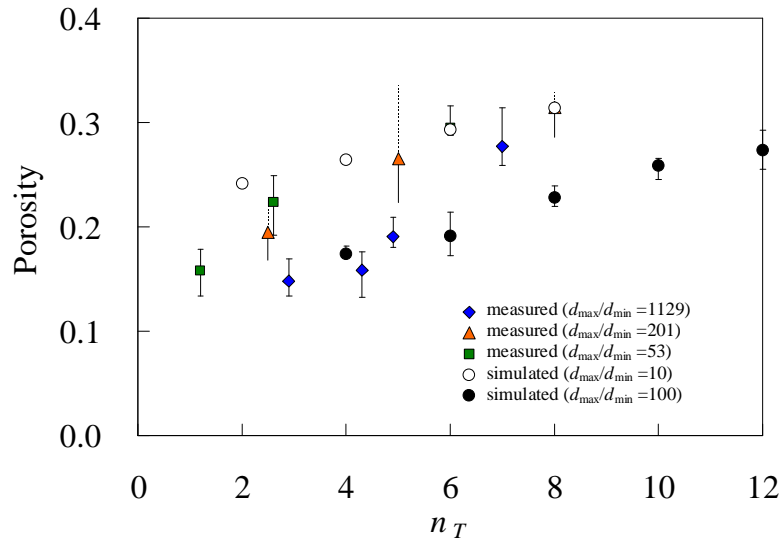
Fig.4.24 Comparison between the measured porosity and simulated porosity for Talbot distribution with different Talbot number.

4.5 Measurement of Actual Riverbed Porosity

4.5.1 Sampling location and riverbed condition

A field measurement technique is applied to obtain the porosity of surface layer and the sub-surface layer in a dry part of the streambed. The location of the field measurement is at a point bar of Uji River located in front of Ujigawa Open Laboratory, DPRI, Kyoto University (Figure 4.25). The condition of bed material is shown in Figure 4.26. The bed is vertically stratified with the coarse armor layer on the surface.

Fig.4.25   Location of field experiment for measuring the porosity of actual riverbed material; located at the point bar of Uji River in front of Ujigawa Open Laboratory, DPRI, Kyoto University (map from Google Earth).
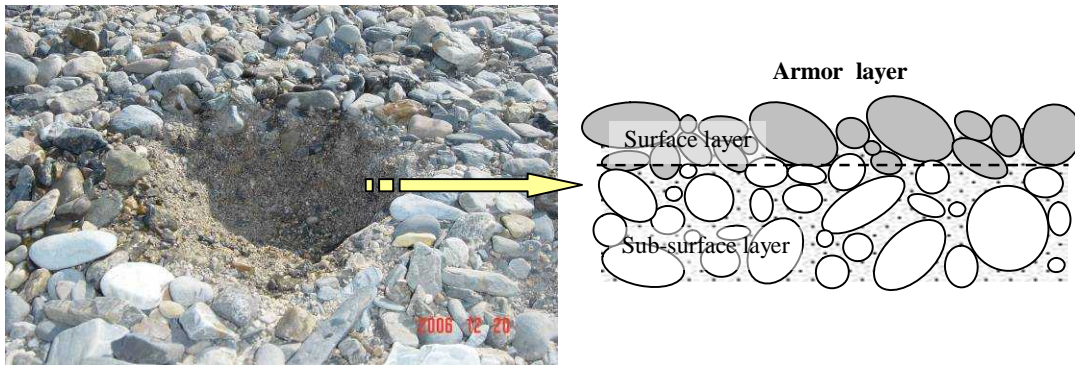
Fig.4.26   Condition of riverbed material at sampling location; the bed is vertically stratified with the coarse armor layer on the surface.

4.5.2 Field measurement in riverbed with armor coat

Measurement is conducted in the upstream part of the point bar at three different locations for surface and sub-surface material. The general process of porosity measurement in the field follows the procedure that described in sub section 4.4.2. The differences are the control of surface condition and the sampling of surface layer material.

(1)   Surface layer

As the surface layer usually consists of coarser material than the sub-surface layer, the outline of bed surface is rough (Figure 4.27(a)). On the other hand, the outline of surface of the sub-surface layer appearing after the removal of the surface layer is rather smooth (Figure 4.27(b)). If the surface sample is not sufficiently smooth, it misses the volume of voids between the surface particles and consequently the measured porosity of the surface layer becomes too small. In order to estimate the porosity of the sample adequately, the surface of the sample needs to be smooth as possible. One possible way to obtain this condition is the filling the space between particles in the surface layer with salt as shown in Figure 4.27(c). The conditions of bed surface material are shown in Photo 4.2.

126
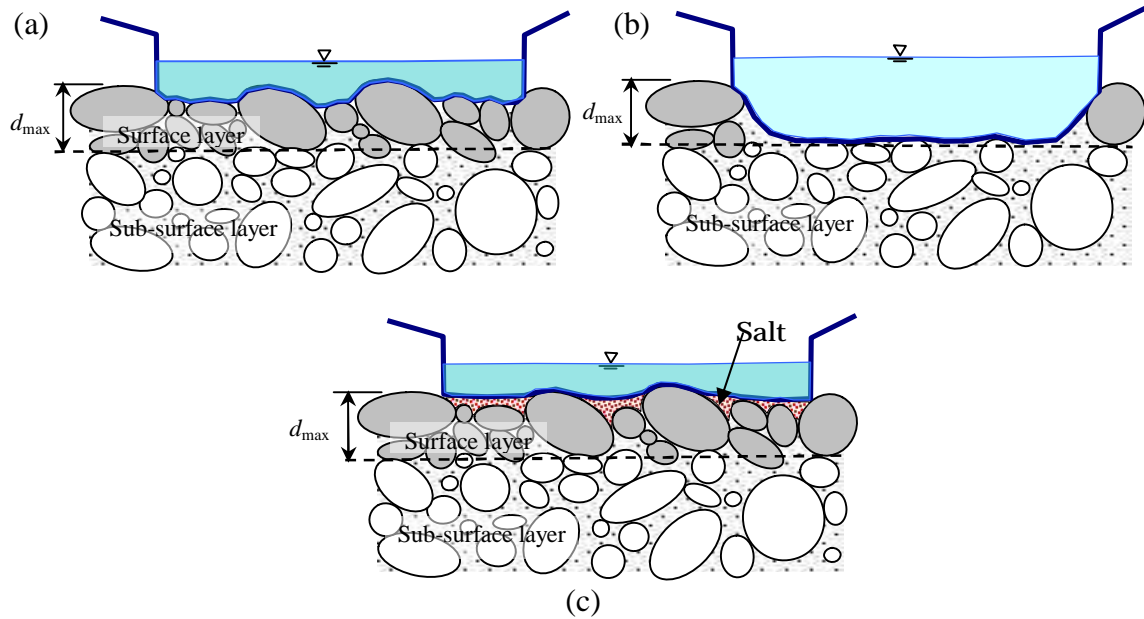
Fig.4.27 The outlines of bed material; (a) initial outline of bed surface (without salt), (b) outline of surface of the sub-surface layer (c) outline of bed surface with salt.
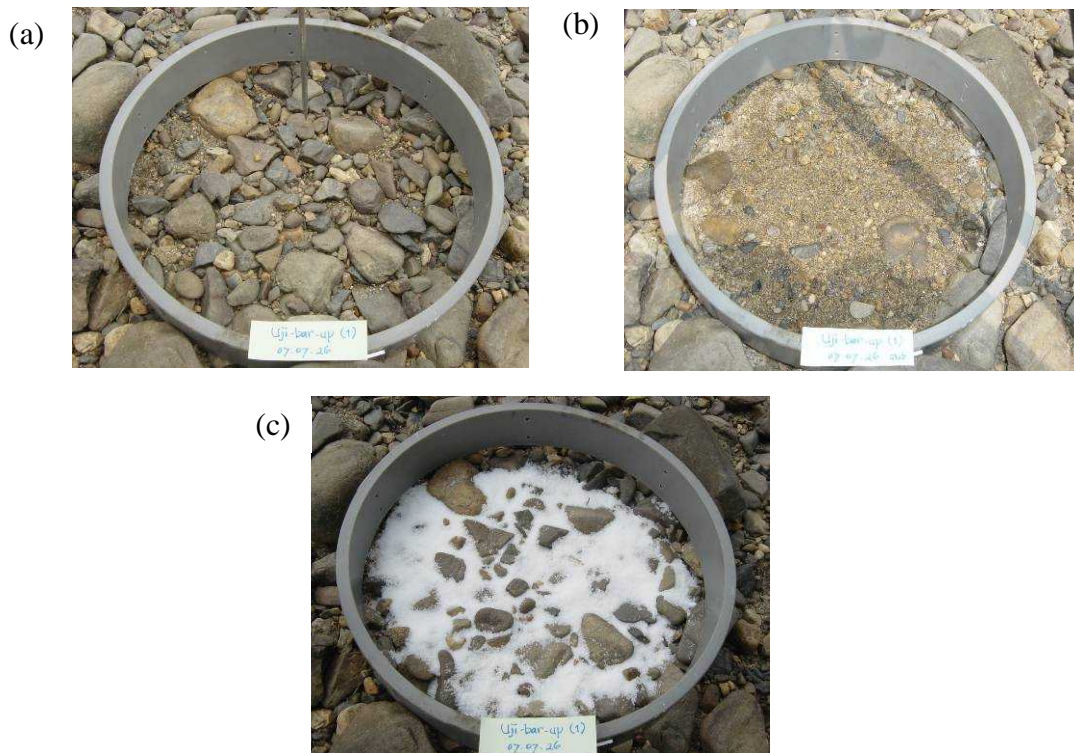
Photo 4.2 The conditions of bed material; (a) initial condition of bed surface, (b) condition of surface of the sub-surface layer (c) condition of bed surface with salt.

The surface layer is three dimensional and can only be sampled volumetrically. The thickness of the surface layer is described as extending from the bed-surface plane down to the bottom side of the largest particle size (d_{max}) or a frequently occurring large surface particle size (d_{dom}). The surface layer which is sampled over the entire thickness of the surface layer consists of surface particles plus those sub-surface particles that are at a depth less than the d_{max} of the surface layer (grey particles in the Figure 4.27). The surface bed materials are sampled three times for each location. Before measuring the volume of the sample, the salt included in the sample should be dissolved and washed away from the sediment sample.

The average grain size distributions of the surface layer are shown in Figure 4.28. Based on the identification method of grain size distribution type, the grain size distribution of surface layer is classified into M-Talbot distribution. Ratio of maximum and minimum diameters for the surface layer is 847 and the average Talbot numbers is 3.8.
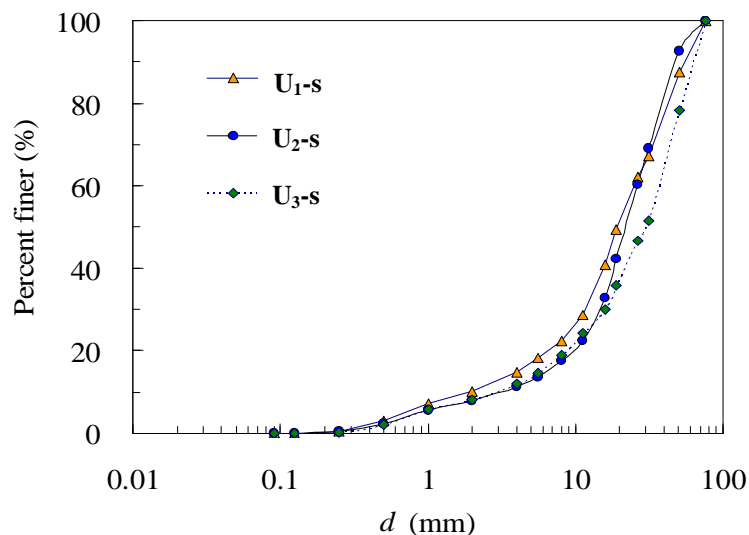
Fig.4.28 Grain size distribution of the surface layer at the sampling location of Uji River bar.

(2) Sub-surface layer

Sub-surface layer is the sediment under the surface layer. In order to measure the porosity and to sample the sub-surface sediment, the overlying surface layer first needs to be removed by taking a volumetric surface layer sample. The procedure for measuring the porosity is same as the measurement method shown in Figure 4.17. Sub-surface sediments are sampled to the same thickness as the surface layer thickness. The grain size distributions of the sub-surface layer are shown in Figure 4.29. Based on the identification method of grain size distribution type, the grain size distribution of sub-surface layer is classified into bimodal distribution.
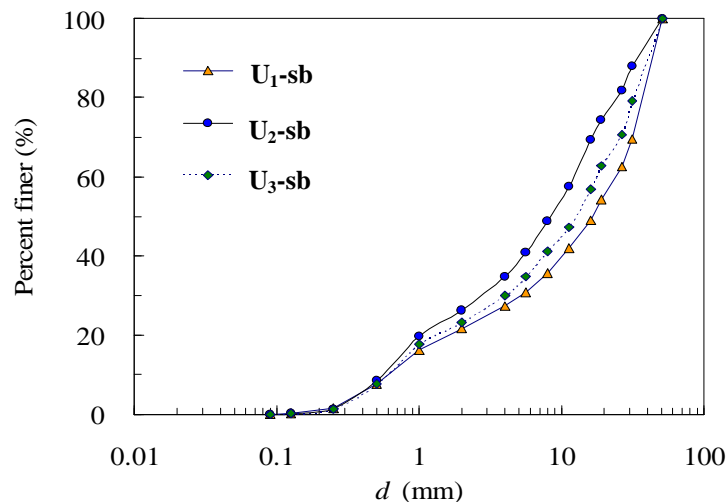
Fig.4.29 Grain size distribution of the sub-surface layer at the sampling location of Uji River bar.

4.5.3 Porosity of actual riverbed material

Measurement results are shown in Figure 4.28. The porosity of armor layer measured without salt ranged from 0.181 to 0.199 with the mean value of 0.191, and the porosity measured with salt ranged from 0.228 to 0.231 with the mean value of 0.230. The measured porosity with salt provides the higher porosity than that without salt. Comparing to the

measured porosity of Talbot distribution in the laboratory, the measured porosity of the laboratory experiment is similar with the measured porosity without salt. This result shows that the measured porosity of surface layer in the laboratory is underestimated. This discrepancy may be due to the differences in the compaction degree of the particle packing. The packing of particle of sediment sample in the laboratory experiment is denser than the actual packing in the field. The difficulty in the measurement with salt is to adjust the amount of salt to be filled into the surface of bed layer. If too much salt is filled into the bed surface layer, the porosity of armor layer becomes too high.

The measured porosity of sub-surface layer ranged from 0.134 to 0.156 with a mean value of 0.148. The porosity of sub-surface layer is smaller than that of surface layer because the sub-surface layer contains much more fine sediment than the surface layer. So, the finer materials are filling into the void of larger material. The influence of grain size distribution on porosity varies between sediment layers.
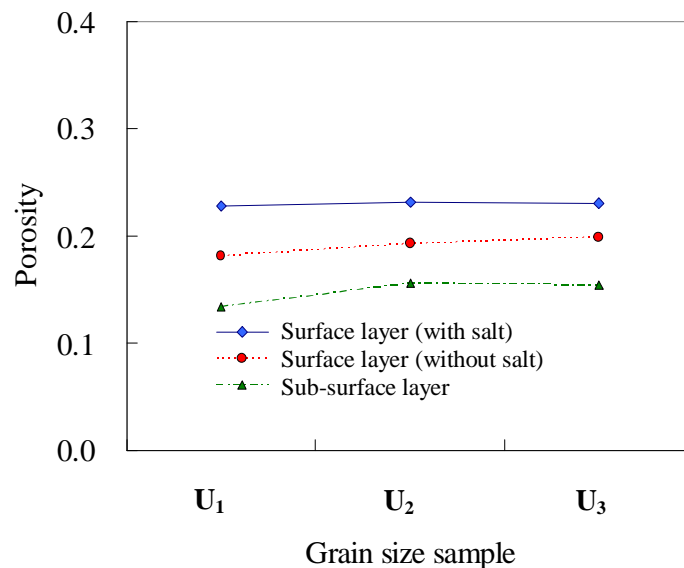
Fig. 4.30 Comparison of the measured porosity, between the surface layer (with salt and without salt) and sub-surface layer.

130

4.6 Summary

Two methods for estimating the porosity of sediment mixtures are presented. One is based on a particle packing simulation model. The other one is based on a direct measurement by a water displacement method. The packing simulation model is available to derive the porosity of spherical particle mixtures with different types of size distribution. Porosity of sediment mixtures depends on not only the grain size distribution but also the compaction degree. As a result of simulation, the compaction degree is given. The validity of the model is assessed with the experimental results, and its validity is confirmed, while the rather large disagreement is pointed out for the case of a uniform size distribution. The defect of this model is that it takes too much time to execute the simulation for the particles with a wide grain size distribution in a vessel. The measurement method can be available for in situ estimation of porosity. This method is simple and applicable for field surveying. However, this method is available only for the dry material.

The results in **Chapter 4** are summarized as follows:

1) Relationship between the grain size distribution and the porosity can be determined by using the characteristic parameters of lognormal and M-Talbot grain size distributions.

2) For lognormal distribution, the porosity depends only on the standard deviation of $\ln d$, σ_L, if the compaction degree is constant. The porosity decreases with an increase in the standard deviation, σ_L, mainly due to the reduction of the volume of void by the occupation of large particles. Simulation results show that the deviation of simulated porosity increases when the standard deviation, σ_L, increases from 0.75 to 1.5. This deviation arises from the effect of vessel size.

3) The trend of porosity change with the standard deviation, σ_L, between

131

the measurement and the simulation is almost similar. However, the measurement result is somewhat larger than the simulated one. The discrepancy may be due to the difference in the shape of particles, the compaction degree, and the inverse grading of the particles. Particularly in the measurement, it is very difficult to mix the sediment evenly. Consequently, the coarser particle lies at higher position than the finer particle. This inverse grading process makes the porosity larger, while in the simulation the particles are mixed evenly. However, in this study, the diagram available for estimating the porosity of lognormal grain size distribution was obtained.

4) For M-Talbot distribution, the simulation result shows that the porosity increases with an increase in the Talbot number, n_T, and a decrease in the ratio of d_{max}/d_{min} gives the higher value of porosity. The relation between porosity and Talbot number for the different ratio of maximum and minimum diameters is expressed by the lines with a same inclination. However, the porosities in the simulation and the measurement are rather different for the same Talbot number and the same ratio of maximum and minimum diameters. The reason of this discrepancy is also the differences in the shape of particle, the compaction degree, and the inverse grading of the particle.

5) For M-Talbot distribution, it is possible to estimate the porosity roughly by means of the presented relation between the porosity and the characteristic parameter of grain size distribution. However, as there is rather larger difference between the simulation and the measurement, more investigation on the influence of the compaction degree is necessary to fix the relation.

6) The porosity of bimodal distribution depends on the percentage of each fraction in the mixture. It is interesting that the minimum porosity appears for a percentage of finer material as in a binary mixture. The porosities in the simulation and the measurement are rather different

for the same proportion of finer materials. The discrepancy between the measured and simulated porosities may be caused by the difference in the uniformity of the sediment mixtures. In the simulation, the particles are packed evenly in the vessel with dense packing, so the porosity is low. However, in the experiment, the coarse fraction lies at the higher position and the finer fraction goes down to the lower position. As each fraction has an almost uniform distribution, the porosity in the measurement method is larger than simulated one and close to the porosity of uniform sediment.

7) A method for measuring the porosity of sediment is proposed. The porosity of sediment mixtures and bed material can be reasonably estimated by measuring the in-situ volume of sediment sample. This method is simple and applicable for field surveying. However, this method is available only for the dry material.

8) In the gravel bed river, the bed is usually stratified vertically with coarse armor layer on the surface. The characteristic of gravel bed material varies between sediment layers. Generally, the surface layer has a M-Talbot distribution and the sub-surface layer has a bimodal distribution. Therefore, the porosity of surface layer is higher than the porosity of sub-surface layer due to the armoring in the surface layer.

9) Compaction degree of bed material in the surface layer is usually rather low compared with the material in the sub-surface layer; consequently, the porosity of surface layer is larger than sub-surface layer.

The relationship between the grain size distribution and the porosity for lognormal and M-Talbot distributions obtained in this chapter is then installed into a bed variation model, which will be discussed in Chapter 5.

References

Aberg, B. (1992a). "Voids ratio of noncohesive soils and similar materials." *Journal of Geotechnical Engineering*, Vol. 118, No.9, pp.1315-1334.

Aberg, B. (1992b). "Hydraulic conductifity of noncohesive soils." *Journal of Geotechnical Engineering*, Vol. 118, No.9, pp.1335-1347.

Aberg, B. (1996a). "Grain size distribution for smallest possible void ratio." *Journal of Geotechnical Engineering*, Vol. 122, No.1, pp.236-239.

Aberg, B. (1996b). "Void sizes in granular soils." *Journal of Geotechnical Engineering*, Vol. 122, No.3, pp.74-77.

Albert, L.J.H, (2005). "Initial porosity of random packing." *Thesis presented to Delft University of Technology*, in partial fulfillment of requirement for Doctor degree.

ASCE Task Committee on Sediment Transport and Aquatic Habitats. (1992). "Sediment and aquatic habitat in rivers systems." *J. Hydraul. Eng.,* Vol.118, No.5,pp.669-687.

Carling, P.A. and Reader, N.A. (1982). "Structure, composition and bulk properties of upland stream gravels." *Earth Surface Processes and Landforms,* Vol.7, pp.349-365.

Cumberland, D.J., and Crawford, R.J. (1987). "The packing of particles." *Handbook of Powder Technology*, Elsevier, New York. Vol.6, 148 pp.

Erman, D. C. & Ligon, F. K. (1988). "Effects of discharge fluctuation and the addition of fine sediment on stream fish and macroinvertebrates below a water-filtration facility." *Environmental Management*, 12, 85-97.

Gayraud, S., Philippe, M. (2003). "Influence of bed-sediment features on the interstitial habitat available for macroinvertebrates in 15 French streams." *Internat. Rev. Hydrobiol.*, Vol. 88, pp. 77-93.

Han, D., Nur A., and Morgan D. (1986). "Effect of porosity and clay content on wave velocities in sandstones." *Geophysics*, Vol.51, No.11, pp.2093-2107.

Hirano, M. (1971). "Riverbed degradation with armoring." *J. Japan Soc. Civil Eng.*, Vol.195, pp.55-65. (in Japanese with English summary)

Koltermann, C.E. and Gorelick, S. M. (1995). "Fractional packing model for hydraulic conductivity derived from sediment mixtures." *Water Resources Research*, Vol.31, No.12, pp.3283-3297.

Marion, D., Nur A., Yin H., and Han D. (1992). "Compresional velocity and porosity in sandy-clay mixtures." *Geophysics*, Vol.57,No.4,pp.554-563.

Milhous, R.T. (2002). "Measurement of the Bed Material of Gravel-Bed Rivers." *Proc. Hydraulic Measurements and Experimental Methods Conference* (CD-ROM). Estes Park, Colorado, USA.

Nolan, G. T. and Kavanagh, P. E. (1993). "Computer simulation of random packings of spheres with log-normal distributions." *Powder Technology*, Vol.76, pp.309-316.

Sohn, H.Y. and Moreland, C. (1968). "The effect of particle size distribution on packing density." *The Canadian Journal of Chemical Engineering*, Vol.46, pp.162-167.

Standish, N. and Borger, D.E. (1979). "The porosity of particulate mixtures." *Powder Technology*, Vol.22, pp.121-125.

Suzuki, M. & Oshima, T. (1983). "Estimation of the co-ordination number in a multi-component mixture of spheres." *Powder Technology*, Vol.35, pp.159-166.

Takemon, Y., Takemon, M., Tanida, K., Nakajima, T., and Mitamura, O. (2003). "Qualitative investigation of hyporheos by the freeze-core-method." *Proc. Fluvial Creature Research Workshop*, pp.235-241. (in Japanese)

Tsutsumi, D., Fujita, M., and Sulaiman, M. (2006). "Changes in the void ratio and void structure of riverbed material with particle size distribution." *River, Coastal and Estuarine Morphodynamics*, Vol. 2, Parker, G., Garcia, M.H., eds., Taylor & Francis, pp. 1059-1065.

Wood, P. J. & Armitage, P. D. (1997). "Biological effect of fine sediment in the lotic environment." *Enviromental Management*, Vol.21, pp.203-217.

Yamada, H. & Nakamura, F. (2002). "Effect of fine sediment deposition and channel works on periphyton biomass in the Makomanai river, northern Japan." River Res. Applic., Vol.18, pp.481-493.

Yu, A. B. and Standish, N. (1993). "A study of packing particles with mixture size distribution." *Powder Technology*, Vol.76, pp.113-124.

Chapter 5

A Bed-porosity Variation Model

5.1 Introduction

5.1.1 Background

(1) Actual condition of porosity change

The installation of dams on a river typically blocks the downstream delivery of sediment and causes the bed degradation and the morphological change. Also, after the dam construction, the riverbed changes qualitatively, and consequently it is covered by an armor coat composed of coarser sediment and with a high porosity. For such reservoir sedimentation issues, recently some sediment managements have been implemented. For example, in Japan, the Dasidaira reservoir and the Unazuki reservoir have a sediment flushing gate and those gates have been operated to remove the sediment deposit to the Kurobe River. Such an artificial sediment supply must influence the downstream reach quantitatively and qualitatively. From an ecological point of view, those human impacts on habitat for fish and aquatic insects are very important and particularly the importance of assessing the change in void structure of the bed material has been strongly pointed out (Milhous, 1982; ASCE Task Committee, 1992; Gayraud and Philippe, 2003).

The porosity of bed material is an essential parameter on the infiltration process in riverbeds. The interstitial space in sediments plays an important role in habitat for aquatic insects. The space of coarser bed material has often been occupied by fine sediment during a flood. In that case, a compact layer may develop that reduces the porosity and the

137

hydraulic conductivity of the riverbed. On the other hand, if an armor coat develops on the bed surface, the interstitial space of coarser bed material is vacant and the porosity of the bed material can be increased. These events often take place in natural rivers and they cause the change in the infiltration system and the habitat condition. A method for assessing the change in interstitial space and porosity of bed material is, therefore, required from an ecological and hydrological point of view.

(2) Experiment on transformation processes of porosity

A flume experiment is conducted to realize the transformation processes of void structure for two situations; one is that only fine sediment is removed from a sediment mixture and another is that a little fine sediment supply into a coarser bed material that is transported as shown in Figure 5.1.
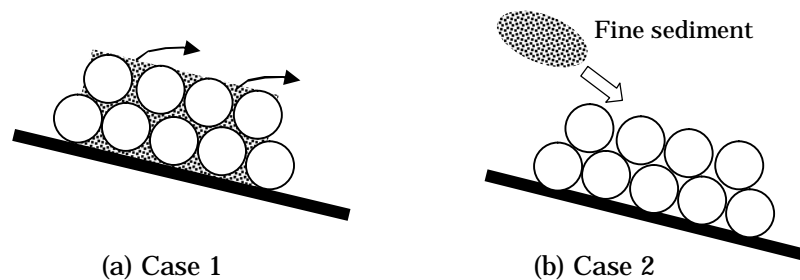
(a) Case 1   (b) Case 2

Fig.5.1 Experimental conditions; (a) Case 1: fine sediment removal from a sediment mixture and (b) Case 2: a little fine sediment supply into a coarser bed material that is transported.

The experiment is conducted in the flume with a width of 0.40 m, a depth of 0.40 m and a working length of 7.0 m at Ujigawa Open Laboratory of DPRI, Kyoto University. The flume walls are made of clear acrylic, allowing direct observation of the transport. The slope of the flume is adjusted to 1/50. Water is circulated, and the water discharge is held nearly constant for all runs. A sediment mixture is originally placed in the working

section and scraped flat. The thickness of the sediment layer over the channel bottom is 5.3 cm. A weir with a height of 10 cm is placed at the end of the working section to investigate the process of sedimentation.

The original bed material is composed of coarse and fine fractions of sediment. The size of coarse fraction ranges from 4.75 mm to 26.5 mm and the median grain size, d_{50}, is 15 mm. The size of fine fraction ranges from 0.5 mm to 4.75 mm and the median grain size, d_{50}, is 2 mm. The grain size distributions of fine fraction, coarse fraction and bed material are shown in Figure 5.2. The fine fraction sediment is used also as the supplied sediment.
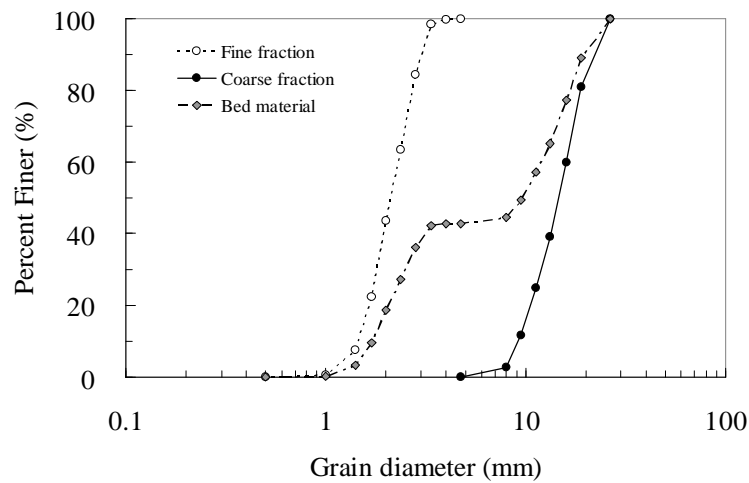
Fig.5.2 The grain size distributions of fine fraction, coarse fraction and bed material.

The experiment consists of two runs, Run 1 and Run 2. In Run 1, no sediment is supplied and the coarse sediment does not move actively. Only fine sediment is removed from the original bed material. This run is continued until the flow brings little sediment. In Run 2, fine sediment is fed constantly from the upstream end of the flume by a conveyor belt. The fine sediment deposits into the coarser bed material. Run 1 is followed by Run 2; the condition of riverbed in the end of Run 1 is used as the initial condition of Run 2. Each run is carried out by 4 steps. Cumulative time steps for Run 1 are 20, 65, 130, 250 minutes and for Run 2 are 30, 50, 66, 82

minutes. Total duration for Run 1 and Run 2 is 332 minutes. The experimental conditions are summarized in Table 5.1. The water depth, *h,* and the velocity, *v,* are the initial average water depth and velocity in the uniform region, respectively. The elevations of the bed and water surface are measured at 0.025 m intervals for 7.0 m working length. These profiles are taken at the end of every step of each run. The surface bed material is sampled at the upper, middle and lower locations before first run and at the end of each run by surface excavation. The sampling points are located at 1 m, 3.5 m and 6 m downstream of the upper end of the flume. The bed material is excavated up to a depth corresponding to the coarsest grain size. All samples are air-dried, weighed and then sieved; providing the grain size distribution of the surface layer.

Table 5.1 Conditions for experimental runs.

Exp.	Q_w (m^3/s)	q_s (10^{-6} m^2/s)	h (m)	v (m/s)	F_r	$\tau*$ (fine)	$\tau*$ (coarse)	Time (min)
Run 1	0.0136	0	0.039	0.879	1.428	0.178	0.026	20, 65, 130, 250
Run 2	0.0136	31.8	0.045	0.754	1.133	0.203	0.030	30,50, 66, 82

Bed variation process in the upstream region of the weir is shown in Figure 5.3(a) and Figure 5.3(b) for Runs 1 and 2, respectively. From those results some important   information can be pointed out. First, in the Run 1, only the fine sediment is removed from the sediment mixture, fine sediment moved and no sediment is supplied from the upper end. Thus, the sediment discharge in the uniform flow region increases in the downstream direction. However, bed degradation does not occur in the uniform flow region, as shown in Fig.5.3(a). Second, in Run 2, the bed level does not go up significantly in the upstream region where back sand does not extend even if fine sediment is supplied to the static equilibrium bed condition. These results differed from the conventional experimental results, that is no

140

sediment supply causes bed degradation and sediment supply to a static equilibrium bed condition causes bed aggradation. The reason why the results differed from the common knowledge is that the porosity of the surface bed material changes in Run 1 and Run 2.
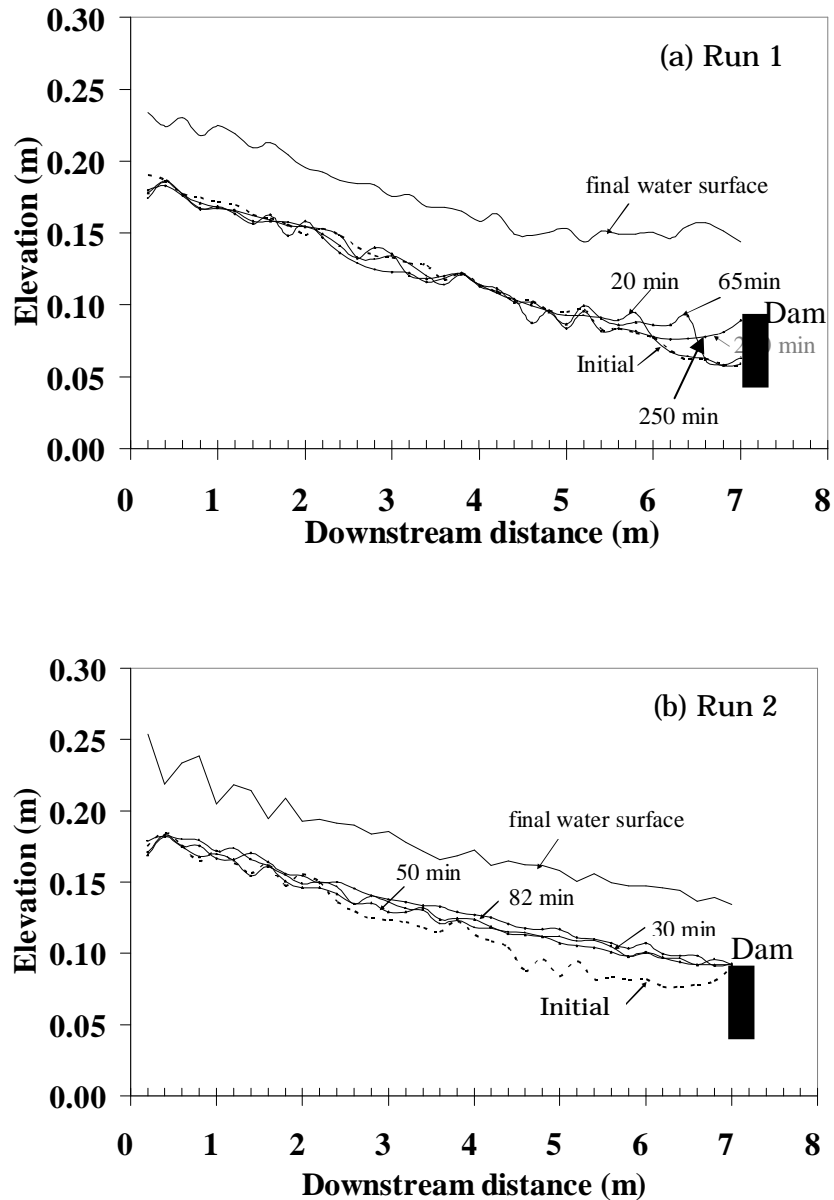

Fig.5.3 Bed surface and water surface profiles in Run 1 and Run 2.

The grain size distributions of surface bed material at the upstream point ($x = 1$ m) and the downstream point ($x = 6$ m) are shown in Figure 5.4. These samples are taken before Run 1 and at the end of Run 1 and Run 2. The percentage of fine sediment is initially 37% and 22% at the upstream point and the downstream point, respectively. In Run 1, the fine sediment in the bed surface moves from the upstream region to the downstream region. As a result, the fine sediment proportion at the upstream point decreases to 5% from 37% and increases to 26% from 22% at the downstream point. As the bed level does not change at the upstream point, this result means the increase in the porosity of bed material.

Sediment feeding in Run 2 makes the surface bed material much finer. Actually, the fine sediment proportion at the upstream point exceeds the original value up to 64% because of too much sediment supply. Figure 5.4 (b) shows the surface bed material at the downstream point is almost substituted by the supplied fine sediment.

(3) Review of riverbed variation models

A numerical simulation method for bed variation is one of the tools for assessing the riverbed deformation. Some bed variation models are available to the numerical analysis on topographical and morphological changes of rivers (Lopez and Falcon, 1999; Papanicolau *et al.*, 2004; Meier and Reichert, 2005). Ashida *et al.* (1988) have made some discussions on the mechanism of armoring phenomena, taking an idea of particle exchange within bed layers as well as selective entrainment into account. Wu and Chou (2003) adopted a combination of the active layer concept and two-layer treatment to outline the framework of sediment transport system, which allowed incorporation of subsurface sand into the surface layer through the mechanisms of upward entrainment and bed degradation. However, they could not provide information on the change in porosity.
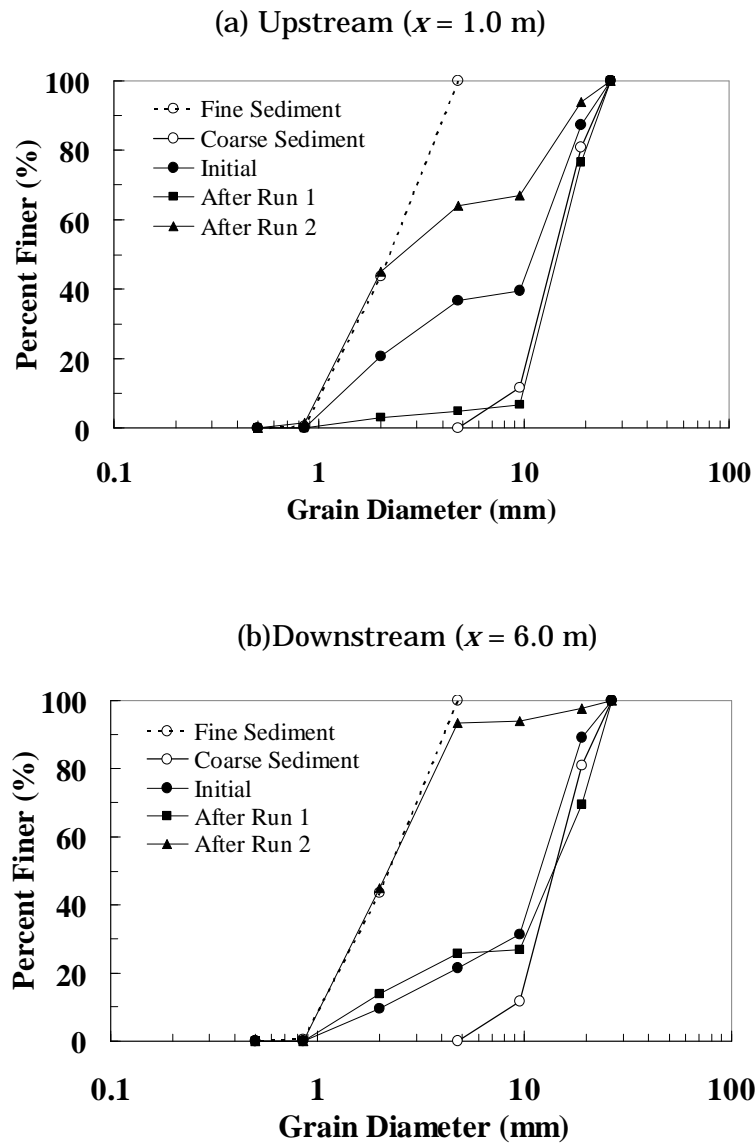
Fig.5.4 Grain size distributions of surface bed material at the upstream ($x = 1$ m) and the downstream ($x = 6$ m).

So far, engineers and researchers have conventionally assumed that the porosity of bed material is a constant in their bed variation models, regardless of whether the particle size of the bed material is uniform. However, if only fine sands are removed from a riverbed composed of sediment mixtures or they deposit into the voids of coarser bed material, the porosity of the bed material must change significantly as shown in 5.1.1.(2). For these situations, it is very clear that fixing the porosity at a constant value is inadequate in calculating the bed variation. Hirano (1971) has presented a bed variation model for sediment mixtures, and also pointed out this necessity of considering the change of porosity in some cases. After his activity, many other researchers have developed the numerical bed variation model, but nobody has proposed a model that available for the analysis of change of porosity.

5.1.2 Purpose of the study

This study aims at developing a bed-porosity variation model that available for the analysis of the change in porosity of bed material as well as the bed variation. The relationship between the grain size distribution and the porosity could be determined by the geometric properties of the grain size distribution (Sulaiman, *et al.*, 2007). The porosity was assumed to be a function of characteristic parameters of grain size distribution as described in Chapter 4. An exchange model of bed material and transport sediment is introduced to obtain the time and space variations of porosity and grain size distribution of bed material. To eliminate the complexity of the calculation of water surface profile and to eliminate the irrationality caused by hydraulic jumps, MacCormack scheme is used. MacCormack method can handle flows containing shocks or discontinuities such as flows over pit or flows around the vicinity of large roughness elements.

5.2 Governing Equations

5.2.1 Basic concept

Riverbeds vary with the local change in the sediment discharge. The water flow in river depends on the water discharge, the geometry of the river, and the boundary conditions, and is normally unsteady and non-uniform. Thus, the sediment transport is also non-uniform. The sediment discharge depends on the hydraulic conditions and the grain size distribution of riverbed material. The non-uniformity of sediment transport causes the riverbed to deform and resultantly the other geometry of the river to change. The local change in sediment discharge of each particle size causes the grain size distribution of bed material to change. Therefore, to calculate the riverbed variation, it is necessary to carry out the calculation of the sediment discharge and the change in the grain size distribution simultaneously.

The previous bed variation model assumed that the porosity is constant; therefore, the time differential term on the porosity in the continuity equation of sediment can be neglected. A schematic diagram for the previous riverbed variation analysis is shown in Figure 5.5 and a schematic model for calculating the riverbed variation is illustrated in Figure 5.6. It is recognized that the previous model can create a reliable numerical simulation result. The model, however, has not been employed to an extreme condition such as a situation where fine sand deposits into the void structure of static gravel beds. If the model is applied to such a condition, the result of the model may not fit well with the condition because the porosity is not constant.
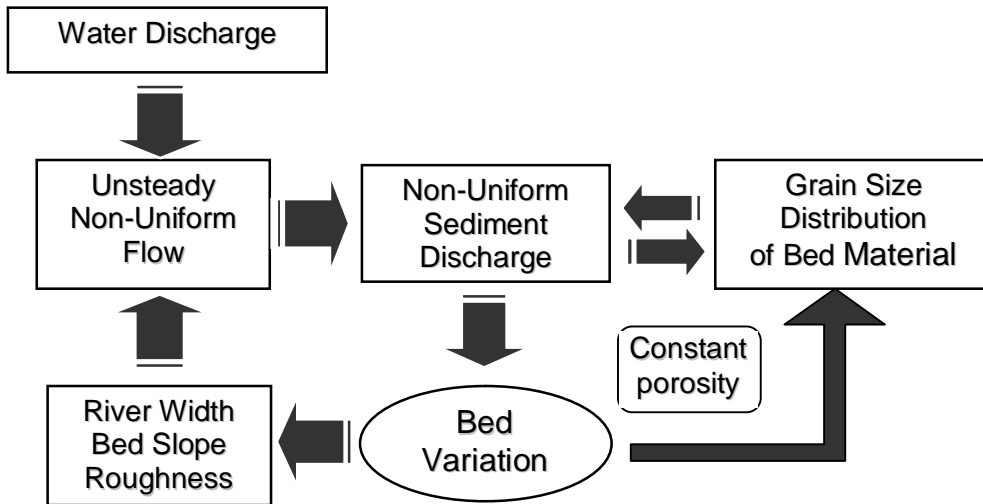
Fig.5.5   Previous bed variation analysis assumed the porosity is constant.
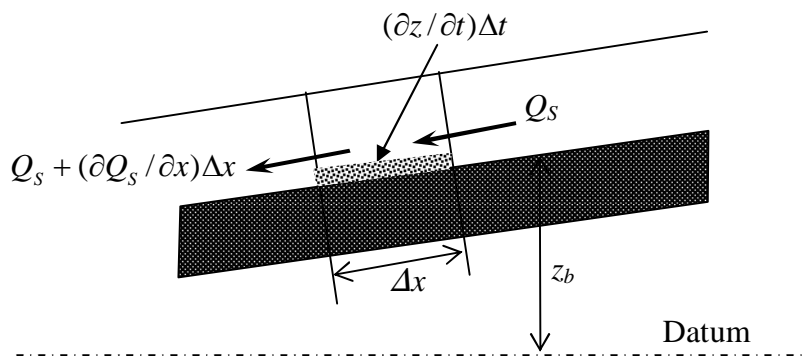

Fig.5.6 Continuity of sediment transport.

As no doubt that porosity of bed material is not constant and dependent on the grain size distribution, the time differential term on the porosity in the continuity equation of sediment must be considered. In this chapter, a bed-porosity variation model is presented. A schematic diagram for this bed-porosity variation analysis is shown in Figure 5.7. According to the previous exchange model between bed material and transported sediment such as Hirano's model, the change of grain size distribution in a time interval can not be obtained without the change in bed elevation in the time interval. If the change of grain size distribution is not obtained, the time change of porosity, λ, is not analyzed. This means that the continuity equation of sediment is an implicit equation. To solve this matter, and to simplifying the analysis, the changes in the grain size distribution and porosity in the original mixing layer are obtained temporally and then the change in bed elevation using the temporal grain size distribution is calculated.
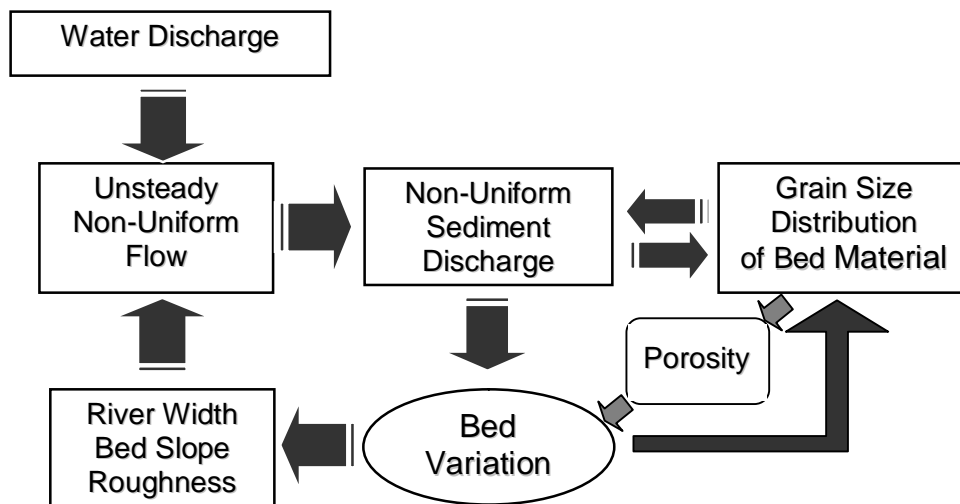
Fig.5.7 Presented bed variation analysis considering the changes in porosity.

147

Porosity is dependent on the grain size distribution of bed material and its compaction degree. In this study, the compaction degree is considered empirically and the porosity is assumed to be a function of characteristic parameters of grain size distribution. There were some types of grain size distribution as explained in Chapter 3, such as lognormal distribution and M-Talbot distribution. For obtaining the porosity of each type of distribution, the relation between the characteristic parameters and the porosity of each type is needed. The method for identifying the grain size distribution type and the method for estimating the porosity have been described in Chapter 3 and Chapter 4, respectively. A flow chart of relation between main routine of bed variation model and the subroutine of identifying of grain size distribution and estimating the porosity is shown in Figure 5.8.
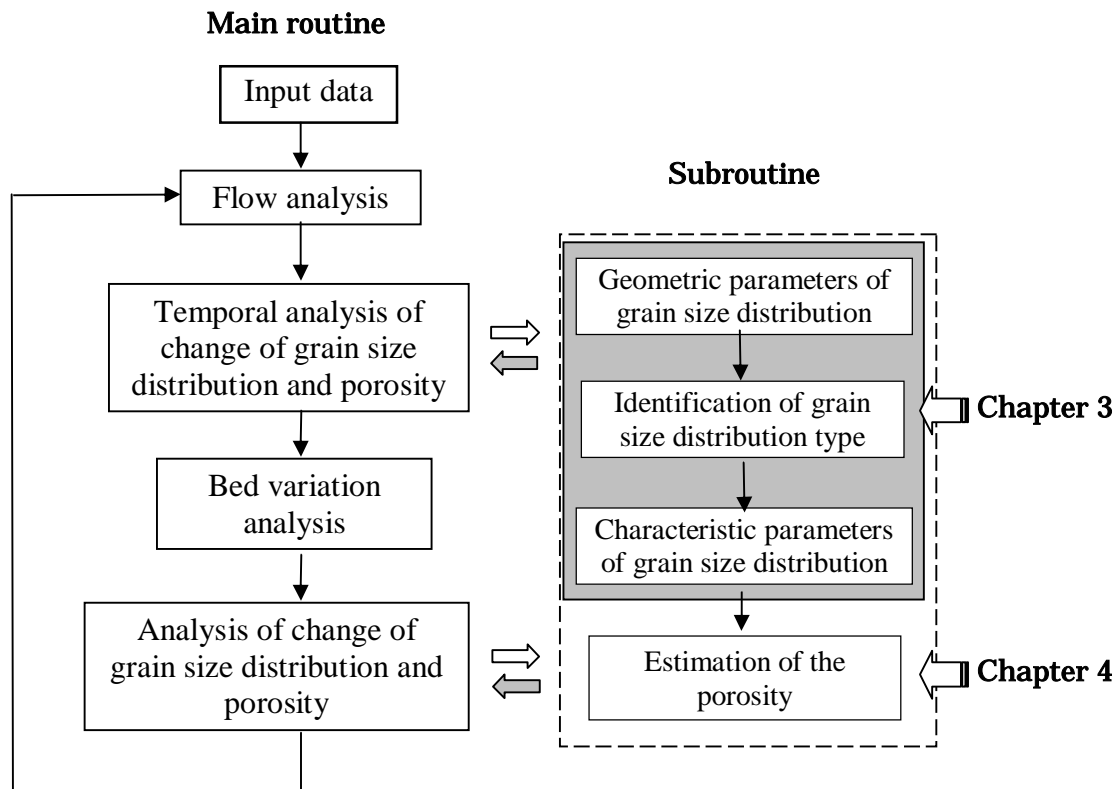
Figure 5.8 Flow chart of the bed-porosity variation model

In this subroutine, the grain size distribution is analyzed geometrically by using indices γ (Eq.3.8) and β (Eq.3.9). After the geometric parameters are found out, the grain size distribution is identified by using the diagram of relation between β and γ shown in Figure 3.10 to determine the distribution type. The characteristic parameters of grain size distribution are obtained by a fitting curve method. Lognormal distribution has one characteristic parameter ($\Pi_1 = \sigma_L$) and M-Talbot distribution has two characteristic parameters ($\Pi_1 = d_{max}/d_{min}$, $\Pi_2 = n_T$), where σ_L = standard deviation of ln$d$, d_{max} = maximum grain size, d_{min} = minimum grain size and n_T = Talbot number.

5.2.2 Basic equations

One dimensional bed-porosity variation is analyzed by the continuity equation of water, the energy equation for flows and the continuity equation of sediment combined with the sediment exchange model of transported material and bed material. As an exchange model, Hirano's model is used. The basic equations are as follows:

(a) Continuity equation of water:

$$\frac{\partial Bh}{\partial t} + \frac{\partial Q}{\partial x} = 0 \tag{5.1}$$

where B = channel width, h = water depth, Q = water discharge, t = time and x = distance in streamwise direction.

(b) Energy equation for flows:

$$\frac{\partial Q}{\partial t} + \frac{\partial}{\partial x}\left(\frac{1}{2}gBh^2 + \frac{Q^2}{Bh}\right) = gBh(i_b - i_f) \tag{5.2}$$

where g = gravity acceleration, i_b = bed slope and i_f = energy gradient. The flow energy is dissipated by the bed shear stress, so that the energy gradient can be expressed as follows:

$$i_f = \frac{\tau_b}{\rho g R} \tag{5.3}$$

where τ_b = riverbed shearing force, R = hydraulics radius, and ρ = water density. τ_b is given as follows:

$$\tau_b = \frac{1}{8} f \rho v^2 \tag{5.4}$$

Therefore, the energy gradient is given by the following equation:

$$i_f = \frac{1}{8} f \frac{v^2}{g R} \tag{5.5}$$

where v = average water velocity and f = friction coefficient.

Using the Manning's resistance law, the energy gradient is rewritten as follows:

$$i_f = \frac{n^2 v^2}{R^{4/3}} \tag{5.6}$$

where n = Manning coefficient.

The water depth and velocity at the specified locations can be calculated under the given initial and boundary conditions by using Eq. (5.1), (5.2) and (5.6). After the water depth is obtained, the shear velocity, u_* and non dimensional tractive force, τ_*, can be calculated using the following equations:

$$u_* = \sqrt{g R i_f} \tag{5.7}$$

$$\tau_* = \frac{u_*^2}{s g d} \tag{5. 8}$$

where $s = \sigma/\rho - 1$, and σ = density of sand.

(c) Continuity equation of total sediment:

The change in bed elevation is calculated using the equation of continuity of sediment discharge shown below:

$$\frac{\partial}{\partial t}\int_{z_o}^{z_b}\{1-\lambda(t,x,z)\}dz + \frac{1}{B}\frac{\partial Q_S}{\partial x} = 0 \tag{5.9}$$

where λ = porosity of bed material, z_b = bed level, z_0 = a reference level, z = a vertical axis, and Q_s = sediment discharge.

(d) Continuity equation of each sediment fraction:

For sediment mixtures, bed material is classified into n fractions. Continuity equation of each fraction is written as:

$$\frac{\partial}{\partial t}\int_{z_o}^{z_b}\{1-\lambda(t,x,z)\}p_j(t,x,z)dz + \frac{1}{B}\frac{\partial Q_{Sj}}{\partial x} = 0 \tag{5.10}$$

where j = grade of sediment fraction, p_j = mixing ratio of j-th fraction in bed material, and Q_{sj} = sediment discharge of j-th fraction.

(e) Porosity and grain size distribution

Porosity is dependent on the grain size distribution of bed material and its compaction degree. In this study, the compaction degree is considered empirically and the porosity is assumed to be a function of characteristic parameters of grain size distribution.

$$\lambda = f_n\left(\Pi_1,\Pi_2,\Pi_3,\ldots\ldots\right) \tag{5.11}$$

where Π_1, Π_2, Π_3….= characteristic parameters of grain size distribution.

5.2.3 Sediment transport rate

(1) Uniform sediment

The total sediment discharge, Q_S, is calculated by using Ashida and Michiue's bed load transport formula and Ashida and Michiue's suspended load formula. Ashida and Michiue (1972) proposed a bed-load transport formula with taking the influence of critical shear stress on the movement of grains into consideration:

$$\frac{q_b}{\sqrt{\left(\frac{\sigma}{\rho}-1\right)gd^3}} = 17\tau_{*e}^{3/2}\left(1-\frac{\tau_{*c}}{\tau_*}\right)\left(1-\frac{u_{*c}}{u_*}\right) \tag{5.12}$$

where τ_{*e} = non-dimensional effective bed shear stress, τ_{*c} = non-dimensional critical bed shear stress, and τ_* = non-dimensional total bed shear stress. These are defined as follows:

$$\tau_{*c} = \frac{u_{*c}^2}{(\sigma/\rho-1)gd}, \ \tau_* = \frac{u_*^2}{(\sigma/\rho-1)gd}, \tau_{*e} = \frac{u_{*e}^2}{(\sigma/\rho-1)gd}$$

The effective shear velocity, u_{*e}, involved in τ_{*e} is calculated with the following formula proposed by Ashida and Michiue (1972):

$$\frac{v}{u_{*e}} = 6 + 5.75\log\frac{R}{d(1+2\tau_*)} \tag{5.13}$$

where, u_{*e} = effective shear velocity and τ_* = tractive force. The total bed shear stress is associated with the average energy slope and the effective bed shear stress is dependent on the local energy slope.

The suspended load transport rate is calculated by using the concentration distribution of the suspended sediment and the vertical velocity profile:

$$Q_{sus} = q_{sus}B = B\int_a^h C(z)u(z)dz \tag{5.14}$$

where, Q_{sus} = suspended load transport rate and q_{sus} = suspended load transport rate per width. The concentration distribution is calculated by using the following Lane-Kalinske distribution (Lane and Kalinske, 1941):

$$\frac{C(z)}{C_a} = \exp\left[\frac{w_0}{\varepsilon_{zm}}(a-z)\right] \tag{5.15}$$

where, C_a = concentration at the reference point, w_0 = settling velocity of particle, ε_{zm} = the depth averaged diffusion coefficient, a = reference level and z = elevation.

The reference level is set at a height of 5% of the water depth:

$$a = 0.05h \tag{5.16}$$

In an equilibrium state, the concentration at the reference level can be expressed using the pick up rate, q_{su}, as follows:

$$C_a = \frac{q_{su}}{w_o} \tag{5.17}$$

Ashida and Fujita (1986) showed photograph taken by a high speed video camera to demonstrate the motions of suspended sediment particles in stream, and proposed the following pick up rate:

$$q_{su} = \frac{2}{3}K\sqrt{\frac{6}{\pi(s+1)}}\int_{\eta_0}^\infty u_*\sqrt{ck^2\eta - \frac{\pi}{8}C_{Do}\xi_o^2}\cdot\phi(\eta)d\eta \tag{5.18}$$

where, $\eta_o = (\pi/8)C_{Do}\xi_o^2/(ck^2)$, $C_{Do} = 2 + 24v/(w_o d)$, v = kinetic viscosity, c = coefficient of lift force, k = coefficient of sheltering effect, and K = 0.035.

The function ϕ is given by the following equation:

$$\phi(\eta) = \frac{1}{\sqrt{2\pi}} \exp(-\frac{1}{2}\eta^2)$$ (5.19)

This equation depends on the two parameters, w_0/u_* and the particle diameter, and the riverbed gradient as well, which relates to the life period of the turbulence affecting the suspended sediment. Figure 5.9 shows the difference in the pick up rate equation among those proposed by Ashida and Michiue, Itakura and Kishi, and Ashida and Fujita. The equation proposed by Ashida and Fujita can take account of the sheltering effect of cobbles and pebbles, so it can be used for evaluating the pick up rate for non-uniform sediment.
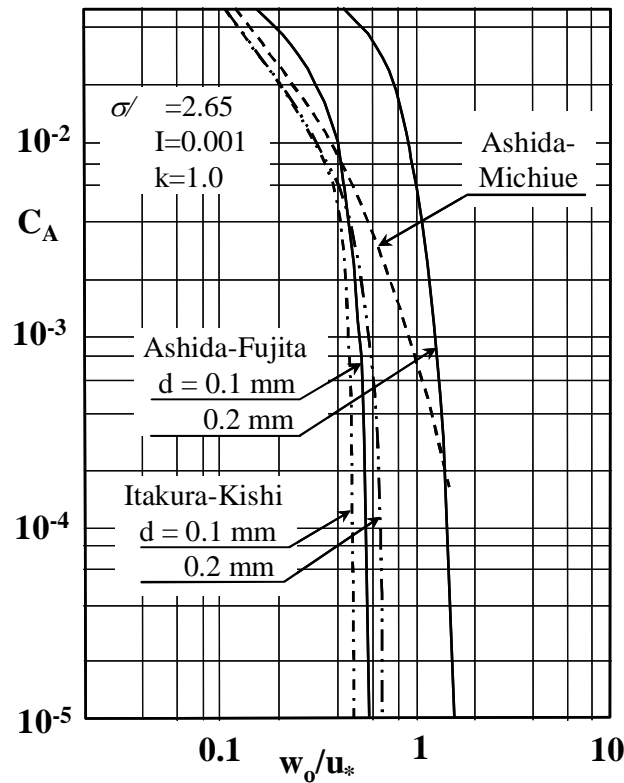
Fig.5.9 Concentration at the reference point.

The depth averaged diffusion coefficient is calculated as follows:

$$\varepsilon_{zm} = \frac{\beta \kappa u_* h}{6}$$ (5.20)

154

where, β = a proportional constant, normally β =1 to 1.2, κ = Karman constant (κ =0.4 for clear water).

Assuming that the water velocity can be represented by the average velocity, v, the equation (5.14) can be rewritten into the following form:

$$Q_{sus} = q_{sus}B = BvC_a \frac{h}{6Z}\left(1 - \exp(-6Z)*\exp(6Za/h)\right) \tag{5.21}$$

where $Z = \dfrac{w_0}{\beta\kappa u_*}$.

Total sediment discharge is the sum of the bed load transport rate and suspended transport rate:

$$Q_s = Q_b + Q_{sus} \tag{5.22}$$

(2) Sediment mixtures

Sediment discharge for each grain size fraction is calculated by using bed load transport rate and suspended load transport rate for non-uniform sediment. The bed load transport rate for each fraction for general flow conditions is expressed as follows:

$$\frac{q_{bj}}{\sqrt{\left(\dfrac{\sigma}{\rho}-1\right)gd_j^{\,3}}} = 17 p_{sj}\tau_{*ej}^{3/2}\left(1 - \frac{\tau_{*cj}}{\tau_{*j}}\right)\left(1 - \frac{u_{*cj}}{u_*}\right) \tag{5.23}$$

where q_{bj} = the bed load transport rate of j-th fraction, d_j = grain size of j-th fraction and p_{sj} = percentage of j-th fraction in surface layer,

$$\tau_{*cj} = \frac{u_{*cj}^2}{(\sigma/\rho-1)gd_j} \;,\; \tau_{*j} = \frac{u_{*j}^2}{(\sigma/\rho-1)gd_j} \;,\; \tau_{*ej} = \frac{u_{*ej}^2}{(\sigma/\rho-1)gd_j}$$

For suspended load transport rate, the concentration at reference level for each fraction, C_{aj} , is obtained by multiplying by the proportion

factor p_{sj}. Then the Eq. (5.14) is used to obtain the suspended load transport rate:

$$C_{aj} = p_{sj} \frac{q_{suj}}{w_o} \qquad (5.24)$$

$$q_{susj} = vC_{aj} \frac{h}{6Z} \left(1 - \exp(-6Z) * \exp(6Za/h)\right) \qquad (5.25)$$

where, q_{suj} = pick up rate for each groups and q_{susj} = suspended load transport rate per width for each group.

The sediment discharge of j–th fraction is the sum of the bed load transport rate and suspended load transport rate of j–th fraction:

$$Q_{sj} = Q_{bj} + Q_{susj} \qquad (5.26)$$

5.2.4 Porosity estimation

As stated in the pervious section, the porosity is assumed to be dependent only on the characteristic parameters of grain size distribution (Eq.(5.11)). There are some types of grain size distribution as described in Chapter 3 such as lognormal distribution and M-Talbot distribution. Lognormal distribution has a parameter ($\Pi_1 = \sigma_L$) and M-Talbot distribution has two parameters ($\Pi_1 = d_{max}/d_{min}$, $\Pi_2 = n_T$,) where σ_L = standard deviation of $\ln d$, d_{max} = maximum grain size, d_{min} = minimum grain size and n_T = Talbot number. The porosity of lognormal and M-Talbot distribution can be obtained by using the relationship between the characteristic parameters and the porosity as shown in Figure 4.21 and Figure 4.24 for lognormal distribution and M-Talbot distribution, respectively. For binary mixtures with much different size, there were two cases of mixing, i.e., coarse packing and fine packing as described in Chapter 4. The porosities of these mixtures were expressed by Eq.(4.9) and Eq.(4.16) for coarse packing and fine packing, respectively.

5.3 An Exchange Model of Bed Material and Transported Sediment

The space distribution of porosity of bed material and its time variation are necessary to solve Eq.(5.10). To obtain them, it is convenient to make a multi-layer structure in riverbed as shown in Figure 5.10. Each layer is numbered from the surface layer (i.e., 1st layer is surface layer). According to Hirano's model, the thickness of each layer is assumed to be a constant which is equal to the maximum size of bed material. The exchange between bed material and transported sediment is assumed that it takes place only within the surface layer and the sediment transportation from an upper layer to the lower layer is neglected. These assumptions are contradicted with a fact that finer sediment possibly drops into the lower layer of gravel-cobble bed. For convenience sake, however, the condition is excluded in this model. Thus, in Fig.5.10 the sediment mass in the sections L_1 and L_2 is conserved during time Δt. The equations are solved by means of a finite differential method. So, the calculation grid structure whose lateral and vertical intervals are Δx and a, respectively, is made in riverbed.
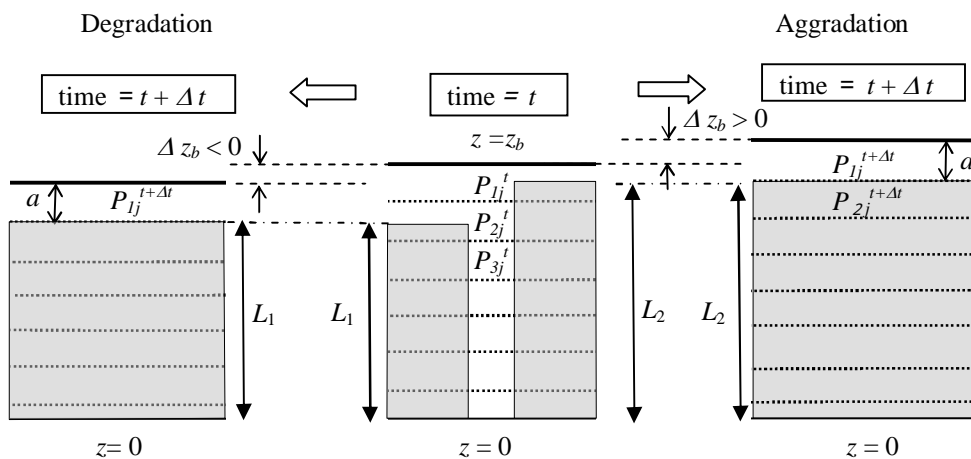
Fig.5.10 An employed multi-layer model.

If the porosity is not constant, the first term of Eq.(5.10) for bed degradation condition and bed aggradation condition can be expressed as follows:

(a) Bed degradation $(\partial z_b / \partial t < 0)$:

$$\frac{\partial}{\partial t} \int_{z_o}^{z_b} \{1 - \lambda(t,x,z)\} p_j(t,x,z) dz$$

$$= \left\{ \left(1 - \lambda_1^{t+\Delta t}\right) p_{1j}^{t+\Delta t} a - \left(1 - \lambda_1^t\right) p_{1j}^t a + \left(1 - \lambda_2^t\right) p_{2j}^t \Delta z_b \right\} / \Delta t$$

$$= \left\{ p_{1j}^{t+\Delta t} a - \lambda_1^{t+\Delta t} p_{1j}^{t+\Delta t} a - p_{1j}^t a + \lambda_1^t p_{1j}^t a + \left(1 - \lambda_2^t\right) p_{2j}^t \Delta z_b \right\} / \Delta t$$

$$= \left\{ a\left(p_{1j}^{t+\Delta t} - p_{1j}^t\right) - \lambda_1^{t+\Delta t} p_{1j}^{t+\Delta t} a + \lambda_1^{t+\Delta t} p_{1j}^t a - \lambda_1^{t+\Delta t} p_{1j}^t a + \lambda_1^t p_{1j}^t a + \left(1 - \lambda_2^t\right) p_{2j}^t \Delta z_b \right\} / \Delta t$$

$$= \left\{ a\left(p_{1j}^{t+\Delta t} - p_{1j}^t\right) - \lambda_1^{t+\Delta t} a\left(p_{1j}^{t+\Delta t} - p_{1j}^t\right) + p_{1j}^t a\left(\lambda_1^t - \lambda_1^{t+\Delta t}\right) + \left(1 - \lambda_2^t\right) p_{2j}^t \Delta z_b \right\} / \Delta t$$

$$= a\left(1 - \lambda_1^{t+\Delta t}\right) \frac{\left(p_{1j}^{t+\Delta t} - p_{1j}^t\right)}{\Delta t} - a p_{1j}^t \frac{\left(\lambda_1^{t+\Delta t} - \lambda_1^t\right)}{\Delta t} + \left(1 - \lambda_2^t\right) p_{2j}^t \frac{\Delta z_b}{\Delta t}$$

$$= \frac{\partial p_{1j}}{\partial t} a\left(1 - \lambda_1^{t+\Delta t}\right) - a p_{1j}^t \frac{\partial \lambda_1}{\partial t} + \left(1 - \lambda_2^t\right) p_{2j}^t \frac{\partial z_b}{\partial t}$$

Eq.(5.10) can be written as:

$$\frac{\partial p_{1j}}{\partial t} a\left(1 - \lambda_1^{t+\Delta t}\right) - a p_{1j}^t \frac{\partial \lambda_1}{\partial t} + \left(1 - \lambda_2^t\right) p_{2j}^t \frac{\partial z_b}{\partial t} + \frac{1}{B} \frac{\partial Q_{Sj}}{\partial x} = 0$$

$$\frac{\partial p_{1j}}{\partial t} = \frac{p_{1j}^t}{\left(1 - \lambda_1^{t+\Delta t}\right)} \frac{\partial \lambda_1}{\partial t} - \frac{1}{\left(1 - \lambda_1^{t+\Delta t}\right) aB} \frac{\partial Q_{Sj}}{\partial x} - \frac{\left(1 - \lambda_2^t\right)}{a\left(1 - \lambda_1^{t+\Delta t}\right)} p_{2j}^t \frac{\partial z_b}{\partial t} \tag{5.27}$$

$\lambda_1^{t+\Delta t}$, that is necessary for calculate Eq.(5.27), is associated with the grain size distribution of 1st layers at time $t+\Delta t$. To simplify the numerical method, the porosity of 1st layer at time $t+\Delta t$ is tentatively calculated by the porosity of 1st layer at time t. Eq.(5.27) can be rewritten as follows:

$$\frac{\partial p_{1j}}{\partial t} = \frac{p_{1j}}{(1 - \lambda_1)} \frac{\partial \lambda_1}{\partial t} - \frac{1}{(1 - \lambda_1) aB} \frac{\partial Q_{Sj}}{\partial x} - \frac{(1 - \lambda_2)}{a(1 - \lambda_1)} p_{2j} \frac{\partial z_b}{\partial t} \tag{5.28}$$

(b) Bed aggradation $(\partial z_b / \partial t \geq 0)$:

$$\frac{\partial}{\partial t} \int_{z_o}^{z_b} \{1 - \lambda(t,x,z)\} p_j(t,x,z) dz$$

$$= \left\{ \left(1 - \lambda_1^{t+\Delta t}\right) p_{1j}^{t+\Delta t} a - \left(1 - \lambda_1^{t}\right) p_{1j}^{t} \left(a - \Delta z_b\right) \right\} \Big/ \Delta t$$

$$= \left\{ \left(1 - \lambda_1^{t+\Delta t}\right) p_{1j}^{t+\Delta t} a - \left(1 - \lambda_1^{t+\Delta t}\right) p_{1j}^{t} a + \left(1 - \lambda_1^{t+\Delta t}\right) p_{1j}^{t} a - \left(1 - \lambda_1^{t}\right) p_{1j}^{t} \left(a - \Delta z_b\right) \right\} \Big/ \Delta t$$

$$= \left\{ \left(1 - \lambda_1^{t+\Delta t}\right) a \left(p_{1j}^{t+\Delta t} - p_{1j}^{t}\right) + p_{1j}^{t} a - \lambda_1^{t+\Delta t} p_{1j}^{t} a - a p_{1j}^{t} + p_{1j}^{t} \Delta z_b + \lambda_1^{t} p_{1j}^{t} a - \lambda_1^{t} p_{1j}^{t} \Delta z_b \right\} \Big/ \Delta t$$

$$= \left\{ \left(1 - \lambda_1^{t+\Delta t}\right) a \left(p_{1j}^{t+\Delta t} - p_{1j}^{t}\right) - p_{1j}^{t} a \left(\lambda_1^{t+\Delta t} - \lambda_1^{t}\right) + p_{1j}^{t} \left(1 - \lambda_1^{t}\right) \Delta z_b \right\} \Big/ \Delta t$$

$$= a \left(1 - \lambda_1^{t+\Delta t}\right) \frac{p_{1j}^{t+\Delta t} - p_{1j}^{t}}{\Delta t} - p_{1j}^{t} a \frac{\lambda_1^{t+\Delta t} - \lambda_1^{t}}{\Delta t} + p_{1j}^{t} \left(1 - \lambda_1^{t}\right) \frac{\Delta z_b}{\Delta t}$$

$$= \frac{\partial p_{1j}}{\partial t} a \left(1 - \lambda_1^{t+\Delta t}\right) - a p_{1j}^{t} \frac{\partial \lambda}{\partial t} + p_{1j}^{t} \left(1 - \lambda_1^{t}\right) \frac{\partial z_b}{\partial t}$$

Eq.(5.10) can be written as:

$$\frac{\partial p_{1j}}{\partial t} a \left(1 - \lambda_1^{t+\Delta t}\right) - a p_{1j}^{t} \frac{\partial \lambda_1}{\partial t} + \left(1 - \lambda_1^{t}\right) p_{1j}^{t} \frac{\partial z_b}{\partial t} + \frac{1}{B} \frac{\partial Q_{Sj}}{\partial x} = 0$$

$$\frac{\partial p_{1j}}{\partial t} = \frac{p_{1j}^{t}}{\left(1 - \lambda_1^{t+\Delta t}\right)} \frac{\partial \lambda_1}{\partial t} - \frac{1}{\left(1 - \lambda_1^{t+\Delta t}\right) aB} \frac{\partial Q_{Sj}}{\partial x} - \frac{p_{1j}^{t}}{a} \frac{\partial z}{\partial t} \tag{5.29}$$

$\lambda_1^{t+\Delta t}$, is necessary for calculate Eq.(5.29). To simplify the numerical method, similar with the bed degradation case, the porosity of 1st layer at time $t+\Delta t$ is tentatively calculated by the porosity of 1st layer at time t. Thus, Eq.(5.29) can be rewritten as follows:

$$\frac{\partial p_{1j}}{\partial t} = \frac{p_{1j}}{(1 - \lambda_1)} \frac{\partial \lambda_1}{\partial t} - \frac{1}{(1 - \lambda_1) aB} \frac{\partial Q_{Sj}}{\partial x} - \frac{1}{a} p_{1j} \frac{\partial z_b}{\partial t} \tag{5.30}$$

159

In the case of constant porosity, Eq.(5.28) and Eq.(5.30) are written as:

$$\frac{\partial p_{1j}}{\partial t} = \frac{-1}{(1-\lambda)aB}\frac{\partial Q_{Sj}}{\partial x} - \frac{p_{2j}}{a}\frac{\partial z_b}{\partial t} \quad (\partial z/\partial t < 0) \tag{5.31}$$

$$\frac{\partial p_{1j}}{\partial t} = \frac{-1}{(1-\lambda)aB}\frac{\partial Q_{Sj}}{\partial x} - \frac{p_{1j}}{a}\frac{\partial z_b}{\partial t} \quad (\partial z/\partial t \geq 0) \tag{5.32}$$

These equations were also presented by Hirano (1971).

5.4 Numerical Simulation Method

5.4.1 Standard Successive Approximation

To solve Eq.(5.1), (5.2), (5.9) and (5.10), some numerical simulation methods can be employed. One of them is a standard successive approximation method. For flow analysis, the calculation method is same as before. Eq.(5.9) and (5.10) are solved by means of a finite differential method. So, the calculation grid structure whose lateral and vertical intervals are Δx and a, respectively, is made in riverbed. Considering the mass balance of sediment in the multi-layer structure as shown in Figure 5.11, the increase in bed elevation Δz_b during time Δt under both condition of degradation and aggradation, is expressed as follows:
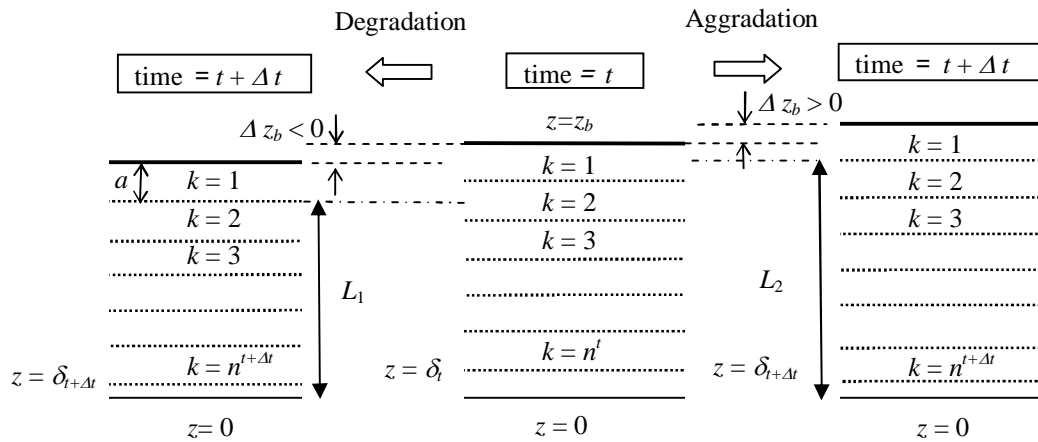
Fig. 5.11 An employed multi-layer model.

(1) Degradation condition ($\Delta z_b < 0$)

Initial absolute volume of bed material above $z = 0$:

$$\int_0^{z_b^t} (1 - \lambda)dz = \sum_{k=3}^{n^t} \left(1 - \lambda_k^t\right)a + \int_0^{\delta^t} \left(1 - \lambda^t\right)dz + \left(1 - \lambda_2^t\right)\left(a + \Delta z_b\right) - \left(1 - \lambda_2^t\right)\Delta z_b + \left(1 - \lambda_1^t\right)a$$

(5.33)

Absolute volume of bed material after degradation:

$$\int_0^{z_b^{t+\Delta t}} (1 - \lambda)dz = \sum_{k=2}^{n^{t+\Delta t}} \left(1 - \lambda_k^{t+\Delta t}\right)a + \int_0^{\delta^{t+\Delta t}} \left(1 - \lambda^{t+\Delta t}\right)dz + \left(1 - \lambda_1^{t+\Delta t}\right)a$$

(5.34)

Absolute sediment volume of L_1 is not changed, thus,

$$\sum_{k=2}^{n^{t+\Delta t}} \left(1 - \lambda_k^{t+\Delta t}\right)a + \int_0^{\delta^{t+\Delta t}} \left(1 - \lambda^{t+\Delta t}\right)dz = \sum_{k=3}^{n^t} \left(1 - \lambda_k^t\right)a + \int_0^{\delta^t} \left(1 - \lambda^t\right)dz + \left(1 - \lambda_2^t\right)\left(a + \Delta z_b\right)$$

(5.35)

Substituting Eq.(5.33), (5.34) and (5.35) to the first term of Eq.(5.9):

$$\frac{\partial}{\partial t}\int_0^{z_b}(1 - \lambda)dz = \frac{\left(1 - \lambda_1^{t+\Delta t}\right)a + \left(1 - \lambda_2^t\right)\Delta z_b - \left(1 - \lambda_1^t\right)a}{\Delta t}$$

(5.36)

$$\frac{\partial}{\partial t}\int_0^{z_b}(1 - \lambda)dz = \frac{1}{\Delta t}\left\{\left(\lambda_1^t - \lambda_1^{t+\Delta t}\right)a\right\} + \frac{\Delta z_b}{\Delta t}\left(1 - \lambda_2^t\right)$$

(5.37)

Substituting Eq.(5.37) to Eq.(5.9):

$$\frac{1}{\Delta t}\left\{\left(\lambda_1^t - \lambda_1^{t+\Delta t}\right)a\right\} + \frac{\Delta z_b}{\Delta t}\left(1 - \lambda_2^t\right) + \frac{1}{B\Delta x}\left(Q_{Si}^t - Q_{Si-1}^t\right) = 0$$

(5.38)

$$\Delta z_b = \frac{1}{1 - \lambda_2^t}\left\{\left(\lambda_1^{t+\Delta t} - \lambda_1^t\right)a - \frac{\Delta t}{B\Delta x}\left(Q_{Si}^t - Q_{Si-1}^t\right)\right\}$$

(5.39)

161

Second term of Eq (5.9) is expressed by backward differential as shown in Eq.(5.38) when it is sub critical flows. When it is super critical flows, Eq.(5.39) should be converted into forward differential shown in Eq.(5.40):

$$\Delta z_b = \frac{1}{1-\lambda_2^t}\left\{\left(\lambda_1^{t+\Delta t} - \lambda_1^t\right)a - \frac{\Delta t}{B\Delta x}\left(Q_{S\,i+1}^t - Q_{S1}^t\right)\right\} \tag{5.40}$$

where λ^t_n = porosity of n-th layer at time t, and $Q_{si}{}^t$ = sediment discharge at time t and i-th section.

(2) Aggradation condition ($\Delta z_b > 0$)

Initial absolute volume of bed material above $z=0$:

$$\int_0^{z_b^t}\left(1-\lambda\right)dz = \sum_{k=2}^{n^t}\left(1-\lambda_k^t\right)a + \left(1-\lambda^t\right)\Delta z_b \int_0^{\delta^t}\left(1-\lambda^t\right)dz + \left(1-\lambda_1^t\right)\left(a-\Delta z_b\right) \tag{5.41}$$

Absolute volume of bed material after aggradation:

$$\int_0^{z_b^{t+\Delta t}}\left(1-\lambda\right)dz = \sum_{k=2}^{n^{t+\Delta t}}\left(1-\lambda_k^{t+\Delta t}\right)a + \int_0^{\delta^{t+\Delta t}}\left(1-\lambda^{t+\Delta t}\right)dz + \left(1-\lambda_1^{t+\Delta t}\right)a \tag{5.42}$$

Absolute sediment volume of L_2 is not changed, thus,

$$\sum_{k=2}^{n^{t+\Delta t}}\left(1-\lambda_k^{t+\Delta t}\right)a + \int_0^{\delta^{t+\Delta t}}\left(1-\lambda^{t+\Delta t}\right)dz = \sum_{k=2}^{n^t}\left(1-\lambda_k^t\right)a + +\left(1-\lambda_1^t\right)\Delta z_b \int_0^{\delta^t}\left(1-\lambda^t\right)dz$$

$$\tag{5.43}$$

Substituting Eqs.(5.41), (5.42) and (5.43) to first term of Eq.(5.9):

$$\frac{\partial}{\partial t}\int_0^z\left(1-\lambda\right)dz = \frac{\left(1-\lambda_1^{t+\Delta t}\right)a - \left(1-\lambda_1^t\right)\left(a-\Delta z_b\right)}{\Delta t} \tag{5.44}$$

$$\frac{\partial}{\partial t}\int_0^z\left(1-\lambda\right)dz = \frac{1}{\Delta t}\left\{\left(\lambda_1^t - \lambda_1^{t+\Delta t}\right)a\right\} + \frac{\Delta z_b}{\Delta t}\left(1-\lambda_1^t\right) \tag{5.45}$$

Substituting Eq.(5.45) to Eq.(5.9):

$$\frac{1}{\Delta t}\left\{\left(\lambda_1^t - \lambda_1^{t+\Delta t}\right)a\right\} + \frac{\Delta z_b}{\Delta t}\left(1 - \lambda_2^{t+\Delta t}\right) + \frac{1}{B\Delta x}\left(Q_{Si}^t - Q_{Si-1}^t\right) = 0 \qquad (5.46)$$

$$\Delta z_b = \frac{1}{1-\lambda_1^t}\left\{\left(\lambda_1^{t+\Delta t} - \lambda_1^t\right)a - \frac{\Delta t}{B\Delta x}\left(Q_{Si}^t - Q_{Si-1}^t\right)\right\} \qquad (5.47)$$

Second term of Eq.(5.9) is expressed by backward differential as shown in Eq.(5.46) when it is sub critical flows. When it is super critical flows, Eq.(5.47) should be converted into forward differential shown in Eq.(5.48):

$$\Delta z_b = \frac{1}{1-\lambda_1^t}\left\{\left(\lambda_1^{t+\Delta t} - \lambda_1^t\right)a - \frac{\Delta t}{B\Delta x}\left(Q_{Si+1}^t - Q_{Si}^t\right)\right\} \qquad (5.48)$$

(3) Tentative grain size distribution and porosity

$\lambda_1^{t+\Delta t}$, that necessary to calculate Eqs.(5.39) and (5.47), is associated with the grain size distribution of 1st layer at time $t+\Delta t$. As described before, Eqs.(5.9),(5.11),(5.28) and (5.30) are a set of implicit differential equations. To simplify the numerical method, the grain size distribution of 1st layer at time $t+\Delta t$ is tentatively calculated by Eq.(5.49):

$$p_{1j}^{t+\Delta t} = \frac{p_{1j}^t\left(1-\lambda_1^t\right)a\Delta x B - \Delta t\left(Q_{Si,j}^t - Q_{Si-1,j}^t\right)}{\left(1-\lambda_1^t\right)a\Delta x B - \Delta t\left(Q_{Si}^t - Q_{Si-1}^t\right)} \qquad (5.49)$$

This grain size distribution is used only for determining the porosity $\lambda_1^{t+\Delta t}$ and the grain size distribution of 1st layers at time $t+\Delta t$ is recalculated by Eqs.(5.28) or (5.30). Eq. (5.49) is obtained by considering the sediment budget only in the 1st layer at time t. Therefore, this distribution differs from the grain size distribution in the 1st layer at time $t+\Delta t$. To reduce the difference, it is necessary to take smaller interval time Δt so that Δz_b is much smaller.

The vertical exchange of sediment under the 2nd layer is not considered. The new grain size distribution under the 2nd layer at time $t+\Delta t$ is obtained by rearrangement of the bed layer structure and the renewal of grain size distribution in the 1st layer. Based on these conditions, Eq.(5.10) is then described as follows:

(a) Bed degradation:

$$\frac{\partial p_{1j}}{\partial t} = \frac{p_{1j}}{(1-\lambda_1)} \frac{\partial \lambda_1}{\partial t} - \frac{1}{(1-\lambda_1)aB} \frac{\partial Q_{Sj}}{\partial x} - \frac{(1-\lambda_2)}{a(1-\lambda_1)} p_{2j} \frac{\partial z_b}{\partial t} \qquad (5.50)$$

(b) Bed aggradation:

$$\frac{\partial p_{1j}}{\partial t} = \frac{p_{1j}}{(1-\lambda_1)} \frac{\partial \lambda_1}{\partial t} - \frac{1}{(1-\lambda_1)aB} \frac{\partial Q_{Sj}}{\partial x} - \frac{1}{a} p_{1j} \frac{\partial z_b}{\partial t} \qquad (5.51)$$

These equations are expressed in finite differential form as

(a) Bed degradation:

$$\frac{\Delta p_{1j}}{\Delta t} = \frac{p_{1j}}{(1-\lambda_1)} \frac{\Delta \lambda_1}{\Delta t} - \frac{1}{(1-\lambda_1)aB} \frac{Q_{Si+1,j} - Q_{si,j}}{\Delta x} - \frac{(1-\lambda_2)}{a(1-\lambda_1)} p_{1j} \frac{\Delta z_b}{\Delta t} \qquad (5.52)$$

(b) Bed aggradation:

$$\frac{\Delta p_{1j}}{\Delta t} = \frac{p_{1j}}{(1-\lambda_1)} \frac{\Delta \lambda_1}{\Delta t} - \frac{1}{(1-\lambda_1)aB} \frac{Q_{Si+1,j} - Q_{Si,j}}{\Delta x} - \frac{1}{a} p_{1j} \frac{\Delta z_b}{\Delta t} \qquad (5.53)$$

5.4.2 MacCormack Scheme

(1)   Conservation form

The system of differential equations is solved by the MacCormack explicit finite difference scheme using alternatively forward and backward

finite differences. The MacCormack method can automatically find the location of hydraulic jumps, and does not need to select the backward or forward differential. Moreover, all the basic equations are rewritten into a conservation form, so that both the water surface and riverbed calculations can be executed in a single algorithm. The basic equations, including 1) the equation of continuity of water flow, 2) momentum conservation law, and 3) the equation of continuity of sediment transport are rewritten into a conservation form as shown below:

$$\frac{\partial U}{\partial t} + \frac{\partial E}{\partial x} = C \tag{5.54}$$

where t = the time, x = the longitudinal flow direction. U, E, and C are expressed as follows:

$$U = \begin{pmatrix} Bh \\ Q \\ \int_{z_o}^{z_b}(1-\lambda)dz \end{pmatrix}, \quad E = \begin{pmatrix} Q \\ \frac{1}{2}gBh^2 + \frac{Q^2}{Bh} \\ \frac{Q_s}{B} \end{pmatrix}, \quad C = \begin{pmatrix} 0 \\ gBh(i_b - i_f) \\ 0 \end{pmatrix} \tag{5.55}$$

where B = the channel width, h = the water depth, Q = the water discharge, z_b = the elevation of channel bed, g = the gravity acceleration, Q_S = the sediment discharge, λ = the porosity of the bed materials, i_b = the channel slope, i_f = the energy slope.

The MacCormack method is a simultaneous calculation of the water level and riverbed elevation using the Predictor level and Corrector level equations derived from Eq.(5.54). The Predictor level equation is a forward differential, while the Corrector level equation is a backward differential, though it is possible to substitute each other. To prevent instability of calculation, it is necessary to add a term to give artificial viscosity, as shown below:

Predictor level (see Fig. 5.12):

$$\overline{U}_i = U_i^j - \frac{\Delta t}{\Delta x}\left\{E_{i+1}^j - E_i^j + \left(D_{i+1}^j - D_i^j\right)\right\} + \Delta t C_i^j \qquad (5.56)$$

Corrector level (see Fig 5.13):

$$U_i^{j+1} = \frac{1}{2}\left(U_i^j + \overline{U}_i\right) - \frac{\Delta t}{2\Delta x}\left\{\overline{E}_i - \overline{E}_{i-1} - \left(\overline{D}_i - \overline{D}_{i-1}\right)\right\} + \frac{\Delta t}{2}\overline{C}_i \qquad (5.57)$$

where D = artificial viscosity

The terms $\overline{E}$, $\overline{D}$, $\overline{C}$, are those calculated using the results of the Predictor level calculation. The artificial viscosity can be given by the following equation:

$$D_i^j = K u_{*i} h_i \left(U_{i+1}^j - 2U_i^j + U_{i-1}^j\right)\ \left(\frac{1}{\Delta x}\right) \qquad (5.58)$$

where K = the coefficient of artificial viscosity given by the following equation:

$$K = \begin{bmatrix} k_v & 0 & 0 \\ 0 & k_v & 0 \\ 0 & 0 & k_z \end{bmatrix} \qquad (5.59)$$

Generally k_v = 1 to 5 and k_z is smaller than k_v by one order.

(2)   Water depth, water discharge and bed level

When U_1, U_2 and U_3 are first, second and third components of U, the water depth and the water discharge are obtained as:

$$h = U_1 / B \qquad (5.60)$$

$$Q = U_2 \qquad (5.61)$$

m   m-1 m-2   3   2   1

D_m D_{m-1} D_{m-2} D_3 D_2 D_1

t

$t+\Delta t$

U_m U_{m-1} U_{m-2} - U_3 U_2 U_1

E_m E_{m-1} E_{m-2} - E_3 E_2 E_1

C_m C_{m-1} C_{m-2} - C_3 C_2 C_1
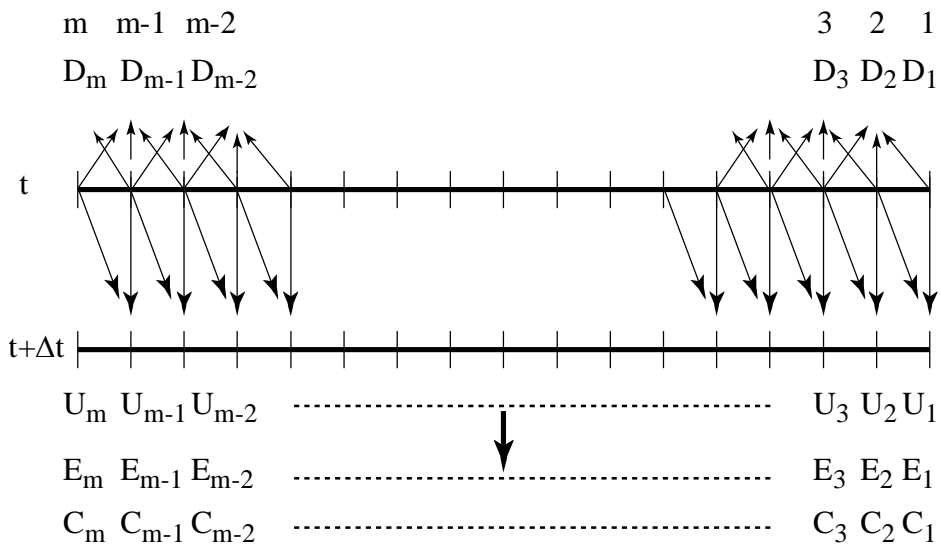
Fig.5.12 Predictor scheme.

m   m-1 m-2   3   2   1

D_m D_{m-1} D_{m-2} D_3 D_2 D_1

t

$t+\Delta t$

U_m U_{m-1} U_{m-2} - U_3 U_2 U_1

E_m E_{m-1} E_{m-2} - E_3 E_2 E_1

C_m C_{m-1} C_{m-2} - C_3 C_2 C_1
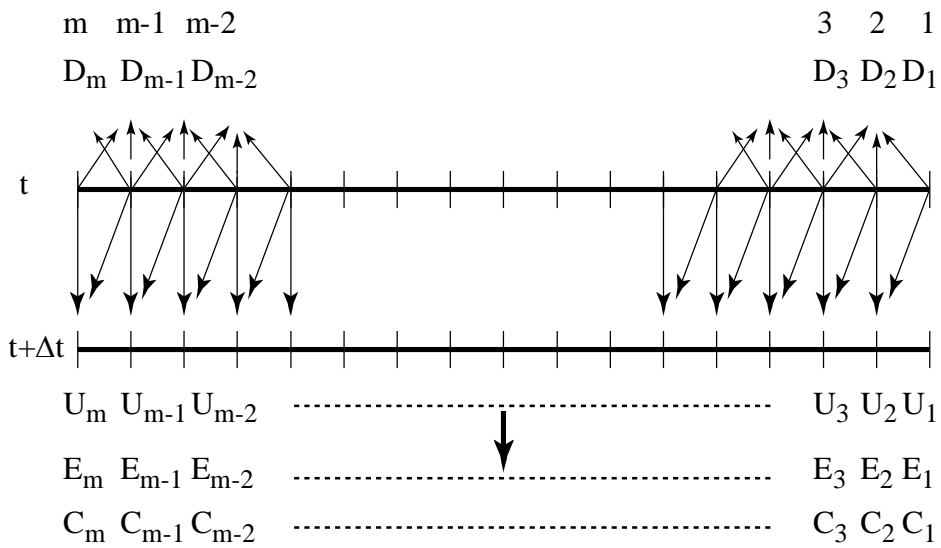
Fig.5.13 Corrector scheme.

167

Bed level is obtained as follows:

$$U_3 = \int_{z_o}^{z_b}(1-\lambda)dz = z_b - z_o - \int_{z_o}^{z_b}\lambda\,dz = z_b - R(z) \tag{5.62}$$

where $\quad R(z) = z_o + \int_{z_o}^{z_b}\lambda\,dz$

Therefore, the increase in bed level is expressed by

$$\Delta z_b = \Delta U_3 + \Delta R \tag{5.63}$$

where

$$\Delta R = R(z_b^{t+\Delta t}) - R(z_b^t) = \int_{z_o}^{z_b+\Delta z}\lambda dz - \int_{z_o}^{z_b}\lambda dz \tag{5.64}$$

(3)   A layer model

A layer model is necessary to calculate Eq.(5.64). The gray area in Fig.5.14 is not disturbed with bed variation at all. Therefore, ΔR is obtained as follows:

Bed degradation:

$$\Delta R = \left(\lambda_1^{t+\Delta t} - \lambda_1^t\right)a + \lambda_2^t\Delta z_b \tag{5.65}$$

Bed aggradation:

$$\Delta R = \left(\lambda_1^{t+\Delta t} - \lambda_1^t\right)a + \lambda_1^t\Delta z_b \tag{5.66}$$
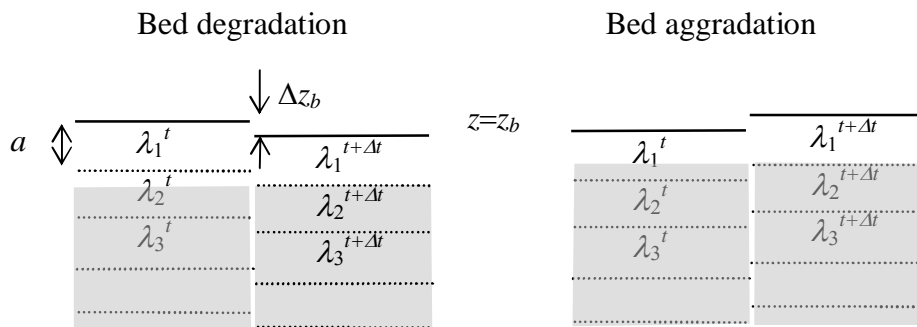
Fig.5.14 A layer model.

Therefore,

Bed degradation:

$$\Delta z_b = \frac{\left(\lambda_1^{t+\Delta t} - \lambda_1^t\right)a + \Delta U_3}{1 - \lambda_2^t} \tag{5.67}$$

Bed aggradation:

$$\Delta z_b = \frac{\left(\lambda_1^{t+\Delta t} - \lambda_1^t\right)a + \Delta U_3}{1 - \lambda_1^t} \tag{5.68}$$

In Eq.(5.67) and (5.68), $\lambda_1{}^t$ and $\lambda_2{}^t$ are obtained from Eq.(5.11). However, $\lambda_1{}^{t+\Delta t}$ is not obtained because the grain size distribution at time $t+\Delta t$ is not calculated yet. So, using the following equation, the percentage of each fraction of the bed material, $p_j{}^{t+\Delta t}$, at time $t+\Delta t$ is temporally calculated as follows:

$$p_{1j}^{t+\Delta t} = \frac{p_{1j}^t\left(1 - \lambda_1^t\right)aB\Delta x - \dfrac{\partial Bq_{s,j}^t}{\partial x}\Delta x\Delta t}{\left(1 - \lambda_1^t\right)aB\Delta x - \dfrac{\partial Bq_s^t}{\partial x}\Delta x\Delta t} \tag{5.69}$$

(4) Grain size distribution

Grain size distribution is calculated by the following equations.

(a) Bed degradation:

$$\frac{\partial p_{1j}}{\partial t} = \frac{p_{1j}}{(1 - \lambda_1)}\frac{\partial \lambda_1}{\partial t} - \frac{1}{(1 - \lambda_1)aB}\frac{\partial Q_{Sj}}{\partial x} - \frac{(1 - \lambda_2)}{a(1 - \lambda_1)}p_{2j}\frac{\partial z_b}{\partial t} \tag{5.70}$$

(b) Bed aggradation:

$$\frac{\partial p_{1j}}{\partial t} = \frac{p_{1j}}{(1 - \lambda_1)}\frac{\partial \lambda_1}{\partial t} - \frac{1}{(1 - \lambda_1)aB}\frac{\partial Q_{Sj}}{\partial x} - \frac{1}{a}p_{1j}\frac{\partial z_b}{\partial t} \tag{5.71}$$

Finite differential form of Eq.(5.70) and (5.71) are as follows:

(a) Bed degradation:

$$\frac{\Delta p_{1j}}{\Delta t} = \frac{p_{1j}}{(1-\lambda_1)} \frac{\Delta \lambda_1}{\Delta t} - \frac{1}{(1-\lambda_1)aB} \frac{(Q_{Si+1,j} - Q_{Si,j})}{\Delta x} - \frac{(1-\lambda_2)}{a(1-\lambda_1)} p_{2j} \frac{\Delta z_b}{\Delta t}$$

(5.72)

(b) Bed aggradation:

$$\frac{\Delta p_{1j}}{\Delta t} = \frac{p_{1j}}{(1-\lambda_1)} \frac{\Delta \lambda_1}{\Delta t} - \frac{1}{(1-\lambda_1)aB} \frac{(Q_{Si+1,j} - Q_{Si,j})}{\Delta x} - \frac{1}{a} p_{1j} \frac{\Delta z_b}{\Delta t}$$

(5.73)

5.5 An Algorithm for Estimating the Porosity

To establish a bed-porosity variation model, the important point is how to introduce the results in Chapter 3 and Chapter 4 into a bed variation model. Therefore, a sub-program of identifying the grain size distribution type and obtaining the porosity is explained in this section. The sub-program involves four stages as shown in Figure 5.15.

Input data

⇩

Identification and classification

⇩

Obtaining the characteristic parameters
of grain size distribution

⇩

Estimating the porosity
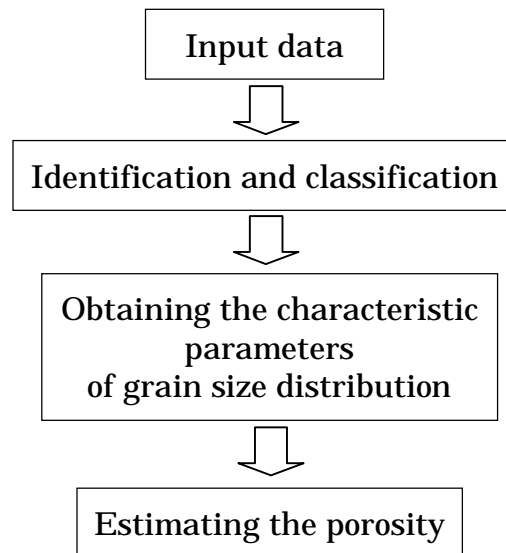
Fig.5.15   Calculation procedure for classifying the grain size
distribution and estimating the porosity.

170

5.5.1 Input grain size distribution

The grain size of bed material is divided into some classes in bed variation model. The representative grain sizes $dd(j)$ of class-j and the proportion $p_s(j)$ are generally used in calculation. However, the minimum grain size and the maximum grain size are necessary to obtain the geometric indices β and γ. To obtain the Talbot number by fitting the grain size distribution with Talbot distribution function, j-th grain size $d(j)$ and the percent finer $f(j)$ are also necessary. Therefore, $d(j)$ and $f(j)$ as well as $dd(j)$ and $p_s(j)$ are used in the calculation program. As the representative grain size $dd(j)$ is the geometric average of the uppermost size and the lowest size of class-j, $d(j)$, $f(1)$ and $f(j)$ are calculated by Eqs.(5.74) ,(5.75) and (5.76), respectively. However, the minimum grain size $d(1)$ or the maximum grain size $d(n)$ is necessary:

$$d(j+1) = \frac{dd(j)^2}{d(j)} \tag{5.74}$$

$$f(1)=0.0 \tag{5.75}$$

$$f(j) = \sum_{j=1}^{j-1} f_s(j) \qquad (j>1) \tag{5.76}$$

5.5.2 Identification and classification

The grain size distribution is then classified into M-Talbot type and lognormal type. The geometric indices β and γ are calculated with the input data on grain size distribution. Then, the geometric type of the grain size distribution is identified using the diagram on classification of grain size distribution type as shown in Figure 3.10.

5.5.3 Obtaining the characteristic parameters of grain size distribution

The characteristic parameters of grain size distribution are obtained by fitting curve method. The characteristic parameter of the lognormal distribution is only standard deviation σ_L. Standard deviation for lognormal distribution is calculated from the grain size distribution data.

$$\sigma_L{}^2 = \sum_{j=1}^{N} \left(\ln d_j - \overline{\ln d} \right)^2 p_{sj} \tag{5.77}$$

The characteristic parameters of M-Talbot distribution are Talbot number, n_T, and ratio of maximum and minimum diameter, d_{max}/d_{min}. The method of least squares is the best way to obtain Talbot number, but the easier method, that is an individually 5 points fitting method, is used in this study. Talbot number by one point fitting for percent finer of $x\%$ is calculated as:

$$n_{T(x\%)} = \frac{\ln\left(f(d_{(x\%)}) \right)}{\ln\left(\dfrac{\log d_{(x\%)} - \log d_{min}}{\log d_{max} - \log d_{min}} \right)} \tag{5.78}$$

After Talbot numbers are obtained for 5 points (16%, 25%, 50%, 75% and 84%), Talbot number is finally obtained from the average of $n_T(x\%)$ as follows:

$$n_T = \frac{n_{T(16\%)} + n_{T(25\%)} + n_{T(50\%)} + n_{T(75\%)} + n_{T(84\%)}}{5} \tag{5.79}$$

5.5.4 Estimating the porosity

The porosity is estimated by using the relation between the characteristic parameters of grain size distribution and the porosity as shown in Figure 4.21 and Figure 4.24 for lognormal and M-Talbot distributions, respectively.

(1) Lognormal distribution

As explained in Chapter 4 that there were some differences in the trend of porosity change with the standard deviation between the measurement and the simulation. The reason seemed due to the difference in compaction degree and the inverse grading in the real sediment packing. It is impossible to consider these effects into the porosity estimation model, but it is necessary to calibrate the estimated porosity.

In this study, the more appropriate porosity is obtained under two assumptions. One is the uniform sediment usually has a porosity of 0.4 and the other is the uniform sediment has a standard deviation less than 0.2. Under these assumptions, the particle packing simulation result is expanded as shown in Fig.5.16. Consequently, the porosity of lognormal distribution is expanded for all standard deviation. The corrected porosity is used to estimate the porosity in the bed-porosity variation model.
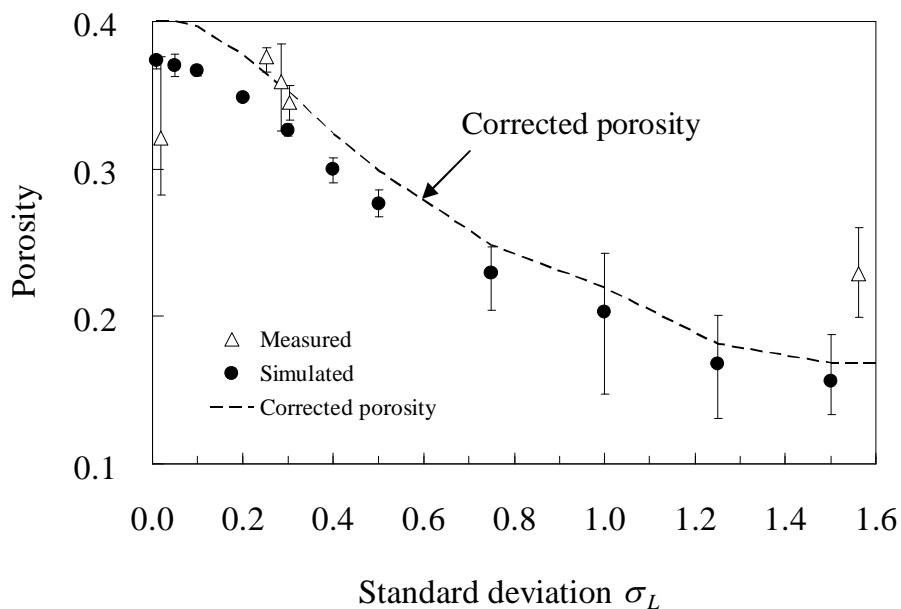
Fig. 5.16   Estimated porosity of lognormal distribution for bed-porosity variation model

(2) M-Talbot distribution

As shown in Figure 4.24, both of the simulation result and the measurement result show that the porosity increases with Talbot number and the ratio of maximum and the minimum grain sizes. The important thing in Fig.4.24 is that simulation result shows the pararel line and has the same inclination even for different ratio of maximum and minimum diameters. This slope represents the changing rate of porosity to Talbot number. Thus, the changing rate seems to be constant. As explained in Chapter 4, there were some differences in the trend of porosity change with the Talbot number between the measurement and the simulation due to the effect of compaction and inverse grading. Therefore, the simulation result and measurement result cannot be used directly. To estimate the porosity in the bed-porosity variation model, the correction of the simulation and measurement results is needed. The basic assumption used is similar to the assumption used in the calibration of lognormal distribution. One is the uniform sediment usually has a porosity of 0.4 and the other is the uniform sediment has a standard deviations less than 0.2. The corrected porosity is obtained as follows. First, the slope of the relationship between porosity and Talbot number is determined. Second, the critical Talbot number where M-Talbot distribution can be recognized as uniform distribution is determined. Based on the simulation result, the increase rate of porosity to Talbot number is $\partial\lambda/\partial n_T$ =0.0125. As the Talbot number increases, the sediment mixtures tend to be uniform. The critical Talbot number can be obtained by using the relation between Talbot number and the standard deviation as shown in Figure 5.17. If the standard deviation of uniform sediment is assumed to be 0.2, the critical Talbot numbers are 8, 18 and 22 for d_{max}/d_{min}=10, 100 and 1000, respectively. The porosity of M-Talbot distribution is estimated based on the slope and the critical Talbot number. The relations are listed in Table 5.2 and shown in Figure 5.18.

174
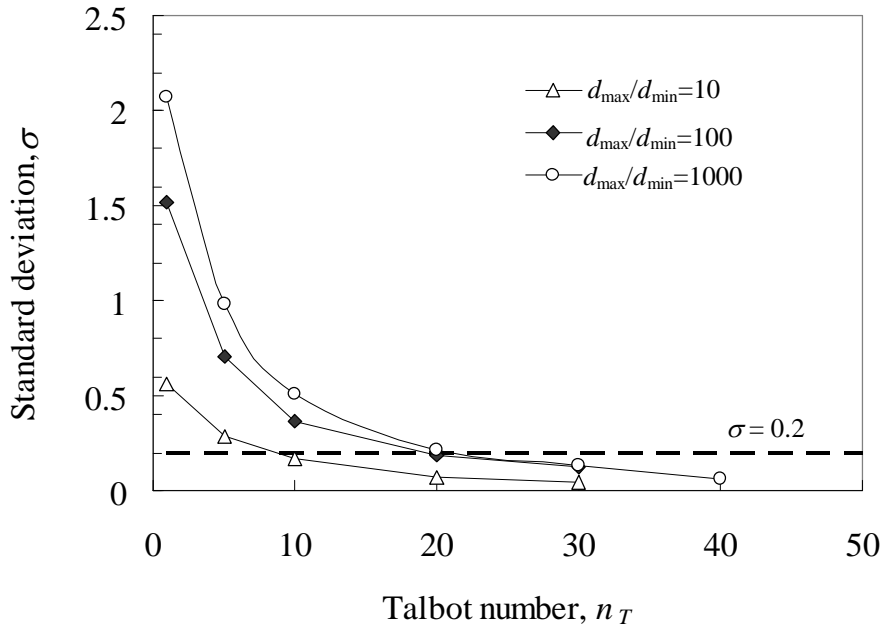
Fig. 5.17 Relationship between Talbot number and standard deviation for M-Talbot distribution

Table 5.2 Porosity of M-Talbot distribution

d_{max}/d_{min}	Porosity (λ)
$100 < d_{max}/d_{min}$	$\lambda = 0.0125n_T + 0.3$
$100 \leq d_{max}/d_{min} < 1000$	$\lambda = 0.0125n_T + 0.2$
$d_{max}/d_{min} \geq 1000$	$\lambda = 0.0125n_T + 0.15$
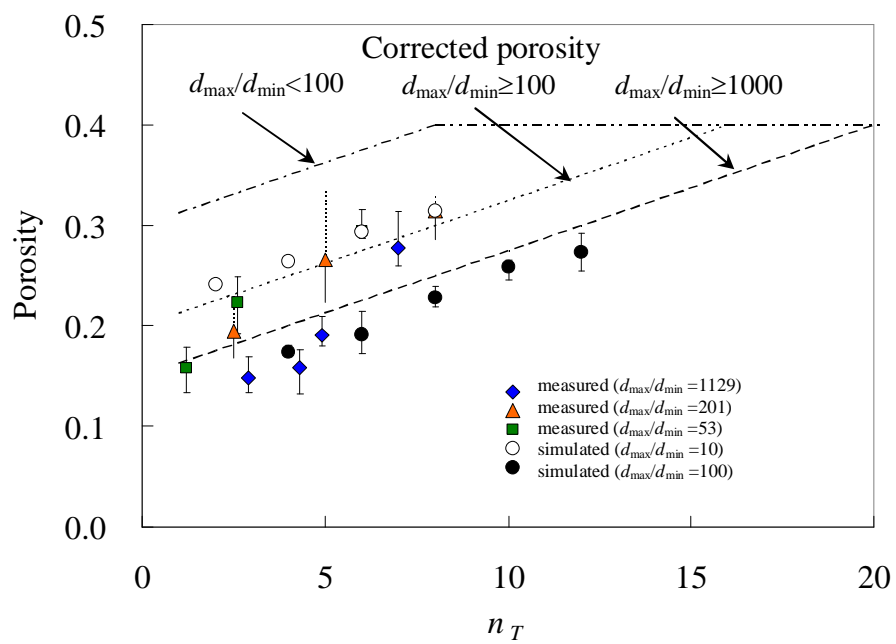
Fig. 5.18 Estimated porosity of M-Talbot distribution for bed-porosity variation model

5.6 Numerical Simulation Results and Discussion

5.6.1 Simulation on bed-porosity variation by standard successive approximation

(1) Condition

The bed-porosity variation model with standard successive approximation is applied to simulate the bed and porosity variation process observed in the flume experiment described in section 5.1.1. The porosity is obtained by a simple analytical model for binary mixtures as presented in Chapter 4 Section 4.2. Porosity is determined from the mixing ratio of finer particle (or coarser particle). The initial bed material is composed of two particle sizes. The diameters of particle are $d_1 = 2$ mm and $d_2 = 13$ mm. The mixing ratio of particle with a size of d_1 is 28%. Initial channel slope is 0.02 and a weir is installed at the downstream end of the channel. The water is supplied at a rate of 0.0136 m³/s.

Simulation is conducted under two conditions. In the Run 1, no fine particle is supplied to the bed material. In the Run 2, fine particle is supplied constantly from the upstream end of the channel at a rate of $q_s = 31.8 \times 10^{-6}$ m²/s. Run 1 is followed by Run 2; the condition of bed material in the end of Run 1 is used as initial condition of Run 2.   Each simulation is carried out by 4 steps as in the experiment.   Cumulative time steps for Run 1 are 20, 65, 130, 250 minutes and for Run 2 are 30, 50, 66, 82 minutes. The simulation conditions are summarized in Table 5.3.

Table 5.3   Simulation conditions on bed variation by standard successive approximation, in the case of binary mixtures.

Simulation	Q_w (m³/s)	q_s (10^{-6} m²/s)	Time (min)
Run 1	0.0136	0	20, 65, 130, 250
Run 2	0.0136	31.8	30,50, 66, 82

To make the improvement of this bed variation model clear, the simulation result is compared with the result calculated by a standard bed variation model on the assumption that the porosity is constant.

(2) Results

Figure 5.19 shows the comparisons of the simulated results by (a) the standard bed variation model and by (b) the presented model with the experimental results. Both simulation results look similar, but there are some differences on the bed variation in the upstream region. The characteristics on bed variation described in section 5.1.1 come from the change in the porosity of bed material. In the Run 1, the experimental result shows that the bed degradation is very small. The simulated result by the standard model shows that the degradation depth is rather larger (Fig.5.19(a)). In the result by the presented model (Fig.5.19(b)), the degradation does not occur; the longitudinal variation of sediment transport cannot cause the bed elevation change but the change in the porosity of the bed material occurs at a location under the condition. Therefore, the presented model can produce the more reasonable bed variation in the upstream region. However, the developing velocity of the delta in the simulation is rather faster than the experimental one. It seems that this disagreement may be due to the applicability of the employed bed load formula that has not developed for a binary mixture with much different grain sizes.
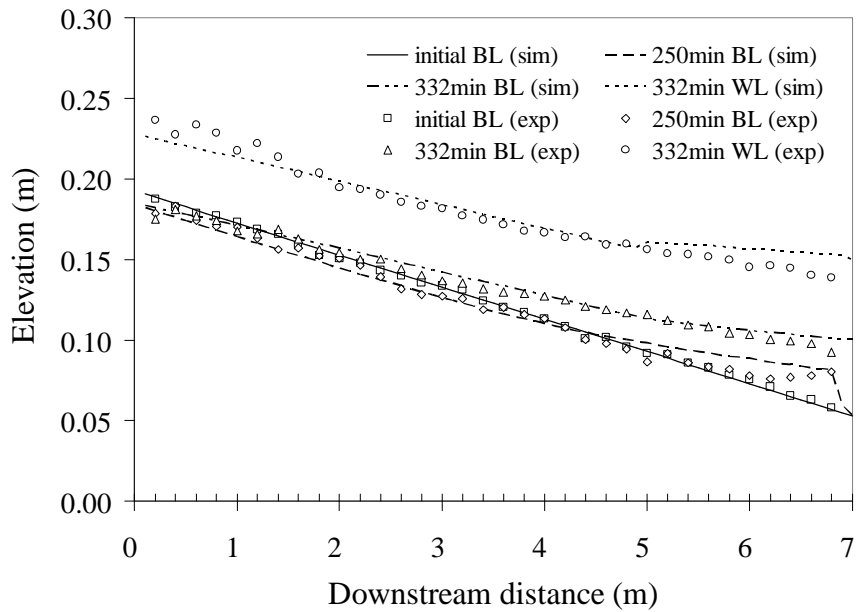
(a) Constant porosity
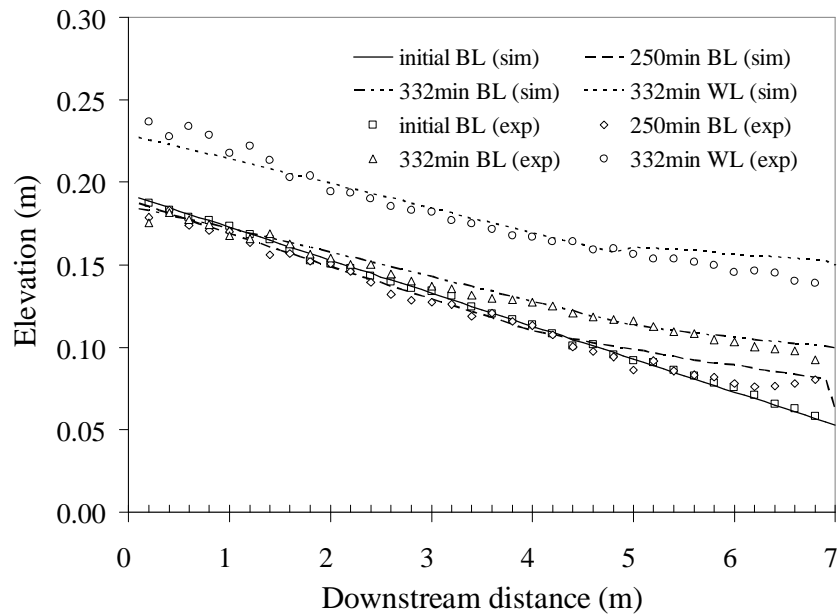
(b) Porosity dependent on grain size distribution

Fig.5.19   Simulation result and experimental result on bed variation;
(a) porosity is assumed to be constant, (b) porosity is
calculated by Eqs.(5.10) and (5.11).

Figure 5.20 shows the longitudinal distributions of the fine sediment proportion simulated by the presented model and obtained in the experiment. The simulated result explains the process of the fine sediment movement; in Run 1, the fine sediment is removed from the bed material in the upstream region and deposits in the downstream region and in Run 2, the supplied fine sediment buries the pore of the bed material. The comparison between the simulated result and experimental result shows the presented model can simulate the tendency of the variation of the grain size distribution.
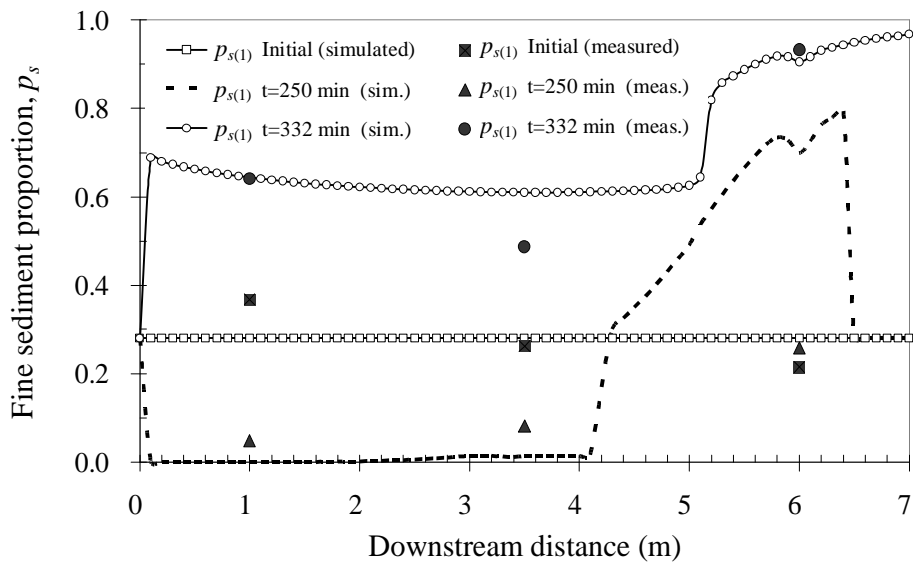
Fig.5.20 Simulation and experiment results on fine sediment proportion of surface bed material

Figure 5.21 shows the simulated result on the longitudinal porosity changes of surface bed layer. After Run 1 (t = 250 min), the porosity of surface layer in the upstream region increases from the original value, because of the entrainment of fine sediment from bed material. The porosity in the downstream region also increases because the fine sediment covers the bed material. Comparing each size of voids in this region, the size in the upstream region is much larger. At the boundary between the both regions,

180

the porosity decreases because of mixing of fine sediment and coarse sediment. After Run 2 (t = 332 min), the fine sediment moves downstream burying the pore of the bed material in the upstream region. Consequently, the porosity decreases. As the delta is composed of the fine sediment only, the porosity of the surface of the delta is approaching to a normal porosity λ_s (in this simulation λ_s =0.40).
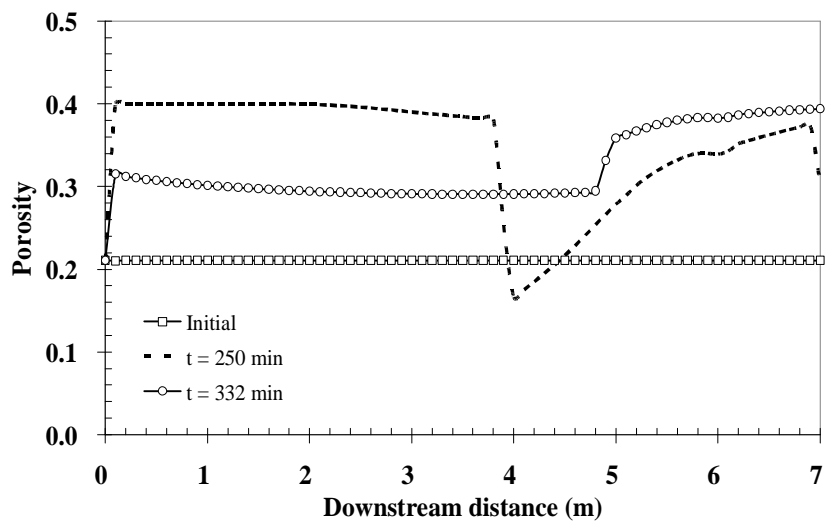
Fig.5.21 Simulation result on longitudinal porosity changes of bed surface layer.

5.6.2 Simulation on bed-porosity variation by MacCormack scheme

The presented bed-porosity variation model is applied to simulation of the bed variation processes on the some conditions by means of MacCormack scheme. Firstly, the model is applied to the bed variation in the case of binary mixtures. Secondly, the model is applied to the bed variation process observed in the flume experiment as described in section 5.1.1. Thirdly, the model is applied to the bed and porosity variation process for bed material with continuous grain size distribution, under two conditions; (1) no sediment supply condition and (2) sediment supply condition.

(1) Bed variation in the case of binary mixtures

a) Conditions

The presented bed-porosity variation model is applied to the bed and porosity variation in a channel with a length of 15 m and a width of 0.5 m. The initial channel slope is 0.02 and at the downstream end of the channel is set at two cases, fixed with a groundsill (without weir) and installed a weir with a height of 0.05 m. The water is supplied at a rate of 0.02 m³/s. Simulation is conducted to observe the bed and porosity variation under two conditions; one is the only fine sediment is removed from a bed sediment mixtures (no sediment supply) and another is the fine sediment supply into a bed material (sediment supply). The initial bed material is composed of two particle sizes. In the case of no sediment supply, the diameters of particle are $d_1 = 0.5$ mm and $d_2 = 20$ mm. The mixing ratio of particles with a size of d_1 is 30%. In the case of sediment supply, the diameters of particle are $d_1 = 1$ mm and $d_2 = 20$ mm. The mixing ratio of particles with a size of d_1 is 10%. The smaller particle diameter is also used as the supplied sediment. Simulation is carried out for four cases i.e., B-1, B-2, B-3, and B-4. A weir is installed to investigate the process of sedimentation in the Case B-2 and B-4. The simulation conditions are summarized in Table 5.4 and shown in Figure 5.22.

Table 5.4 Simulation conditions on bed variation by MacCormack scheme, in the case of binary mixtures.

Simulation	d_1 (mm)	d_2 (mm)	f_1 (%)	f_2 (%)	Q_w (m³/s)	q_s (10^{-6} m²/s)	Downstream end condition
Case B-1	0.5	20	30	70	0.02	0	groundsill
Case B-2	0.5	20	30	70	0.02	0	weir
Case B-3	1.0	20	10	90	0.02	5	groundsill
Case B-4	1.0	20	10	90	0.02	5	weir

For all cases, slope = 0.02
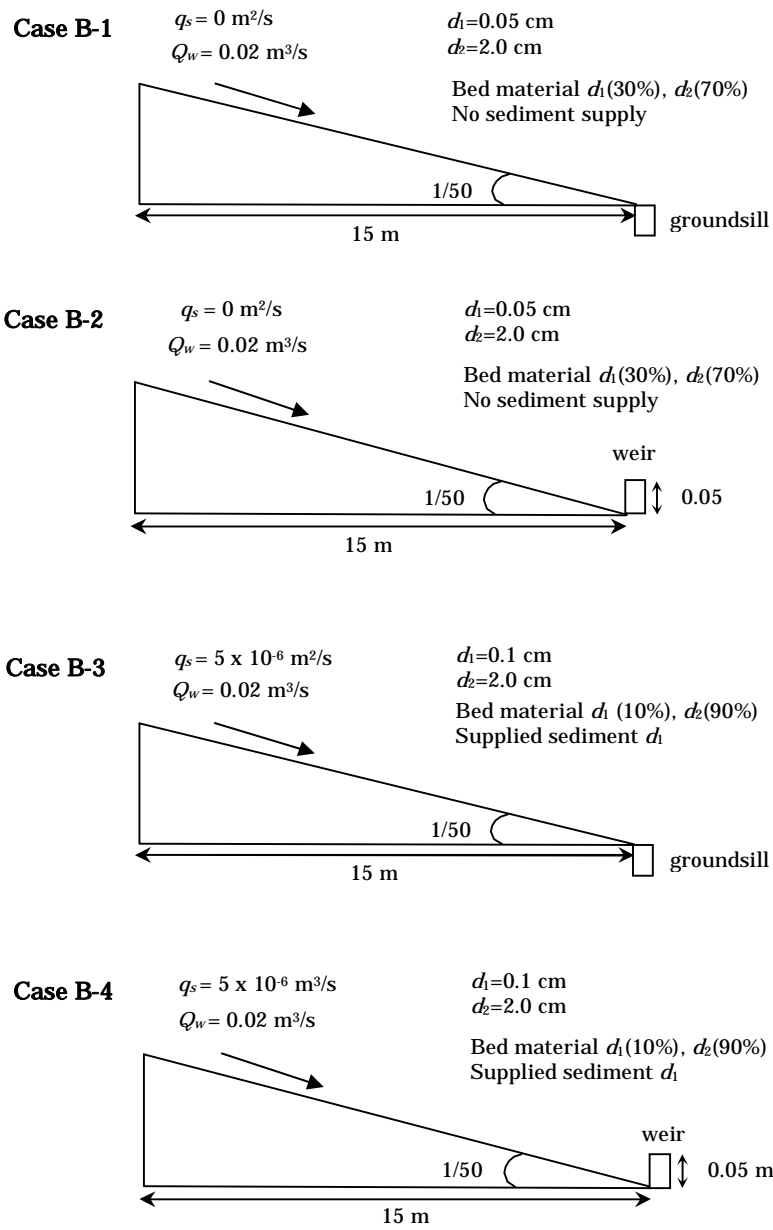
Fig.5.22 Conditions of bed-porosity simulation for binary mixtures.

b) Results

The simulation results on bed and porosity variation for those cases are shown in Fig.5.23, Fig.5.24, Fig.5.25, Fig.5.26, respectively. Each figure shows the bed elevation, the deposition depth variation, the temporal and longitudinal variations of the fine proportion of surface bed material and the porosity of surface layer. The simulation result is compared with the result on the assumption of constant porosity to make the improvement of this bed-porosity variation model clear.

In Case B-1 (Fig.5.23), the simulated result by the presented model shows that the degradation does not occurred, while the simulated result on the assumption of constant porosity shows that the degradation depth is rather larger. The longitudinal variation of sediment transport can not cause the bed degradation in the simulation by the presented model because the coarse sediment does not move, and only fine sediment moves out from the coarse particles layer. The simulated results on the longitudinal distributions of the fine sediment proportion show the process of fine sediment movement. The fine sediment removed from the bed material progressively downstream causes the changes of the proportion of finer materials and the change in porosity.

In Case B-2 (Fig.5.24), a weir is installed at the downstream end of the channel. The simulated result on the assumption of constant porosity shows that the degradation occurs at the upstream and the midstream part of the channel, while on the assumption of not-constant porosity the degradation does not take place. The sedimentation occurs at the downstream part of the channel in both simulations, and the deposition depths are relatively similar. The simulated result on the longitudinal distributions of the fine sediment proportion explains the process of the fine sediment movement under the sedimentation condition. The fine sediment is removed from the bed material in the upstream region and deposits in the downstream region. The porosity of surface layer in the upstream region

184

increases from the original value; because of the entrainment of fine sediment from the bed material. The entrained fine sediment buries the pore of the bed material at the downstream part. The porosity in the downstream region also increases because the fine sediment covers the bed material. Comparing between the void size of surface layer in the upstream region and that in the downstream region, the void size in the upstream region is much larger. At the boundary between the both regions, the porosity decreases because of mixing of fine sediment and coarse sediment.

In Case B-3 (Fig.5.25), fine sediment supply causes the bed aggradation. The simulated result on the assumption of constant porosity shows that the aggradation depths in the upstream and midstream part are rather larger than the simulated result on the assumption of not-constant porosity. The deposition depths at the downstream part near the groundsill decreased to the initial condition in both simulated results. The simulated results on the longitudinal distributions of the fine sediment proportion show the increase in finer proportion in the surface layer at the upstream and the midstream part. Because the fine sediment fills the pores of the coarse bed sediment and causes the decrease in porosity. The porosity at the downstream part near the groundsill is relatively constant during the simulation.

In Case B-4 (Fig.5.26), a weir is installed at the downstream end of the channel and the fine sediment is supplied from the upstream end of the channel. The simulated results on bed elevation and deposition depth show that the aggradation takes place at the upstream and midstream part and the deposition at the downstream part. The simulated result on the assumption of constant porosity shows that the aggradation depths in the upstream and midstream parts are rather larger than the simulated result on the assumption of not-constant porosity. The deposition depths at the downstream part of the channel in both simulations are relatively similar. The proportion of fine sediment in the bed material increases along the

channel and approaches to 1 at the downstream end of the channel. This phenomenon is caused by the deposition of the supplied sediment into the surface bed material. The porosities at the upstream and midstream parts decrease because the supplied fine sediment buries the pore of the bed material. The porosity at the downstream part increases because the fine sediment covers the bed material.

From those results, it can be seen that the differences in the deposition depth (both of aggradation and degradation under the conditions of no sediment supply and sediment supply) at the upstream and midstream part of the channel between the simulation on the assumption of constant porosity and not-constant porosity are rather lager. The comparison of the deposition depths is shown in Figure 5.27. In the case of no sediment supply, only fine sediment moves out from the bed material and the bed level at upstream and midstream part does not change. In the case of fine sediment supply, the supplied fine sediment comes into the layer and fills the pores of coarser sediment. When the change in porosity is not considered, the simulation creates the deposition or erosion as shown in Figure 5.27. These simulation results show that the simulation on the assumption of not-constant porosity produces more reasonable results than the simulation on the assumption of constant porosity.
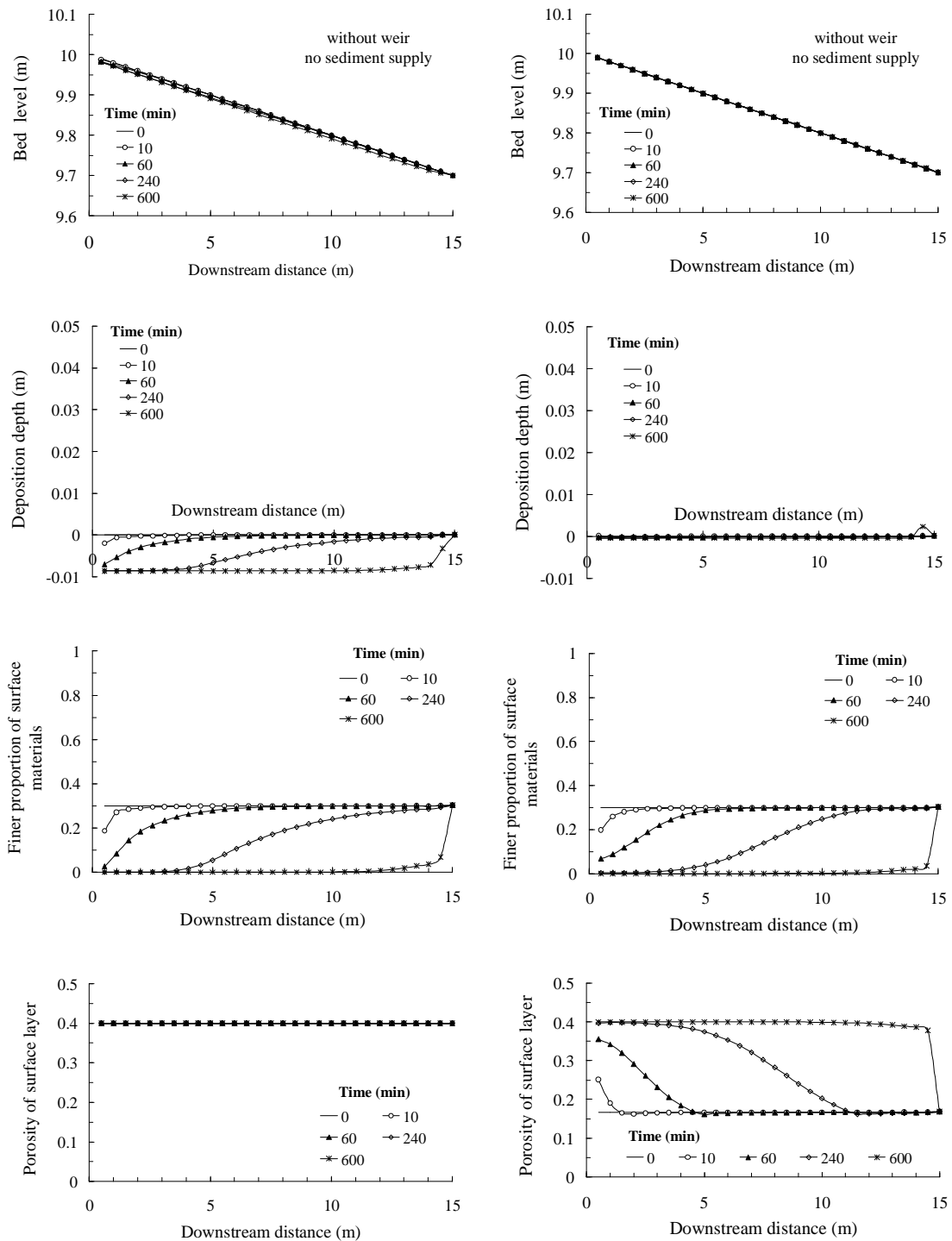
(a) Constant porosity

(b) Porosity dependent on grain size distribution

Fig.5.23 Simulation result on bed and porosity variation of binary mixtures, **Case B-1** (without weir and no sediment supply); (a) porosity is assumed to be constant, (b) porosity is calculated by Eqs.(5.10) and (5.11).
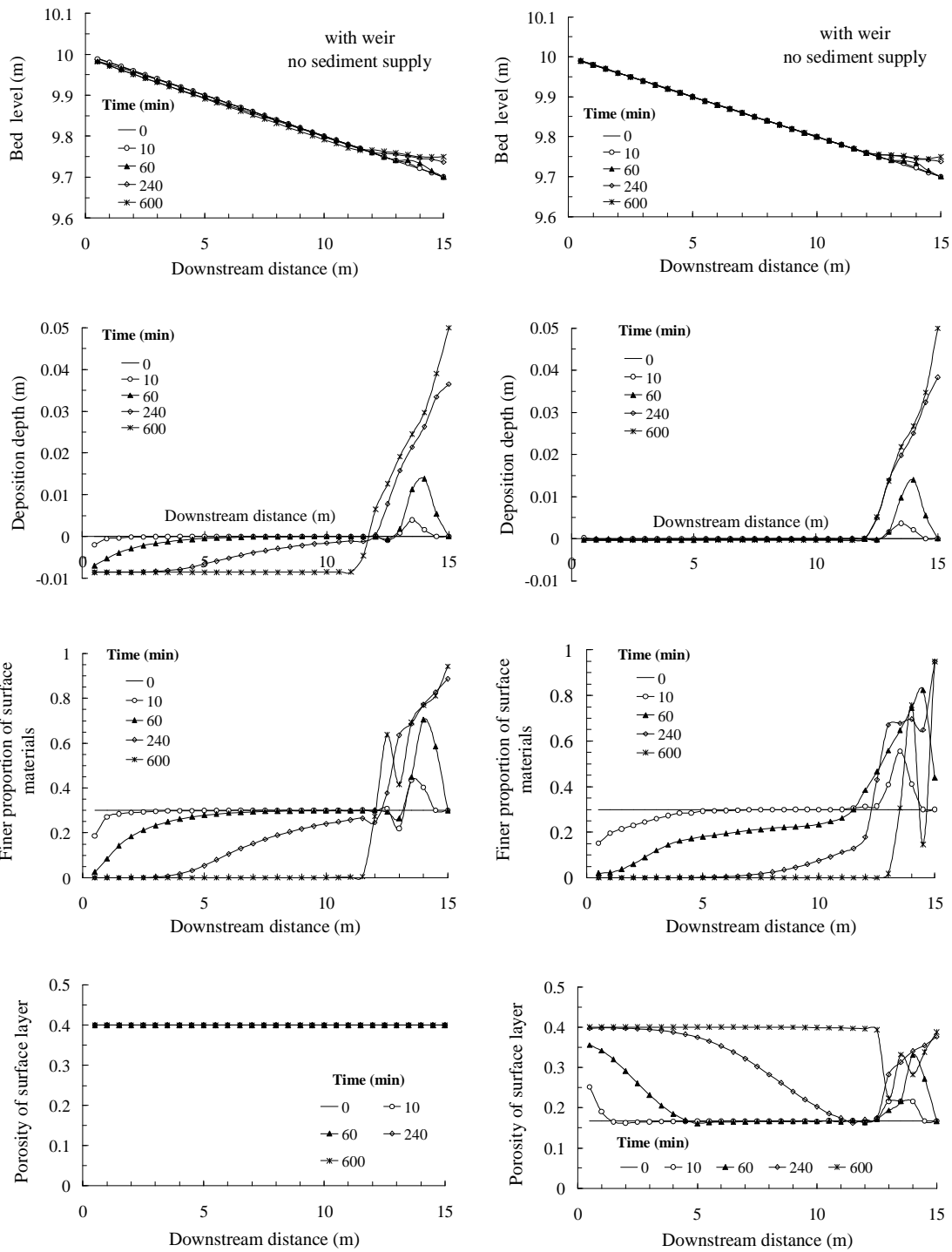
(a) Constant porosity

(b) Porosity dependent on grain size distribution

Fig.5.24 Simulation result on bed and porosity variation of binary mixtures, **Case B-2** (with weir and no sediment supply); (a) porosity is assumed to be constant, (b) porosity is calculated by Eqs.(5.10) and (5.11).

188
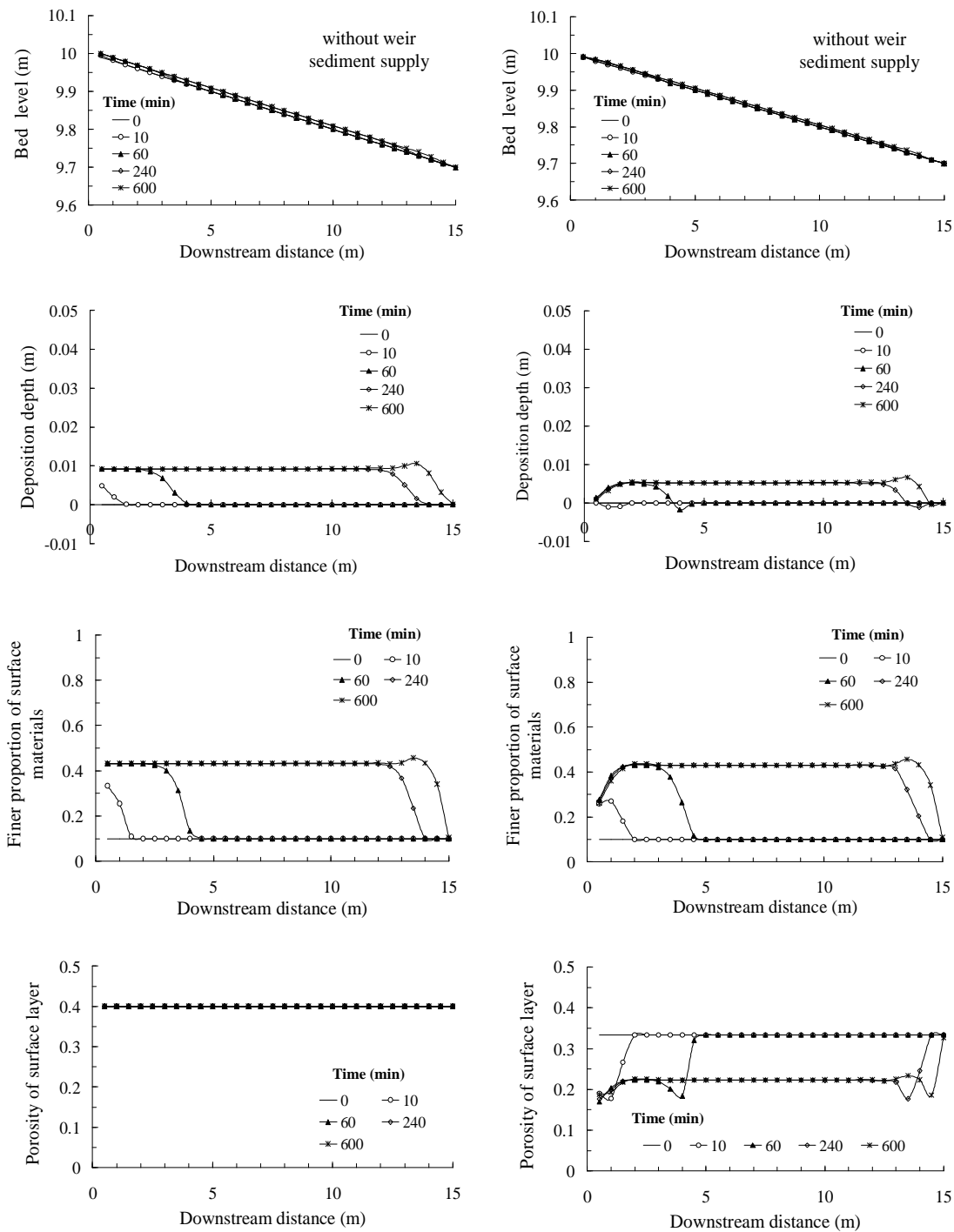
(a) Constant porosity

(b) Porosity dependent on grain size distribution

Fig.5.25 Simulation result on bed and porosity variation of binary mixtures, **Case B-3** (without weir and sediment supply); (a) porosity is assumed to be constant, (b) porosity is calculated by Eqs.(5.10) and (5.11).

189
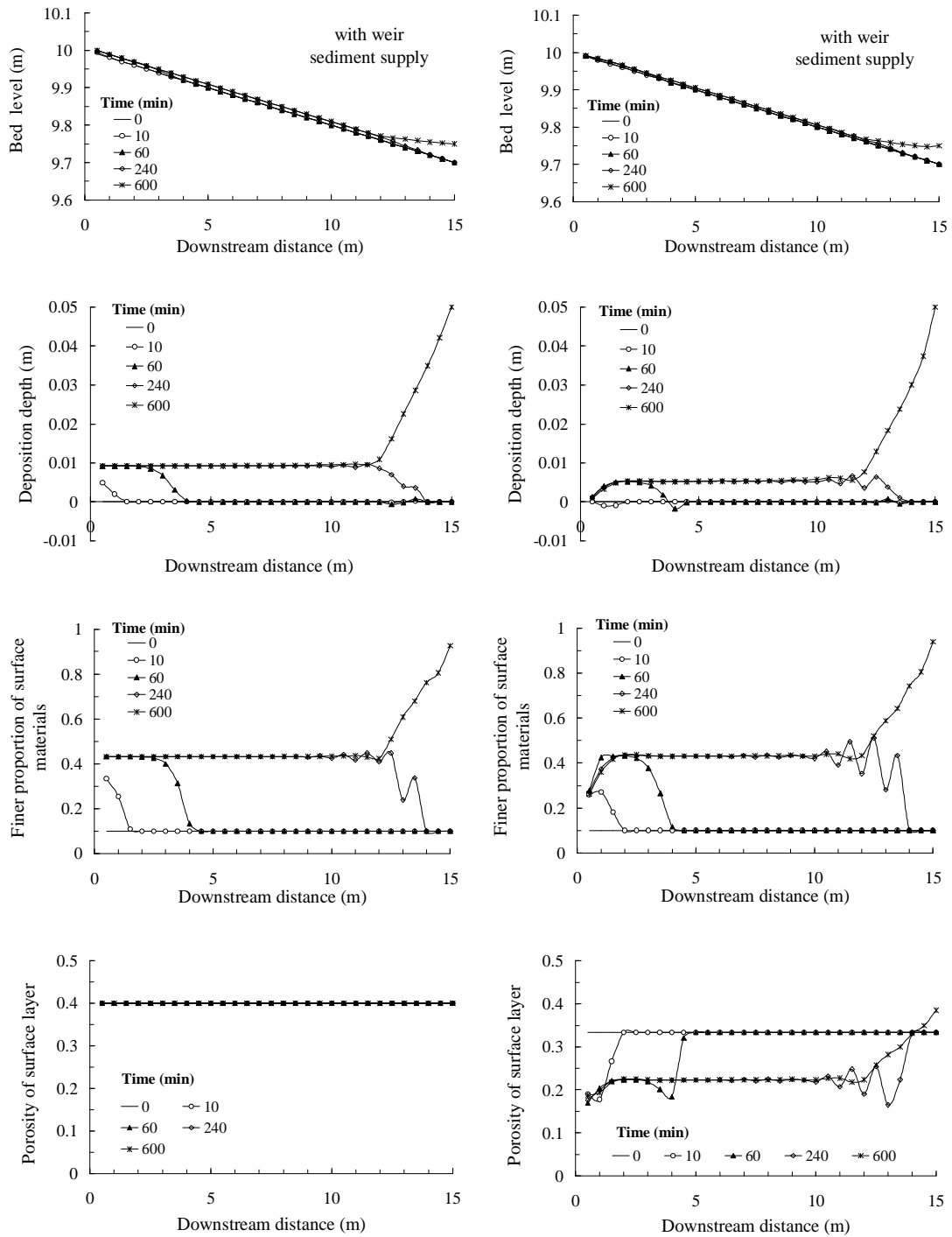
(a) Constant porosity

(b) Porosity dependent on grain size distribution

Fig.5.26 Simulation result on bed and porosity variation of binary mixtures, **Case B-4** (with weir and sediment supply); (a) porosity is assumed to be constant, (b) porosity is calculated by Eqs.(5.10) and (5.11).
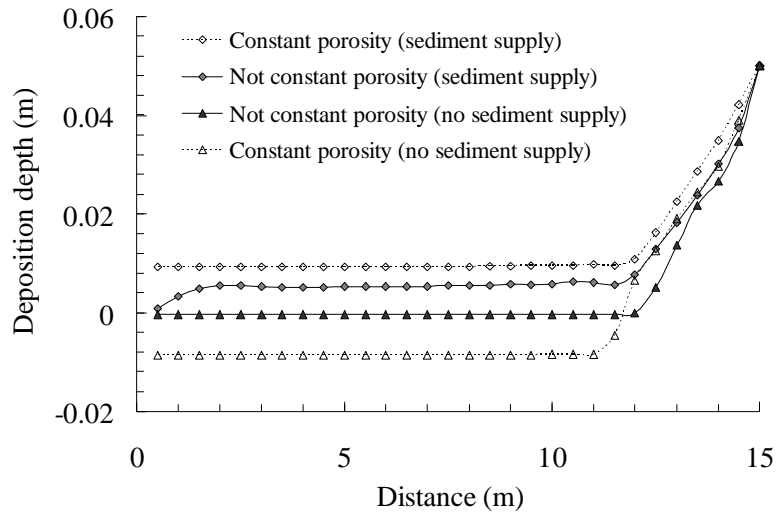
Fig.5.27 Comparison between deposition depths with assumption of constant porosity and not constant porosity.

Figures 5.28 and 5.29 show the simulation results on bed and porosity variation of binary mixtures, under two conditions of; (a) no sediment supply, and (b) sediment supply, in the cases of groundsill installation (no sedimentation case) and weir installation (sedimentation case), respectively. In the former case (Fig.5.28), when no sediment is supplied to the bed material, the fine sediment moves out from the bed material. The surface bed material becomes coarser and the mean diameter of surface bed material becomes larger. The proportion of finer material decreases along the channel and the porosity increases. In the case that sediment is supplied to the bed material, the supplied sediments come into the layer and fill the pores of coarser material. This process causes the changes in the elevation and the composition of bed material. The proportion of finer materials in the surface bed material increases. And as consequence, the porosity decreases.

191

(a) No sediment supply   (b)   Sediment supply
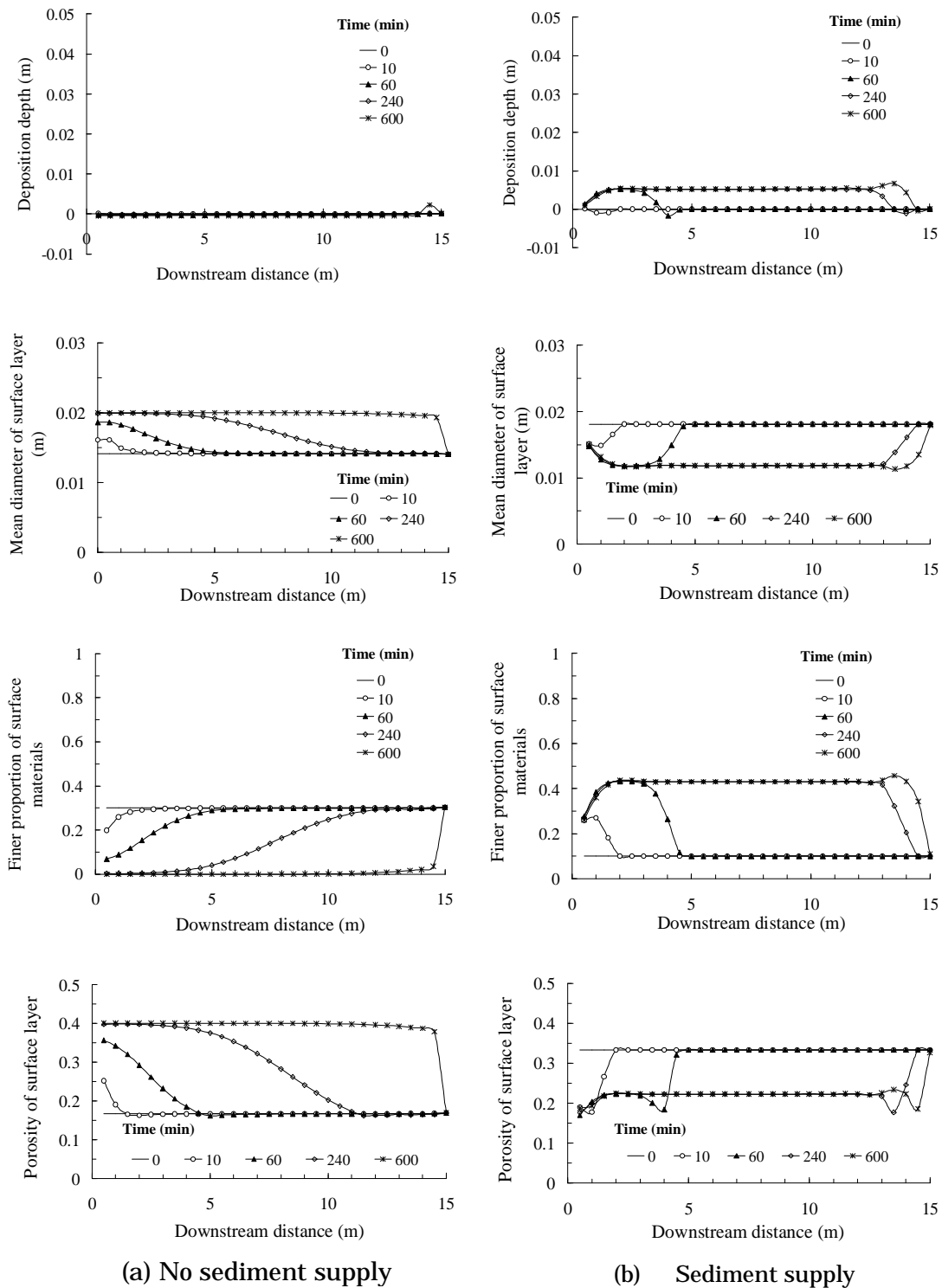
Fig.5.28 Simulation results on bed and porosity variation of binary mixtures, in the case of no sedimentation, under two conditions of; (a) no sediment supply, (b) sediment supply.

(a) No sediment supply   (b) Sediment supply
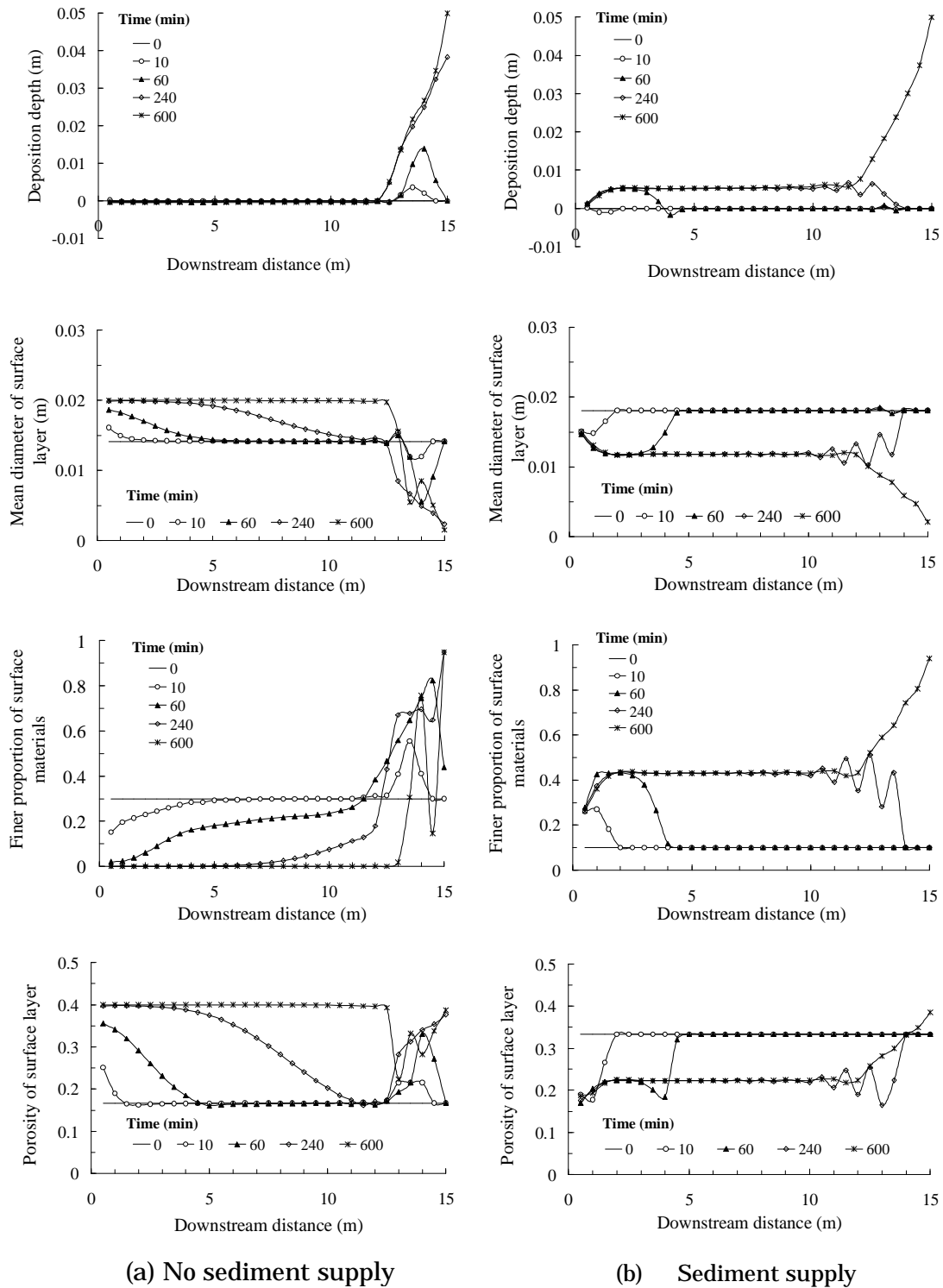
Fig.5.29 Simulation results on bed and porosity variation of binary mixtures, in the case of sedimentation, under two conditions of; (a) no sediment supply, (b) sediment supply.

In the second case (sedimentation case) (Fig.5.29), when no sediment is supplied to the bed material, fine material at the upstream and midstream part moves to downstream and deposits at the downstream part. Bed profile at the upstream and midstream part does not change, but the mean diameter and the porosity of surface layer change. As almost all of the finer material move to the downstream, the bed material at the upstream and midstream part is composed of coarse sediment only. The porosity of the surface bed material is approaching to the normal porosity (the porosity of uniform sediment), λ_s, which in this simulation $\lambda_s = 0.40$. At the downstream part, fine sediment covers the bed material, so the proportion of fine sediment increases up to 1 and the porosity increases to the normal porosity, λ_s. At the boundary between the upstream and downstream regions the porosity decreases because of mixing of the coarse sediment and fine sediment.

In this model, the grain size distribution and the porosity of each layer of the bed material are stored. Thus, the model can provide the result on the vertical distribution of porosity. The vertical distributions of ratio of finer sediment and porosity of bed material at three locations (i.e., $x = 1.0$ m, $x = 7.5$ m, and $x = 14.0$ m from the upstream end of channel), 600 min after the water and sediment supply are shown in Figure 5.30 and Figure 5.31. Figure 5.30 shows the simulated results in the case that no weir is installed in the downstream end of channel (no sedimentation case). Figure 5.31 shows the simulated results in the case that a weir is installed in the downstream end of channel (sedimentation case).

In Case B-1 (Fig.5.30(a)), the fine sediment in the surface layer moves out from the bed material cause the decrease in proportion of finer sediment along the channel from the initial condition approaching to zero. That means almost all of the surface bed material is covered by coarse sediment. As consequence, the porosity increases and approaches to the normal porosity.

In Case B-3 (Fig.5.30(b)), the fine sediment fills the voids between the coarse sediment. It causes the increase in the proportion of finer sediment in the surface layer along the channel and the decrease in porosity. The decrease in porosity in the upstream part is larger than the midstream and downstream parts.

In Case B-2 (Fig.5.31(a)), the proportion of the finer sediment at the upstream and midstream part decreases to zero, due to the removal of fine sediment from the bed material. This situation causes an increase in the porosity of bed material that approaches to the normal porosity. In this condition, the bed material is only composed of coarse sediment. In the contrary, the proportion of finer sediment at the downstream part increases while the porosity also increases. This situation occurs because the surface bed material is covered by the finer materials.

In Case B-4 (Fig.5.31(b)), the proportion of finer sediment at the upstream and midstream parts increases slightly in the flow direction, and the porosity decreases. At the downstream part where sedimentation takes places, the proportion of finer sediment increases rapidly, because the surface bed material is covered by the finer material. The porosity of bed material at the layer No. 1 is similar with the initial condition, and a minimum porosity is observed at the layer No. 3. The porosity decreases to the minimum value because of mixing of fine sediment and coarse sediment in the initial surface bed layer as schematically shown in Figure 5.32. The vertical distribution of the porosity of the sedimentation near the weir is adequately calculated.

Thus, the simulation results show that the presented model can produce a reasonable distribution of porosity of the riverbed material in the longitudinal and vertical directions in the case of binary mixtures.
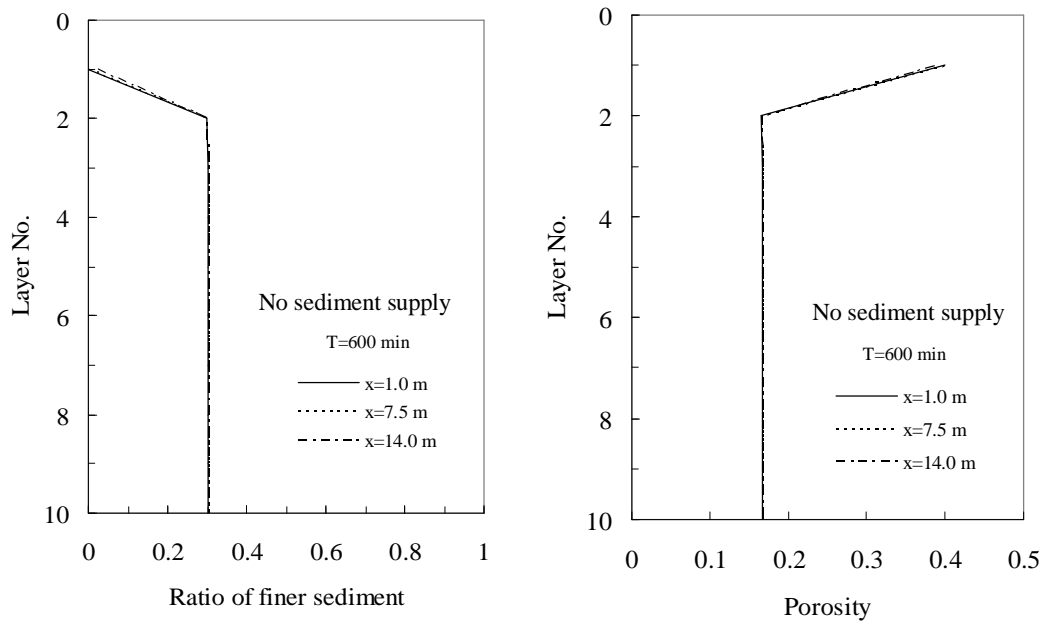
(a) Case B-1 (no sediment supply)
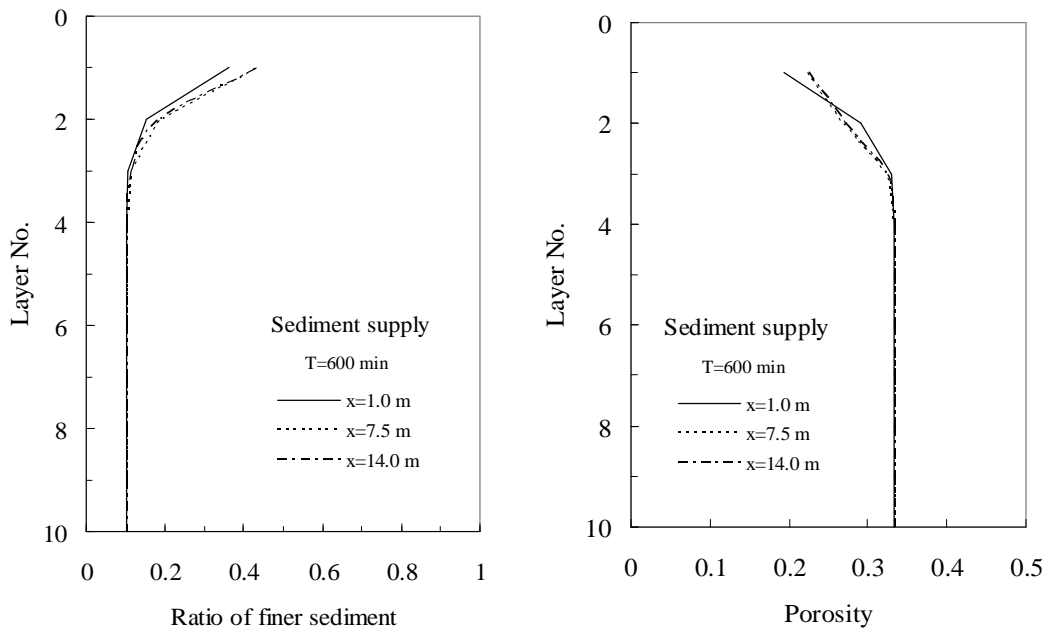
(b) Case B-3 (sediment supply)

Fig.5.30 Simulation results on vertical distribution of ratio of finer sediment and porosity, (a) Case B-1 and (b) Case B-3.
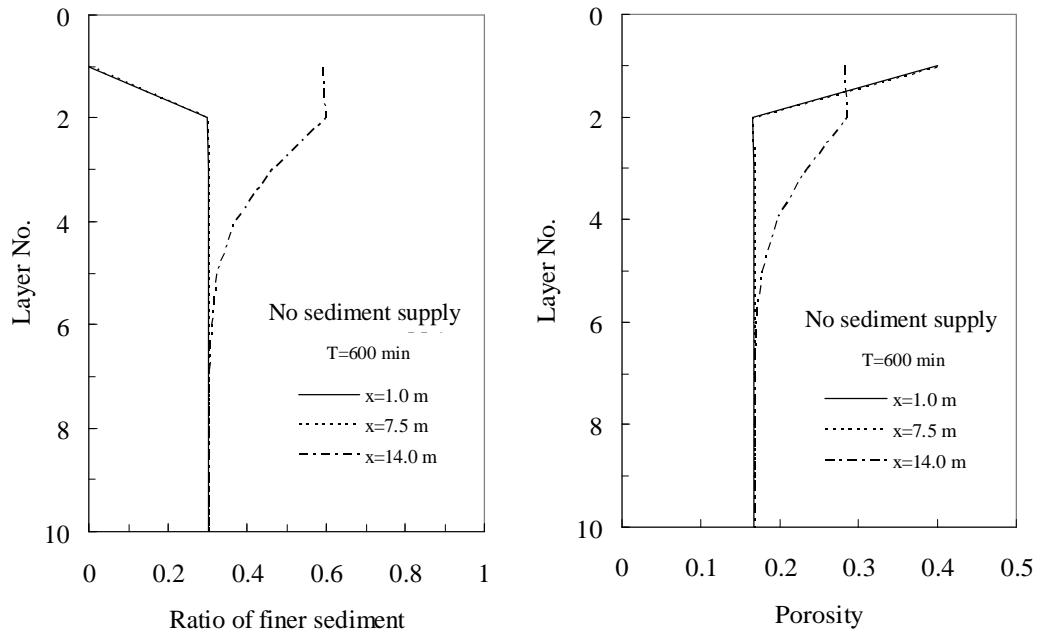
(a) Case B-2 (no sediment supply)
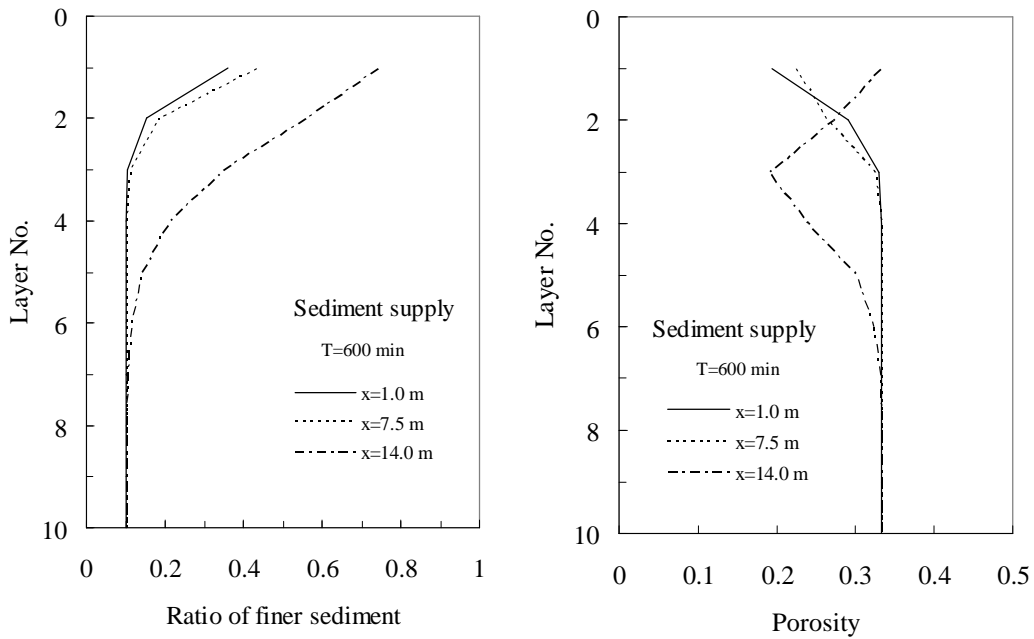
(b) Case B-4 (sediment supply)

Fig.5.31   Simulation results on vertical distribution of ratio of finer sediment and porosity, (a) Case B-2 and (b) Case B-4.
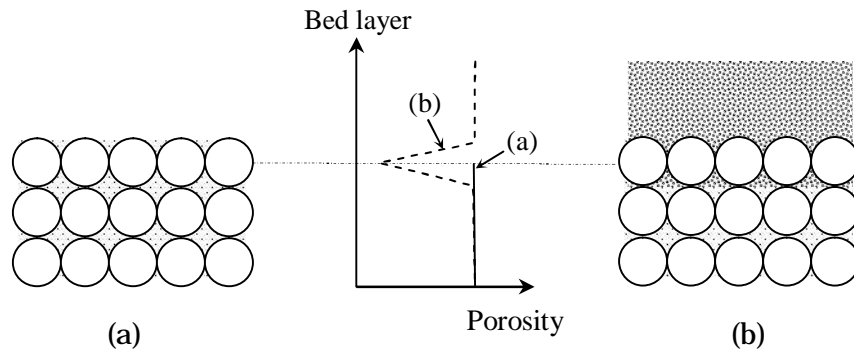
Fig.5.32 Schematic diagram of mixing between fine sediment and coarse sediment in the surface bed material at the downstream part of the channel and its porosity; (a) before sediment supply and (b) after sediment supply.

(2) Comparison between the simulated results on bed variation by MacCormack Scheme and the experimental results

The bed-porosity variation model with MacCormack scheme is applied to simulate the bed variation observed in the flume experiment as described in section 5.1.1. The simulations are carried out on the assumption of constant porosity and not-constant porosity. The simulation conditions are the same as the description in sub-section 5.6.1(1). The comparisons between the simulated results and the experimental results are shown in Figure 5.33. Figure 5.33(a) shows the comparison between the simulated result on the assumption of constant porosity and the experimental result. Figure 5.33(b) shows the comparison between the simulated result on the assumption of not-constant porosity and the experimental result. Both of the simulation results show the almost similar bed variation. However, some differences on the bed variation at the upstream region can be pointed out. The experimental result shows that the bed degradation is very small. The characteristics on bed variation come from the change in the porosity of bed material. If the porosity is assumed to be constant in the model, the

degradation depth is rather larger. In the model considering the porosity changes, degradation does not occur. The presented model produces more reasonable results if the porosity is assumed to be not constant.
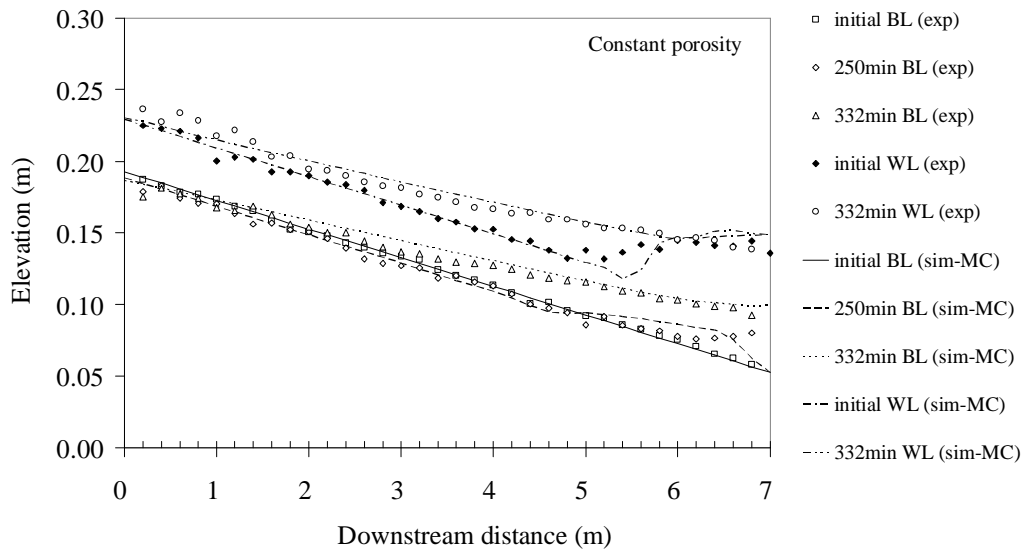
(a) Constant porosity
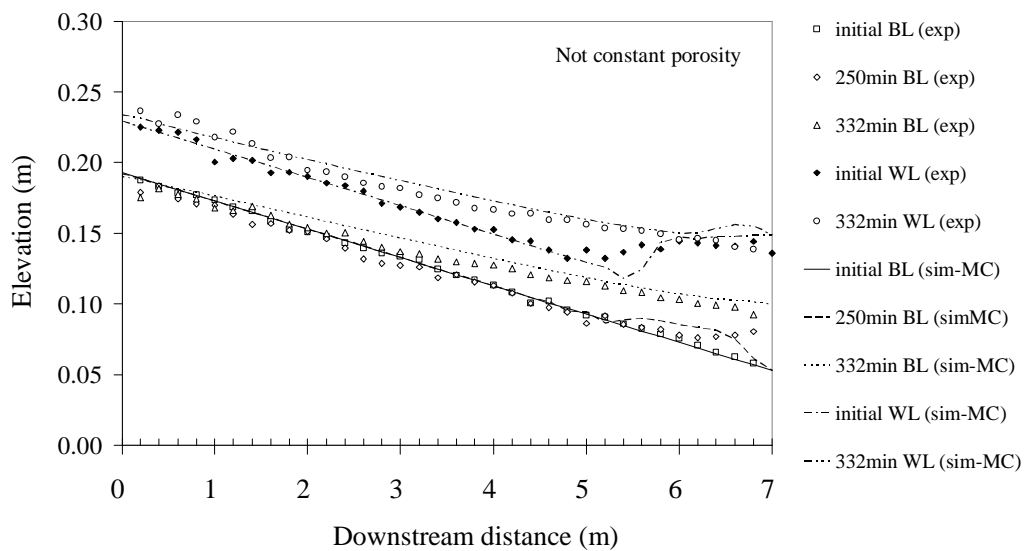
(b) Porosity dependent on grain size distribution

Fig. 5.33 Simulation results (by MacCormack scheme) and experimental result on bed variation; (a) porosity is assumed to be constant, (b) porosity is calculated by Eqs.(5.10) and (5.11)

(3) Simulation on bed and porosity variation in the case of sediment mixtures with continuous grain size distribution

a) Conditions

The presented bed-porosity variation model is applied to the bed variation in a channel with a length of 15 m and a width of 0.5 m. Simulation is carried out to observe the bed and porosity variation under two conditions; one is no sediment supply condition and another is sediment supply condition. The simulation conditions are summarized in Table 5.5 and shown in Figure 5.34 for no sediment supply condition and Figure 5.35 for sediment supply condition. The initial channel slopes are 0.01 and 0.02. A weir with a height of 0.05 m is installed in some cases to investigate the process of sedimentation. The initial bed material has a grain size distribution ranging from 1.0 mm to 10 mm. The distribution type of initial bed material is lognormal for the first condition and M-Talbot type for the second condition. A histogram and corresponding sieve curve of the mixtures used for initial bed material are shown in Figure 5.36. The mean diameter of the mixtures, $d_m = 5$ mm. The water is supplied at a rate of 0.02 m³/s. Under this condition, the maximum grain can not be transported. The total simulation time is 600 min.

Table 5.5   Simulation conditions on bed variation by MacCormack scheme, in the case of sediment mixtures with continuous grain size distribution.

Simulation	Bed material	Slope	Q_w (m³/s)	q_s (10^{-5} m²/s)	Downstream end condition
Case C-1	Lognormal	0.01	0.02	0	groundsill
Case C-2	Lognormal	0.01	0.02	0	weir
Case C-3	Lognormal	0.02	0.02	0	weir
Case C-4	M-Talbot	0.01	0.02	8 (3~6 mm)	groundsill
Case C-5	M-Talbot	0.01	0.02	8 (3~6 mm)	weir
Case C-6	M-Talbot	0.01	0.02	8 (1~4 mm)	groundsill

No sediment supply

Case C-1
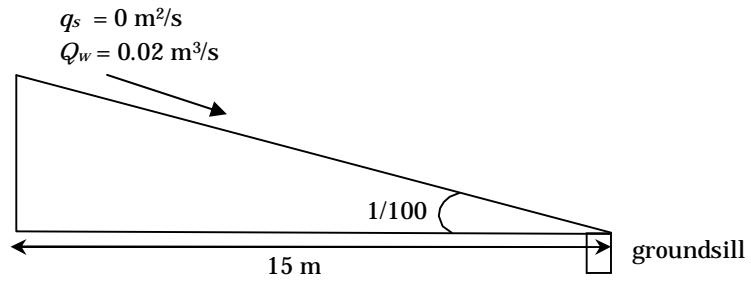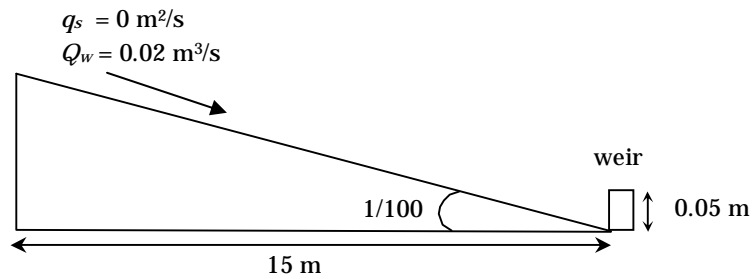
q_s = 0 m²/s
Q_w = 0.02 m³/s

1/100

15 m

groundsill

Bed material: Lognormal type
No sediment supply

Case C-2

q_s = 0 m²/s
Q_w = 0.02 m³/s

weir

1/100

0.05 m

15 m

Bed material: Lognormal type
No sediment supply

Case C-3

q_s = 0 m²/s
Q_w = 0.02 m³/s

weir

1/50

0.05 m

15 m
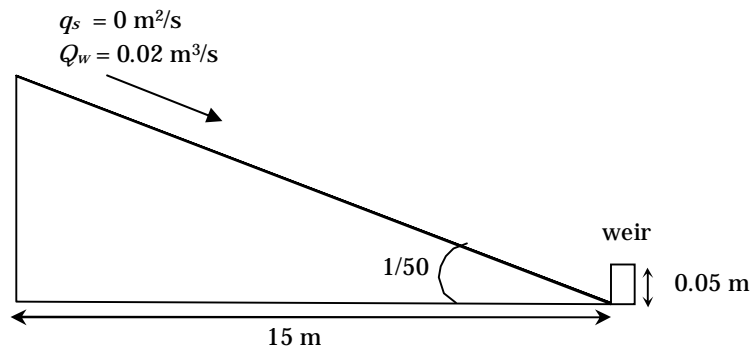
Bed material: Lognormal type
No sediment supply

Fig.5.34 Simulation conditions on bed-porosity variation in the case of sediment mixtures with continuous grain size distribution (No sediment supply condition).

Sediment supply

Case C-4
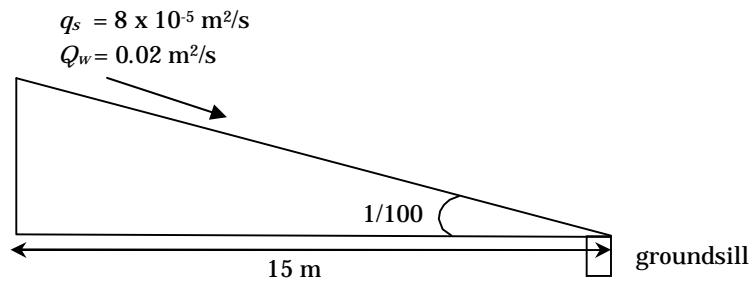
$q_s = 8 \times 10^{-5}$ m²/s
$Q_w = 0.02$ m²/s

1/100

15 m

groundsill

Bed material: M-Talbot type
Sediment supply: Middle size of bed material (2.8~5.9 mm)

Case C-5

$q_s = 8 \times 10^{-5}$ m²/s
$Q_w = 0.02$ m²/s

weir

1/100

0.05 m

15 m

Bed material: M-Talbot type
Sediment supply: Middle size of bed material (2.8~5.9 mm)

Case C-6

$q_s = 8 \times 10^{-5}$ m²/s
$Q_w = 0.02$ m²/s

1/100

15 m

groundsill
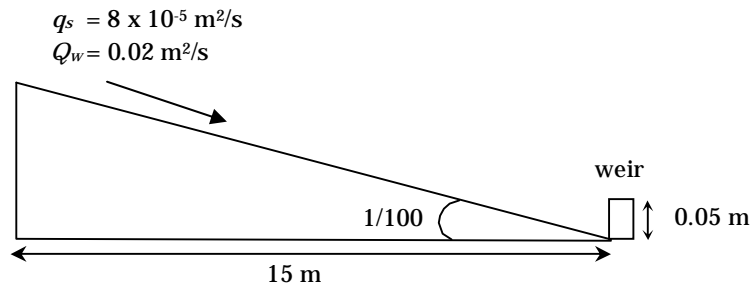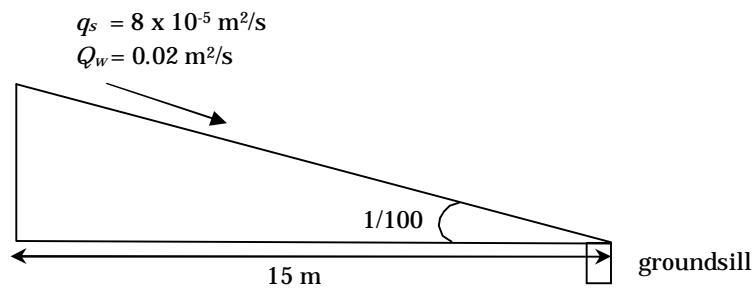
Bed material: M-Talbot type
Sediment supply: Lower size of bed material (1.4~4.5 mm)

Fig.5.35 Simulation conditions on bed-porosity variation in the case of sediment mixtures with continuous grain size distribution (Sediment supply condition).

(a) Lognormal distribution (b) M-Talbot distribution
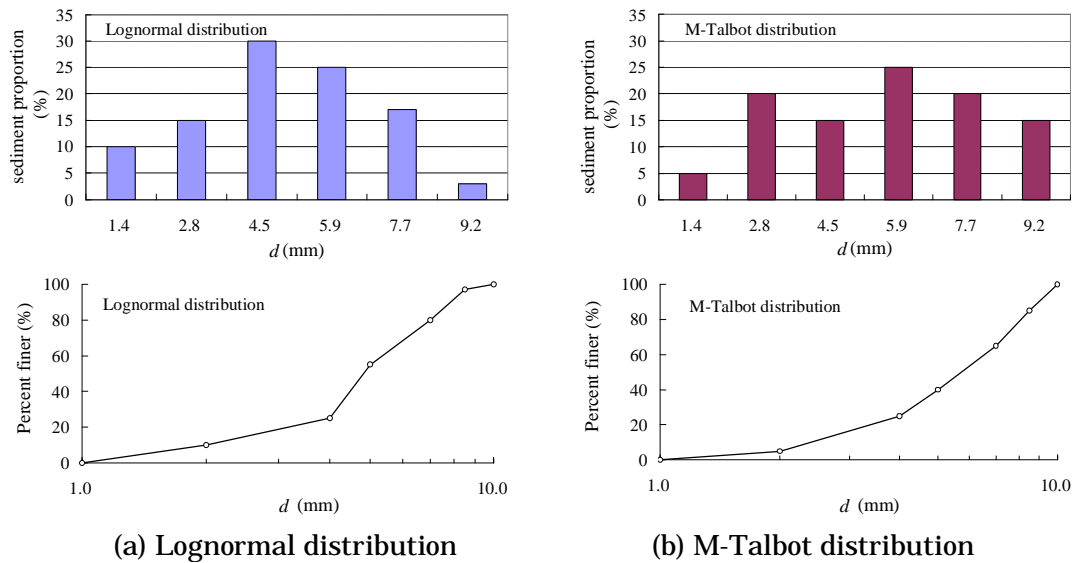
Fig.5.36 Sediment proportion and cumulative distribution of initial bed material; (a) Lognormal distribution, and (b) M-Talbot distribution.

b) Results

The simulation results on bed and porosity variation for six cases i.e., C-1, C-2, C-3, C-4, C-5, and C-6 are shown in Fig.5.37, Fig.5.39, Fig.5.41, Fig.5.43, Fig.5.45 and Fig.5.47, respectively. Each figure shows the changes in bed profile, the deposition depth, the mean diameter variation, the porosity and the type of the grain size distribution. The changes of grain size distribution of each case are shown in Fig.5.38, Fig.5.40, Fig.5.42, Fig.5.44, Fig.5.46, and Fig.5.48, respectively.

Figure 5.37(a) and 5.37(b) show the evolution of bed profiles and deposition depth in the simulation of Case C-1. The bed surface decreases along the channel during the simulation time, due to the removal of fine fraction from the bed material. The fine fraction of bed material is eroded and the degradation propagates to the downstream. Temporal and longitudinal variation of the mean diameter of surface layer is shown in Figure 5.37(c). Mean diameter of surface materials gradually becomes larger than the initial mean diameter. This means that the fine fraction moves to the downstream and the surface bed material at the upper part becomes

coarser than the bed material at the downstream part. Therefore, the porosity of surface bed material at the upstream part is larger than that at the downstream part as shown in Figure 5.37(d). Evolution of grain size distribution of surface bed material at three different locations; upstream, midstream and downstream part are shown in Figure 5.38. It is clearly shown that the grain size distribution gradually changes from the initial distribution to M-Talbot type of grain size distribution. The time and longitudinal variation of distribution type is shown in Figure 5.37(e).

In Case C-2 (Fig.5.39), a weir with a height of 5 cm is installed at the downstream end of the channel and the hydraulic condition of simulation is similar with Case C-1. Figure 5.39(a) and 5.39(b) show that the bed degradation occurs at the upstream part and the bed aggradation occurs at the downstream part. The fine fraction of bed material at the upstream part moves to the downstream and deposited in front of the weir. The bed material at the upstream and midstream parts become coarser and the mean diameter of surface bed material increases as shown in Fig.5.39.(c). At the downstream part near the weir, the fine fraction of bed material increases and the mean diameter of the surface bed material decreases, but the porosity increases as shown in Figure 5.39(b). The reason why the porosity increased at the downstream near the weir is that the bed material becomes more uniform than the initial bed material. The grain size distribution at the upstream and midstream parts become M-Talbot distribution, while the lognormal distribution is kept at the downstream as shown in Figure 5.39(e) and 5.40.

In Case C-3 (Fig.3.41), the channel slope is 0.02 and a weir with a height of 5 cm is installed at the downstream end of the channel. Figure 5.41(a) shows that the bed elevation at the upstream part goes down drastically and the degradation is large. The erosion depth is around 0.14 m at the end of upstream channel as shown in Fig.3.41(b). The mean diameter of surface bed material along the channel increases drastically as shown in

Figure 5.41(c). This means that only coarse fraction material remains in the bed surface layer. The porosity increases to 0.34 at the downstream and 0.4 at the upstream part of the channel as shown in Figure 5.41(d). The grain size distribution finally changes to M-Talbot distribution as shown in Figure 5.41(e) and 5.42.

These simulation results show that no sediment supply causes the bed degradation and the increase in the mean grain size and the porosity of surface layer. The surface bed material becomes progressively coarser and coarser.

The following three cases of simulation show the effect of sediment supply on bed variation:

In Case C-4 (Fig.5.43), the sediment mixtures with a minimum diameter of 2.8 mm and the maximum diameter of 5.9 mm, that is the middle fraction of the initial bed material, is supplied to a channel composed of the bed material with M-Talbot distribution as shown in Figure 5.35(b). The sediment supply rate is 0.00008 m²/s (consists of 0.00001 m²/s of 2.8 mm, 0.00002 m²/s of 4.5 mm, and 0.00005 m²/s of 5.9 mm). The initial slope is 0.01 and at the downstream end of the channel is fixed with a groundsill. The results on bed and porosity variation are shown in Figure 5.43. The simulated results on bed variation and deposition depth (Fig.5.43(a) and Fig.5.43(b)) show the degradation takes places along the channel. The erosion depth at the upstream end of the channel is 0,04 m. The mean diameter of surface bed material along the channel decreases while the porosity increases. This situation is caused by the supplied sediment that contains finer material than the initial bed material. The time variation of the grain size distribution at the upstream, midstream and downstream parts are shown in Figure 5.43. The grain size distributions of bed material change to the lognormal distribution. The grain size distribution at the upstream part changes suddenly after the sediment is supplied to the bed material.

In Case C-5 (Fig.5.45), a weir with a height of 5 cm is installed at the downstream end of the channel and the hydraulic condition of simulation is similar with Case C-4. The simulated results on bed elevation and deposition depth (Fig.5.45(a) and Fig.5.45(b)) show the aggradation takes places along the channel. The mean diameter of bed material decreases, as illustrated in Fig.5.45(c). This is caused by the deposition of the supplied sediment into the surface bed material, but the porosity increases as shown in Figure 5.45(d). The increase in porosity is due to the sediment deposition on the surface bed material that has more uniform grain size distribution than initial surface bed material as shown in   Figure 5.46. The grain size distribution of surface bed material finally has a lognormal distribution (Fig.5.45(e)).

In Case C-6 (Fig.5.47), the sediment mixture with the minimum diameter of 1.4 mm and a maximum diameter of 4.5 mm, that is the finer fraction of the initial bed material, is supplied to the channel. The sediment supply rate is 0.00008 m²/s   (consists of 0.00001 m²/s of 1.4 mm, 0.00002 m²/s of 2.8 mm, and 0.00005 m²/s of 4.5 mm).   Figure 5.47(a) and 5.47(b) show the degradation occurs along the channel even if sediment is supplied into the channel. This condition may be caused by the effect of sediment supply. The finer sediment supply can reduce the grain size of the bed material and increase the transport capacity (Curran and Wilcock, 2005). The effect of finer sediment supply can be seen from the changes of the mean diameter (Fig.5.47(c)) and the grain size distribution of surface layer (Fig.5.48). The finer fraction of sediment increases and consequently the mean diameter of surface bed material decreases. The increase in the finer fraction in the bed material mixture causes the decrease in porosity as shown in Figure 5.47(d). The grain size distribution of bed material finally has a lognormal distribution.   The fine sediment supply can cause the degradation in the channel due to the increase in transport capacity; and reduces the mean diameter and the porosity of surface bed material.

q_s = 0 m²/s
Q_w = 0.02 m³/s

Case C-1

1/100

15 m

Bed material: Lognormal type
No sediment supply

(a) Bed profile

(b) Deposition depth

(c) Mean diameter of surface layer

(d) Porosity of surface layer

(e) Type of grain size distribution
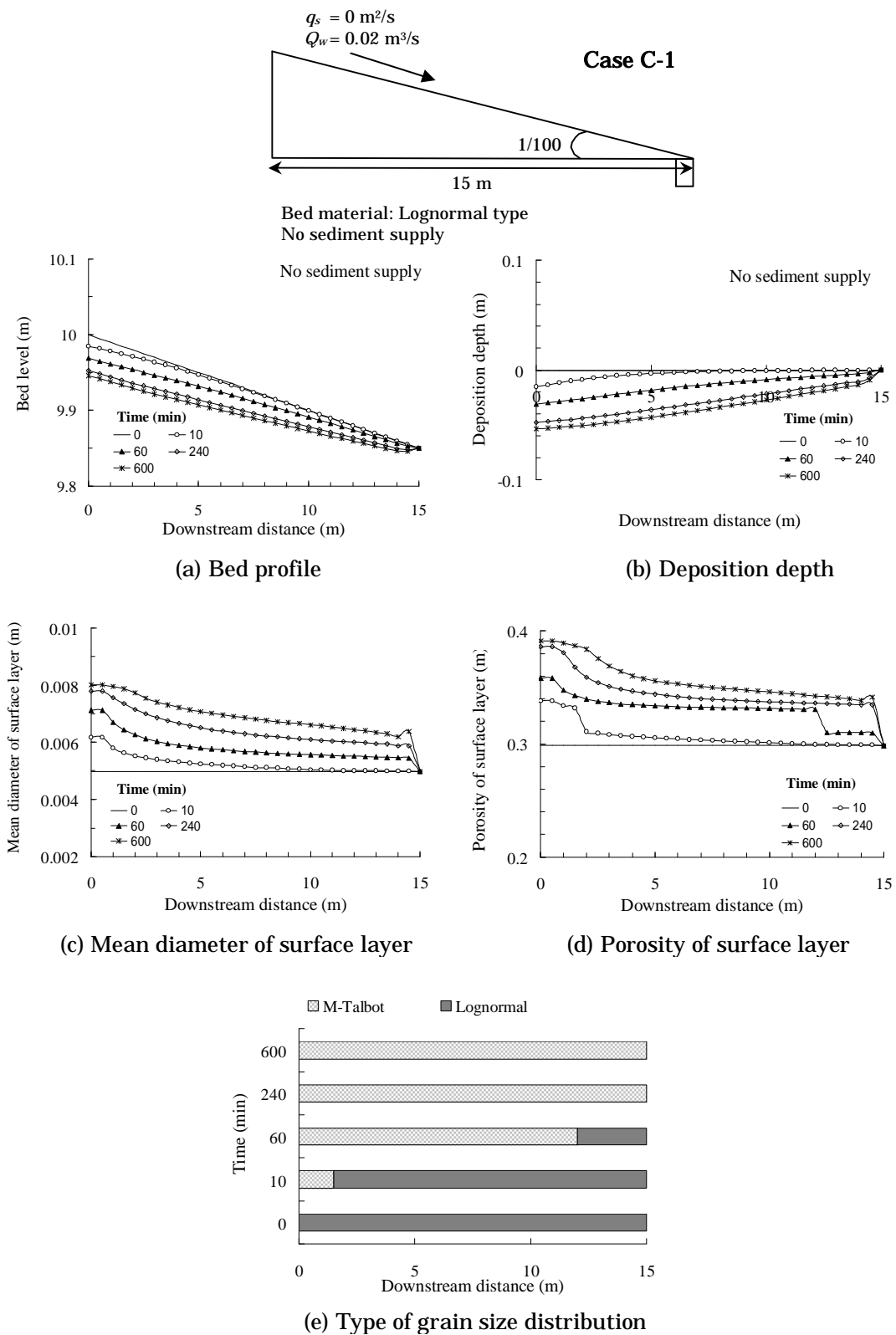
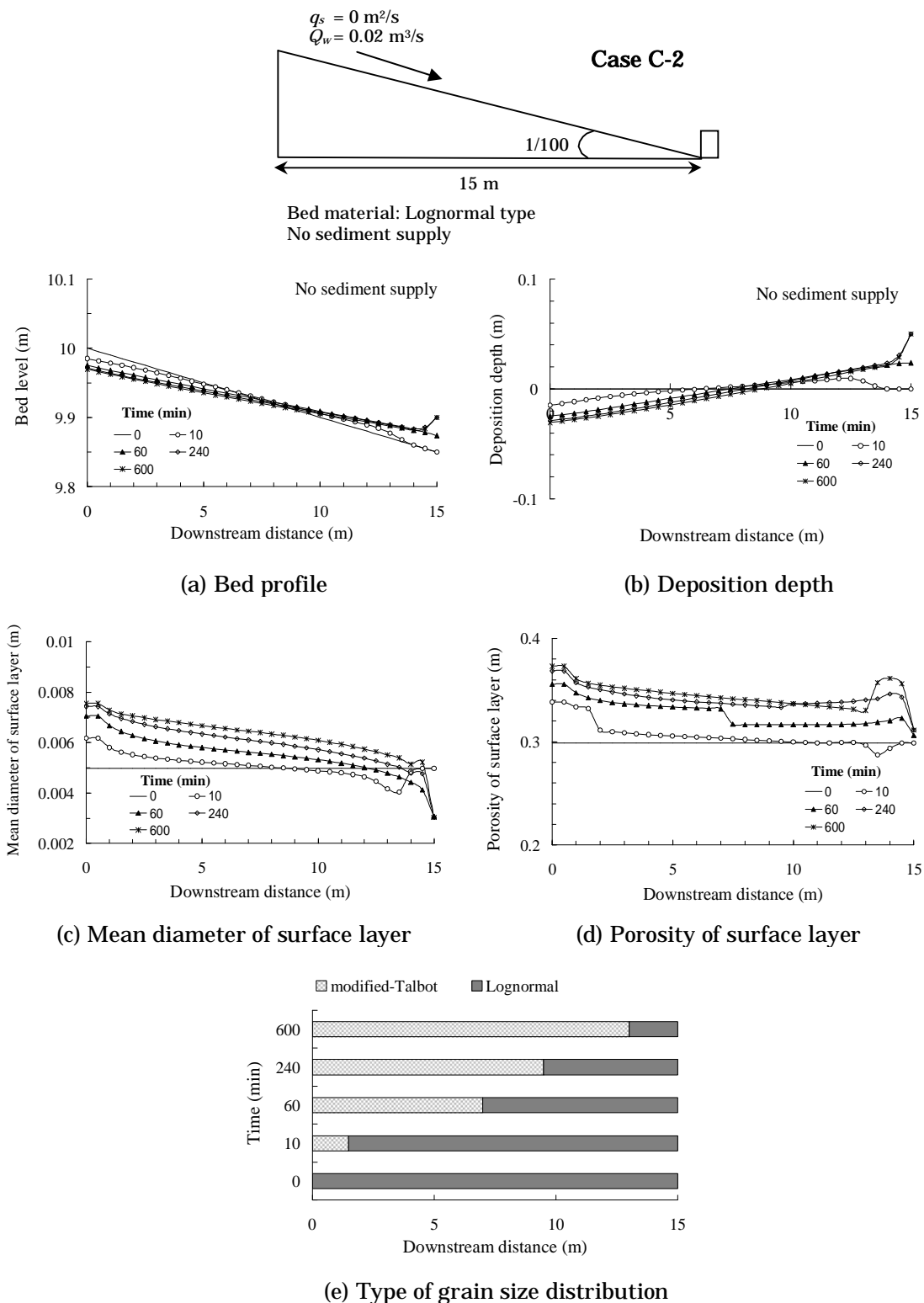**Fig.5.37**   Simulation results on bed and porosity variation (**Case C-1**).
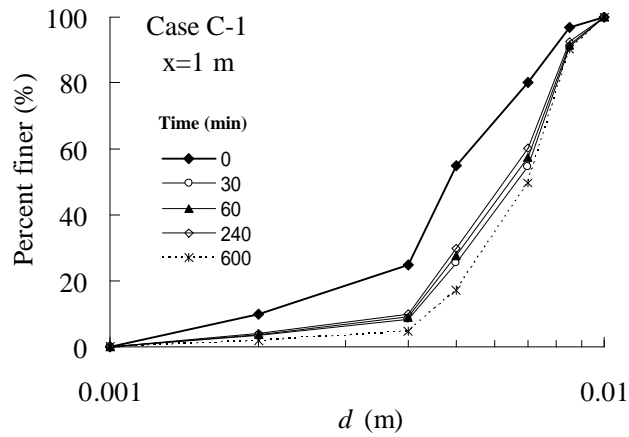
(a) Upstream ($x = 1$ m)
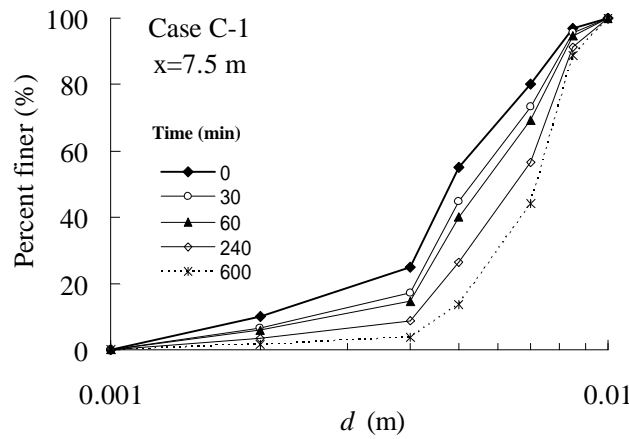
(b) Midstream ($x = 7.5$ m)
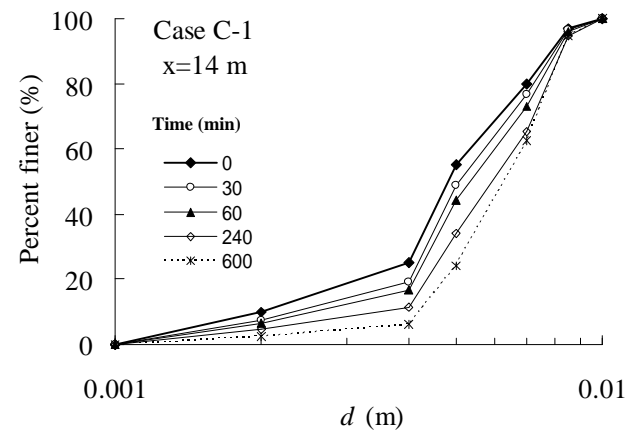
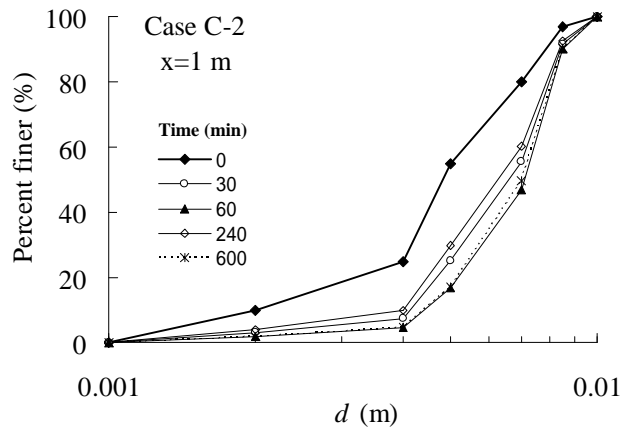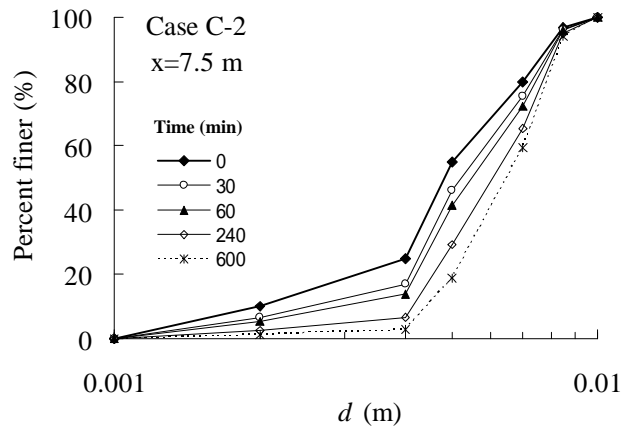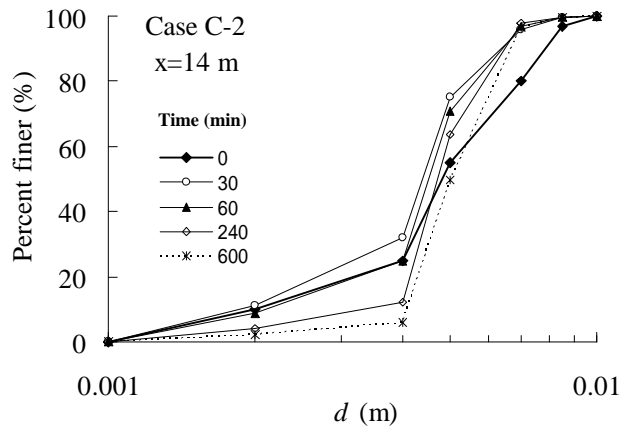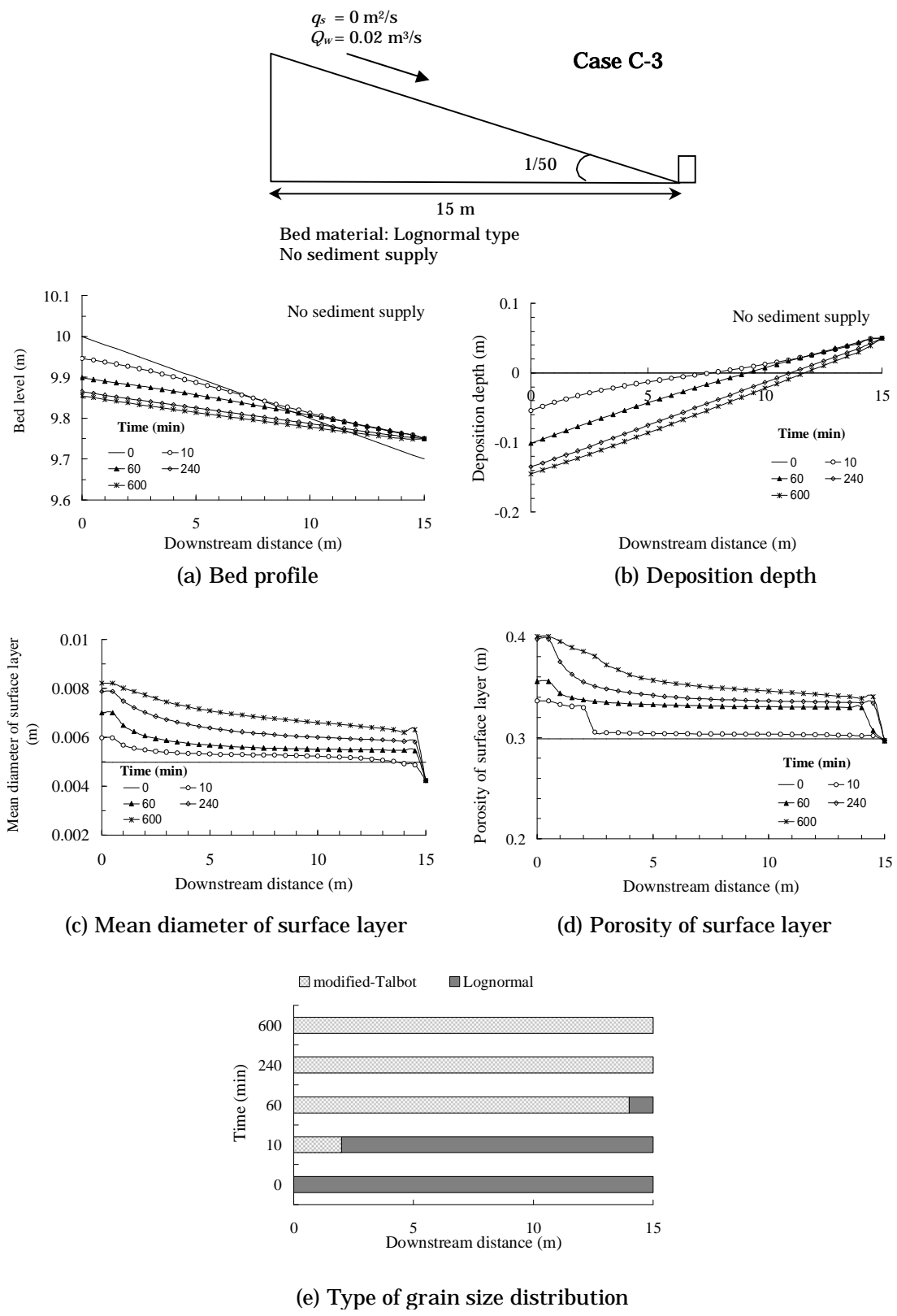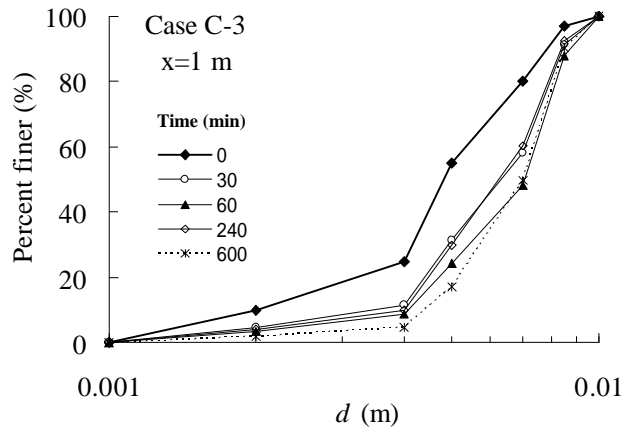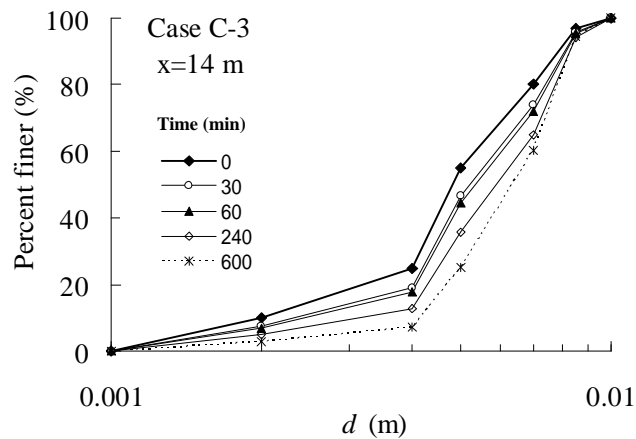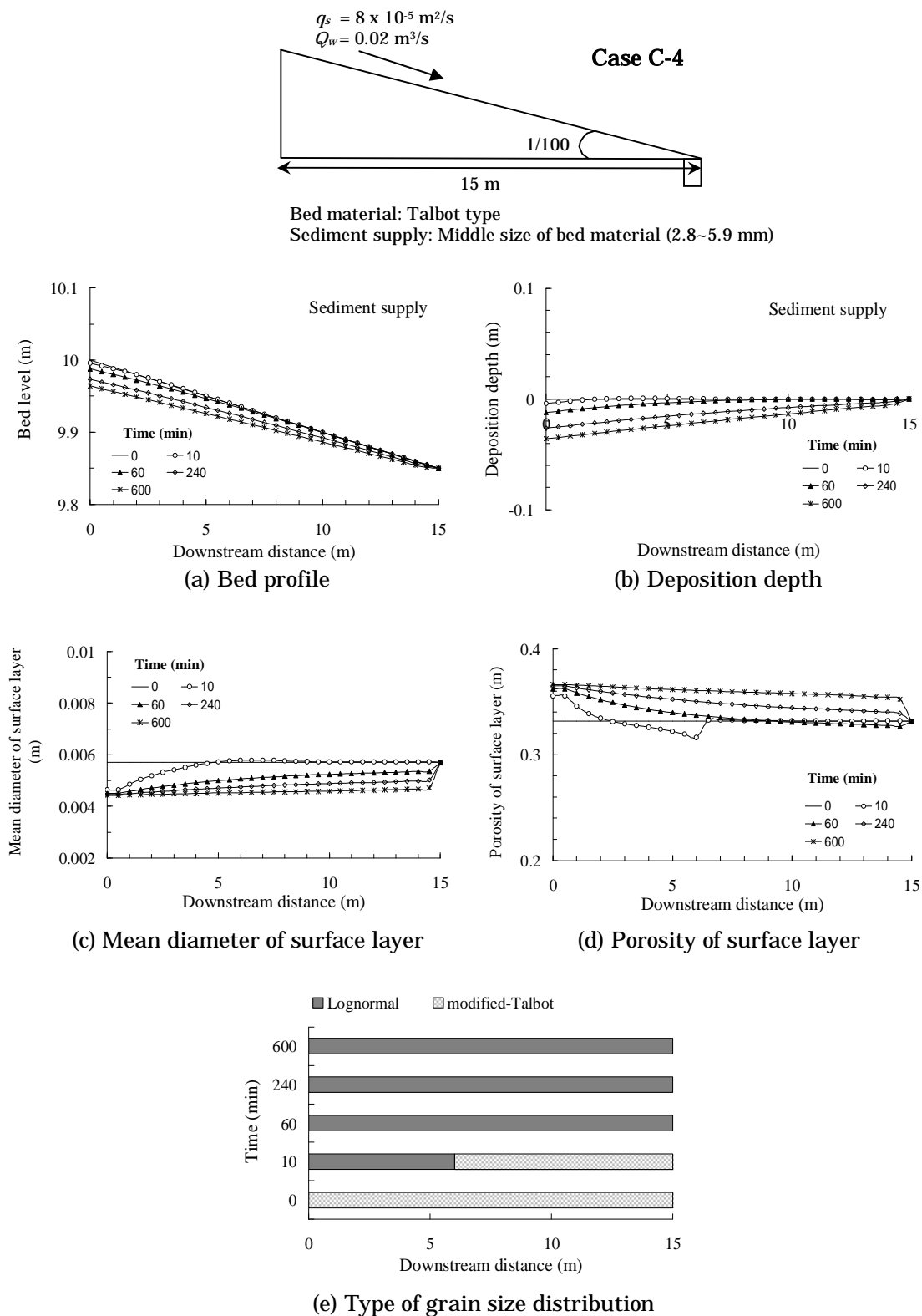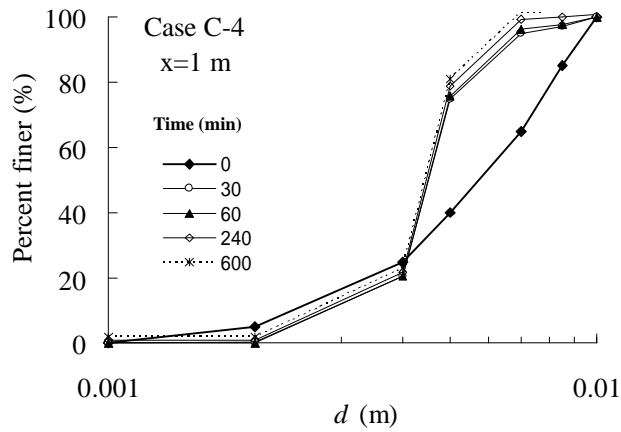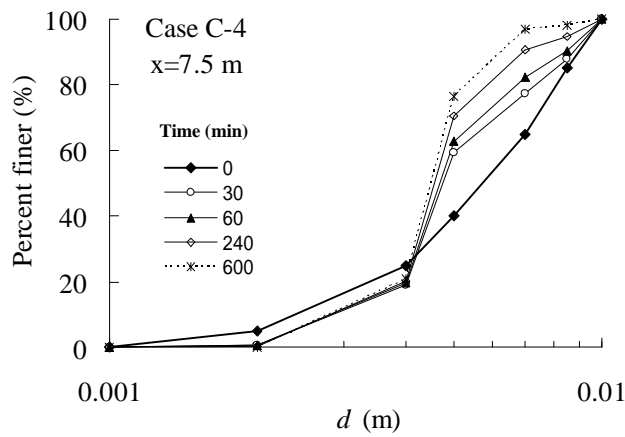(c) Downstream ($x = 14$ m)

Fig.5.38 Grain size distributions of surface bed material at the upstream ($x = 1$ m), midstream ($x = 7.5$ m), and downstream ($x = 14$ m), in the **Case C-1.**

208

Fig.5.39   Simulation results on bed and porosity variation (**Case C-2**).

(a) Upstream (x = 1 m)

(b) Midstream (x = 7.5 m)

(c) Downstream (x = 14 m)

Fig.5.40 Grain size distributions of surface bed material at the upstream (x = 1 m), midstream (x = 7.5 m), and downstream (x = 14 m), in the **Case C-2.**
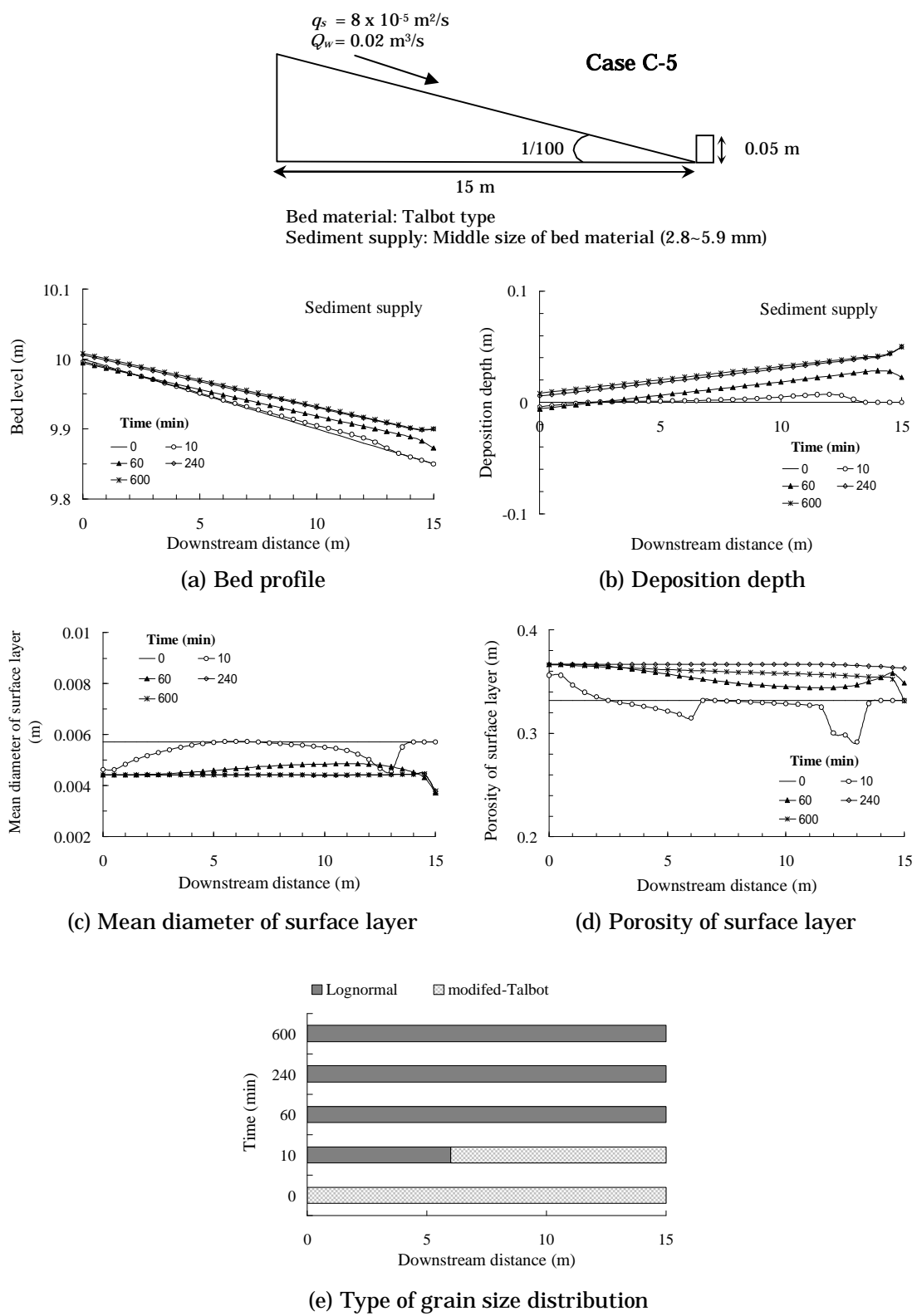
210

$q_s = 0$ m²/s
$Q_w = 0.02$ m³/s

Case C-3

1/50

15 m

Bed material: Lognormal type
No sediment supply

(a) Bed profile

(b) Deposition depth

(c) Mean diameter of surface layer

(d) Porosity of surface layer

(e) Type of grain size distribution

Fig.5.41   Simulation results on bed and porosity variation (**Case C-3**).

(a) Upstream ($x = 1$ m)
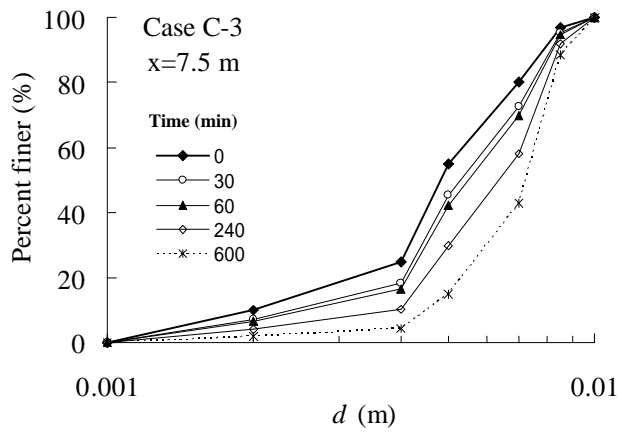
(b) Midstream ($x = 7.5$ m)
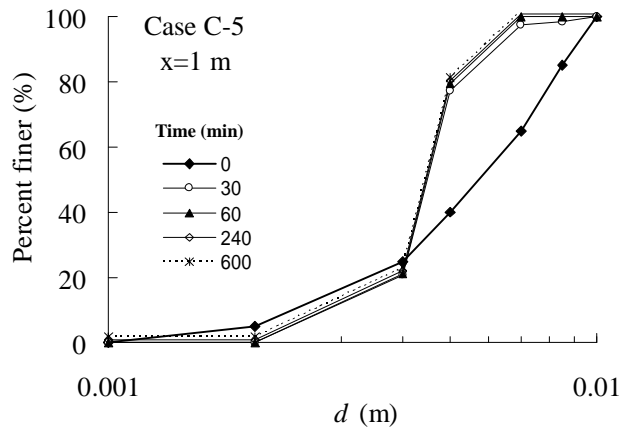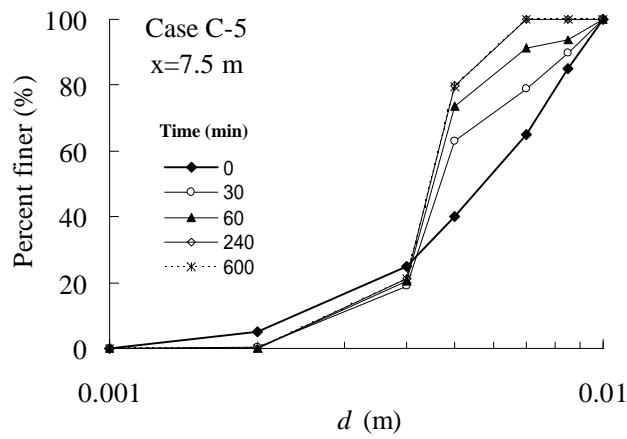

(c) Downstream ($x = 14$ m)

Fig.5.42 Grain size distributions of surface bed material at the upstream ($x = 1$ m), midstream ($x = 7.5$ m), and downstream ($x = 14$ m), in the **Case C-3.**

$q_s = 8 \times 10^{-5}$ m²/s
$Q_w = 0.02$ m³/s

Case C-4

1/100

15 m

Bed material: Talbot type
Sediment supply: Middle size of bed material (2.8~5.9 mm)

(a) Bed profile

(b) Deposition depth

(c) Mean diameter of surface layer

(d) Porosity of surface layer

(e) Type of grain size distribution

Fig.5.43   Simulation results on bed and porosity variation (**Case C-4**).

213

(a) Upstream ($x = 1$ m)
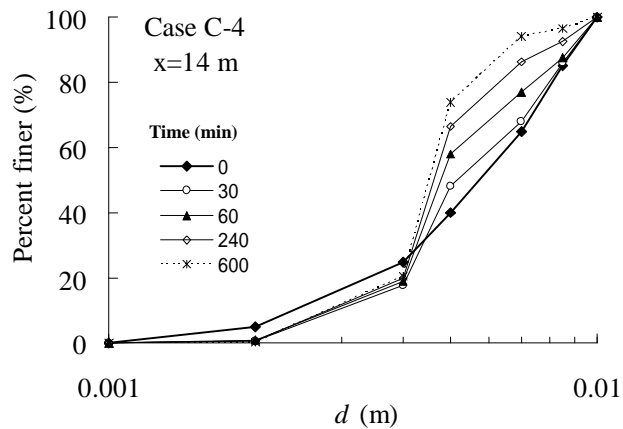
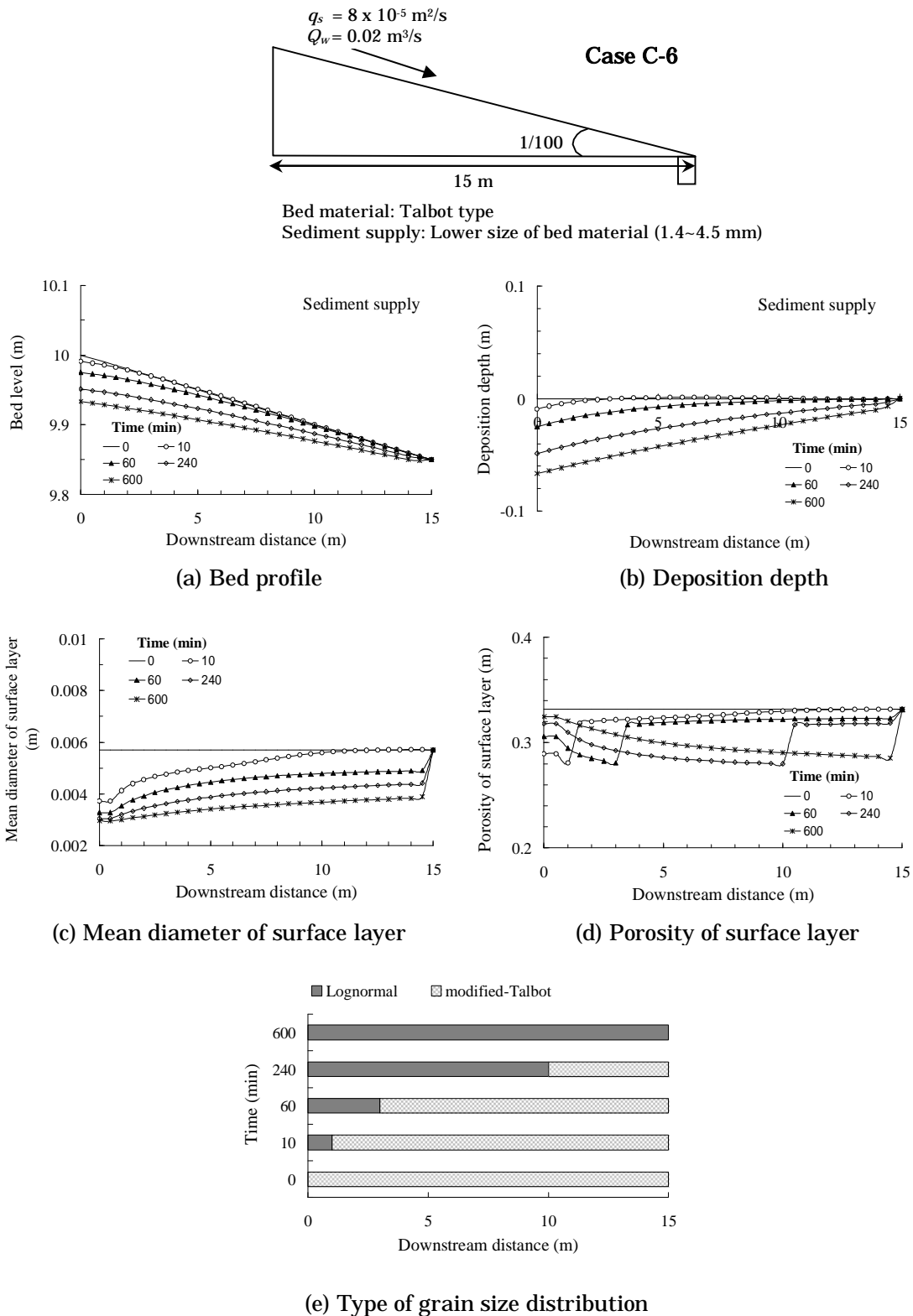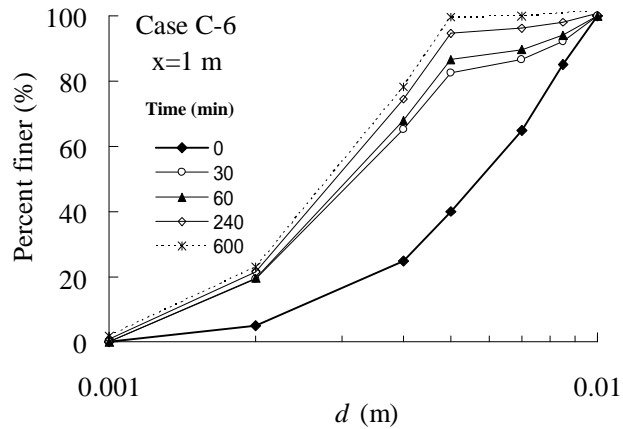(b) Midstream ($x = 7.5$ m)

(c) Downstream ($x = 14$ m)

Fig.5.44 Grain size distributions of surface bed material at the upstream ($x = 1$ m), midstream ($x = 7.5$ m), and downstream ($x = 14$ m), in the **Case C-4.**

214

Case C-5

$q_s = 8 \times 10^{-5}$ m²/s
$Q_w = 0.02$ m³/s

1/100

0.05 m

15 m

Bed material: Talbot type
Sediment supply: Middle size of bed material (2.8~5.9 mm)

(a) Bed profile

(b) Deposition depth

(c) Mean diameter of surface layer

(d) Porosity of surface layer

(e) Type of grain size distribution

Fig.5.45   Simulation results on bed and porosity variation (**Case C-5**).

215

(a) Upstream ($x = 1$ m)

(b) Midstream ($x = 7.5$ m)
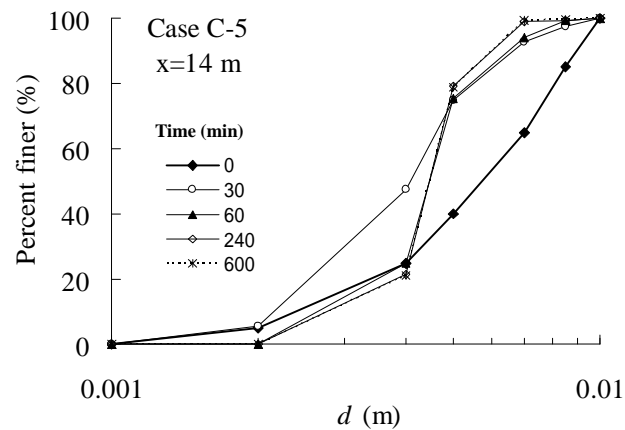
(c) Downstream ($x = 14$ m)

Fig.5.46 Grain size distributions of surface bed material at the upstream ($x = 1$ m), midstream ($x = 7.5$ m), and downstream ($x = 14$ m), in the **Case C-5.**
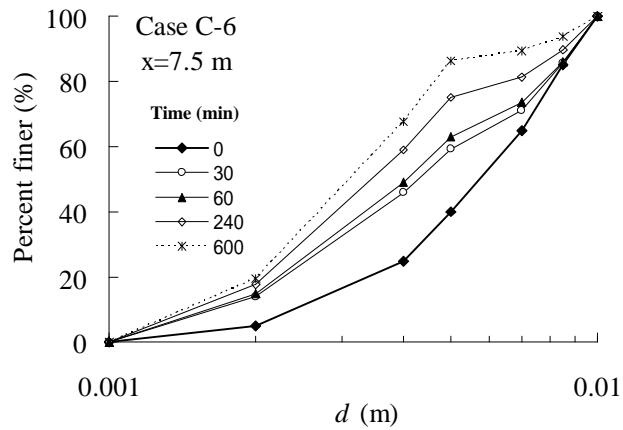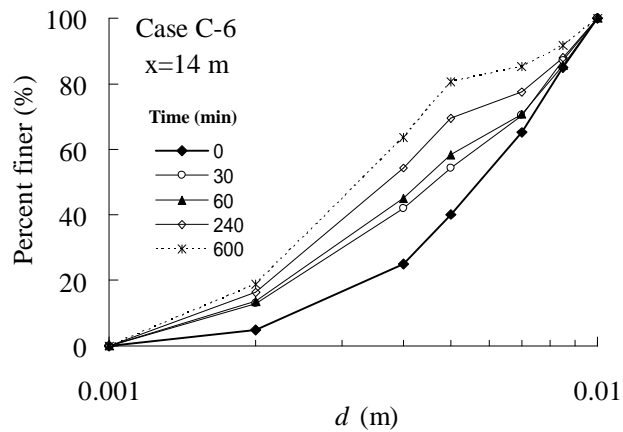
216

q_s = 8 x 10⁻⁵ m²/s
Q_w = 0.02 m³/s

Case C-6

1/100

15 m

Bed material: Talbot type
Sediment supply: Lower size of bed material (1.4~4.5 mm)

(a) Bed profile

(b) Deposition depth

(c) Mean diameter of surface layer

(d) Porosity of surface layer

(e) Type of grain size distribution

Fig.5.47   Simulation results on bed and porosity variation (**Case C-6**).

(a) Upstream ($x = 1$ m)

(b) Midstream ($x = 7.5$ m)

(c) Downstream ($x = 14$ m)

Fig.5.48 Grain size distributions of surface bed material at the upstream ($x = 1$ m), midstream ($x = 7.5$ m), and downstream ($x = 14$ m), in the **Case C-6.**

218

The simulation results show that the presented bed-porosity variation model produces a reasonable result on the change in porosity as well as the bed variation in the case of sediment mixtures with continuous grain size distribution.

5.7 Summary

As no doubt that the porosity of bed material is not constant and dependent on the grain size distribution, the time differential term on the porosity in the continuity equation of sediment must be considered. A one-dimensional bed-porosity variation model is developed for the analysis of the change in porosity of bed material as well as the bed variation. Porosity is dependent on the grain size distribution of bed material and its compaction degree. In this study, the compaction degree is empirically considered and the porosity is assumed to be a function of characteristic parameters of grain size distribution. Analytical model on porosity of binary mixtures with much different grain sizes and the relationship between the characteristic parameters of grain size distribution and porosity presented in Chapter 4 are introduced into the bed variation model. The type and the characteristic parameters of grain size distribution are identified by using an identification method presented in Chapter 3. An exchange model of bed material and transport sediment is introduced to obtain time and space variations of grain size distribution and porosity of bed material. A flume experiment is conducted to realize the transformation processes of void structure for two conditions; one is the only fine sediment is removed from a sediment mixtures (no sediment supply) and another is the fine sediment deposit into a coarse bed material (sediment supply).

Two numerical methods are employed to solve the governing equations, i.e., standard successive approximation method and MacCormack scheme. The bed-porosity variation model with standard successive approximation is applied to simulate the bed and porosity variation process observed in the flume experiment. To make clear the improvement of this bed variation model, the simulation result is compared with the result calculated by a standard model on the assumption that the porosity is constant. The bed-porosity variation model by means of MacCormack scheme is applied to simulation of the bed variation processes on the some conditions. Firstly, the model is applied to the bed variation in the case of binary mixtures. Secondly, the model is applied to the bed variation process observed in the flume experiment. Thirdly, the model is applied to the bed and porosity variation process for bed material with continuous grain size distribution, under two conditions; (1) no sediment supply condition and (2) sediment supply condition.

The results on experiment of bed variation and simulation of bed-porosity variation model are as follows:

1) The situation of non-equilibrium sediment movement without bed variation is experimentally investigated. This characteristic is caused by the change in the porosity of bed material. The experiment clearly shows that a bed variation model must be able to analyze the processes of two conditions. One is the fine sediment moves to downstream and buries the pore of surface bed material and another is the removal of fine sediment from the bed material without bed degradation.

2) The comparison between the simulated result by means of standard successive approximation and the experimental result shows that the presented model can simulate the tendency of the variation of the grain size distribution and produces a reasonable result on the change in porosity as well as the bed variation. The comparison between the simulated result by means of MacCormack scheme and the

220

experimental result also shows the similar result.

3) In the case of binary mixtures, the simulation results by means of MacCormack scheme show that the simulation on the assumption of not-constant porosity produce more reasonable results than the simulation on the assumption of constant porosity. The model can produce a distribution of porosity of the riverbed material in the longitudinal and vertical directions.

4) In the case of sediment mixtures with continuous grain size distribution, the simulation is carried out to observe the bed and porosity variation under two conditions; one is no sediment supply condition and another is sediment supply condition. The simulation results show that no sediment supply causes the bed degradation, and the increase in both the mean grain size distribution and the porosity of surface layer. The grain size distribution becomes progressively coarser and coarser. The fine sediment supply can causes the degradation in the channel due to the increase in the transport capacity; and reduce both the mean diameter and the porosity of surface bed material. The bed-porosity variation model was also able to produce the changes of grain size distribution type.

5) The validity of the presented bed-porosity variation model in the case of sediment mixtures with continuous grain size distribution has not been verified yet, but it is believed that this model has a good performance for the analysis of bed and porosity variation. It can be applied for the problems on bed variation and ecosystem in the downstream of dam.

References

ASCE Task Committee on Sediment Transport and Aquatic Habitats (1992). "Sediment and aquatic habitat in rivers systems." *Journal of Hydraulics Engineering*, Vol. 118: 669-687.

Ashida, K. and Michiue, M. (1972). "Study on Hydraulic Resistance and Bed-load Transport Rate in Alluvial Streams." *Proc. Japan. Soc. of Civil Eng.*, No.206, pp.59-69 (in Japanese).

Ashida, K. and Fujita, M. (1986). "Stochastic model for particle suspension in open channels." *J. Hydro. And Hydr. Eng.,* JSCE, Vol.4, No.2, pp.21-46*.*

Ashida, K., Egashira, S., and Nishino, T. (1988)."Mechanism of armouring phenomena in movable beds." *Annuals, Disas. Prev. Res. Inst., Kyoto Univ.*, Vol. 31(B-2), pp.423-441 (in Japanese with English summary).

Curran, J.C. and Wilcock, P.R. (2005). "Effect of Sand Supply on Transport Rates in a Gravel-Bed Channel." *Journal of Hydraulics Engineering*, Vol. 131, pp.961-967.

Gayraud, S., Philippe, M. (2003). "Influence of bed-sediment features on the interstitial habitat available for macroinvertebrates in 15 French streams." *Internat. Rev. Hydrobiol.*, Vol.88, pp.77-93.

Hirano, M. (1971). "River-bed degradation with armoring." *J. Japan Soc. Civil Eng.*, Vol.195, pp.55-65. (in Japanese with English summary).

Lane, E.W. and Kalinske, A.A. (1941). "Engineering calculation of suspended sediment." Trans. A.G.U., Vol.22, pp.603-607.

Lopez, J.L. Falcon, M.A. (1999). "Calculation of bed changes in mountain streams." *Journal of Hydraulics Engineering*, Vol. 125, pp.263-270.

Meier, W.K. and Reicchert, P. (2005). "Mountain streams-modeling hydraulics and substance transport." *Journal of Environmental Engineering*, Vol. 131, pp.252-261.

Milhous, R.T. (1982). "Effect of sediment transport and flow regulation on the ecology of gravel-bed rivers." *Gravel-bed Rivers*. Edited by Hey, R.D., Bathurst, J.C. and Thorne, C.R, John Wiley & Sons, pp.819-842.

Papanicolau, A.N., Bdour, A., and Wicklein, E. (2004). "One-dimensional hydrodynamic/sediment transport model applicable to steep mountain streams." *Journal of Hydraulic Research*, Vol.42, No.4. pp.357-375.

Sulaiman, M., Tsutsumi, D., and Fujita, M. (2007). "Porosity of Sediment Mixtures with Different Type of Grain Size Distribution." *Annual Journal of Hydraulic Engineering,* JSCE*,* Vol.51, pp.133-138.

Wu, F.-C., and Y.-J. Chou (2003). "Simulation of gravel-sand bed response to flushing flows using a two-fraction entrainment approach: Model development and flume experiment." *Water Resources Research*, Vol.39, No.8, p.1211.

Chapter 6

Conclusions and Recommendations

The sediment movement system in a river basin consists of sediment production process in the mountainous region, sediment supply process to the torrents and sediment deposition process in the lower reach and coastal area. The system is influenced by the natural impacts as well as human-induced impacts. Both impacts affect the topographical feature and ecosystem in the basin including the coastal area. In volcanic basins, particularly in Indonesia, the topographical changes of the rivers are mainly dependent upon some following factors: the impact of volcanic eruption that causes the severe bed aggradation, the development of the sediment control works that causes the bed degradation in the downstream, the construction of dams and weirs that causes the bed degradation in the downstream and coastal erosion, uncontrolled sediment mining that causes the riverbed degradation in the downstream, and deforestation that causes the severe erosion in river basins. Conventionally, these problems are addressed locally for each control area. Local countermeasure for sediment-related problems may give a negative influence on the other reach, and thus the integrated sediment control measure is strongly necessary. The targets of integrated sediment management are: 1) to prevent disasters, 2) to reduce the negative influence of sediment on river, 3) to utilize the sediment resources effectively, and 4) to conserve the river and coastal environment. To achieve those goals, the research on the feasible and effective sediment management methods and the development of some tools for sediment management should be promoted.

A numerical simulation method for bed variation is one of the tools necessary for integrated sediment management. As the void of riverbed material plays an important role in the fluvial geomorphology, the infiltration system in riverbeds and the river ecosystem, the change of void with the bed variation is one of the concern issues in eco-hydraulic and river management. Thus, the development of a bed variation model considering the changes in porosity is strongly required and it is expected that the model contributes in the analysis of those problems as a tool of the integrated sediment management.

The objectives of this study were; (1) to figure out the recent sediment-related problems in a volcanic river basin as well as the impacts on riverbed variation and ecosystem, a case study in Merapi volcanic area and Progo River basin, Indonesia, (2) to develop a method for classifying and identifying the type of grain size distribution, (3) to develop two methods for estimating the porosity of different type of grain size distribution, (4) to develop a fundamental framework of quantitative and qualitative bed variation model and a bed-porosity variation model.

The results obtained in the previous chapters are summarized as follows:

In **Chapter 2**, the sediment-related problems in volcanic area (particularly in Mt. Merapi and Progo River, Indonesia) and the impacts on bed variation and ecosystem were pointed out. The sediment-related problems persist in the upper reach, the middle reach, also in the lower reach. Some problems are triggered by the natural activities such as volcanic activity of Mt. Merapi and heavy rainfalls, and many others occurs due to the human interfere such as deforestation, construction of sabo dams and sand mining. The activities of Merapi Volcano have caused severe sediment-related disasters, including pyroclastic flows and debris flows. Frequent eruptions produced a tremendous amount of volcanic loose deposit on the slope of Mt. Merapi and disasters in the downstream area. At another

side, uncontrolled sand mining has caused serious problems in the watershed, such as bank erosion, riverbed degradation, unstableness of river structures and environmental effects. One of the critical issues of uncontrolled sand mining in Merapi volcanic area is the riverbed degradation in the Lower Progo River. The riverbed degradation has threatened the existing social infrastructures, which induced serious negative impacts on the regional development. Removal of finer material through sand mining also caused bed coarsening due to changes in grain size distribution.

A qualitative analysis in this chapter showed that the sand mining could be an effective method to control the excess sediment, in order to keep the riverbed in an appropriate level for water utilization and river ecosystem, if the sand mining activities are properly managed. Therefore, the sustainable sand mining management is an important point as a part of the sediment control plan and the regional development to reduce and mitigate the disasters.

In **Chapter 3**, a method for classifying and geometrically identifying the type of grain size distribution was presented. There are some typical types of grain size distribution. In this study, it was assumed that the porosity of bed material was dependent on the type. Thus, the method is necessary for a bed-porosity variation model. First, grain size distribution was classified into some typical types and those characteristic parameters were found out. Then the grain size distribution was geometrically identified by using geometric indices γ and β. Based on the geometrical analysis of typical grain size distributions, a diagram on classification of grain size distribution type was indicated. The presented identification method was then applied to the natural grain size distribution data and the validity of the method was verified. The results in **Chapter 3** are summarized as follows:

1) Unimodal distribution could be classified into three typical types of distribution namely; Talbot distribution, lognormal distribution and anti-Talbot distribution and the characteristic parameters of each type were found out.

2) It is well known that the bed material in mountain streams has Talbot distribution. The characteristic parameters of this distribution are the maximum grain size, d_{max}, and a coefficient, n. However, fitting the Talbot-like wide grain size distribution of bed material by using this function gives the much larger difference in the range of finer sizes. Therefore, the original Talbot distribution function was modified with considering the minimum grain size distribution, and in this study, it was called as modified-Talbot distribution or M-Talbot distribution. The characteristic parameters of M-Talbot distribution were the Talbot number, n_T, and the ratio of the maximum and minimum diameters of particle, d_{max}/d_{min}.

3) The geometric indices γ and β, that designate the relative locations of the grain size for percent finer of 50% (d_{50}) and the grain size for the peak probability density (d_{peak}) between the minimum size and the maximum size were found out for classification of the distribution type, namely M-Talbot type, lognormal type and M-anti-Talbot type.

4) A diagram on classification of grain size distribution was presented. The diagram presented the relation between geometric indices γ and β and the domain of each typical unimodal distribution, i.e., M-Talbot, lognormal and M-anti-Talbot distribution. The validity of the diagram was then verified by the comparison with the result by means of visual identification.

5) The diagram on classification of grain size distribution could be applied to classify the actual grain size distributions into three types. The grain size distributions of surface bed material in the midstream of Japanese Rivers tended to be M-Talbot distribution, while the grain size

distributions in the downstream tended to be lognormal distribution. The grain size distribution of sub-surface bed material had bimodal distribution. Sediments produced on the bare slope were identified as Talbot distribution. Deposited materials had variety typical grain size distributions depending on the deposit location and the source of material.

In **Chapter 4**, two methods for estimating the porosity of sediment mixtures were presented. One was based on a particle packing simulation model. The other one was based on a measurement by a water displacement method. The packing simulation model was available to derive the porosity of spherical particle mixtures with different types of size distribution. Porosity of sediment mixtures depended on not only the grain size distribution but also the compaction degree, but the model could not control the compaction degree. As a result of simulation, the compaction degree was given. The validity of the model was assessed with the experimental results, and its validity was then confirmed. The defect of this model was that it took too much time to pack the particles with a wide grain size distribution in a vessel. The measurement method could be used in situ estimation of porosity. This method was very simple and applicable for field surveying. However, this method was available only for the dry material.

The results in **Chapter 4** are summarized as follows:
1) The porosity of sediment mixtures could be determined by the characteristic parameters of the grain size distribution.
2) For lognormal distribution, the porosity depended only on the standard deviation of $\ln d$, σ_L, if the compaction degree was constant. The porosity decreased with an increase in the standard deviation, σ_L, mainly due to the reduction of the volume of void by the occupation of large particles. Simulation results showed that the deviation of simulated porosity increased when the standard deviation, σ_L, increased from 0.75 to 1.5.

This deviation arose from the effect of vessel size.

3) The trend of porosity change with the standard deviation between the measurement and the simulation was almost similar. However, the measurement result was somewhat larger than the simulated one. The discrepancy might be due to the difference in the shape of particle, the compaction degree, and the inverse grading of the particles. Particularly in the measurement, it was very difficult to mix the sediment evenly. Consequently, the coarser particle lay at higher position than the finer particle. This inverse grading process made the porosity larger, while in the simulation the particles were mixed evenly. However, the diagram available for estimating the porosity of lognormal grain size distribution was obtained.

4) For M-Talbot distribution, the simulation results showed that the porosity increased with an increase in the Talbot number, n_T, and a decrease in the ratio of d_{max}/d_{min} gave the higher value of porosity. The relation between porosity and Talbot number for the different ratio of maximum and minimum diameters was expressed by the lines with a same inclination. However, the porosities in the simulation and the measurement were rather different for the same Talbot number and the same ratio of maximum and minimum diameters. The reason of this discrepancy was also the differences in the shape of particle, the compaction degree, and grading of the particle.

5) For M-Talbot distribution, it is possible to estimate the porosity roughly by means of the presented relation between the porosity and the characteristic parameter of grain size distribution. However, as there was rather larger difference between the simulation and the measurement, more investigation on the influence of the compaction degree is necessary to fix the relation.

6) The porosity of bimodal distribution depends on the percentage of each fraction in the mixture. It was interesting that the minimum porosity

appeared for a percentage of finer material as in a binary mixture. The porosities in the simulation and the measurement were rather different for the same proportion of finer materials. The discrepancy between the measured and simulated porosities might be caused by the difference in the uniformity of the sediment mixtures. In the simulation, the particles were packed evenly in the vessel with dense packing, so the porosity was low. However, in the experiment, the coarse fraction lay at the higher position and the finer fraction went down to the lower position. As each fraction had an almost uniform distribution, the porosity in the measurement method was larger than simulated one and close to the porosity of uniform sediment.

7) A method for measuring the porosity of sediment was proposed. The porosity of sediment mixtures and bed material could be reasonably estimated by measuring the in-situ volume of sediment sample. This method was very easy and applicable to the field survey.

8) In the gravel bed river, the bed was usually stratified vertically with coarse armor layer on the surface. The characteristic of gravel bed material varied between sediment layers. Generally, the surface layer has a M-Talbot distribution and the sub-surface layer has a bimodal distribution. Therefore, the porosity of surface layer was higher than the porosity of sub-surface layer due to the armoring in the surface layer.

9) Compaction degree of bed material in the surface layer was usually rather low compared with the material in the sub-surface layer; consequently, the porosity of surface layer was larger than sub-surface layer.

In **Chapter 5**, a one-dimensional bed-porosity variation model for the analysis of the change in porosity of bed material as well as the bed variation was developed. As no doubt, that porosity of bed material is not constant and

dependent on the grain size distribution, the time differential term on the porosity in the continuity equation of sediment must be considered. Analytical model on porosity of a mixture of two particle groups with much different grain sizes and the relationship between the characteristic parameters of grain size distribution and the porosity presented in Chapter 4 were introduced into the bed variation model. The type and the characteristic parameters of grain size distribution were identified by using an identification method presented in Chapter 3. An exchange model of bed material and transport sediment was introduced to obtain the time and space variations of grain size distribution and porosity of bed material.

Two numerical methods were employed to solve the governing equations, i.e., a standard successive approximation and MacCormack scheme. The standard successive approximation method was applied to simulate the bed and porosity variation process observed in the flume experiment. To make clear the improvement of this bed variation model, the simulation result was compared with the result calculated by a standard model on the assumption that the porosity was constant. MacCormack scheme was applied to simulation of the bed variation processes on the some conditions. Firstly, the model was applied to the bed variation in the case of binary mixtures. Secondly, the model was applied to the bed variation process observed in the flume experiment. Thirdly, the model was applied to the bed and porosity variation process for bed material with continuous grain size distribution, under two conditions; (1) no sediment supply condition and (2) sediment supply condition.

The results on the experiment of bed variation and the simulation of bed-porosity variation are as follows:

1) The situation of non-equilibrium sediment movement without bed variation was investigated experimentally. This characteristic was caused by the change in the porosity of bed material. The experiment clearly showed that a bed variation model must be able to analyze the

processes of two conditions. One was the fine sediment moved to downstream and buried the pore of surface bed material and another was the removal of fine sediment from the bed material without bed degradation.

2) The comparison between the simulation result by means of the standard successive approximation method and the experimental result showed the presented model could simulate the tendency of the variation of the grain size distribution and produced a reasonable result on the change in porosity as well as the bed variation. The comparison between the simulation result by means of MacCormack scheme and the experimental result also showed similar results.

3) In the case of binary mixtures, the simulation results by means of MacCormack scheme showed that the simulation on the assumption of not-constant porosity produced more reasonable results than the simulation on the assumption of constant porosity. The model could produce a reasonable distribution of porosity of the riverbed material in the longitudinal and vertical directions.

4) In the case of sediment mixtures with continuous grain size distribution, simulation was carried out to observe the bed and porosity variation under two conditions; one was no sediment supply condition and second was sediment supply condition. The simulation results showed that no sediment supply caused the bed degradation, and the increase in the mean grain size and the porosity of the surface layer. The grain size distribution was progressively coarser and coarser. The fine sediment-supply on the bed material caused the bed degradation in the channel because the transport capacity was larger than the sediment discharge. In addition, it reduced the mean diameter and the porosity of surface bed material. The bed-porosity variation model was also able to produce the changes of grain size distribution type.

5) The validity of bed-porosity variation model in the case of sediment mixtures with continuous grain size distribution had not been verified yet, but it was believed that this model had a good performance for the analysis of bed and porosity variation. It could be applied for the problems on bed variation and ecosystem in the downstream of dam.

Through the model simulation, laboratory experiment, and field observation, the porosity of particles and sediments mixtures have been investigated. Special attention was paid to the relationship between the porosity and the grain size distribution. The porosity of sediment mixtures could be determined by the characteristic parameters of the grain size distribution for lognormal and M-Talbot distribution. The relation was then introduced into a bed variation model.

A one-dimensional bed-porosity variation model proposed in this study is different from the conventional model from a viewpoint of considering the porosity of bed material. Hence, the proposed model is available for the analysis of the change in porosity of bed material as well as the bed variation. The model contributes in two aspects; from the hydraulics point of view, the model provides an improvement of the accuracy in the riverbed variation calculation and from ecological point of view, the model provides the changes in porosity with the bed variation. In the case of binary mixtures, the validity of the model has been verified using a data set provided by the experiment and the simulation result showed that the model produced a reasonable result on the change in porosity as well as the bed variation. In the case of sediment mixtures with continuous grain size distribution, although the validity of the model has not been verified yet, the simulation result showed the model available for analysis of bed and porosity variation.

Future work is required to improve the performance of the model. The following points are recommended to be considered:

1) To assess the validity of the model in the case of sediment mixtures with continuous grain size distribution, a laboratory experiment is necessary to be conducted. After the validation process, to examine the applicability of the model, its application to the real river is necessary to be conducted.

2) In this study, the porosity was assumed as a function of characteristic parameters of grain size distribution and the compaction degree was considered empirically. However, there were differences between the simulation results and measurement results of the porosity. The discrepancy might be due to the influence of the compaction degree, the uniformity of the mixtures of sediment and the inverse grading of the particles. Hence, future research on how to include these factors should be considered.

3) The characteristic parameters of the unimodal grain size distribution were found out and could be used to determine the porosity of sediment mixtures. However, considering the riverbed material can have the bimodal grain size distribution, it is necessary to find out the characteristic parameters of the bimodal distribution and relate it to the porosity.

Acknowledgments